FABRICATION OF TISSUE ENGINEERING SCAFFOLDS USING STEREOLITHOGRAPHY

A Dissertation
Presented to
The Academic Faculty

by

Benita M. Comeau

In Partial Fulfillment
of the Requirements for the Degree
Doctor of Philosophy in the
School of Chemical & Biomolecular Engineering

Georgia Institute of Technology
December 2007

FABRICATION OF TISSUE ENGINEERING SCAFFOLDS USING STEREOLITHOGRAPHY

Approved by:

Dr. Clifford L. Henderson, Advisor
School of Chemical & Biomolecular Engineering
Georgia Institute of Technology

Dr. Mark Prausnitz
School of Chemical & Biomolecular Engineering
Georgia Institute of Technology

Dr. Carson Meredith
School of Chemical & Biomolecular Engineering
Georgia Institute of Technology

Dr. David Rosen
The George W. Woodruff School of Mechanical Engineering
Georgia Institute of Technology

Dr. Peter Ludovice
School of Chemical & Biomolecular Engineering
Georgia Institute of Technology

Dr. Yadong Wang
The Wallace H. Coulter Department of Biomedical Engineering
Georgia Institute of Technology and Emory University

Date Approved: August 7, 2007

This thesis is dedicated to by husband Jon, without whom I would never have undertaken or completed the graduate school adventure.

ACKNOWLEDGEMENTS

During my time at Georgia Tech, there have been many individuals who have contributed their time and effort to this work. I would like to thank my advisor, Clifford L. Henderson, for his support and guidance. I am especially appreciative of the amount of freedom he has extended to me over the years, in terms of research topics and areas of investigation. I would also like to thank my other committee members, Dr. Carson Meredith, Dr. Peter Ludovice, Dr. Mark Prausnitz, Dr. David Rosen, and Dr. Yadong Wang, whose time and input have significantly improved the quality of my work. In particular, I would like to thank Dr. Meredith for generously sharing his cell culture lab space with me, Dr. Yadong Wang whose donation of fibroblasts made this work possible, and Dr. Rosen who offered me all of the resources at the Georgia Tech RPMI laboratory.

I would also like to acknowledge the invaluable help and support that I received from my fellow Georgia Tech graduate students. All of the Henderson group members have always been there for me. Celesta White, Cody Berger and Trevor Hoskins welcomed me into the group, and Ashwini Sinha, Michael Romeo, Richard Lawson, Yueming Hua, and Cheng-Tsung Lee have all lent a hand in the following years. I appreciate that Ameya Limaye shared his SLA insights, and I am grateful for the help from my friends Gracy Wingkono and Charlene Rincon in the cell lab. Several undergraduates, Ben Katz, Jonanna Stanton, and Amin Zargar, worked closely with me on various branches of my project. I truly appreciate their work and effort.

There have also been many friends at Tech, without whom I would have been colder, hungrier and less sane. These include the Becks, the Haydens, Mikkel Thomas, and Karla Dennis; all of you made meals more fun and setbacks seem less disastrous. Thank you especially to my friends Harley and Emily Hayden who welcomed me into their home for a tough last semester. I also want thank to my officemate, Karla Dennis, whose wonderful cookies and warm friendship always helped make studying and work so much better. I truly value all of you, and these friendships will be some of the best things that I carry away with me from Georgia Tech.

Finally, I would not be here today without the loving support from all of my incredible family. My in-laws, Phillip, Penny and Alisa Comeau, have truly made me a part of their family these last five years. My mother, Maggie Kuo, has always encouraged me to work up to my potential and continues to be a role model for me of an independent, intelligent, thoughtful woman. Amy Kuo, my sister, my best friend and partner-in-crime, has always been a source of joy in my life and I know she will always be there for me, no matter what happens. I certainly would not be here today without the love and guidance of my father, Hong-Hsiang Kuo, PhD, who set me on the course to become a chemical engineer by passing on the curiosity about science from his father, through him, and finally to me. I will never forget my first lesson about convective cooling from my dad, while eating ice cream on a windy summer day. Of course, there is one final thank you to write, and that goes to my extraordinary husband, Jon Comeau, PhD. I would never have come to graduate school without your support, and it is your constant love and strength that has sustained me during all of the hard times. Jon, I love you always.

TABLE OF CONTENTS

LIST OF TABLES

LIST OF FIGURES

SUMMARY

In summary, the work in this thesis is towards fabricating a hierachrically structured, tissue engineering scaffold using stereolithography and photolithographic methods. An overview of the tissue engineering field is given, putting the fabrication of tissue engineering scaffolds using stereolithography in the context of the current state of the art. A non-cytotoxic set of photo-acid generators was identified which may be used in photoresists for the cell patterning process. A novel method for evaluating the toxicity of these small molecules by doping them into a polymer matrix is presented, and shows good agreement with earlier studies on photoinitiators that was done by directly adding them to the cell media. The challenges and benefits of patterning cells using photolithographic means is highlighted, and cell patterning using traditional photoresist polymers is demonstrated, without the need for the synthesis of highly specialized bioresist polymers. In order to consistently achieve cell patterns with these materials, a special cell seeding procedure that includes a wash step after one hour of incubation is necessary. These findings open a larger material space for using photoresists to pattern cells, and offer a much simpler method for cell patterning than most of the currently used methods. The cell patterning mechanisms were investigated using a quartz crystal microbalance with dissipation (QCMD) and show why the patterning procedure works well. The QCMD results show that the unexposed, fully-protected polymer surfaces have the lowest amount of fibronectin adsorption and there is no frequency shift upon introduction of a cell suspension, showing that the surface resists cell adhesion and

spreading. Thus, a wash step after one hour of incubation easily removes the cells in these regions, leaving only the cells in the exposed, de-protected areas.

The mirror-array based stereolithographic apparatus that was built in the laboratory is documented, along with some of the specialized components that were built to hold and align the mirror array. In particular, a design change in the mounting of the mirror array allows for ease of focusing the image on the resin surface, without having to account for keystone type corrections, and thus this system can resolve below the size of individual mirrors with the smallest achievable line size of 5 μm. There is discussion of the synthesis and theoretical considerations for formulating a stereolithographic test resin, which is capable of undergoing rapid polymerization, acid-catalyzed de-protection of a low energy activation group, and incorporation of a degradable linkage. Unfortunately, this initial test resin did not demonstrate cell patterning; however, the MOM-protected methacrylic acid still shows promise and may be used as starting point for future work. A simple degradable linkage, diallyl fumarate, was successfully incorporated through photopolymerization and demonstrates that the degradation of the polymer may be tuned by formulating the resin with a mixture of monomers. Finally, the overall conclusion and suggestions for the future directions this work may take are discussed.

CHAPTER 1

INTRODUCTION TO TISSUE ENGINEERING STRATEGIES

There is a great need for the development of robust tissue engineering strategies to improve our current medical capabilities. One definition of tissue engineering is "the application of engineering principles to create devices for the study, restoration, medication, and assembly of functional tissues from native or synthetic sources" [1]. The need for understanding how to assemble functional tissues arises from the shortage of donor organs, and the need to treat injuries and disease. For example, as of April 2004, there were 83,888 total candidates listed on the national organ transplant waiting list, and about 17 patients die each day while waiting for an organ [2].

While the promise of engineering complete organs is certainly alluring, the current state of technology is not yet capable of generating complex, functioning structures. The most recent successes have been in the culturing of two-dimensional (2D) tissues, not organs. For example, several synthetic skin tissues have been engineered that can be used to treat a wide range of medical ailments where skin cannot normally regenerate after an injury [3]. A main reason that engineered skin has progressed this far is that it does not require very complex cell architectures or a large network of vessels to transport nutrients and oxygen. For other large three-dimensional (3D) organs, it is necessary to provide a transportation network and a complex arrangement of different cell types; and these are just two of the many challenges that confront researchers in this area.

There are three main approaches to tissue engineering: 1) the use of isolated cells or cell substitutes to replace those cells that supply the needed function; 2) the delivery of tissue-inducing substances, such as growth and differentiation factors, to targeted locations; 3) growing cells in three-dimensional scaffolds [4]. The first two methods can be applied when the injury or defect is small and well contained. For the healing of larger wounds or defects, these two methods become quite limited; and the third approach has become a very active area of research. A key component to this third strategy is a scaffold which provides a 3D architecture for the cells to grow on. The design of the scaffold should include a high degree of interconnected porosity for nutrient and waste transport. Additionally, it may be necessary for more than one cell type to be present in the tissue. Thus, the scaffold must allow for different cell types to grow in the correct orientation to one another and differentiate appropriately. Finally, of course, the scaffold should be tailored in size and shape to the diseased or injured area that the new tissue will replace. The basic scheme is illustrated below (Figure 1.1).

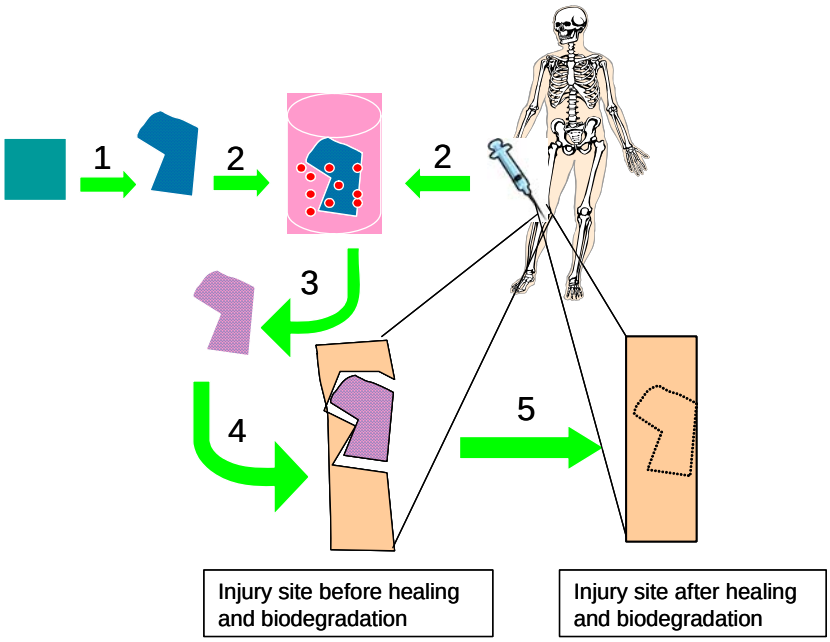

Figure 1.1: General tissue engineering scaffold strategy

The main steps are: 1) build a tissue engineering scaffold in the desired geometry from an engineered starting material; 2) seed the scaffold with the appropriate cell types from the patient or donor; 3) allow the cells to grow and differentiate into functioning tissues; 4) implant the final tissue structure at the site of injury; and 5) bio-degradation of the tissue engineering scaffold material, leaving just the functioning tissue at the injury site. Clearly, there are a multitude of engineering challenges to complete this approach, and it is beyond the scope of this thesis to examine all of them. The work presented here is focused on the front end of this process: identifying suitable materials for a novel fabrication process, and testing the compatibility of these materials with cell seeding.

Applications of Tissue Engineering

Due to the broad definition of tissue engineering, tissue engineering strategies may be employed to treat ailments in every part of the body. There are many cell therapy strategies which involve the direct transplant of functioning cells into the reconstruction/rehabilitation site (Table 1.1).

Table 1.1: Overview of cell therapies where isolated cells are transplanted to regain function lost due to disease, and the associated problems [5].

Cell Therapy	Disease	Use	Problems
Bone marrow	immune deficiency leukemia	transplantation	rejection reactions
Keratinocytes	burns ulcers	transplantation	no skin structures such as hair, sweat glands or sebaceous glands
Chondrocytes	damaged cartilage	transplantation	deficient stability
Myoblasts	muscular dystrophy	transplantation	immune reaction
Cardiomyocytes	Cardiac infarction	transplantation	deficient integration, function
Islet cells	diabetes mellitus	transplantation	stop production of insulin
Dopaminergic neurons	Parkinson's disease	transplantation	stop specific function

With the problems presented by direct transplantation of cells, one may realize that it might be advantageous to transplant whole, functioning tissues into the diseased area. In order to reduce the risk of immune rejection, and because there is a shortage of donor tissue and organs, it becomes necessary to engineer functioning tissues from isolated cells. This leads to the use of scaffold-based tissue engineering strategies. As mentioned earlier, this strategy is most suited for the regeneration of large areas of tissue, or for the repair of tissue where cells will not normally re-grow. Table 1.2, below, gives

several examples of the use of tissue engineering scaffolds for the treatment of disease through implantation.

Table 1.2: Uses of tissue constructs for the regeneration of lost function in the basic tissue types [5].

Tissue replacement	Disease	Use	Problems
Neural constructs	separation of the spinal cord, degeneration of the retina	implantation	insufficient differentiation
Muscle constructs	lack of muscle tissue	implantation	insufficient function, inadequate connection
Connective tissue constructs	damage in form giving cartilage, comminuted fracture of bones, measures of reconstruction	implantation	mechanical stability, stability of form
Blood vessels	aneurysms, arteriosclerosis	implantation	mechanical stability
Heart valves	defects of the heart valves	implantation	calcification, lacking function

It is clear from Tables 1.1 and 1.2 that tissue engineering therapies may have great promise in treating diseases in all of the tissues in our body; however, these methods have not been fully developed and perfected. Both of these points, the promise of vast medical treatments and great scientific and engineering challenges, have driven many researchers and entrepreneurs into the rapidly growing field of tissue engineering.

Commercialization of Tissue Engineering

While there are a myriad of potential applications for tissue engineering, there are only a few great success stories. The reason for this is that there are several major hurdles that are inherent to most tissue engineering strategies: immune reaction or the

rejection of foreign cells or tissues, the lack of the complex structures that exist in our natural tissues, and the difficulty in maintaining proper cell function. These hurdles underlie many of the problems associated with tissue therapies given in Tables 1.1 and 1.2 above. Although these problems persist, there have been a few commercial tissue engineering successes. It is useful to examine these case studies to understand the state of the art, and to predict how this field may progress.

The major success story in the commercialization of scaffold-based tissue engineering is in the treatment for skin wounds. One of the main uses for artificial skin is for burn patients. While grafting a patient's own skin on the wound would be the most ideal therapy, severely burned patients may not have enough healthy skin for grafting or may be too weak for surgery [6]. Additionally, there are situations where a patient is unable to heal a skin wound, as in the case of diabetic ulcers. Thus, there was a need for artificial skin that doctors could use as wound dressing and/or to help promote healing.

Apligraf®, Dermagraft® and Becaplermin (Regranex®) are all products developed for the treatment of diabetic ulcers, and are a useful case study since they illustrate the breadth of the three main tissue engineering techniques discussed earlier. Apligraf® is a two-layered, tissue construct that most closely mimics the natural structure of skin as it is composed of a lower dermal layer (bovine type I collagen and human fibroblasts) and an upper epidermal layer (human keratinoctyes that are differentiated, to replicate the human epidermal architecture). While Apligraf® is supplied as a living tissue, Dermagraft® is a cryopreserved engineered skin-substitute product. Another key difference between these two products is that Dermagraft® consists of human fibroblasts seeded on a bioadsorbable mesh scaffold, whereas Apligraf® does not contain any synthetic scaffolding material.

Finally Regranex® is a gel that contains platelet derived growth factors without any cells. All three of these products are approved therapies for diabetic ulcers, and are even covered by standard, national healthcare insurance policies [7]. The acceptance of these products in general medicine not only showcases the great potential for highly efficacious treatments via tissue engineering strategies, but also paves the way for future engineered tissue products.

The Future of Tissue Engineering

The future is promising for many tissue engineering strategies. The potential market is very large, as a recent report indicates that the market size for heart valve replacement and skin repair products are $225 and $5945 million respectively, and eventually tissue engineering may provide therapies and treatments for diseases which account for nearly half of the United States annual healthcare costs [12]. The discrepancy between the heart valve and skin repair product categories offers an interesting insight to this emerging technology. That is, in certain categories, such as skin repair, there are no other developed strategies for treatment; whereas the heart valve market is already developed. Thus, some of the greatest potential for tissue engineering may lie in the development of completely new areas of therapy for previously untreatable disorders. Also, with the myriad of disorders and research areas, it becomes more evident that there is not a single tissue engineering strategy that will be the optimum solution for all diseases and injuries. Instead, there will be specific strategies to target specific needs.

Fabrication of Tissue Engineering Scaffolds

Tissue engineering scaffolds have been widely studied, with the hope of designing scaffolds that can support complex, 3D tissues. Also, many constructs have been prepared with the idea of studying cell to cell interactions. There are several widely accepted requirements for a tissue engineering scaffold [4]. First, the scaffold must have a high porosity, with the proper pore size and structure to facilitate transport. Along with this, a high surface area is necessary. The scaffold must also have adequate mechanical strength to maintain the desired structure. In addition to these structural elements, the scaffold must behave appropriately in a biological manner, i.e. be biocompatible. Biocompatibility is "the ability of a material to perform with an appropriate host response in a specific application" [13]. This may require that the scaffold be biodegradable and of the proper chemistry to facilitate positive cell interactions for the enhancement of cell adhesion, growth, migration, and differentiation.

Conventional scaffolds commonly lack substantial mechanical strength, and there is difficulty in controlling porosity, pore distribution, and pore interconnectivity. Additionally, the chemical nature of these scaffolds is typically homogenous. That is, there is no mechanism for creating additional chemical functionality, distinct from the bulk chemistry, in a specified geometry on the scaffold. The ability to chemically modify selected areas on a scaffold is one method to direct cell growth in deliberate patterns; which is necessary for the engineering of complex, functioning tissues.

A major difficulty and shortcoming in all of the current tissue engineering technologies is developing a method to generate hierarchical structure via a tissue engineering scaffold. Currently, most tissue engineering scaffolds are made of a single

bulk material and it is difficult to position several cell types in a specific manner. This is necessary if one is to realize the fully potential of engineering tissues.

Fabrication Methods

Many routes for creating a 3D scaffold have been studied, including 2D layer by layer methods [14, 15], direct fabrication of 3D forms through inject-able hydrogels [16], polymer-porogen methods such as salt leaching [4], and rapid prototyping methods [17-19]. The 2D layer routes mentioned above typically apply layering methods to create hierarchical order in the scaffold. That is, by careful dispensing of the layering materials, a scaffold may be formed with varying material and cell type.

There is considerable interest in using rapid prototyping (RP) and solid free-form fabrication (SFF) methods to create three dimensional cell constructs with rationally designed porous network structures. These fabrication methods allow one to design a part using computer aided design (CAD) techniques, and then translate that design directly into a 3D part. The benefit is that 3D geometry may be very well controlled by the designer. The challenge, then, is to find materials and fabrication techniques that are compatible with cell growth and function. This task is not trivial as these methods were initially developed for rapid prototyping, without planning for a bio-compatible process.

One rapid prototyping method is the three dimensional printing (3DP) process developed at the Massachusetts Institute of Technology (MIT). This process uses a powder starting material and a suitable binder. The part is formed in a layer-by-layer manner as the binder is jetted onto the appropriate regions of powder that are to become the solid part. Several groups have used 3DP with aliphatic polymers as the matrix material. Materials such as poly(L-lactide) (PLA) [20] and copolymers of poly(lactide-

coglycolide) (PLGA) [21] have been studied. Another group has investigated the use of 3DP with starch-based polymers formulated from cornstarch, dextran, and gelatin with water-based binders [22]. Pressure assisted microsyringe is another SFF method that has been tested. This method was developed at the University of Pisa, and operates by using a microsyringe to deposit a layer of the desired polymer, in the desired geometry. Each layer is laid down on top of the others by adjusting the z-height of the syringe, until a complete 3D object is formed. The layers can consist of different patterns and materials, if required. G. Vozzi et. al. has successfully demonstrated this fabrication technique with PLGA [15]. Both 3DP and pressure assisted microsyringe offer good control of the final part geometry. However, both are limited in the minimum feature size by the syringe control of the binder or polymer, and the 3DP is further limited as it requires a powder pre-material and a binder.

Soft lithography refers to several different molding methods. One is micromolding, which is just solvent casting a polymer on a polymer mold. For example, G. Vozzi et. al. produced PLGA scaffolds using a PDMS mold [15]. The PDMS mold is formed by casting PDMS on a mold made of patterned photoresist. Microfluidic molding is another soft lithography technique where a PDMS mold is reversibly sealed to a substrate, and PLGA is cast by the application of a negative pressure to the cavity between the mold and substrate. A third soft lithographic technique is spin coating where the desired polymer is spun onto a mold, and then peeled off. The main drawback for these soft lithography methods is the complexity in the fabrication process. For each part, a stamp or mold must be fabricated in addition to the desired geometry.

All of these techniques provide a means to accurately control the 3D structure of the tissue engineering construct. It becomes possible to direct not only the overall shape of the construct, but also to design the inner porous structure. However, it is difficult to specifically tailor the chemical composition of the constructs as they are being built. In the layer by layer methods, one may change the material of construction for each layer, but this introduces many complexities to the fabrication process. Also, the layer thickness is coupled to the size of the scaffold. As the scaffold size increases, it will not be possible to increase the number of layers indefinitely. Thus, at some point, the layer thickness must increase, and some of the detail in the engineering design will be lost. These limitations have to the investigation of a different fabrication approach, stereolithography (SL).

Stereolithography Methods

Stereolithography utilizes a straightforward set-up of a vat of monomer and photoinitiator, a laser, and a computer for control. In this method, a 3D form is designed on the computer, and then electronically "sliced" so that it is represented by a series of layers. These image layers are then fed into the computer that controls the SL laser. The laser then follows the shape of each layer in the vat. At each location in the vat that absorbs power from the laser, a polymerization event will occur. This is illustrated in Figure 1.2.

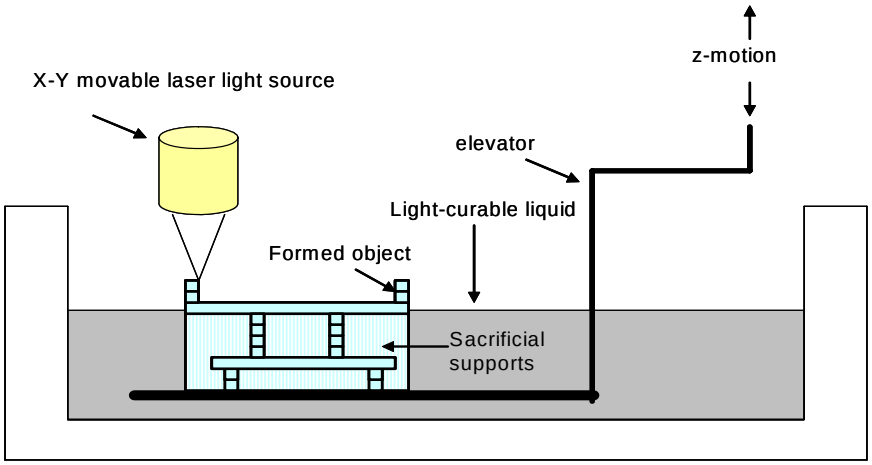

Figure 1.2: Schematic of stereolithographic apparatus.

A variety of photosensitive materials and cell types have been studied for use with SL-made scaffolds. One research group has explored this area using a biodegradable resin comprised of diethyl fumarate (DEF), poly(propylene fumarate) (PPF), bisacylphosphin oxide, and Irgacure 819 as the photoinitiator [19]. Their goal was to use SL to manufacture biodegradable scaffolds for bone. They used an SLA 250 machine, with a 325 nm UV laser. They were successful in building a 3D object with the biodegradable resin, but no detailed data was given regarding the properties of the finished part.

Another group of researchers used copolymers of ε-caprolactone and trimethylene carbonate in an SL machine to create biodegradable, photocured, tissue engineering substrates [23]. The liquid copolymers were crosslinked in their custom designed SL tool, which used a Hg-Xe lamp as the UV light source. The preparation of the copolymers was done using a ring opening polymerization. They succeeded in making a

small well on the millimeter scale. Subsequent papers examined the degradation behavior of these materials [24, 25]. While these methods show promise for using SL in biological application to create 3D physical hierarchical structure, there is no easy means by which chemical hierarchical order may be designed.

Cell Patterning Techniques

In order for proper cell function and differentiation in engineered tissues, it is often necessary to grow cells in specific patterns. The importance of cell alignment and pattern is evident when one examines natural tissue structures, and examples are shown below in Figure 1.3

.

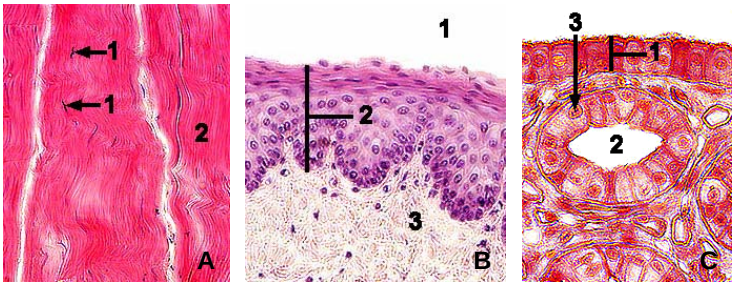

Figure 1.3: Microscope images showing cell patterns in tissues [26]. A) Dense connective tissue from tendon showing 1= fibroblasts nuclei, and 2 = collagen fibers. B) Esophagus section lined with stratified squamous epithelium. 1 = lumen of esophagous, 2 = stratified squamous epithelium, 3= connective tissue. C) Kidney section showing tubules made of simple cuboidal epithelial cells. 1= outer wall, 2= kidney tubules, 3= nucleus of epithelial cell.

There are several methods to pattern cells. Indirect methods first pattern biologically relevant molecules or create a physical topography, and then cells are added to the chemical or physical template. For instance, grooved topographies have been used to

align cells in order to direct the cell function through the cell morphology [27]. This patterning technique uses traditional microfabrication methods of photolithography and plasma etch to etch micron sized grooves into a glass slide, and the cells are grown in the grooves. Another indirect method is to pattern a biomolecule using a microfabricated stamp, for instance, neurons were grown on grids of patterned molecules such as laminin and polylysine [28]. Both of these techniques are useful methods for studying cell behavior, but do not translate well for making larger 3D structures.

In more direct methods of cell patterning, cells are placed directly in the desired physical alignment, as in the before mentioned layer-by-layer methods. Another interesting method of cell patterning involves using thermally responsive polymers [29, 30]. These polymers change conformation with temperature, and can become cell repulsive or cell adhesive. Thus, cells are seeded across this material and then small cooling elements are placed in specific regions. These regions change conformation and the cells in those regions may be washed away and a second cell type may be seeded in their place. While this is more direct type of cell patterning, it again is difficult to translate into a 3D, larger structure.

Another recently developed cell patterning method uses the biological equivalent of a photoresist, referred to as a "bioresist", that can be used to direct cell growth on 2D surfaces [31]. The material used in this work is composed of a copolymer of methyl methacrylate and 3-(t-butoxycarbonyl)-N-vinyl-pyrrolidone (NVP), Figure 1.4.

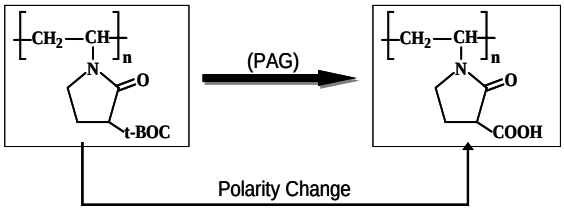

Figure 1.4: Bioresist Chemistry

A photoacid generator (PAG) is incorporated with this polymer, and the mixture may be exposed and developed to generate topographic features, similar to a conventional chemically amplified resist (CAR). By exposing the features and heating the sample, without development in aqueous base, the deprotection reaction occurs and modifies the polymer hydrophilicity, but no topographic pattern is produced. This hydrophilic pattern is capable of directing patterned cell growth [31]. Using these materials to directly fabricate 3D scaffolds is challenging and requires methods analogous to the 2D layer-by-layer assemblies mentioned earlier. However, the use of similar materials with stereolithography could present a more facile route to producing complex, 3D, physically and chemically hierarchically structured scaffolds.

Development of Hierarchical Tissue Scaffolds using Stereolithography

The overall goal of this work is to develop new methods and materials for the fabrication of hierarchically structured, 3D tissue scaffolds. Conventional scaffolds commonly lack substantial mechanical strength, and there is difficulty in controlling porosity, pore distribution, and pore interconnectivity. Additionally, the chemical nature

of these scaffolds is typically homogenous. That is, there is no mechanism for creating additional chemical functionality, distinct from the bulk chemistry, in a specified geometry on the scaffold. The ability to chemically modify selected areas on a scaffold is one method to direct cell growth in deliberate patterns; which is necessary for the engineering of complex, functioning tissues. The general aim of this work is to address these issues through the application of stereolithography (SL) to the fabrication of hierarchically structured tissue engineering scaffolds.

Chemical control requires photopolymerizable materials that can also be selectively chemically modified during the SL part building process. The system under investigation utilizes an acid-catalyzed de-protection event to change the surface chemistry of an SL-made polymer. This method is analogous to conventional chemically amplified photoresists. The chemical modification alters the surface properties, affecting how proteins interact with the surface and thereby affecting how cells interact with the surface. Several cell seeding techniques were explored to find a robust method of patterning cells with photo-resist materials. Protein adsorption has been characterized on various protected and de-protected surfaces using a quartz crystal microbalance with dissipation to demonstrate the capacity of this system to direct protein adsorption, leading to directed cell adhesion. A custom-built SL apparatus was built to facilitate this work, and various test resins were synthesized.

References

[1] *Biomaterials Science: An Introduction to Materials in Medicine*. San Diego: Academic Press, 1996.

[2] "United Network for Organ Sharing", www.transplantliving.org, accessed May, 2004.

[3] W. Leventon, "Synthetic Skin; Can robots, computers, and chip-making techniques save tissue engineering and bring internal organs to market?," in *IEEE Spectrum*, 2002.

[4] P. X. Ma, "Scaffolds for tissue fabrication," *Materials Today (Oxford, United Kingdom)*, vol. 7, pp. 30-40, 2004.

[5] W. W. Minuth, R. Strehl, and K. Schumacker, *Tissue Engineering Essentials for Daily Laboratory Work*. Weinheim: Wiley-VCH Verlag GmbH & Co. KGaA, 2005.

[6] R. A. Brenner, "Burn Survivor Resource Center," http://www.burnsurvivor.com/skin_substitutes.html, 2002, accessed May 2004.

[7] C. H. Corporation, "Cigna HealthCare Coverage Position, Wound Healing: Tissue-Engineered Skin Substitutes and Growth Factors, Coverage Position Number 0068," Cigna HealthCare 5/15/2004, revised 5/15/2007 2007.

[8] D. O. Freytes, S. F. Badylak, T. J. Webster, L. A. Geddes, and A. E. Rundell, "Biaxial strength of multilaminated extracellular matrix scaffolds," *Biomaterials*, vol. 25, pp. 2353-2361, 2004.

[9] T. W. Gilbert, T. L. Sellaro, and S. F. Badylak, "Decellularization of tissues and organs," *Biomaterials*, vol. 27, pp. 3675-3683, 2006.

[10] T. W. Gilbert, D. B. Stolz, F. Biancaniello, A. Simmons-Byrd, and S. F. Badylak, "Production and characterization of ECM powder: implications for tissue engineering applications," *Biomaterials*, vol. 26, pp. 1431-1435, 2005.

[11] S. Badylak, S. Meurling, M. Chen, A. Spievack, and A. Simmons-Byrd, "Resorabable bioscaffold for esophageal repair in a dog model," *J. Pediatr. Surg.*, vol. 35, pp. 1097-1103, 2000.

[12] *Biomaterials in the Design and Reliability of Medical Devices*, 1 ed. Natick, MA: Springer, 2003.

[13] D. F. Williams, "Definitions in Biomaterials. Proceedings of a Consensus Conference of the European Society for Biomaterials," presented at Consensus Conference of the European Society for Biomaterials, Chester, England, 1987.

[14] T. H. Ang, F. S. A. Sultana, D. W. Hutmacher, Y. S. Wong, J. Y. H. Fuh, X. M. Mo, H. T. Loh, E. Burdet, and S. H. Teoh, "Fabrication of 3D chitosan-hydroxyapatite scaffolds using a robotic dispensing system," *Materials Science &*

Engineering, C: Biomimetic and Supramolecular Systems, vol. C20, pp. 35-42, 2002.

[15] G. Vozzi, C. Flaim, A. Ahluwalia, and S. Bhatia, "Fabrication of PLGA scaffolds using soft lithography and microsyringe deposition," *Biomaterials*, vol. 24, pp. 2533-2540, 2003.

[16] J. A. Burdick and K. S. Anseth, "Photoencapsulation of osteoblasts in injectable RGD-modified PEG hydrogels for bone tissue engineering," *Biomaterials*, vol. 23, pp. 4315-4323, 2002.

[17] B. Dhariwala, E. Hunt, and T. Boland, "Photopolymerizable Hydrogels and Stereolithography" *Tissue Engineering*, vol. 10, pp. 1316-1322, 2004.

[18] G. T. M. Chu, G. A. Brady, W. Miao, J. W. Halloran, S. J. Hollister, and D. Brei, "Ceramic SFF by direct and indirect stereolithography," *Materials Research Society Symposium Proceedings*, vol. 542, pp. 119-123, 1999.

[19] M. N. Cooke, J. P. Fisher, D. Dean, C. Rimnac, and A. G. Mikos, "Use of stereolithography to manufacture critical-sized 3D biodegradable scaffolds for bone ingrowth," *Journal of Biomedical Materials Research, Part B: Applied Biomaterials*, vol. 64B, pp. 65-69, 2003.

[20] J. Zeltinger, J. K. Sherwood, D. A. Graham, R. Mueller, and L. G. Griffith, "Effect of pore size and void fraction on cellular adhesion, proliferation, and matrix deposition," *Tissue engineering*, vol. 7, pp. 557-72, 2001.

[21] S. S. Kim, H. Utsunomiya, J. A. Koski, B. M. Wu, M. J. Cima, J. Sohn, K. Mukai, L. G. Griffith, and J. P. Vacanti, "Survival and function of hepatocytes on a novel three-dimensional synthetic biodegradable polymer scaffold with an intrinsic network of channels," *Annals of surgery*, vol. 228, pp. 8-13, 1998.

[22] C. X. F. Lam, X. M. Mo, S. H. Teoh, and D. W. Hutmacher, "Scaffold development using 3D printing with a starch-based polymer," *Materials Science & Engineering, C: Biomimetic and Supramolecular Systems*, vol. C20, pp. 49-56, 2002.

[23] T. Matsuda, M. Mizutani, and S. C. Arnold, "Molecular Design of Photocurable Liquid Biodegradable Copolymers. 1. Synthesis and Photocuring Characteristics," *Macromolecules*, vol. 33, pp. 795-800, 2000.

[24] M. Mizutani and T. Matsuda, "Liquid acrylate-endcapped biodegradable poly(e-caprolactone-co-trimethylene carbonate). II. Computer-aided stereolithographic microacrhitectural surface photoconstructs," *Journal of Biomedical Materials Research*, vol. 62, pp. 395-403, 2002.

[25] M. Mizutani and T. Matsuda, "Liquid acrylate-endcapped biodegradable poly(e-caprolactone-co-trimethylene carbonate). I. Preparation and visible light-induced photocuring characteristics," *Journal of Biomedical Materials Research*, vol. 62, pp. 387-394, 2002.

[26] R. Gillis, "A/P Lab," http://bioweb.uwlax.edu/aplab/, 2002, accessed May 2007.

[27] M. J. Dalby, M. O. Riehle, S. J. Yarwood, C. D. W. Wilkinson, and A. S. G. Curtis, "Nucleus alignment and cell signaling in fibroblasts: response to a micro-grooved topography," *Experimental Cell Research*, vol. 284, pp. 274-282, 2003.

[28] A. K. Vogt, L. Lauer, W. Knoll, and A. Offenhausser, "Micropatterned Substrates for the Growth of Functional Neuronal Networks of Defined Geometry," *Biotechnology Progress*, vol. 19, pp. 1562-1568, 2003.

[29] M. Yamato, C. Konno, M. Utsumi, A. Kikuchi, and T. Okano, "Thermally responsive polymer-grafted surfaces facilitate patterned cell seeding and co-culture," *Biomaterials*, vol. 23, pp. 561-567, 2001.

[30] M. Yamato, O. H. Kwon, M. Hirose, A. Kikuchi, and T. Okano, "Novel patterned cell coculture utilizing thermally responsive grafted polymer surfaces," 2001.

[31] W. He, C. R. Halberstadt, and K. E. Gonsalves, "Lithography application of a novel photoresist for patterning of cells," *Biomaterials*, vol. 25, pp. 2055-2063, 2004.

CHAPTER 2

CYTOCOMPATIBILITY OF PHOTOACID GENERATORS FOR THE FORMULATION OF CYTOCOMPATIBLE PHOTORESISTS

Photolithography is the dominant technology for generating two-dimensional patterns in the microelectronics and microfabrication industries. The need to pattern cells has attracted many researchers to the investigation of photolithography as a means for enabling preferential cell attachment and cell alignment. Most of the work using photolithography for cell patterning has been indirect. That is, photolithography has been used to generate topographical patterns or patterns of important biomolecules, and these cues have then directed cell adhesion. However, it has recently been shown that deprotection-based photoresist chemistries, adapted from chemically amplified photoresists, can be used directly to pattern cells. This new cell patterning strategy has the potential to make significant impacts in a variety of areas including tissue engineering, biosensors, and fundamental cell studies.

For this method of cell patterning to become useful, a cytocompatible, photolithographic material set must be developed. The critical component for deprotection-based lithographic materials is the photoacid generator (PAG). The PAG generates a photoacid via light exposure, which subsequently catalyzes the deprotection reaction of a protected polymer. In this work, NIH3T3 fibroblast cells were plated on poly(hydroxystyrene) (PHOST) surfaces that have been doped with various PAGs. PHOST was selected as the matrix polymer since its chemical structure serves as a well-defined mimic of traditional plasma-treated polystyrene culture substrates. While the

inclusion of certain PAGs was observed to hinder cell adhesion and growth, other PAGs appear to have little negative effect on the fibroblasts. These PAGs, which are the most cytocompatible, are the best candidates to incorporate into material formulations that are intended to pattern cells. Of the PAGs studied in this work, the Ciba 263 PAG [1] was found to be the most cytocompatible.

Introduction

The directed, organized growth of mammalian cells is of extreme interest and importance to many current bioengineering applications. This may include growing cells to be directly integrated into MEMS devices such biosensors [2], creating in vitro neural networks [3], [4], designing cell co-cultures [5, 6], and fabricating engineered tissues and organs [7, 8].

Recently, Gonsalves and co-workers have shown that cells may be patterned directly in two dimensions on biocompatible materials which incorporate a mechanism to locally switch the hydrophilicity of the material surface through pattern-wise exposure to light [9]. Their materials function based on the same basic mechanism as chemically amplified photoresists [10] and thus have been referred to as "bioresists"[9]. In our work, we have explored the extension of this basic idea to other material systems and have found that even conventional photoresist materials, such as tetrahydropyranyl (THP) ether protected poly(hydroxystyrene) (PHOST), may be used in the same fashion to generate cell patterns (Figure 2.1). Inclusion of just a few weight percent of a photoacid generator (PAG) into the THP ether protected PHOST polymer produces a material which can be utilized as a conventional photoresist. Exposure of a film of the material to

ultraviolet light results in generation of photoacid in the exposed areas. This photoacid then catalyzes the deprotection reaction, removing the THP ether group to regenerate the hydroxyl groups on the PHOST (Figure 2.2). This deprotection of the polymer in the exposed areas causes a significant change in the polarity, or hydrophilicity, of the polymer in those areas. This change in polymer polarity can be utilized to form topographic relief patterns in the polymer film by immersing the film in an aqueous alkaline developer solution, as is done in conventional chemically amplified photoresist processing [10]. While such topographic cues can be used to align and pattern cells, our interest is more focused on using local control of material surface chemistry to perform selective cell seeding, alignment, and patterning. Therefore, we have explored the ability to use deprotection reaction-based polymer chemistries to produce materials that can change their polarity and hydrophilicity locally to enable cell patterning without requiring topographical cues. In the case of the THP ether protected PHOST we have shown that this material is capable of locally directing cell adhesion and growth (see Figure 2.1) in a manner similar to what has been described by others for different polymers [9],[11].

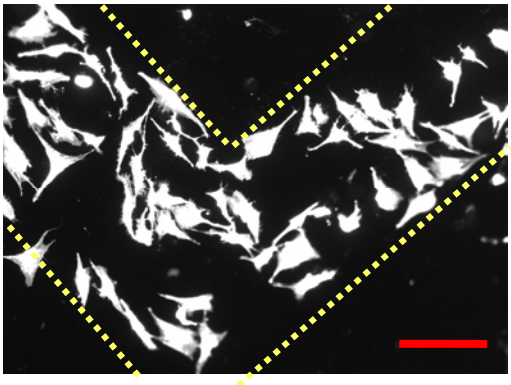

Figure 2.1: Fibroblasts growing in a pattern-wise manner on an exposed, de-protected region, of THP-PHOST. Scale bar = 200 μm.

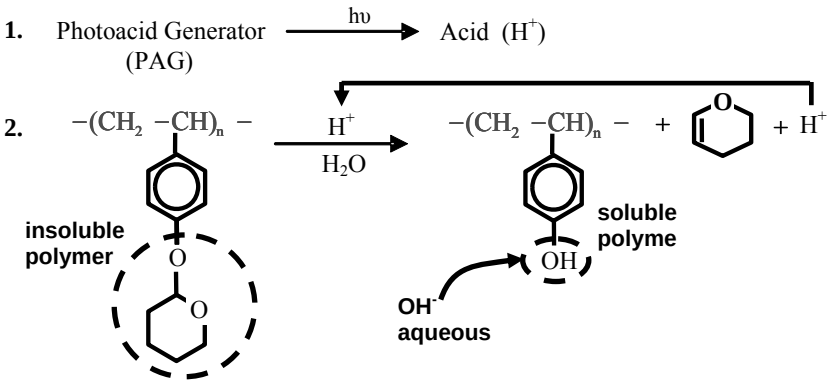

Figure 2.2: Chemically amplified photoresist deprotection reaction of THP protected PHOST.

What is most intriguing about the idea of patterning cells using such deprotection reaction-based chemistry is the ease of the patterning (i.e. requiring only patterned UV exposure) and thus the relatively straightforward manner in which this type of cell patterning may be integrated with other microfabrication processes. One critical aspect of this approach is the potential cytocompatibility problems that may arise with the use of such lithographic material chemistries. The most obvious and immediate concern is the compatibility of the PAGs required for this methodology since they are small molecules which may cross the cell membrane, change the local cell environment, and produce a toxic reaction. For this reason, the work presented in this paper is focused on studying PAG cytocompatibility in order to identify suitable PAG material choices for further cell patterning work and to potentially develop guidelines for future material choices. In this work, a new method for evaluating the cytocompatibility of the PAG materials was developed which is based on culturing cells on polymer films doped with the PAG of interest. This method was adopted to more closely mimic the real end use conditions of

the PAG materials and their method of presentation to cells. Several photoinitiators were also included in this study so that comparisons could be made using the toxicity results generated by methods in this work to previous photoinitiator toxicity experiments which were performed using different methodologies and conditions [12, 13].

Materials and Methods

Materials

Polyhydroxystyrene (PHOST) was obtained from TriQuest, LP. Propylene glycol methyl ether acetate (PGMEA, 99%) was purchased from Aldrich. The Irgacure 651 and 2959 photoinitiators and the 263, 268, 1311, 1325 and 1397 photoacid generators were obtained from Ciba [1]. The triphenylsulfonium triflate (TPS) photoacid generator was purchased from Aldrich. Circular 22 mm Corning brand glass coverslips were used as substrates on which the doped polymer films were cast. Hexamethyldisilazane (HMDS) was purchased from Aldrich and used as a surface priming agent for the glass substrates before polymer film coating. Cell growth studies were performed in Corning six well ultra low attachment plates. Trypsin and Dulbecco's Minimum Essentials medium (DMEM, Cellgro 10-013-CM) were obtained from Cellgro, and bovine calf serum was purchased from Hyclone.

Polyhydroxystyrene coated surfaces

Solid PHOST was dissolved in PGMEA at a concentration of 10% PHOST by weight with respect to the total solution. Glass coverslips were placed on a 130^{o}C hotplate to dehydrate the surface. HMDS was then spin coated onto the glass at 5000

rpm for 6 seconds, and the coverslips were again placed on the 130°C hotplate to vaporize any un-reacted material. This HMDS priming step produces a surface which is terminated with methyl groups, and thus produces good coatings when spin casting using organic solutions. The HMDS prime step is necessary for producing films that adhere well to glass when immersed in aqueous cell culture conditions for at least 72 hours. PHOST solutions were then spin coated onto the glass coverslips by ramping to 2000 rpm at a rate of 100 rpm/sec and holding at 2000 rpm for 40 seconds. Finally, the coated coverslips were baked at 130°C for 3 minutes to remove residual casting solvent.

Photoinitiators and PAGs

For each sample containing a photoinitiator or PAG, the initiator or PAG was dissolved in the PHOST solution at 2% by weight with respect to PHOST. We chose to do a constant loading by weight percent in order to be analogous to previous studies of photoinitiators, as that is the traditional method by which photoactive preparations are made [12, 13]. Coincidentally, for the PAG molecules studied in this work, the weight percent correlates closely to the molar loading of the amount of photoacid generated from the PAG for many of the PAGs studied as the molecular weights of the compounds are similar (shown in Table 2.1). Also, while the large 263 and 268 PAGs are about twice the mass of the smaller PAG molecules, they also generate two photoacids per molecule. In this way, the mass loading percent was held constant as in prior studies, and the molar amount of acid produced in each sample also remained comparable. However, to fully examine the toxicity from the point of view of equivalent initial molar loadings of PAG, samples were also prepared with a constant molar PAG loading of 1.75×10^{-5} moles per 3 grams of 10 wt% PHOST solution. The large PAGs which produce two photoacids per

molecule were loaded at half of this molar concentration since this would be the equivalent formulation in terms of practical use for these materials. The initiators and PAGs used in this study are summarized in Table 2.1.

UV Exposure

Every sample was exposed to 1000 mJ of unfiltered UV light from a mercury arc lamp source. This large exposure dose was used to ensure that all of the photoinitiator or PAG was decomposed into its radical or acid form. After exposure, the samples were baked at 130^{o}C for 90 seconds, to simulate a typical post-exposure bake. The samples were then kept in a biological fume hood, under the UV sterilization light, to ensure that the samples were sterile and ready for cell plating. As we used UV light for sterilization, it was not possible to prepare unexposed samples in this same manner. Other means of sterilization, such as immersion in 70% ethanol and autoclaving, were tried without success. The ethanol was aggressive towards the PHOST films; promoting the films to delaminate from the glass surface. The autoclave process also degraded some of the films, producing samples that had a bubbly appearance under the light microscope.

Table 2.1: Photoinitiators and Photoacid Generators examined in the toxicity study

Name (Supplier)	Effective Wavelength	Molecular Mass	Structure
Irgacure 2959 (Ciba)	365 nm photoinitiator	224.2566 g/mol	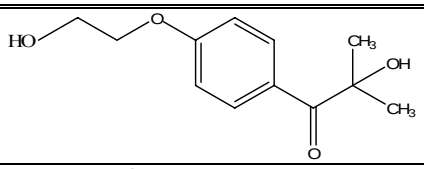
Irgacure 651 (Ciba)	365 nm photoinitiator	256.3012 g/mol	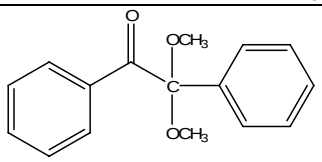
CGI 263 (Ciba)	248 nm photoacid generator	662.6284 g/mol	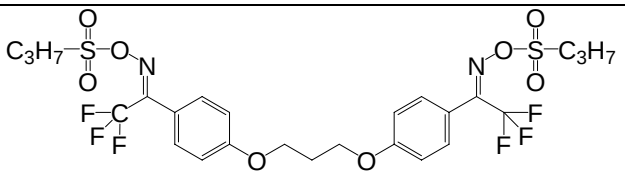
CGI 268 (Ciba)	248 nm photoacid generator	758.7164 g/mol	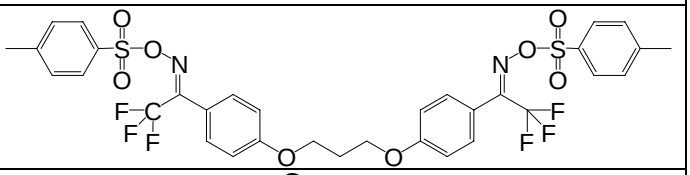
CGI 1311 (Ciba)	365/248 nm photoacid generator	396.4907 g/mol	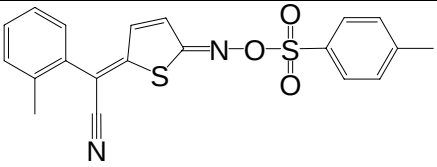
CGI 1325 (Ciba)	365/248 nm photoacid generator	418.5727 g/mol	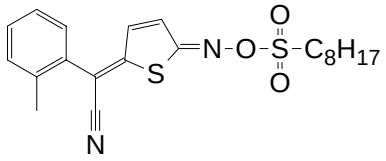
CGI 1397 (Ciba)	365/248 nm photoacid generator	348.4467 g/mol	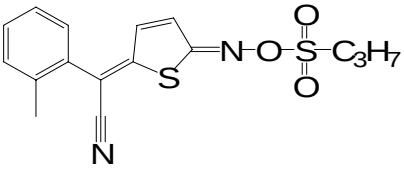
Triphenyl-sulfonium Triflate (TPS-T) (Aldrich)	248 nm photoacid generator	412.4535 g/mol	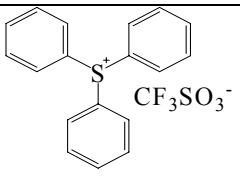

Cell Culture

NIH3T3 fibroblasts were cultured in Dulbecco's Minimum Essentials medium (DMEM, Cellgro 10-013-CM) supplemented with 10% bovine calf serum (BCS, Hyclone) and 1% Antibiotic-Antimycotic Solution (Cellgro 30-004-CL). Fibroblasts were grown up in tissue cultured polystyrene dishes from P2 frozen stock until they reached approximately 80% confluency, and the cells used for in this work varied from P4 to P10. [14]. The subconfluent fibroblast monolayers were dissociated from the culture dish using Trypsin EDTA 1x (0.05% Trypsin/0.53mM EDTA in HBSS, Cellgro 30-004-CL) and were resuspended in fresh media at a concentration of 24×10^4 cells/ml. During re-suspension and cell plating, cell samples were always vigorously siphoned up and down in the pipette to ensure cells were not aggregated.

Cell Plating for 24 Hour Attachment Study

During the entire plating procedure all samples were maintained in a UV light-free environment. Ultra-low attachment six well polystyrene plates (Corning 3471) were used to isolate each sample, allowing cells to only adhere to the sample surface. Samples were presoaked in Dulbecco's phosphate buffered saline (DPBS) w/ Mg^{2+} and Ca^{2+} (Cellgro 21-030-CM) for 5 minutes. The DPBS was removed and 18×10^4 cells in 3.75 ml of culture media were added to each well. This was done by adding 0.75 ml of the 24×10^4 cells/ml suspension to 3 ml of fresh media in each well. The 3 ml of media were added first to each sample well so that the glass coverslips were soaked in media, and then the cell suspension was added. The samples were placed in an incubator at 37^oC and 5% CO_2 for 24 hours to allow for cell adhesion and spreading across the sample surface.

Imaging for 24 hour cell attachment study

Live cell staining solution was prepared by adding 10 μl of Calcein AM (1mM in DMSO, Molecular Probes) to 10 ml of dPBS w/ Ca^{2+} & Mg^{2+}. Samples were rinsed 3 times in DPBS w/ Ca^{2+} & Mg^{2+} to remove all plating media and unattached cells. Samples were then incubated at 37°C and 5% CO_2 for 45 minutes in 1ml of live cell staining solution. After incubation, the samples were rinsed once with DPBS w/ Ca^{2+} & Mg^{2+} to remove the staining solution and then each sample was imaged using fluorescent microscopy. Five regions (center, left, right, top, and bottom) of each sample were imaged with a 10x objective (1.2 mm x 0.9 mm). The number of cells were counted in each section, and analyzed for the mean and standard deviation.

Cell Plating for 72 hour cell proliferation study

The cell plating procedure was identical to the attachment study except the initial plating concentration was lower. Each well was plated with 9×10^4 cells in 3 ml of fibroblast growth media. The cells were then placed in the incubator and allowed to adhere to the surface for 24 hours. The original cell growth media was removed and replaced with fresh media after 24 hours to remove any dead or non-attached cells. This left a surface with only attached cells that were allowed to grow for an additional 48 hours, making an overall incubation period of 72 hours.

Imaging and analysis for 72 hour cell proliferation study

Imaging for the cell proliferation study was performed using light phase microscopy at periodic time intervals during the study since a staining procedure could cause long term toxicity. Images of each sample were taken at three time points: 24 hours, 48 hours, and 72 hours. At each time point one 4x image was taken of the center

of each sample as well as five 10x images (center, top, bottom, right, and left regions of each sample). The 4x picture (2.2 mm x 1.65 mm) was used to qualitatively analyze cell aggregation across the sample as well as to observe cell proliferation over time. The 10x pictures (0.825 mm x 0.62) were counted to determine the average cell count and standard deviation of the number of cells present on each sample surface. Pairwise comparisons were made for all samples using the Student t-test. Significant differences are noted on the plots for pairs with a t-probability < 0.05.

Results and Discussion

This study was originally motivated by the finding that traditional chemically amplified photoresist materials, which rely on an acid catalyzed polymer deprotection mechanism, may be used for cell patterning. The main goals of the work were to determine which PAGs are suitable for formulating lithographic materials used for applications involving cell patterning, and to establish general guidelines for choosing cytocompatible PAGs.

PHOST was chosen as a model matrix polymer material for use as a cell growth substrate, as it is chemically similar, in principle, to tissue culture treated polystyrene. Dissolving the polymer in organic solvent allows for the addition of PAGs and initiators directly to the PHOST matrix, and also permits the use of spin coating to create a thin polymer layer on glass cover slips. The use of glass cover slips provides for simple cell imaging using optical microscopy.

Cell attachment- 24 hour study

First, it was important to establish that this method of measuring cytocompatibility would give comparable results to previous cytocompatibility studies. Earlier studies have shown cytocompatibility trends with radical photoinitiators used for cell immobilization in hydrogel matrices [12, 13]. The authors of these previous works have shown that the Irgacure 651 initiator is highly toxic to fibroblasts, and that the Irgacure 2959 was the most cell-friendly [12, 13]. We have also included these initiators in our study, to show that a similar trend is observed. It is important to note that this work was performed in a different manner than the previous studies. In our experiments, the fibroblasts were grown on a polymer surface which had been doped with the initiator or PAG under investigation. The previous papers examined cells grown with initiators dissolved directly in the cell growth media. There are two main reasons for adopting this new strategy: (1) the incorporation of the PAGs into a solid polymer matrix better mimics their desired use in our applications and (2) many of the common photoacid generators are insoluble or sparingly soluble in aqueous solutions.

The results of this experiment show that the CGI 263 and 268 PAGs were the best suited for cell growth, in both the case of constant mass and mole loading (Figure 2.3). The 26X series of PAGs are non-ionic and relatively large and bulky; and thus also produce large bulky photoproducts. We hypothesize that these characteristics hinder their transport through the cell membrane, thereby reducing their toxicity. Also, one may note that the 26X series PAGs differ from the 13XX series PAGs only in the non-acid photo-product. This may suggest that it is actually the portion of the molecule that does not generate an acid which has the greater effect on cell growth. It may be that the large

non-acid photoproducts of the 26X series are more difficult to transport across the cell membrane than the smaller photoproducts from the 13XX series. To further test these results, samples with constant molar loading were examined for the 2959, 651, 263, and TPS conditions. These give very comparable results, which is not surprising as the molar and mass loadings are not widely dissimilar. The data in Figure 2.3 are presented in relative cell number, which is the number of cells on a particular surface divided by the number on the PHOST control surface for that six well dish. Relative cell number is used so that results obtained under slightly different conditions (different days, different dishes, slightly different cell seeding densities) may be compared.

It should be noted that unexposed samples were also prepared and plated without the UV exposure and there was no significant difference between the plain PHOST control material and those samples that contained initiators or PAGs (data is not shown). However, all of these samples, including the PHOST control, had significantly lower numbers of cells than the exposed samples, possibly due to the lack of a sterilization step.

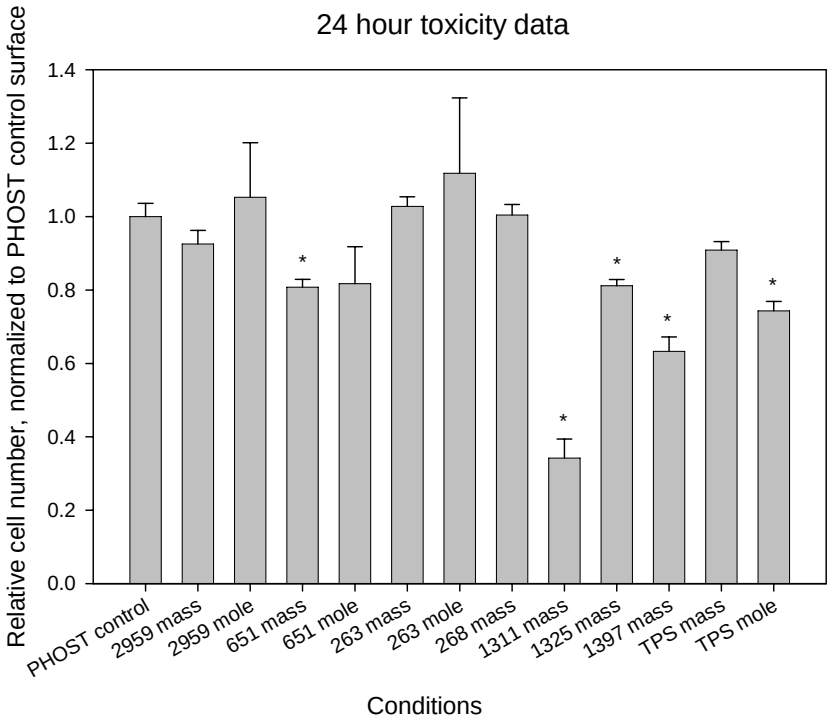

Figure 2.3: 24 hour study of PAG cytocompatibility with NIH/3T3 fibroblast. Constant weight and molar loadings are shown, designated by "mass" and "mole" respectively. Relative survival is the number of cells counted on a particular surface divided by the number of cells counted on the plain PHOST control surface. The error bars represent 95% confidence. Conditions that are significantly different from control PHOST (t probability < 0.05 on Student t-test) are marked with an asterisk (*).

The repeatability of this experiment was also examined to evaluate the usefulness of this type of toxicity study for new materials. The Irgacure 651 initiator and the Ciba 263 PAG were run in two separate experiments. As observed in Figure 2.4, the two runs give very comparable results, lending confidence to the repeated use of this experimental assay to test for the cytocompatibility of potential PAGs and initiators.

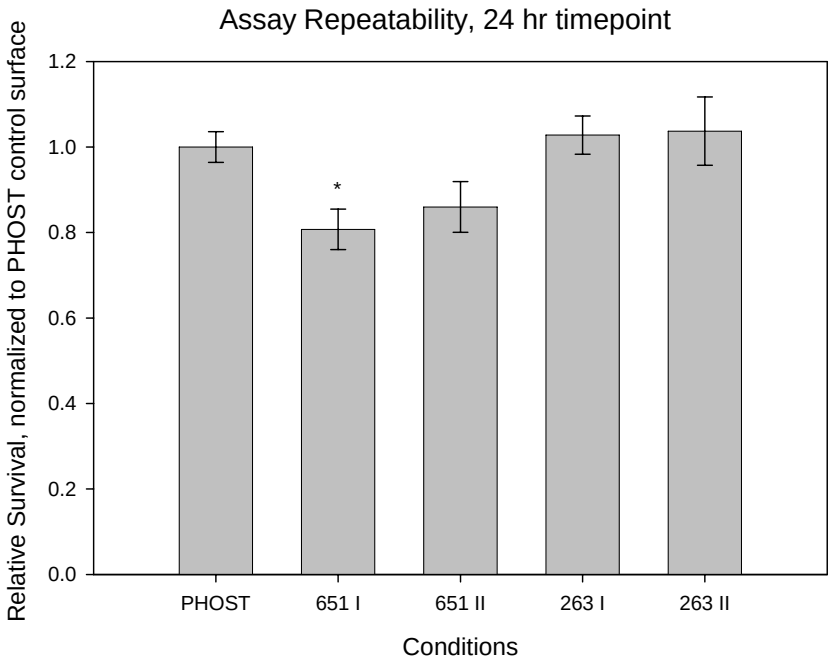

Figure 2.4: Repeatability of cytotoxicity assay of culturing cells on doped polymer substrates. Relative survival is the number of cells counted on a particular surface divided by the number of cells counted on the plain PHOST control surface. Error bars represent 95% confidence. Conditions that are significantly different from control PHOST (t probability < 0.05 on Student t-test) are marked with an asterisk (*).

It should be noted that the worst performer in the 24 hour study was the CGI 1311 PAG (Figure 2.3). While there was a very low number of live cells adhered to the surface after 24 hours, a very high standard deviation was also observed for this sample. This high standard deviation is a reflection of the "patchiness" that is observed during the initial cell plating. The cells tend to cluster together, and do not adhere evenly across the surface. This is evident in Figure 2.5 where a comparison is shown of three conditions: the plain PHOST substrate, the CGI 263 doped substrate, and the CGI 1311 substrate. As one may see, the cells on both the PHOST and CGI 263 materials are evenly spaced across the surface; whereas in the CGI 1311 sample the cells cluster together in only a

few regions. For this reason, there are some microscope images which show very few cells, and other images which look more comparable to the control substrate. This leads to a high standard deviation for the cell count numbers, and a larger range for the 95% confidence interval. The reasons for this patchiness in the cell plating in the CGI 1311 sample are not well understood at this time, but such non-uniform plating and growth behavior is likely to be undesirable.

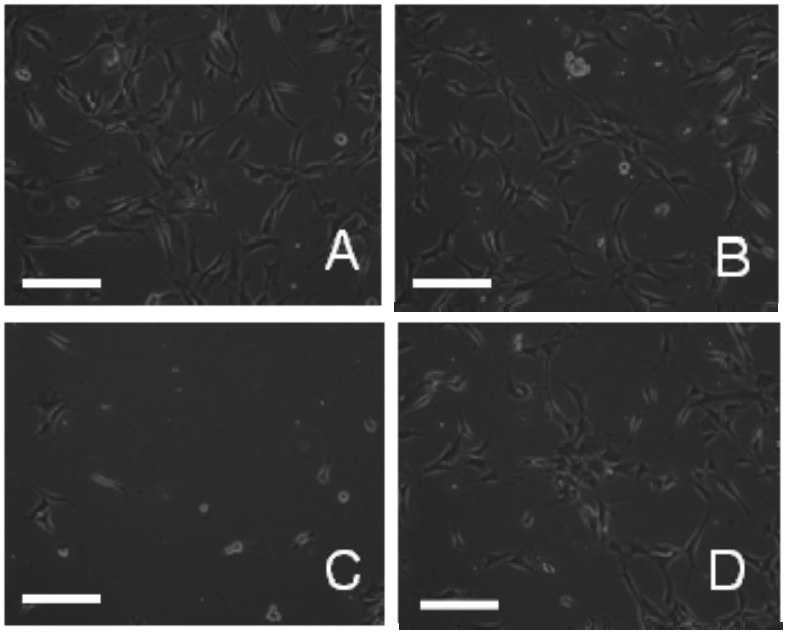

Figure 2.5: Comparison of cell growth on various substrates: (A) PHOST control with no PAG or initiator, (B) PHOST with Ciba 263 PAG, (C&D) 2 regions from PHOST with Ciba 1311 PAG. Scale bar = 0.2 mm.

Cell proliferation- 72 hour study

From the 24 hour study, we can identify substrates that are initially less cytotoxic to the fibroblasts. However, we would like to know how the cells will behave over time.

Thus, the purpose of this set of experiments was to observe how cells grow and proliferate on these different materials over a longer time period. The study was run under constant mass loading conditions to be consistent with previous studies, and the standard methods of formulating photoactive materials. The observation was stopped after 72 hours because the cells had grown to confluency. In a post-confluent culture, fibroblasts tend to grow on top of each other. This causes large sheets of cells to peel off all of the samples, and makes accurate quantification of cell numbers by microscopy impossible.

It is evident from Figure 2.6 that both the CGI 263 and Irgacure 2959 behave quite similarly to the PHOST control over the entire period; supporting our statement that these are the least cytotoxic PAG and initiator studied. It is also interesting to note that while CGI 1311 and TPS conditions had low, non-uniform initial cell attachment, the cells were able to recover significantly over the 72 hour period. The Irgacure 651 is the only initiator or PAG which continually hindered cell growth over the entire 72 hour study. When the data are plotted together as in Figure 2.7, it becomes quite apparent that the Irgacure 651 is the one compound that stands apart from the rest. The two trendlines presented in Figure 2.7 are exponential curve fits for the PHOST control data and Irgacure 651 data. While both curve fits are good, with R^2 values greater than 0.95, it is clear that the Irgacure 651 samples are not exhibiting the rapid exponential growth phase that is expected of a growing and dividing cell culture.

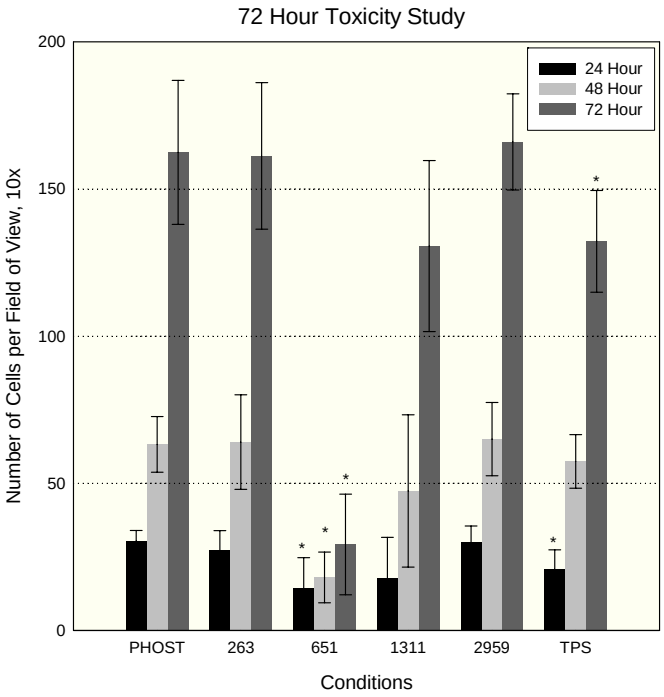

Figure 2.6: Toxicity results over a 72 hour period for constant mass loading. Error bars represent 95% confidence. Conditions that are significantly different from control PHOST (t probability < 0.05 on Student t-test) are marked with an asterisk (*).

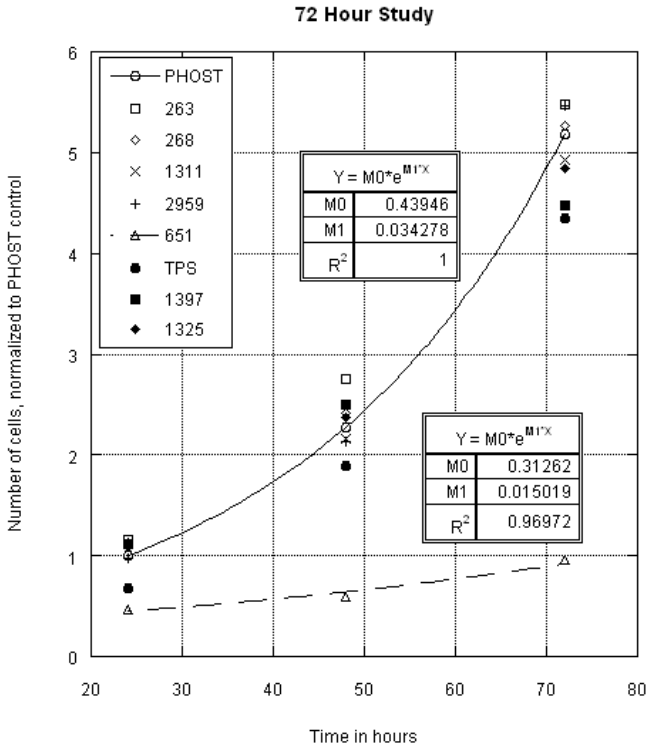

Figure 2.7: 72 hour toxicity data shown with cell number versus time. Trendlines are shown for the PHOST and 651 data sets.

Conclusions

It is significant to note that the most suitable PAGs, from a cytocompatibilty standpoint, are the Ciba CGI 263 and 268. These PAGs have several features which may account for their relatively benign behavior. They are large, non-ionic molecules that generate large non-acid photoproducts. We hypothesize that these characteristics hinder their transport across the cell membrane, reducing their toxicity.

While the CGI 263 and 268 PAGs are the best recommendations, several other PAGs show promise if initial cell uniformity is not important. The CGI 1311 and TPS PAGs both had lower initial cell numbers due to patchy cell seeding, but the cells in those dishes were able to recover in a 72 hour time period. Thus, for applications where it is only important for cells to grow to confluency, these other PAGs may be considered. However, if initial seeding uniformity is critical, the 26X PAGs are shown to be the best choice. The only condition which exhibited long-term toxicity and suppression of cell growth was the PHOST substrate doped with the Irgacure 651 initiator. This matches well with previous work done on photoinitiator toxicity [12], [13], lending credibility to this new method of evaluating the cytotoxicity of photo-active molecules.

It is interesting to note that the toxicity effect of the photoinitiators and PAGs seemed to be exhibited by a lack of initial adherence to the surface. That is, for the 651, TPS and 1311 samples, the initial number of adhered cells was reduced at 24 hours. However, for the TPS and 1311 PAG conditions, the cell number was able to recover over the 72 hour period; whereas the number of viable cells in the 651 photoinitiator condition remained quite low. This may suggest that: there are distinct different toxicity mechanisms for the different PAGs and photoinitiators, that the diffusion of the PAGs

and initiators through the polymer to the cells or their leaching into solution differ, or that the inherent level of toxicity exhibited by the other PAGs is not as great as the 651 initiator.

References

[1] "Photoacid Generators for Microlithography," Ciba Specialty Chemicals 2003.

[2] Y. Lei, P. Mulchandani, W. Chen, J. Wang, and A. Mulchandani, "Whole Cell-Enzyme Hybrid Amperometric Biosensor for Direct Determination of Organophosphorous Nerve Agents With p-Nitrophenyl Substituent," *Biotechnology and Bioengineering*, vol. 85, pp. 706-713, 2004.

[3] S. Tatic-Lucic, Y.-C. Tai, and J. A. Wright, "Silicon-Micromachined Neurochips for In Vitro Studies of Cultured Neural Networks," *Internaltional Conference on Solid-State Sensors and Actuators: Transducers '93*, pp. 943-946, 1993.

[4] M. Jungblut, C. Schwind, W. Knoll, K. Graf, and C. Thielemann, "Micropatterned neural nets on different solid surfaces," *European Cells and Materials*, vol. 6, pp. 48, 2003.

[5] S. N. Bhatia, U. J. Balis, M. L. Yarmush, and M. Toner, "Microfabrication of Hepatocyte/Fibroblast Co-cultures: Role of Homotypic Cell Interactions," *Biotechnology Progress*, vol. 14, pp. 378-387, 1998.

[6] I.-K. Kang, G. J. Kim, O. H. Kwon, and Y. Ito, "Co-culture of hepatocytes and fibroblasts by micropatterned immobilization of b-galactose derivatives," *Biomaterials*, vol. 25, pp. 4225-4232, 2004.

[7] T. Takezawa, "A strategy for the development of tissue engineering scaffolds that regulate cell behavior," *Biomaterials*, vol. 24, pp. 2267-2275, 2003.

[8] P. X. Ma, "Scaffolds for tissue fabrication," *Materials Today (Oxford, United Kingdom)*, vol. 7, pp. 30-40, 2004.

[9] W. He, C. R. Halberstadt, and K. E. Gonsalves, "Lithography application of a novel photoresist for patterning of cells," *Biomaterials*, vol. 25, pp. 2055-2063, 2004.

[10] L. F. Thompson, C. G. Willson, and M. J. Bowden, *Introduction to Microlithography*. Washington DC: American Chemical Society, 1994.

[11] D. V. Nicolau, T. Taguchi, H. Tanigawa, and S. Yoshikawa, "Control of the neuronal cell attachment by functionality manipulation of diazo-naphtho-quinone/novolak photoresist surface," *Biosensors & Bioelectronics*, vol. 11, pp. 1237-1252, 1996.

[12] S. J. Bryant, C. R. Nuttelman, and K. S. Anseth, "Cytocompatibility of UV and visible light photoinitiating systems on cultured NIH/3T3 fibroblasts in vitro," *Journal of Biomaterials Science, Polymer Edition*, vol. 11, pp. 439-457, 2000.

[13] C. G. Williams, A. N. Malik, T. K. Kim, P. N. Manson, and J. H. Elisseeff, "Variable cytocompatibility of six cell lines with photoinitiators used for polymerizing hydrogels and cell encapsulation," *Biomaterials*, pp. 1211-1218, 2005.

[14] "Cryogenic Preservation of Animal Cells," American Type Culture Collection, Manassas, VA No. 3, 2001.

CHAPTER 3

CELL SEEDING METHODS FOR CELL PATTERNING ON CHEMICALLY AMPLIFIED MATERIALS

Introduction

Directing cells to grow in particular patterns has application for many research areas, such as tissue engineering, cell-based biosensors, and fundamental cell studies. Not only is it important to specify the location where cells should grow, it may also be necessary to direct the cells to grow in specific orientations or geometries.

Currently, the most prevalent method is to first generate patterns of cell adhesive or repulsive molecules onto a surface, and then seed cells on this material. This may be done by methods such as micro-molding [1], stamping [2], and microfluidic systems [3]. While these techniques are successful in making the patterned cell cultures, they all require lengthy fabrication processes to first make the mold or stamp, using standard photolithographic methods, followed by the process to actually pattern the molecules of interest.

Photolithography is the industry standard for making patterns in microelectronics and microfabrication. The key component to modern photolithography is the chemically amplified resist (CAR). A positive tone resist contains a polymer with an acid-labile protecting group, and a photoacid generator (PAG). When the CAR is exposed to light, the PAG produces an acid molecule, which can catalyze the de-protection of the polymer, as seen in Figure 3.1.

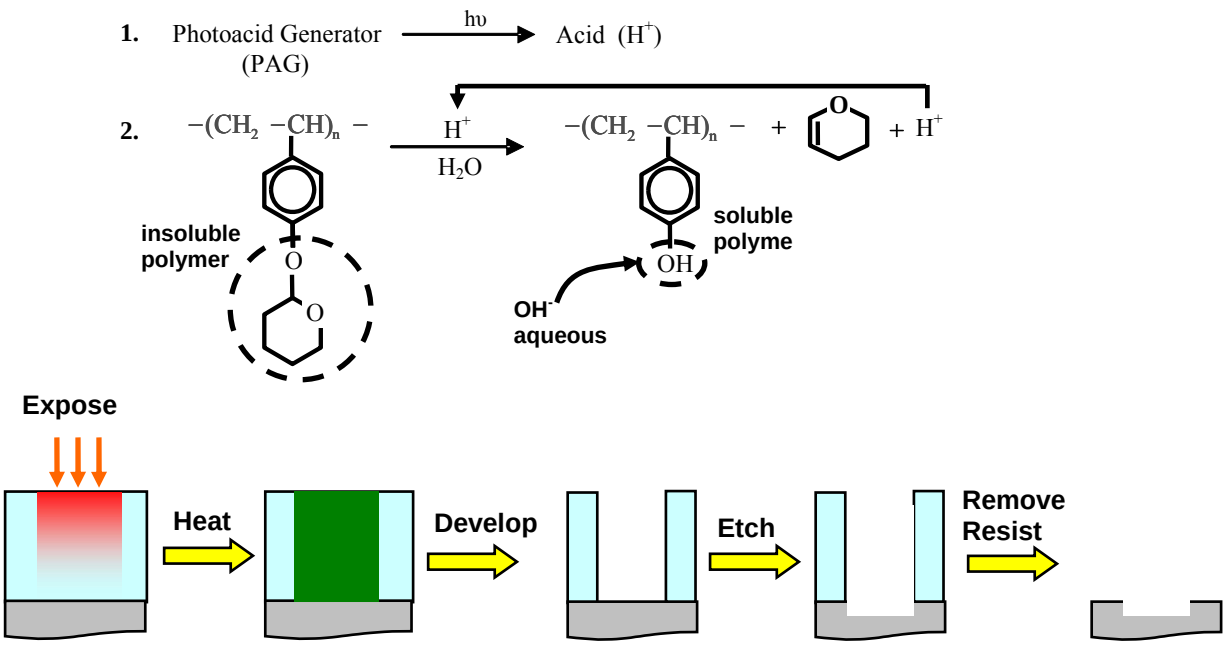

Figure 3.1: Chemically amplified resist process

The de-protection reaction switches the hydrophilicity of the polymer, changing its solubility. In traditional microfabrication strategies, this change in solubility is exploited to make topographical patterns through subsequent development and etch steps.

Photolithography is often used indirectly to pattern cells, as it is part of standard microfabrication processes. For instance, it is a key component of the micro-molding and stamping methods mentioned above [1, 2]. In addition, several groups have studied using photolithography to define regions of biologically relevant molecules, and then using these molecules to define cell patterns. For example, photolithography was used to define regions of immobilized mouse IgG protein [4], and to generate domains of N-(2-aminoethyl)-3-aminopropyl-trimehtoxysilane (EDS) which were then found to localize the seeding of human bone-derived cells [5].

While lithography seems to be an integral part of many cell patterning techniques, there have been few attempts to directly translate the lithographic patterning method into cell patterns. The earliest paper, by Nicolau et. al., investigated the use of diazo-naphtho-quinone (DNQ)/novolak photoresist systems for the patterning of neuronal cells [6]. This work was not successful and perhaps is the reason further cell patterning work using photoresists was not highly pursued. However, it should be noted that the DNQ/novolak resist system is not a CAR, and does not use an acid catalyzed de-protection reaction to switch its solubility. More recently, the Gonsalves group was successful in demonstrating direct cell patterning using photolithography, through the use of a non-traditional resist material [7]. They synthesized a "bio-resist", combining the chemistry of CARs with a known biocompatible polymer backbone, N-vinyl pyrroliodone (NVP).

The aim of this work is to continue investigations into direct patterning of cells by photolithographic methods using CAR chemistry, and to examine the cell seeding conditions which lead to successful cell patterning. We hypothesize that cells may be patterned with materials used in traditional CARs without the need for specialized biomaterial synthesis, if suitable material characteristics are combined with appropriate cell seeding methods. In particular, we initially postulated that by reducing the amount of cell to cell interactions during the initial period of cell attachment, we may enhance the cell to surface interactions, thus resulting in better recognition of the surface patterns by the cells. The enhancement of the surface pattern recognition would allow us to broaden the spectrum of usable materials for photoresist cell patterning. To test this idea, we seeded cells using serum-free and protein-free media to reduce the concentration of molecules that may facilitate cell interactions. The interesting finding, however, is that

with the proper patterned materials, only an intermediate wash step is needed during seeding to remove weakly attached cells and retain the cells growing in the specified pattern, and regular serum-containing media may be used throughout.

Materials and Methods

Materials

Polytertbutylmethacrylate (PTBMA) was obtained from Aldrich. Propylene glycol methyl ether acetate (PGMEA, 99%), the triphenylsulfonium triflate (TPS) photoacid generator, and poly(tert-butyl methacrylate) were purchased from Aldrich. Circular 22 mm Corning brand glass coverslips were used as substrates on which the polymer films were cast. Hexamethyldisilazane (HMDS) was purchased from Aldrich and used as a surface priming agent for the glass and silicon substrates before polymer film coating. Cell growth studies were performed in Corning six well ultra low attachment plates. Trypsin and Dulbecco's Minimum Essentials medium (DMEM, Cellgro 10-013-CM) were obtained from Cellgro, and bovine calf serum was purchased from Hyclone.

Cell culture

NIH3T3 fibroblasts were cultured in Dulbecco's Minimum Essentials medium (DMEM, Cellgro 10-013-CM) supplemented with 10% bovine calf serum (BCS, Hyclone) and 1% Antibiotic-Antimycotic Solution (Cellgro 30-004-CL). Fibroblasts were grown up in tissue cultured polystyrene dishes from P2 frozen stock until they reached approximately 80% confluency, and the cells used for in this work varied from

P4 to P10. [8]. The subconfluent fibroblast monolayers were dissociated from the culture dish using Trypsin EDTA 1x (0.05% Trypsin/0.53mM EDTA in HBSS, Cellgro 30-004-CL) and were resuspended in fresh media. During re-suspension and cell plating, cell samples were always vigorously siphoned up and down in the pipette to ensure cells were not aggregated.

Cell seeding

For all experiments, the patterned substrate was first placed into a cell culture dish under sterile conditions. A small amount of liquid (media, serum-free media or Cellgro Free) was placed into the well to cover the substrate. Then the appropriate amount of cell suspension was added. The dishes were swirled slightly by hand to distribute the cells and media evenly over the surface, and then placed into an incubator at 37^{o}C, with no further agitation.

Cell seeding in serum-containing growth media

After cells were dissociated from the culture dish and re-suspended in media, the cell suspension was counted. The appropriate dilution was made to make a final cell suspension of 15 x 10^4 cells/ml.

For some experimental groups a wash step was used after one hour of incubation at 37^{o}C. These samples were removed from the incubator after one hour, rinsed three times with DPBS with calcium and magnesium, and then fresh serum-containing growth media was placed into the culture well.

Cell seeding in serum-free growth media

After cells were dissociated from the culture dish and re-suspended in media, the cell suspension was centrifuged at 1500 rpm for 5 minutes. The media was carefully removed, leaving the cell pellet. The cells were then re-suspended in DMEM without serum. The cells were counted and the appropriate dilution was made to make a final cell suspension of 15 x 10^4 cells/ml in DMEM without serum.

After one hour of incubation at 37^{o}C, the samples were removed from the incubator, and the DMEM was carefully removed via suction pipet and replaced with fresh serum-containing growth media.

Cell seeding in protein-free media

After cells were dissociated from the culture dish and re-suspended in media, the cell suspension was centrifuged at 1500 rpm for 5 minutes. The media was carefully removed, leaving the cell pellet. The cells were then re-suspended in Cellgro Free media, which does not contain proteins. The cells were counted and the appropriate dilution was made to make a final cell suspension of 15 x 10^4 cells/ml in Cellgro Free.

After one hour of incubation at 37^{o}C, the samples were removed from the incubator, and the Cellgro Free was carefully removed via suction pipet and replaced with fresh serum-containing growth media.

HMDS surface treatment for improved polymer adhesion

Two types of substrates were used for making patterned polymer samples: circular glass cover slips and small silicon pieces about 2 cm x 2 cm. To enhance the adhesion of the polymer to these substrates, they were pre-treated with HMDS. The HMDS was either applied directly to the substrate in liquid form, or through a vapor

deposition process. When applied as a liquid, the HMDS was pipetted onto the substrate, and then the sample was spun at 4000 rpm to remove the excess HMDS. For vapor deposition, the samples were placed under vacuum, and the HMDS vapor was introduced using a stream of nitrogen as the carrier gas. The method of HMDS application did not affect the cell study results, and this surface was never in contact with the cell growth environment.

Preparation of patterned polymer samples on silicon and glass

For individual patterning samples, the PTBMA solution was spun on at 2000 rpm with a 100 rpm/sec ramp rate for 40 seconds. The samples were then soft baked at 120^{o}C for 90 seconds. The samples were then placed under a UV exposure lamp and exposed to 248 nm light through a chrome-on-quartz mask. The samples were then post-exposure baked at 180^{o}C for 3 minutes to fully catalyze the de-protection reaction.

Preparation of patterned polymer surfaces for dose array on whole wafer

The dose arrays were performed on whole 4 inch wafers. The photo-responsive PTBMA solution was spun on the wafer in the same manner as for the patterned polymer samples; 2000 rpm, with a 100 rpm ramp rate, for 40 seconds. The wafer was soft baked at 120^{o}C for 90 seconds. The wafer was then placed under the 248 nm exposure lamp on a moveable stage, under a small square opening of 1 cm x 1 cm. The stage stepped the wafer in a serpentine pattern, and at each stopping point the shutter was opened for a specified amount of time, resulting in a patterned wafer consisting of 1cm x 1 cm squares of various exposure doses. After all of the areas were exposed, the wafer was post-exposure baked at 180^{o}C for 3 minutes.

Results and Discussion

Cell seeding techniques experiments

For each of the cell seeding techniques, cells were plated onto patterned substrates and allowed to grow for 24 hours. The samples were observed and evaluated for pattern fidelity using phase contrast microscopy and fluorescent microscopy with the live/dead stain, and a summary of the qualitative results is given in Table 3.1.

Table 3.1: Summary of cell patterning results for each cell plating condition

	Condition 1 (serum, no wash)	Condition 2 (serum, wash)	Condition 3 (serum-free)	Condition 4 (protein-free)
Cell patterning	Yes- lower quality	Yes	Sometimes	Sometimes

The qualitative analysis for cell patterning was simply determined by viewing the samples to observe whether cells grew only in the exposed patterns (Figure 3.2). The best cell patterns were obtained using seeding condition 2. When conditions 3 and 4 yielded patterns, the patterns were comparable to those in condition 2, although the seeding was usually not as even. However, when the cells were seeded without serum or protein, they were not well attached to the surface. As a result, these samples frequently resulted in very few cells left on the surface.

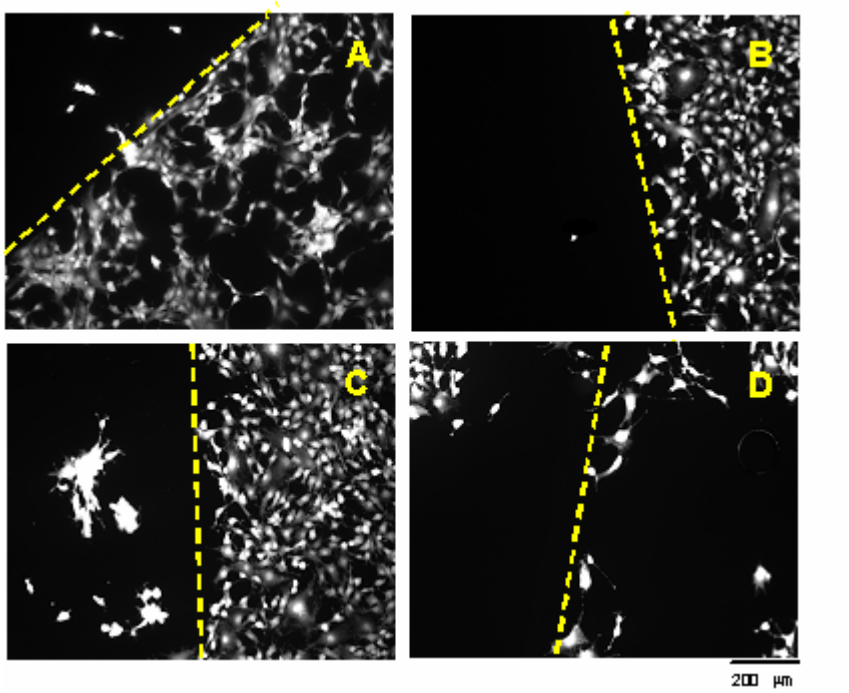

Figure 3.2: Fluorescent microscopy with cells stained live. The yellow lines guide the eye to the boundary between protected and de-protected regions of the polymer. All de-protected regions are on the right side of the yellow lines. A) Serum seeding, very patchy cell adherence with cells extending beyond the surface patterns. B) Serum seeding with wash step, cells seeded evenly across patterned surface with one of the few cells outside of the patterned area. C) Serum-free DMEM seeding with media replacement, cells seeded mostly in the patterned area, but several areas of cells extending outside of the patterned area. D) Cellgro-free seeding with media replacement, very few adherent cells and cells extending outside of the patterned area

To quantify these patterning results, simple 1 cm x 1 cm squares were patterned. Cells were seeded on these samples under the varying conditions. For each sample, five microscope images were taken in and out of the exposed areas. The number of cells in the exposed and unexposed regions was counted, and a ratio of cells in exposed areas to unexposed areas was calculated. The results are shown in the table below (Table 3.2), and it is quite apparent that the best pattern fidelity was obtained under the condition of regular serum containing media with a wash step.

Table 3.2: Average cell numbers and pattern fidelity ratio for each plating condition

Average Number of cells	Media	Media + wash	DMEM	Cellgro Free
Exposed area	280	233	354	191
Unexposed area	12.6	2.8	38.4	17.4
Pattern Fidelity Ratio	23.8	**83.3**	9.2	11

The live/dead stain from Molecular Probes was used to visually determine if the cells in the patterned areas were viable. The pictures below show the same area viewed with red (dead) and green (live) fluorescence (Figure 3.3). These representative pictures show that nearly all of the adhered cells in the patterned areas are indeed alive. The slight red hue is visible only slightly on the background polymer because the exposure time was set to a very long time. One may notice that the cell areas actually show as dark shadows in the picture taken through the red filter, as they are alive. Although few cells are dead, using the dead stain with the long exposure times on the red channel is useful for identifying the patterned regions.

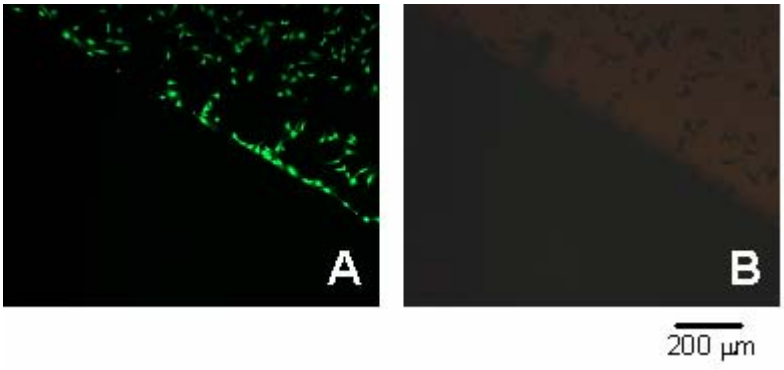

Figure 3.3: Patterned cells stained using live/dead stain. A) Region under green fluorescence, live stain. B) Same region under red fluorescence, dead stain. Notice cells are black, not lit, because they are live. The red stain is very faintly showing the outline of the photo-de-protected region.

Additionally, fluorescent microscopy was used to visualize the cells before and after the wash step. The following pictures (Figure 3.4) show cells with stained nuclei, before and after the wash step, in a similar region on the sample chip. It is observed that most of the remaining cells are those on the exposed, circular regions of the polymer.

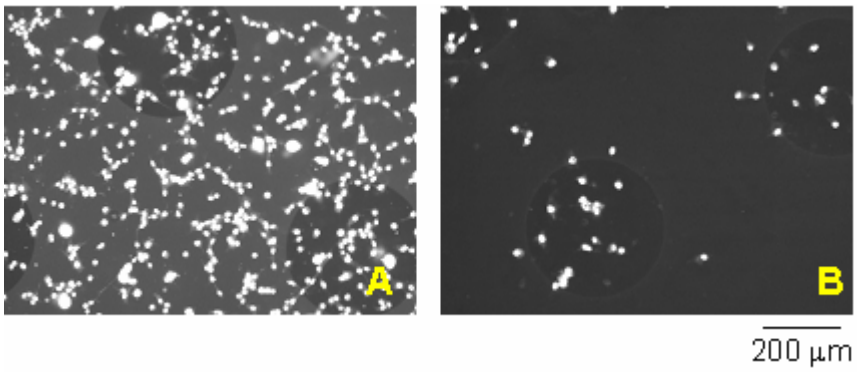

Figure 3.4: Patterned cells stained using nucleus stain. A) Region before wash step. B) Region after wash step.

Pattern stability over time

With the establishment of working cell seeding procedures, experiments were run to determine how stable the cell patterns were over time. PTBMA was patterned and cells were seeded onto the materials using the procedure for condition 2. The samples were allowed to grow over a period of 7 days. During this time, the cells were monitored daily using phase contrast light microscopy. As indicated from the microscope pictures below (Figure 3.5), the cell patterns were maintained over this time period. The experiment was not carried out for longer times as the cells in the patterned regions grew to confluency, and after this point the fibroblasts used in this study begin growing on top of one another and peel of the surface.

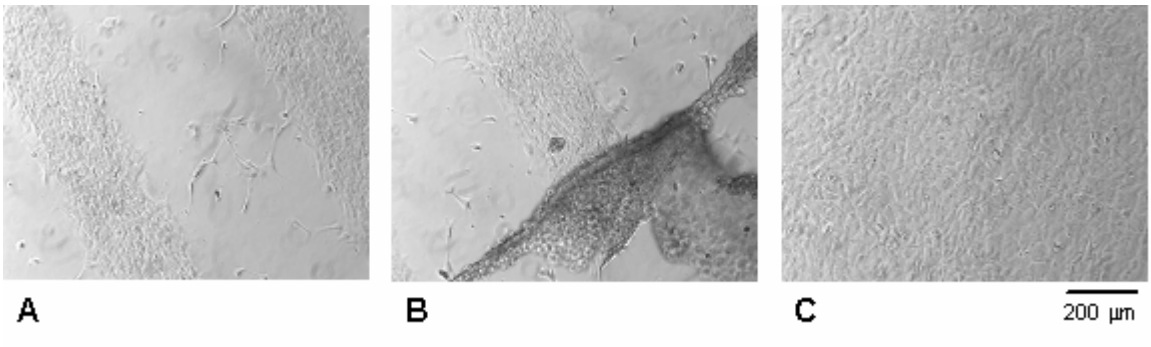

Figure 3.5: Light microscope images of cells growing on patterned surfaces after 7 days. A) Cells maintaining pattern, with few cells starting to bridge un-exposed areas. B) Cells peeling off the surface near a patterned region. C) Cells completely filling exposed region and beginning to grow on top of each other.

Dose array

In order to establish the best exposure conditions for cell patterning, a standard dose array was run on a silicon wafer. The entire wafer was coated with the PTBMA solution, and then small 1 cm x 1 cm regions were exposed to different doses of UV light. The wafer was then seeded with fibroblasts, the cells were stained using the live/dead stain, and the number of live cells in each region was counted (Figure 3.6).

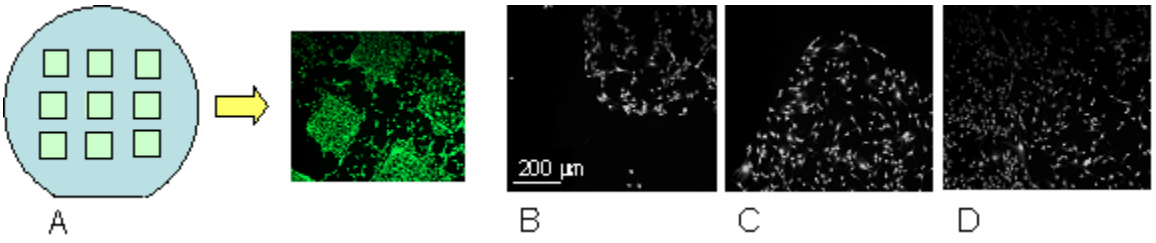

Figure 3.6: A) Picture of dose array translated to cell seeding. B) Fluorescent microscope picture of region from dose array exposed to 3 mJ/cm^2. C) Fluorescent microscope picture of region from dose array exposed to 6 mJ/cm^2. D) Fluorescent microscope picture of region from dose array exposed to 20 mJ/cm^2.

The ratio of the number of cells in each exposed region to the number of cells in the unexposed regions was calculated. This is plotted against the exposure dose, and the optimal dose may be determined (Figure 3.7).

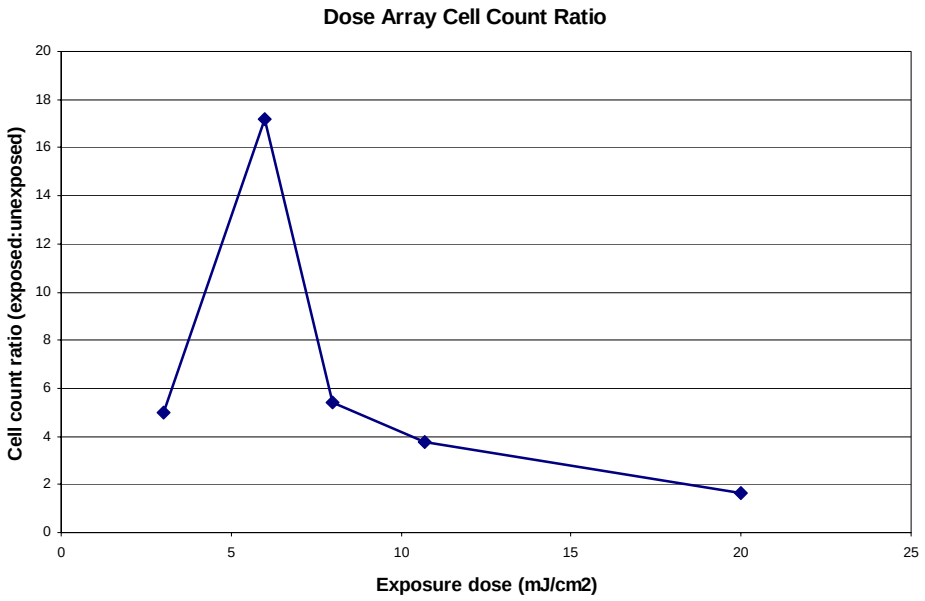

Figure 3.7: Plot of the ratio of the number of cells in the exposed regions to the number of cells in the unexposed regions against the exposure dose delivered to that square in the dose array.

Discussion

The main outcome from this work is that one may use CAR materials to directly pattern fibroblast cells. In order for the pattern to be recognized, a seeding procedure must be used that includes a wash step or change of media after one hour of incubating. The most straightforward method that yields good patterning results is to use regular serum-containing media with a wash of buffered saline after one hour of incubation. This result is surprising, as previous literature suggested that no special plating procedure was needed to pattern cells on a chemically-amplified resist type material [7].

From the ratios of cells in the exposed to unexposed areas, it is obvious that the condition of using regular serum-containing media followed by a wash step, gives the best pattern resolution. That is, the cells are only attached and growing in the patterned region, with very few cells spread out into the non-exposed areas. In the case of using

serum-containing media without a wash step, the cell pattern is evident, but there are significantly more cells adhering outside of the exposed region.

The live/dead viability stain shows that the large majority of the cells in the patterned regions are live. Also, there is some preferential binding of the red ethidium homodimer stain to the exposed areas, which are more hydrophilic. This might be expected as the ethidium homodimer is highly positively charged, and would prefer the de-protected, hydroxyl-terminated surface. Thus, this proves a useful tool when trying to visualize the exposed and unexposed areas in a fluorescent microscope.

It is possible to obtain cell patterns by using serum-free or protein-free media for the initial seeding also. After one hour, the media may be replaced with regular serum-containing growth media. This change of media gives the cells the proper nutrients for growth and also removes the most weakly adhered cells, leaving cells in only the patterned areas. However, this method is not as robust because several attempts have resulted in all of the cells being removed during the change of media. The media change must be done very carefully since the cells are barely adhered to the surface, and even slight bumps or placing the pipette tip too close to the sample can dislodge all of the cells. For this reason, these two seeding methods are not as highly recommended.

The dose array method is one way to determine the optimal exposure dose for cell seeding. From Figure 3.6, it is seen that for this system, a dose of about 6 mJ/cm^2 provides a high patterning ratio. Below this dose, the exposed surface has not received enough energy to fully de-protect, and thus the contrast between the exposed and unexposed regions is low. The reason that there is a decrease in patterning contrast above this dose is an artifact of the exposure system. In the system used for these arrays, there

is a sizable gap between the mask used to generate the square patterns and the wafer. Thus, there is diffusion of light around the masked areas, leading to some flare around the masked areas and the potential for de-protection in the masked areas. This becomes more of an issue at the higher exposure doses, where areas right next to the exposed squares start to receive enough energy to catalyze some de-protection. This is reflected in the decrease in cell seeding contrast at higher doses.

Conclusions and Summary

In conclusion, methods have been established for using acid-catalyzed, chemically amplified photoresist materials to directly pattern fibroblast cells. The recommended method involves seeding fibroblasts in the normal manner, then washing the substrate with buffered saline and replacing the cell growth substrate. This allows weakly adhered cells to be removed and leaves cells growing only in the defined patterns. The patterns have been maintained for seven days in culture, until the fibroblasts have grown to full confluency. This is an important finding as it demonstrates that commercially available resist materials may be used for cell patterning without the need for highly specialized polymer synthesis.

A dose array, which is standard tool used for evaluating resist materials, may also be used to determine the optimal exposure conditions for using photolithographic materials for cell seeding. This an important finding as it allows one to optimize the exposure process for the generation of cell patterns, which is necessary to fully utilize the resist method of patterning cells. The results of this work show an optimal dose of 6 mJ/cm^2, however this will certainly vary depending on the specific configuration of the exposure equipment.

The main insight from this work is that materials originally developed for photolithography in the microfabrication industry may be used to pattern cells, without the need for a development step and the generation of topographical patterns. This greatly expands the number of resist materials that can be used in a biological setting from only the highly specialized "bioresist"[7]. This eliminates the need for synthesizing these special biocompatible protected polymers, and allows researchers to use commercially available chemically amplified resist (CAR) materials. This not only eases the use of CAR materials for cell studies, but also allows for an easier integration of cell seeding combined with microfabrication, which may be beneficial for many areas including cell-based microdevices such as sensors.

In addition, the use of CAR patterning for cell studies would greatly simplify existing cell patterning methods. For instance, two of the most common methods for patterning cells includes the etching of small features into glass and forcing cells into patterns via topographical cues, and the use of microfabricated stamps or microfluidic devices to pattern relevant cell adhesive molecules such as laminin on a surface [9-11]. All of these methods require the full use of photolithography and plasma etch steps to microfabricate structures. By using direct CAR patterning of cells, many of the intermediate fabrication steps are no longer necessary, and the lead time for running these types of studies is greatly shortened.

References

[1] V. A. Liu and S. N. Bhatia, "Three-dimensional photopatterning of hydrogels contg. living cells," *Biomedical Microdevices*, vol. 4, pp. 257-266, 2002.

[2] C. S. Chen, M. Mrksich, S. Huang, G. M. Whitesides, and D. E. Ingber, "Micropatterned surfaces for control of cell shape, position, and function," *Biotechnology Progress*, vol. 14, pp. 356-363, 1998.

[3] D. T. Chiu, N. Li Jeon, S. Huang, R. S. Kane, C. J. Wargo, I. S. Choi, D. E. Ingber, and G. M. Whitesides, "Patterned deposition of cells and proteins onto surfaces by using three-dimensional microfluidic systems," *Proceedings of the National Academy of Sciences of the United States of America*, vol. 97, pp. 2408-2413, 2000.

[4] A. Douvas, P. Argitis, K. Misiako, D. Dimotikali, P. S. Petrou, and S. E. Kakabakos, "Biocompatible photolithographic process for the patterning of biomolecules," *Biosensors & Bioelectronics*, vol. 17, pp. 269-278, 2002.

[5] C. McFarland, C. H. Thomas, C. DeFilippis, J. G. Steele, and K. E. Healy, "Protein Adsorption and Cell Attachment to Patterned Surfaces," *Journal of Biomedical Materials Research*, vol. 49, pp. 200-210, 2000.

[6] D. V. Nicolau, T. Taguchi, H. Tanigawa, and S. Yoshikawa, "Control of the neuronal cell attachment by functionality manipulation of diazo-naphtho-quinone/novolak photoresist surface," *Biosensors & Bioelectronics*, vol. 11, pp. 1237-1252, 1996.

[7] W. He, C. R. Halberstadt, and K. E. Gonsalves, "Lithography application of a novel photoresist for patterning of cells," *Biomaterials*, vol. 25, pp. 2055-2063, 2004.

[8] "Cryogenic Preservation of Animal Cells," American Type Culture Collection, Manassas, VA No. 3, 2001.

[9] C. S. Chen, M. Mrksich, S. Huang, G. M. Whitesides, and D. E. Ingber, "Micropatterned Surfaces for Control of Cell Shape, Position and Function," *Biotechnology Progress*, vol. 14, pp. 356-363, 1998.

[10] D. T. Chiu, N. L. Jeon, S. Huang, R. S. Kane, C. J. Wargo, I. S. Choi, D. E. Ingber, and G. M. Whitesides, "Patterned deposition of cells and proteins onto surfaces using three-dimensional microfluidic systems," *Proceedings of the National Academy of Sciences*, vol. 97, pp. 2408-2413, 1999.

[11] M. J. Dalby, M. O. Riehle, S. J. Yarwood, C. D. W. Wilkinson, and A. S. G. Curtis, "Nucleus alignment and cell signaling in fibroblasts: response to a micro-grooved topography," *Experimental Cell Research*, vol. 284, pp. 274-282, 2003.

CHAPTER 4

QUARTZ CRYSTAL MICROBALANCE INVESTIGATION OF CELL PATTERNING MECHANISM ON RESIST MATERIALS

Introduction

This chapter describes the experiments that were performed using the quartz crystal microbalance to gain insight into the mechanisms that may make cells pattern on photoresist-like materials. It is generally accepted that synthetic materials, without biomimetic properties, acquire bioactivity only after interacting with dissolved proteins [1]. Variations in the surfaces result in the selectivity of the adsorbed proteins. Thus, the initial hypothesis for this study is that the preferential adsorption of proteins from the serum-containing cell growth media onto the patterned polymer surfaces directs the cell adhesion.

In order to study this, a quartz crystal microbalance with dissipation monitoring (QCM-D) was employed. Quartz crystals were coated with various polymer coatings and samples containing proteins or cells were introduced. By monitoring the change in resonance and dissipation of the crystal, the adsorption of the cells and proteins was recorded.

Quartz Crystal Microbalance with Dissipation

The quartz crystal microbalance (QCM) uses the piezoelectric property of quartz to measure small changes in mass. The quartz crystal microbalance with dissipation

(QCM-D) enhances this technique by also measuring the decay in the resonance of the crystal, thus giving insight into the viscoelasticity of the adsorbed layer. A QCM is made of a thin quartz disk, about 0.3 mm thick, with two gold electrodes deposited on either side of the disk. When an AC-field at a frequency close to the crystal's resonant frequency is applied to the disk, the quartz disk will oscillate due to the piezoelectric nature of quartz. The resonant frequency of the oscillation is dependent on the total mass of the crystal. The disk is held in a head assembly which is temperature controlled, and connected to a flow loop (Figure 4.1). The controller measures the frequency and dissipation of oscillation at the resonant frequency, and the third, fifth and seventh overtones.

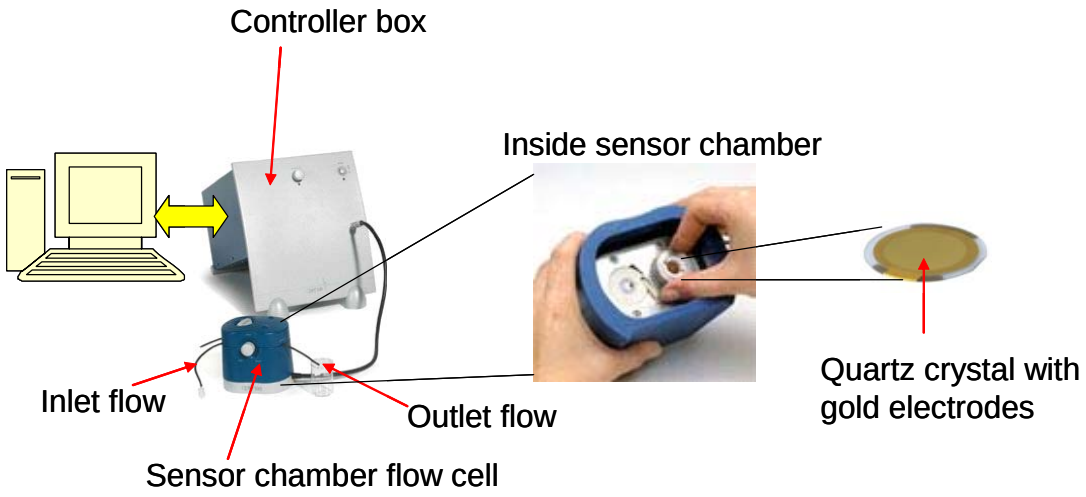

Figure 4.1: QCM-D apparatus, showing the connection between the sensor chamber and controller box, and showing the interior of the sensor chamber and quartz crystal

As binding and release events occur, the total mass of the crystal will appear to change. This change will be reflected in our measurements of the oscillation frequency. By recording the change in resonant frequencies of a vibrating body, the amount of material added or removed can be determined. This relationship between the mass per unit area and frequency is given by the Sauerbrey equation for fundamental resonance (Equation 4.1).

$$\Delta f = \frac{-2\Delta m f_0^{\,2}}{A\sqrt{\mu_q \rho_q}}$$

A = electrode surface area
m = mass
μ_q = shear modulus of quartz
ρ_q = density of quartz
fo = resonant frequency of oscillation

Equation 4.1: Sauerbrey equation

The general Sauerbrey equation may be rearranged, with constant terms combined, to give the relation for calculating mass from frequency change for a 5 MHz crystal, which is what was used (Equation 4.2).

$$\Delta m = \frac{-C \bullet \Delta f}{n}$$

m = mass
C = 17.7 ng/Hz/cm^2 for a 5 MHz crystal
f = frequency of oscillation
n = overtone number (1, 3, 5, 7)

Equation 4.2: Rearrangement of Sauerbrey equation

A flimsy film with a significant viscoelastic nature will not couple completely to the crystal's oscillations, and will actually dampen the oscillation. Thus, measuring the dissipation of the oscillation gives a measure of the film's viscoelasticity (Equation 4.3).

$$D = \frac{E_{lost}}{2\pi E_{stored}}$$

D = dissipation
E_{lost} = energy lost (dissipated) during one oscillation cycle
E_{stored} = energy stored during one oscillation cycle

Equation 4.3: Dissipation equation

QCM-D has been used previously to investigate various bio-chemical interactions. As it is capable of measuring mass uptake in the ng/cm^2 range, it is very useful for studying interactions at these small scales. Also, the gold electrode surfaces may be coated with many different biologically relevant materials, and the measurement chamber is temperature controlled and designed for use with liquid samples. Previous investigators have used this method to detect whole cells as well as proteins on several biologically relevant surfaces such as tantalum[2], titanium dioxide and lipid bilayers[3], and polystyrene surfaces with various treatments [4, 5].

It should be noted that the proportionality between the added mass and the frequency change shown in equations 1 and 2 will hold for even coverage of rigid, well-attached thin films on the active electrode surface. Whole cells do not fall under this range of conditions, as the cell (~10 μm) is much thicker than the depth of the QCM sensor's shear wave (~.25 μm in water). Also, the sensitivity of the QCM sensor varies

by position across the electrode in a Gaussian manner, with a maximum at the center of the sensor. Both of these issues contribute to the finding that the magnitude of the QCM signals do not scale linearly with the number of cells on the surface [4]. Thus, in the investigation of whole cells, only one cell concentration is investigated, with the main goal to differentiate cell behavior on the exposed and unexposed polymer surfaces, not to count the number of cells on the surfaces.

Protein Adsorption Experiments

This section describes the experiments that were preformed to test protein adsorption to different polymer surfaces. To best emulate the cell growth environment, one would want to introduce a solution of fetal or bovine calf serum to the quartz crystal. However, as serum is a complex mixture of proteins and nutrients, the results would be very difficult to interpret as the different components in the mixture are confounding factors and likely impossible to separate.

Thus, to simplify the experiment, a solution of human fibronectin was used. Fibronectin is a well studied glycoprotein found in the extracellular matrix, and is known for its role in cell adhesion and as a guide for cell migration during mammalian development [1, 6].

Materials

The QCM-D apparatus and crystals were obtained from Q-Sense. Human fibronectin was obtained from BD Biosciences (BD #354008). Polyhydroxystyrene (PHOST) polymer was obtained from TriQuest, LP. Protected PHOST polymers were synthesized by C. Berger [7]. Acetone, propylene glycol methyl ether acetate (PGMEA,

99%), and poly(tert-butyl methacrylate) were purchased from Aldrich. The photo-acid generator, 263, was obtained as a sample from Ciba. Trypsin and Dulbecco's Minimum Essentials medium (DMEM, Cellgro 10-013-CM) were obtained from Cellgro, and bovine calf serum was purchased from Hyclone.

Experimental procedure

Coating the QCM-D Crystals

The QCM-D crystals were coated with polyhydroxystyrene (PHOST) protected with tert-butoxycarbonyl (PHOST-tBOC) and tetrahydropyranyl (PHOST-THP). Besides the obvious difference of the protection groups, the PHOST-tBOC is only partially protected (30% of –OH groups are protected) and the PHOST-THP is fully protected, as shown in Figure 4.2.

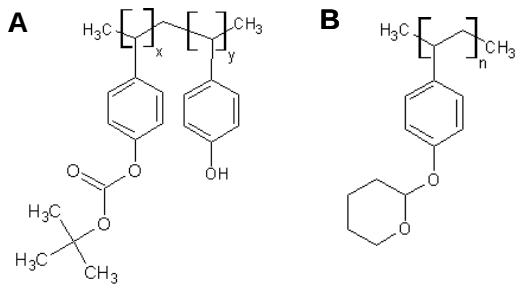

Figure 4.2: Chemical structures for resist materials. A) Partially protected PHOST-tBOC. B) Fully protected PHOST-THP.

The crystals were coated with the polymer by spin coating. The following solutions were used: 2.5 wt% PHOST-tBOC in PGMEA with 3 wt% to solids 263 PAG, and 2.5 weight% PHOST-THP in PGMEA with 3 wt% to solids 263 PAG. Each crystal

was fully coated with one of the solutions, then spun at 500 rpm, 500 rpm/second ramp rate, for 5 seconds, then spun at 4000 rpm, with at 1000 rpm/second ramp rate, for 40 seconds. The crystals were softbaked at 130^{o}C for 90 seconds to remove the solvent. For the de-protected samples, the crystals were then exposed to 50 mJ of 248nm UV light and then post exposure baked for 90 seconds at 130^{o}C to fully catalyze the de-protection reaction. Before the crystals were placed into the measurement chamber a small swab was soaked in acetone and used to clean the gold contact surfaces to ensure a good connection.

Operation of QCM-D Apparatus

Once the QMC-D crystals were coated with the appropriate polymer, they were placed into the QCM-D crystal holding chamber. The fundamental frequency and dissipation were recorded first in air to ensure that the crystal was not damaged during the coating process. Then phosphate buffered saline was introduced to the measurement chamber, and the fundamental frequency and dissipation were measured again. The system was then set to acquire, and the temperature was set to 37^{o}C. The crystal was allowed to equilibrate in the solution until a fairly constant frequency and dissipation were measured. At this time, either a 5 or 10 μg/μl solution of fibronectin in phosphate buffered saline was added to the chamber. The system continued to acquire data until a constant frequency and dissipation was attained again. The acquisition was then stopped and the data was saved. In between each run, the tubing and measurement chamber were thoroughly cleaned with an enzyme cleaner designed to remove proteins, and rinsed with DI water.

Results and Discussion

The following graph shows an example of the raw data taken during a typical QCM-D run. One may observe the period of equilibration in the buffer solution, followed by the introduction of the fibronectin solution, and the mass update by the crystal as a gradual decrease in the frequency of oscillation (Figure 4.3).

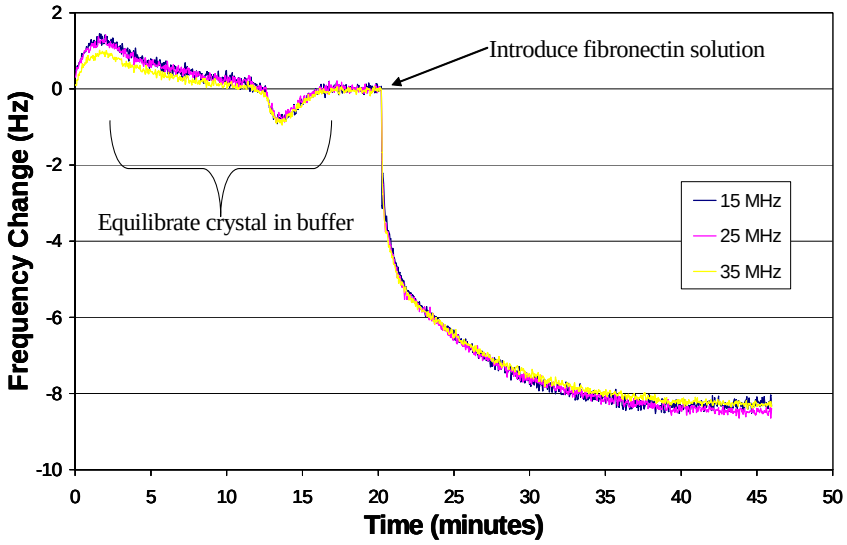

Figure 4.3: Frequency change over time with the addition of a fibronectin protein solution. The first three overtones are shown, normalized.

It should be noted that the three overtones (3^{rd}, 5^{th} and 7^{th} harmonic at 15, 25, and 35 MHz respectively for a 5 MHz crystal) are shown, with the frequency normalized by division by the overtone number, and then the frequency change plotted. The reason these higher overtones are typically used and reported is that they are less noisy than the fundamental frequency at 5 MHz. The data for all three overtones lie on the same plot,

showing that dissipation effects are small and the protein layer behaves mainly as a rigid layer.

For each run, data was collected in this manner, and the change in frequency was recorded. The graph below (Figure 4.4) shows the summary of 3 runs for each sample. One may notice that the partially protected PHOST-tBOC had consistently higher mass uptake, and that the lowest mass uptake was observed for the protected PHOST-THP sample.

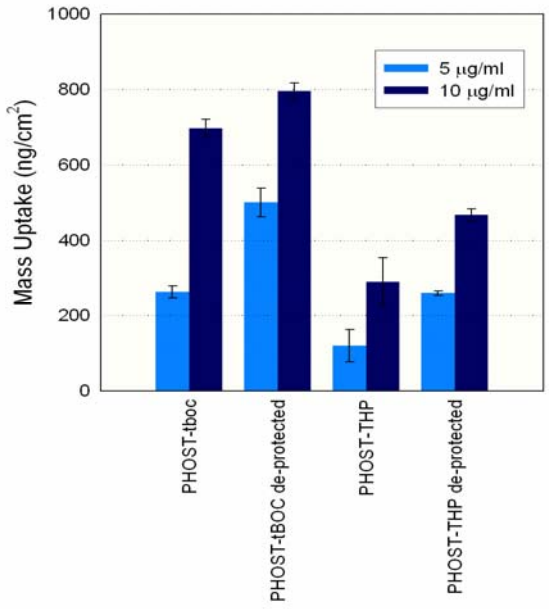

Figure 4.4: Total amount of fibronectin adsorbed for each condition.

These findings are interesting, as initial cell patterning studies on these materials showed that differential cell adhesion is possible on the protected/de-protected PHOST-THP, but

not on the protected/de-protected PHOST-tBOC. The failure mode for the cell patterning is that the cells adhere in all areas, protected and de-protected. This suggests that perhaps there is some threshold amount of adsorbed protein that allows for preferential cell adhesion, since it is only the fully protected PHOST-THP (which has the lowest amount of adsorbed protein) that does not allow for easy cell adhesion. There are many studies in the literature regarding fibronectin and cell adhesion, with some exploring the idea of a threshold amount of protein necessary for cell adhesion [8, 9] and others examining the conformation of the protein on the surface [10, 11], and it is likely that a combination of these effects will determine the cell behavior on a given surface. This work compares well with the threshold studies, one of which finds that 230 ng/cm^2 of fibronectin coating is needed for cells to remain adhered under shear conditions [9]. The data for the PHOST-THP condition in Figure 4.4 are 120 +/- 42 ng/cm^2 and 290 +/- 65 ng/cm^2 (for the 5 and 10 ng/ml conditions respectively) indicating that this condition may not allow for fibronectin adsorption levels above the threshold level needed for firm cell adhesion under shear conditions.

In order to compare these findings with surface properties, the water contact angle for several samples was measured. The data show that the fully protected PHOST-THP has the highest contact angle of about 80^o (Figure 4.5). With increasing exposure dose, the de-protection reaction proceeds, and the water contact angle decreases as the surface becomes more hydrophilic. The large difference in surface energy for the protected PHOST-THP versus the partially protected PHOST-tBOC and exposed surfaces can explain why this surface has the lowest amount of adsorbed protein, and resists cell adhesion.

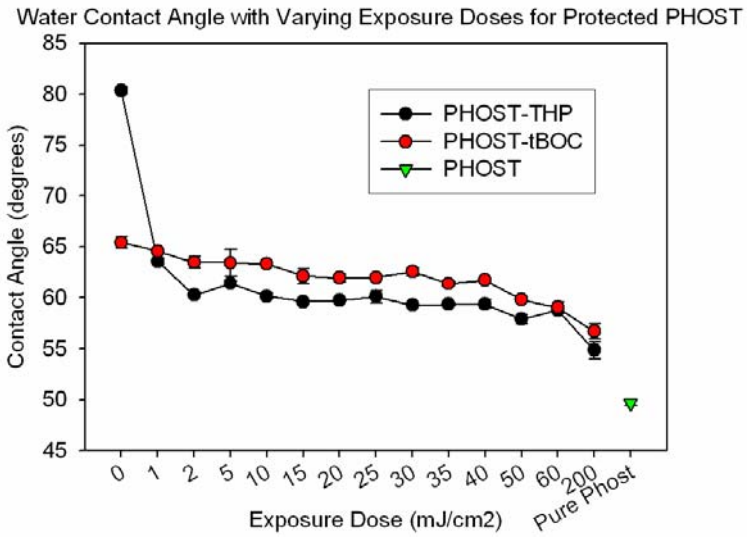

Figure 4.5: Water contact angles plotted against exposure dose for PHOST-THP and PHOST-tBOC surfaces.

Whole Cell Experiments

Materials

Acetone, propylene glycol methyl ether acetate (PGMEA, 99%), the triphenylsulfonium triflate (TPS) photoacid generator, and poly(tert-butyl methacrylate) were purchased from Aldrich. NIH3T3 fibroblast cells were donated. Trypsin and Dulbecco's Minimum Essentials medium (DMEM, Cellgro 10-013-CM) were obtained from Cellgro, and bovine calf serum was purchased from Hyclone.

Experimental procedure

Coating the QCM-D Crystals

The QCM-D crystals were spin coated with poly(tert-butyl methacrylate) (PTBMA). The PTBMA polymer (Figure 4.6) was chosen because the findings from Chapter 3 show that this patterned polymer is capable of giving reliable cell patterns.

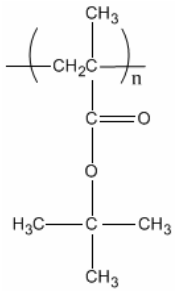

Figure 4.6: Chemical structure of resist material poly(tert-butyl methacrylate) (PTBMA)

The PTBMA solution was made with 10 weight% PTBMA in PGMEA, with 1 weight% to solids of the photo-acid generator TPS. The solution was placed on the crystal, and the crystal was spun at 2000 rpm with a 100 rpm/sec ramp rate, for 40 seconds. The crystal was then soft baked at 120^{o}C for 90 seconds. For those samples that were to be run on exposed, de-protected surfaces, the crystals were then exposed to 248 nm UV light and post-exposure baked for 90 seconds at 180^{o}C. Before the crystals were used, the electrode surfaces were cleaned with acetone to ensure good electrical contacts.

Cell Culture

NIH3T3 fibroblasts were cultured in Dulbecco's Minimum Essentials medium (DMEM, Cellgro 10-013-CM) supplemented with 10% bovine calf serum (BCS, Hyclone) and 1% Antibiotic-Antimycotic Solution (Cellgro 30-004-CL). Fibroblasts were grown up in tissue cultured polystyrene dishes from P2 frozen stock until they reached approximately 80% confluency, and the cells used for in this work varied from P4 to P10. [12]. The subconfluent fibroblast monolayers were dissociated from the culture dish using Trypsin EDTA 1x (0.05% Trypsin/0.53mM EDTA in HBSS, Cellgro 30-004-CL) and were resuspended in fresh media.

Operation of QCM-D Apparatus

Once the QMC-D crystals were coated with the appropriate polymer, they were placed into the QCM-D crystal holding chamber. The fundamental frequency and dissipation were recorded first in air to ensure that the crystal was not damaged during the coating process. Then DMEM was introduced to the measurement chamber, and the fundamental frequency and dissipation were measured again. The system was then set to acquire, and the temperature was set to 37^{o}C. The crystal was allowed to equilibrate in the solution until a fairly constant frequency and dissipation were measured. At this time, cell suspension was added to the chamber. The system continued to acquire until the frequency was fairly constant.

Results and Discussion

Representative plots of the data from the whole cell QCM-D experiments are shown below. The first plot compares the frequency shift observed when cells are added to a PTBMA coated crystal, with and without exposure and de-protection (Figure 4.7).

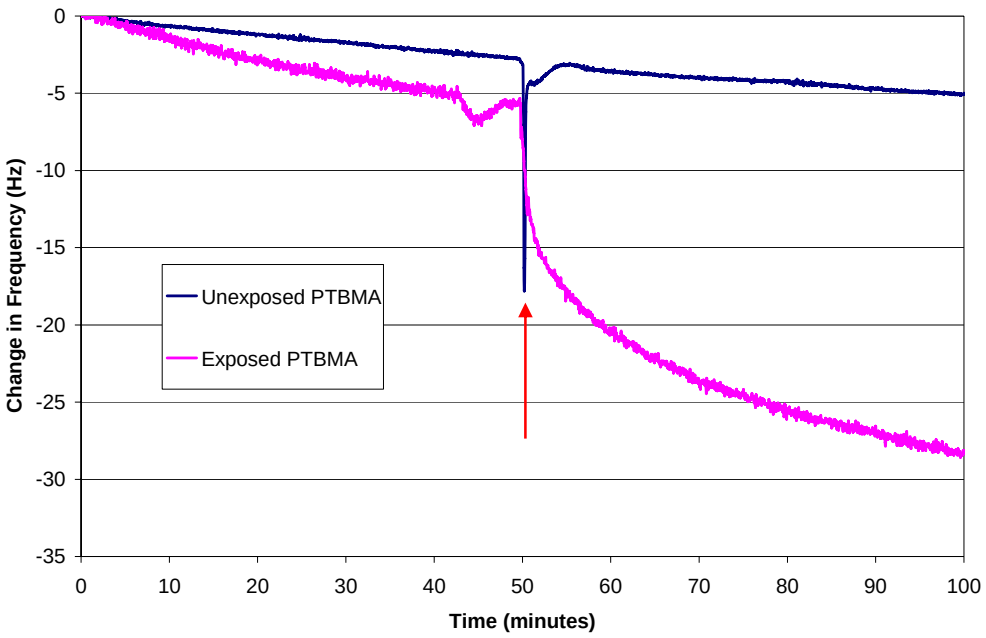

Figure 4.7: Frequency shift as a function of time after introduction of the cell suspension (time of addition of cells shown by arrow). Pink line shows shift for crystal coated with PTBMA and exposed to UV light. Blue line shows shift for crystal coated with PTBMA without any exposure.

It is evident that the unexposed PTBMA coated crystal did not register any significant change in frequency with the addition of the cell suspension. This indicates that the cells in this condition did not adhere to the surface, as the QCM is only capable of sensing cells that have adhered to the surface [4, 13, 14]. Those cells that are dead or

have only settled on the surface do not register as added mass to the crystal, and thus under these conditions no change in frequency is observed.

The next plot (Figure 4.8) shows the dissipation change when cells are added to the protected and de-protected surfaces.

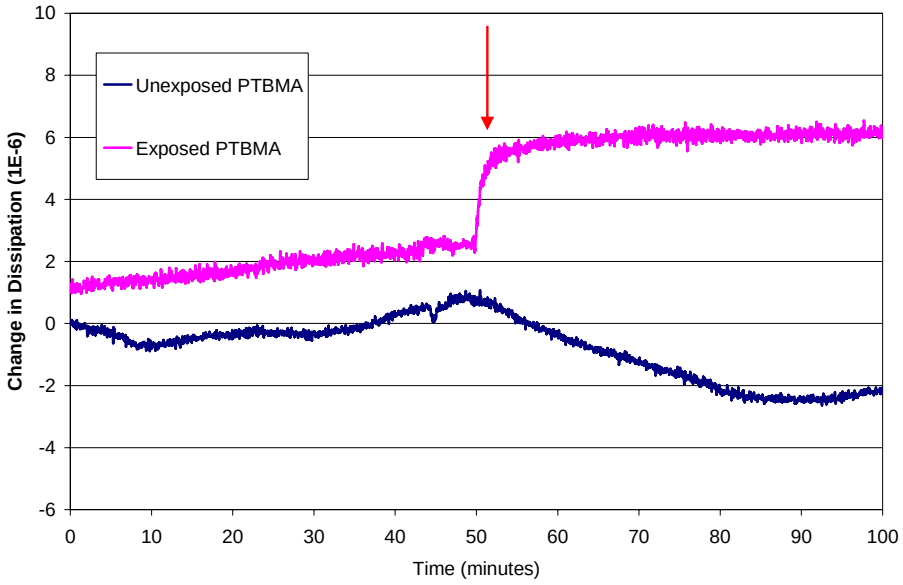

Figure 4.8: The change in Dissipation factor (1E-6) as a function of time after introduction of the cell suspension (time of addition of cells shown by arrow). Pink line shows shift for crystal coated with PTBMA, exposed to UV light, and de-protected. Blue line shows shift for crystal coated with PTBMA without any exposure.

The dissipation factor increases quickly when cells are added to the de-protected PTBMA surface, as expected. As mentioned earlier, this is due to the viscoelastic nature of the cells dissipating some of the energy from the crystal vibration. On the unexposed PTBMA there is no distinct change in the dissipation factor. It appears that there is a

slight downward drift in this particular run, although one should note that the dissipation factor had more drift and variability in this case overall.

The change in dissipation factor plotted against the change in frequency is also a means to discriminate between these two surfaces (Figure 4.9). For the de-protected PTBMA surface, there is a clear increase in dissipation as the frequency decreases. For the unexposed, unmodified PTBMA surface there is no clear trend with frequency and dissipation. It should be noted that in the plot below, the only points shown are those after the addition of the cell suspension to the measurement chamber.

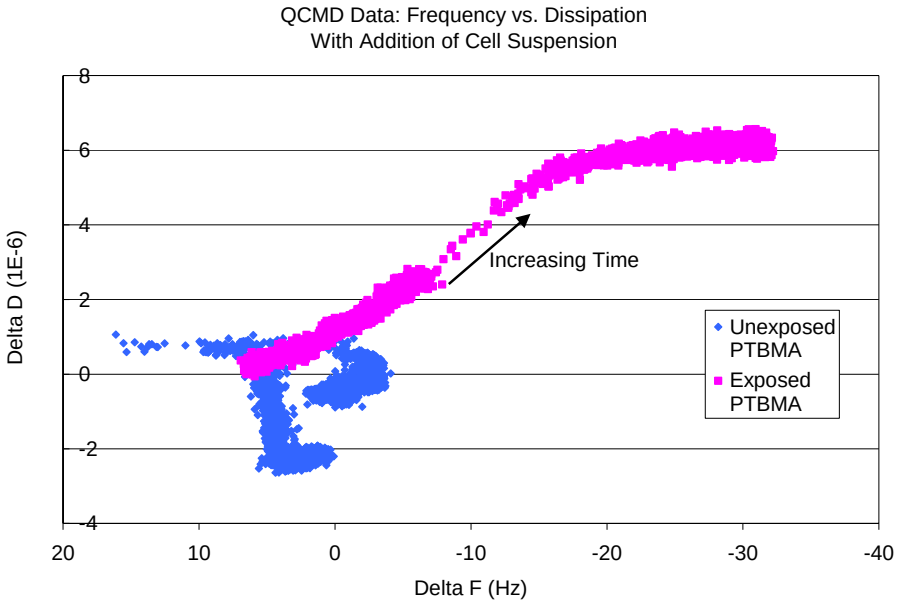

Figure 4.9: The change in Dissipation factor (1E-6) plotted as a function of the change in frequency (Hz). The only points shown are those after the time when the cell suspension was introduced. The black arrow shows the direction of increasing time, with respect to the exposed PTBMA data set. Pink line shows shift for crystal coated with PTBMA, exposed to UV light, and de-protected. Blue line shows shift for crystal coated with PTBMA without any exposure.

The surface energy of PTBMA, as measured by water contact angle, can be used to correlate the cell interaction findings (Table 4.1). As with the PHOST samples, the fully protected PTBMA has a very high contact angle compared to the de-protected PTBMA, with a difference of about 20^{o}, and it is this fully protected surface that resists cell adhesion within the time period studied.

Table 4.1: Water contact angles in degrees for PTBMA, protected and de-protected.

	PTBMA fully protected	PTBMA de-protected	Difference
Average water contact angle	87.3	64.9	22.4

Summary and Conclusions

The QCM-D studies show that there is a significant difference in the amount of fibronectin adsorbed to the protected and de-protected PHOST surfaces. The least amount of fibronectin was added to the protected PHOST-THP surface, which is the only PHOST surface that resists cell adhesion. This suggests that perhaps there is some threshold amount of protein for promoting cell adhesion and that the PHOST-THP does not allow for this critical amount. The measurement of surface energy via water contact angle shows that the fully protected PHOST-THP has the highest contact angle (i.e. most hydrophobic) and has the least amount of protein adsorbed.

For the whole cell experiments, the PTBMA polymer was chosen as the studies from Chapter 3 show that this patterned polymer is capable of generating cell patterns. The findings from the whole cell experiments suggest that cells may only settle and do not adhere on the unexposed, protected PTBMA surfaces. This is evident because there

is no decrease in the frequency upon addition of the cells to the unexposed PTBMA surfaces. Again the water contact angle was measured, and the unexposed, fully protected PTBMA had the highest contact angle and resisted cell adhesion.

These findings are interesting, as they are consistent with the cell seeding methods proposed in the previous chapter. In the unexposed regions of the polymer, the cells may settle lightly on the surface initially without adhering, as there is no frequency shift observed in these conditions. Thus, the wash step after a short incubation time removes these cells, leaving only the cells in the exposed, de-protected regions.

The contact angle measurements consistently show that an increase in hydrophilicity improves fibronectin adsorption and cell adhesion. While the hydrophilicity is a good starting point for identifying potential resists for use in cell patterning, it is certainly not a perfect test. Other researchers have emphasized the importance of other factors, such as the charge of functional groups, in addition to hydrophilicity when considering whether a surface is cell adhesive [11]. Still, this knowledge is very useful in the selection of materials for use in cell patterning via resist methods. For instance, one would not need to formulate resist materials and screen them through cell studies, which can be time consuming and expensive. Instead, the water contact angle may simply be measured on small samples to identify materials that are good candidates for use in cell patterning.

References

[1] *Biomaterials Science: An Introduction to Materials in Medicine*. San Diego: Academic Press, 1996.

[2] C. Modin, A.-L. Stranne, M. Foss, M. Duch, J. Justesen, J. Chevallier, L. K. Anderson, A. G. Hemmersam, F. S. Pedersen, and F. Besenbacher, "QCM-D studies of attachment and differential spreading of pre-osteoblastic cells on Ta and Cr surfaces," *Biomaterials*, vol. 2006, pp. 1346-1354, 2006.

[3] A.-S. Andersson, K. Glasmastar, D. Sutherland, U. Lidberg, and B. Kasemo, "Cell adhesion on supported lipid bilayers," *Journal of Biomedical Materials Research*, vol. 64A, pp. 622-629, 2002.

[4] G. Nimeri, C. Fredriksson, H. Elwing, L. Liu, M. Rodahl, and B. Kasemo, "Neutrophil interaction with protein-coated srufaces studied by an extended quartz crystal microbalance technique," *Colloids and Surfaces B: Biointerfaces*, vol. 11, pp. 255-264, 1998.

[5] C. Fredriksson, S. Kihlman, M. Rodahl, and B. Kasemo, "The Piezoelectric Quartz Crystal Mass and Dissipation Sensor: A Means of Studying Cell Adhesion," *Langmuir*, vol. 14, pp. 248-251, 1998.

[6] B. Alberts, A. Johnson, J. Lewis, M. Raff, K. Roberts, and P. Walter, *Molecular Biology of the Cell, fourth edition*, Fourth ed. New York, NY: Garland Science, 2002.

[7] C. M. Berger, "Measuring Acid Generation Kinetics in Photoresist Films via Capacitance Techniques," in *Chemical Engineering*, vol. Doctor of Philosophy. Atlanta, GA: Georgia Institute of Technology, 2004.

[8] J. Aplin and R. Hughes, "Cell Adhesion on Model Substrata: Threshold Effects and Receptor Modulation," *Journal of Cell Science*, vol. 50, pp. 89-103, 1981.

[9] A. S. Goldstein and P. A. DiMilla, "Effect of adsorbed firbonectin concentration on cell adhesion and deformation under shear on hydrophobic surfaces," *Biomedical Materials Research*, vol. 59, pp. 665-675, 2001.

[10] J. C. Meredith, J. L. Sormana, B. Keselowsky, A. Garcia, A. Tona, A. Karim, and E. J. Amis, "Combinatorial Characterization of Cell Interactions with Polymer Surfaces," *Journal of Biomedical Materials Research*, pp. 483-490, 2003.

[11] K. E. Michael, V. N. Vernekar, B. G. Keselowsky, J. C. Meredith, R. A. Latour, and A. J. Garcia, "Adsorption-Induced Conformational Changes in Fibronectin Due to Interactions with Well-Defined Surface Chemistries," *Langmuir*, vol. 19, pp. 8033-8040, 2003.

[12] "Cryogenic Preservation of Animal Cells," American Type Culture Collection, Manassas, VA No. 3, 2001.

[13] D. Gryte, M. Ward, and W. Hu, "Real-time measurement of anchorage-dependent cell adhesion using a quartz crystal microbalance," *Biotechnology Progress*, vol. 9, pp. 105-108, 1993.

[14] T. Matsuda, A. Kishida, E. H, and Y. Okahata, "Novel instrumentation monitoring in situ platelet adhesivity with a quartz crystal microbalance," *ASAIO J.*, vol. 38, pp. 171-3, 1992.

CHAPTER 5

DESIGN AND ASSEMBLY OF MULTI-WAVELENGTH MICRO-STEREOLITHOGRAPHY SYSTEM

Introduction

As one may recall, the novel fabrication scheme presented in this thesis is to initiate the polymerization reaction with one wavelength of light, and then to catalyze the de-protection reaction by using a second wavelength of light. Commercially available stereolithography apparatuses (SLAs) operate on one fixed wavelength of light [1], making them unsuitable for the proposed method. In order to realize the proposed method of cell patterning in three-dimensions, it is necessary to have an SLA that is capable of exposures of at least two different wavelengths of light. This chapter provides the rationale used in designing our system, the general layout and function of the system, and the documentation for system automation.

Commercial SLA Systems

It is useful to begin with a description of commercial SLA systems. As a brief reminder of the entire SLA process, Figure 5.1 is a diagram showing the main steps in the commercial SLA procedure. First, the part is designed using CAD software, and then specialized software is used to "cut" the 3D computer object into a series of 2D layers. This data is translated into the proper file format and sent to the SLA machine. The parts are built on a mesh platform, where un-reacted resin can drain off the finished parts.

Finally, the finished parts are transferred to a cure oven where they are fully polymerized and crosslinked.

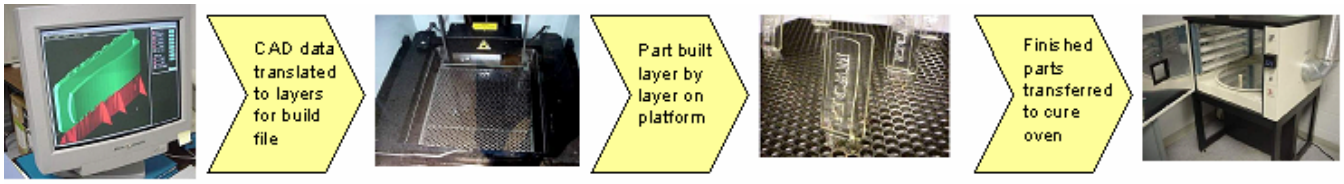

Figure 5.1: Stereolithographic process overview [2]

In the SLA machine, a laser light is directed by a computer-controlled mirror in the shape of each layer. An elevator moves the build platform up and down in the vat of liquid resin, and a sweeper blade runs across the build plane after each layer is written, to smooth the surface. These main components are shown in Figure 5.2.

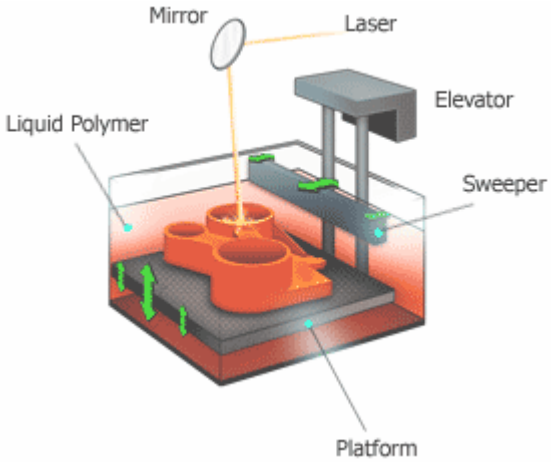

Figure 5.2: Diagram of stereolithography apparatus (SLA) [3]

Our goal is to replicate this build process, substituting a multi-wavelength light source for the laser, and devising a simple, efficient imaging scheme which does not require highly complex manufacture or assembly. It should be noted that these commercial systems work very well, and were in fact used to design and build some of the components used in our custom system. Also, other rapid prototyping technologies are available in the Georgia Tech Rapid Prototyping and Manufacturing Institute (RPMI) facility, but are beyond the scope of this report.

Several commercial SLA machines from 3D Systems are available on campus in the Georgia Tech RPMI: SLA-250/50, SLA-3500, and the SLA Viper Si2 (pictured in Figure 5.3).

Figure 5.3: Photographs of SLA machines available at Georgia Tech. From left to right, photographs of 3D Systems SLA Viper [4], SLA 3500 [4], and SLA 250 [2].

The various SLA models vary in their build speed, feature resolution and platform size. The SLA Viper offers the greatest resolution, using a Neodymium doped Yttrium

Vanadate ($Nd:YVO_4$) solid state laser at 354.7 nm. The "standard" mode has a beam diameter of 0.250 +/- 0.025 mm, and the "high precision" mode offers a beam diameter of 0.075 +/- 0.015 mm. The SLA-3500 also uses a solid state $Nd:YVO_4$ laser, but only has one resolution setting with a beam diameter of 0.20-0.30 mm. Its main advantage is a large build platform with the capacity to build bulkier pieces. Finally the SLA-250/50 uses a Helium Cadmium (HeCd) laser with a fixed wavelength of 325 nm and a spot size of 0.20-0.28 mm. Although it is the older of the machines, it is quite useful for investigating formulations as it can be fitted with custom made "mini vats" that can hold small quantities of experimental resins. Due to the nature of this work, the two machines used were the SLA Viper and SLA-250. The SLA-Viper provided a quick method to build some basic structural components, and the SLA-250 was initially used to understand the SLA build process.

Mirror-Array Based SLA Systems

Mask-projection based SLA systems have been proposed and studied by several research groups since about 1997 [5, 6]. The general set-up of this type of system is shown in Figure 5.4. In this system, each pixel of the image corresponds to a mirror in the array. As the mirrors are turned on and off, images are projected onto the resin surface, and in essence, the mirror array is used as a dynamic mask. These projection-type SLA systems are quite attractive for small-scale laboratories because of the availability of the components and relative simplicity in the assembly. This type of system is especially advantageous for our design because the light source is separate from

the image generation, making it possible to easily adjust the wavelength of light without disrupting the image production.

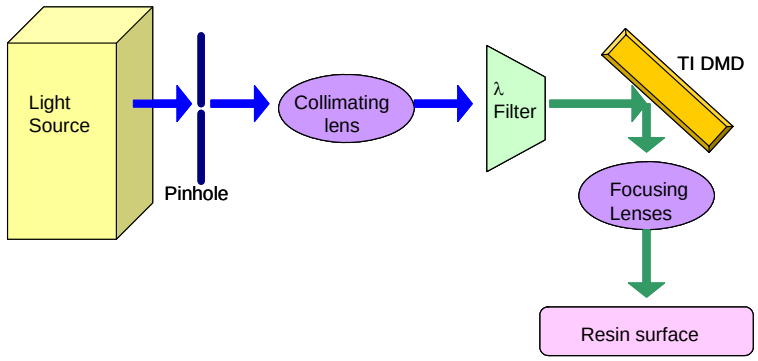

Figure 5.4: General mirror array system

The system we built was inspired by a mirror array SLA designed by Ameya Limaye for his master's thesis in mechanical engineering at Georgia Tech [7]. The basic design is that a collimated light source illuminates a mirror array. The light reflected from the mirror array is then directed down onto the resin surface. A small stage and elevator system move the part lower into the resin vat, the image on the mirror array is changed, and the next layer is exposed. The diagram of A. Limaye's system is shown in Figure 5.5.

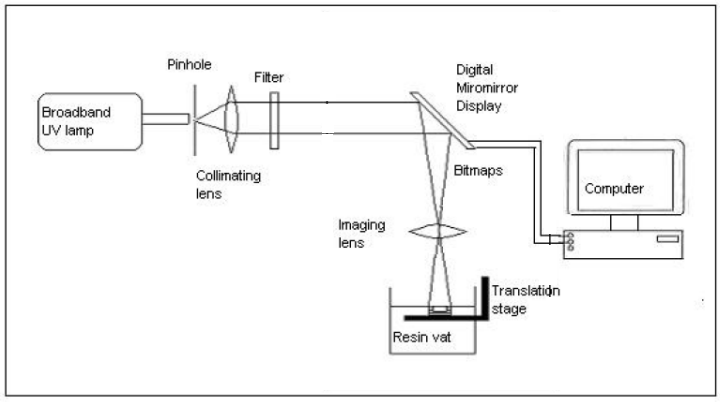

Figure 5.5: Sketch of the basic components in A. Limaye's SLA design [8]

Multi-wavelength SLA System

There are several key differences in the multi-wavelength SLA system built for this work. The most important are the arrangement of the optical components, the path of light, and additional light filters to allow for different wavelengths of light. The multiple wavelength capacity of this system is needed to realize the photopolymerization plus photo-catalyzed de-protection reaction sequence. The optical components and light path are designed to give the most direct projection of the image onto the resin surface, thereby reducing the distortions to the desired image.

In Limaye's design, the mirror array itself is oriented at a 45^{o} angle and is used to turn the light down to the resin surface. This is problematic because the distance that the light travels to the focal plane is different across the area of the mirror array, as shown in Figure 5.6. The distance the blue ray travels (d_{blue}) is larger than the distance the green ray travels (d_{green}). This difference means that for the image to be in good focus, the focal plane would have to be oriented in a 45^{o} angle also. Commercial optical systems, such as

those in projection televisions, can correct for small amounts of this type of error (15-30^{o}), typically called a keystone correction.

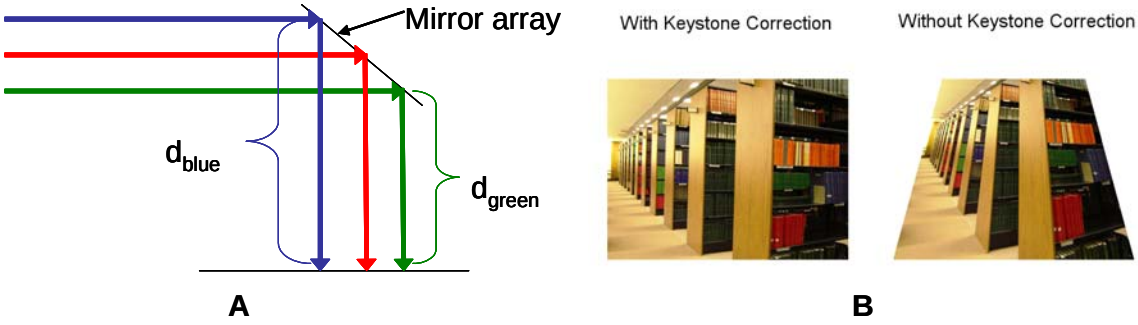

Figure 5.6: A) Schematic showing the difference in distance that the light travels across the mirror array B) A typical keystone correction [9]

To avoid this type of correction, this design orients the mirror array so that the "on" mirrors are parallel to the resin surface, meaning the light may be projected directly perpendicular to the resin surface, as illustrated in Figures 5.7 and 5.8.

Still, in this design, there must be a way to turn the light down towards the resin surface. Two configurations for this were examined: 1) use a piece of quartz at a 45^{o} angle as a beam splitter, 2) use a mirror to turn light up to DMD.

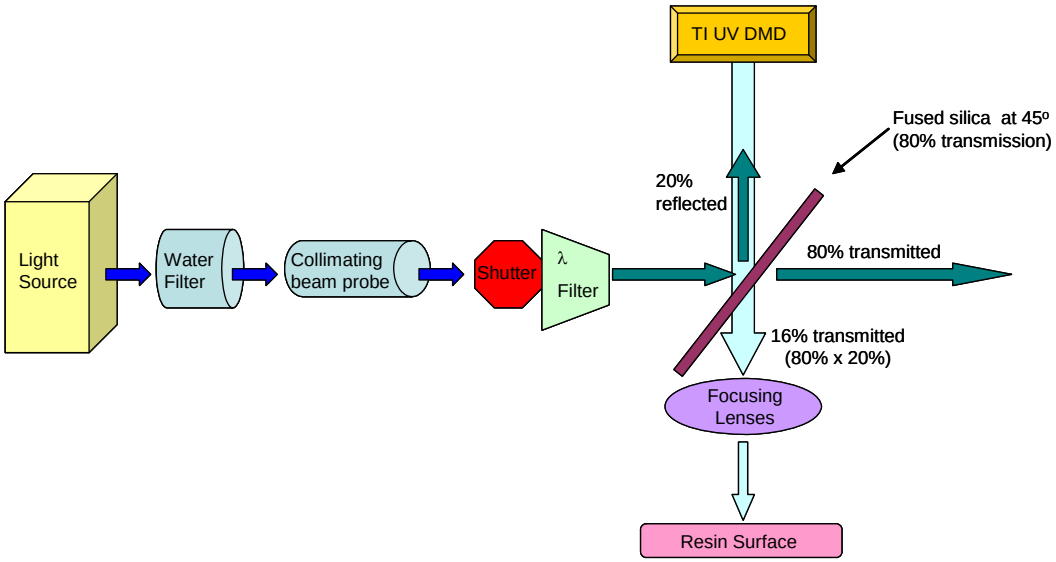

Figure 5.7: Sketch of basic components for the SLA design for this work, Configuration 1.

From the sketch in Figure 5.7, it is apparent that Configuration 1 has a major disadvantage, in that a significant amount of the light intensity is lost through the quartz window, as the quartz used has 80% transmission. This means that by the quartz piece alone, 84% of the light is lost. Thus, the system was re-assembled into configuration 2 (Figure 5.8).

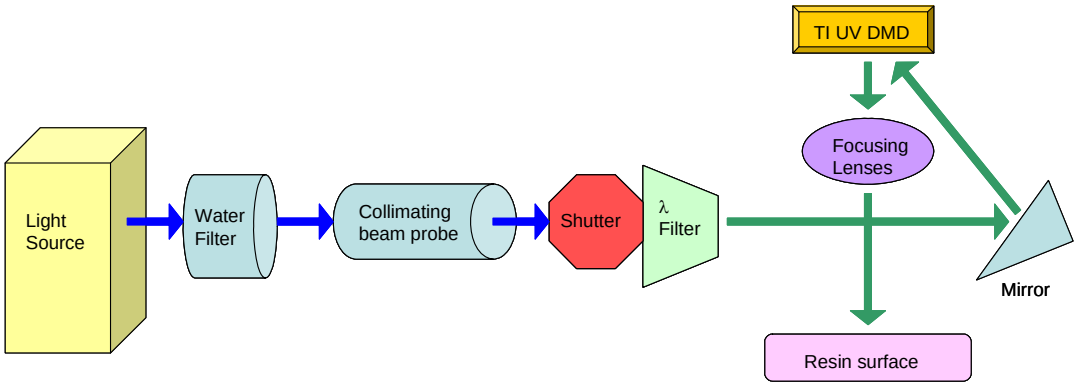

Figure 5.8: Sketch of basic components of SLA system for this work, Configuration 2.

The photographs below (Figures 5.9 and 5.10) show the set-up, as it is assembled in the laboratory. One may notice that most of the set up, except for the lamp housing, is within an optical box. This limits the amount of stray light that may be reflected out into other laboratory work areas. The lamp housing must be kept outside of the box as it produces ozone, and this must be ventilated.

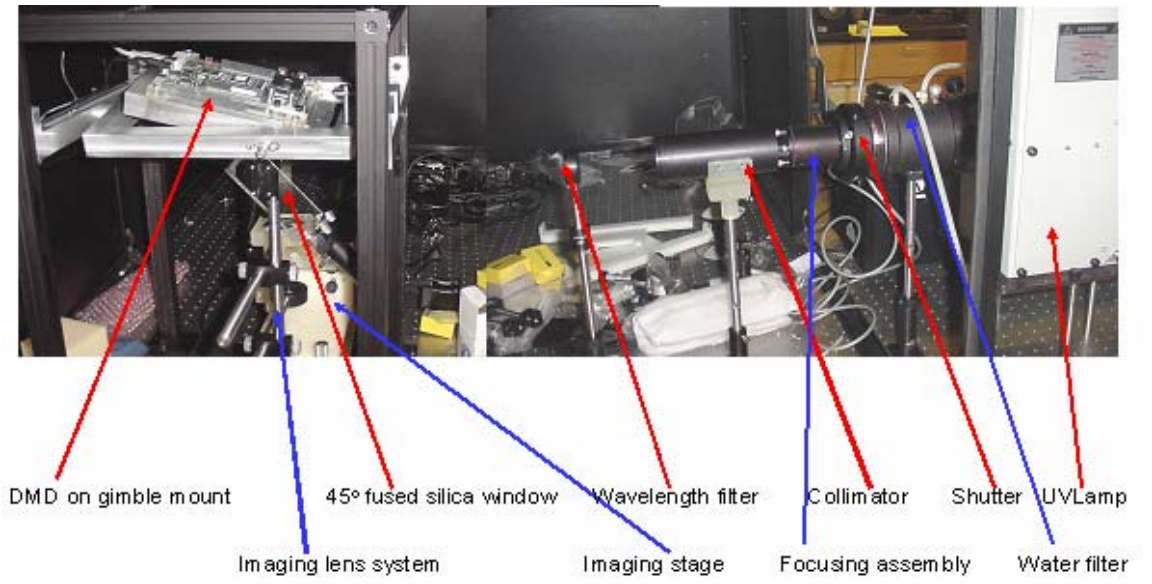

Figure 5.9: Photograph of overall system, configuration 1.

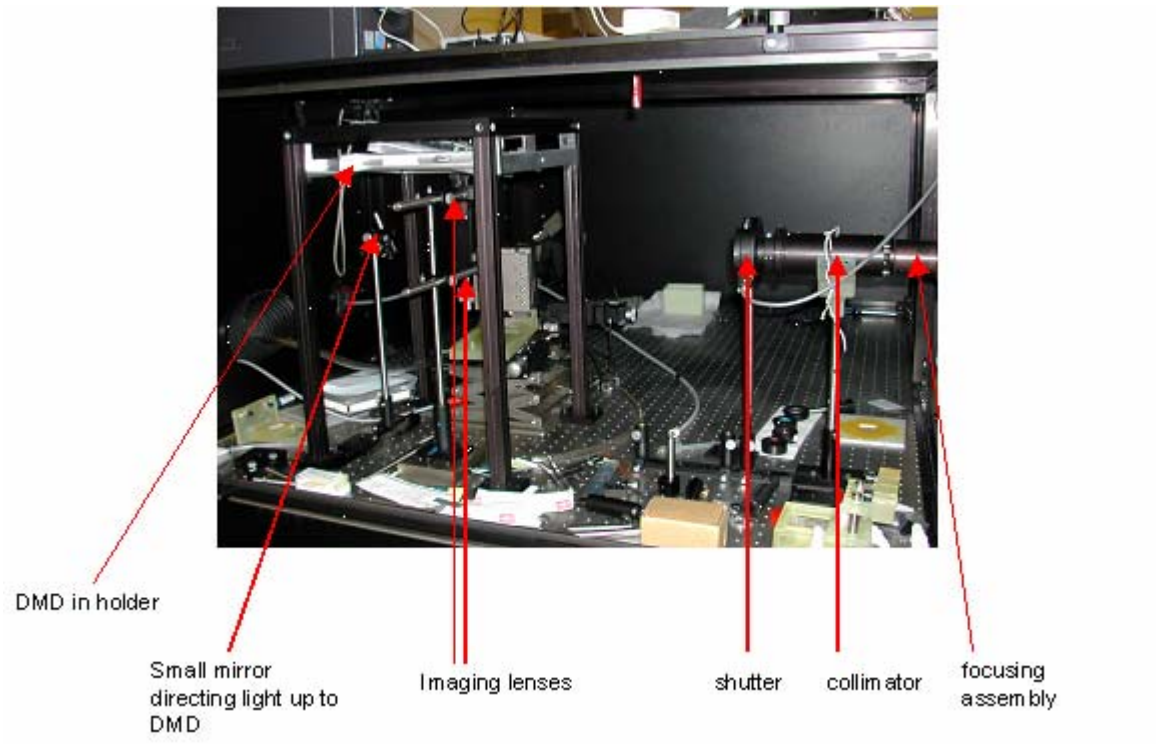

Figure 5.10: Photograph of system set up in configuration 2.

Specialized Design Elements to Accommodate Mirror Array

The greatest difficulty in using the TI DMD comes from the fact that the mirrors rotate on their 45^{o} diagonal axis, with a range of motion from 12 ^{o} to -12^{o} from the horizontal, with a tolerance of +/- 1^{o} (Figures 5.11, 5.12). This arrangement makes it difficult to orient the mirror in space so that the projection is parallel to the resin surface, resulting in a distortion-free image. In our design, we accounted for this problem by designing a special holder for the DMD (Figure 5.14) which sits in an adjustable frame (Figure 5.15). By using these specialized components we can safely fine-tune the position of the DMD in all directions so that the image is projected directly flat onto to the resin surface.

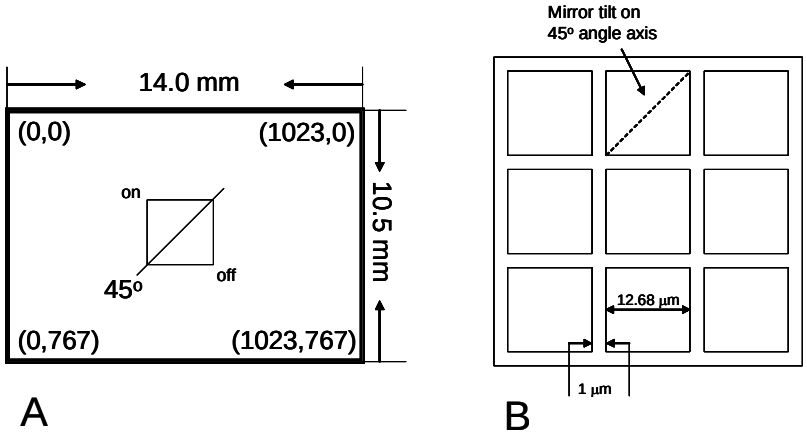

Figure 5.11: DMD chip schematics, adapted from TI DMD Discovery Product Preview Data Sheet, August 30. 2005. (A) Schematic of entire DMD array with coordinates indicating individual mirrors. (B) Schematic showing 9 mirrors of the array with individual mirror dimensions, street width, and tilt angle shown

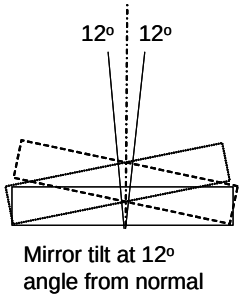

Figure 5.12: DMD mirror sketch showing tilt orientation; adapted from Nayer et. al. 2004

The first piece that was built was a frame for the DMD mirror and board. From the manufacturer, the mirror array is supplied on a printed circuit board which provides the circuitry for control of the mirror (Figure 5.13).

Figure 5.13: Picture of TI-DMD array mounted on circuit board from www.tyrexsales.com

The mirror array may be used in this fashion, without any additional hardware; however, it is more desirable for it to be mounted securely, as it is expensive and delicate. The frame was designed so that the printed circuit board would lie in a small trough, with one end open to expose the mirror array (Figure 5.14).

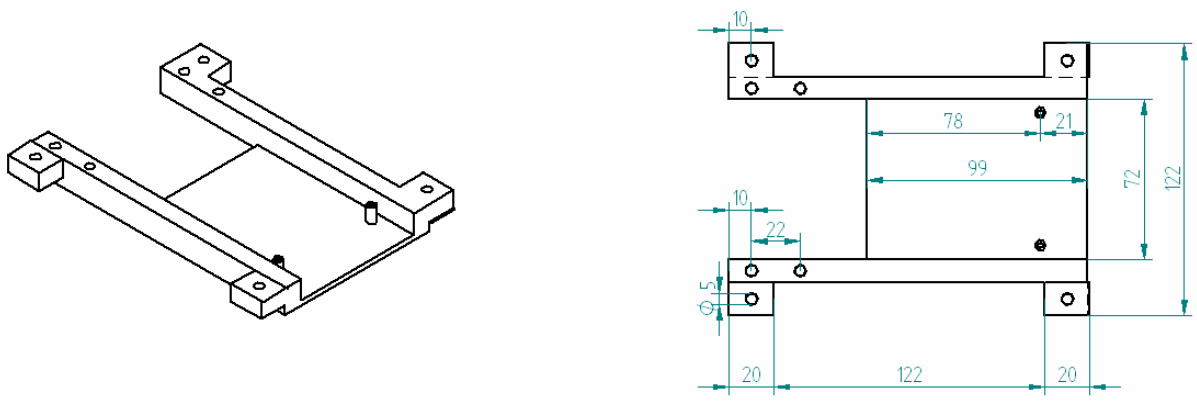

Figure 5.14: Schematic of DMD holder tray. Dimensions are given in millimeters.

The holder was designed using the computer program Solid Edge and then transferred to the SLA Viper for building. The part was post-cured and the stereolithography part was

used directly in the system. Although stereolithography parts are typically used for prototypes as part of the design cycle, for some of the components in this system it was possible to use the parts directly from the stereolithography machine for our final pieces.

This holder was designed along with a metal tower and adjustable mount. Once the DMD array board was secured to the holder tray, the tray could be mounted to the metal adjustable mount (Figure 5.15). The design of this mount was quite important as it is what allows for the compensation of the mirror tilts, so that light may be directed downwards from the array.

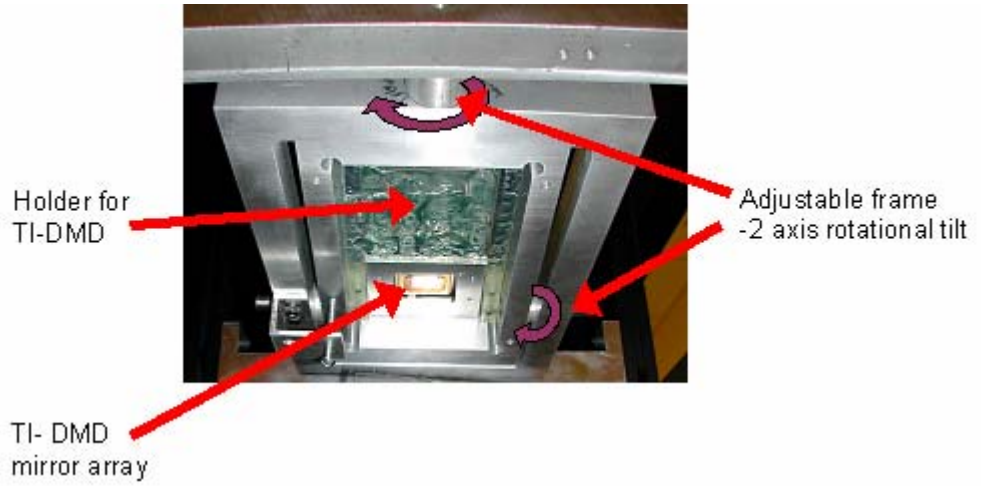

Figure 5.15: Photograph of TI-DMD held in the resin DMD holder which is supported in the metal, adjustable frame

The adjustable mount is then suspended in a large metal tower (Figure 5.16). The tower was designed so that the DMD would be held in a very stable manner, although it still allows for adjustments to be made in the height of the DMD.

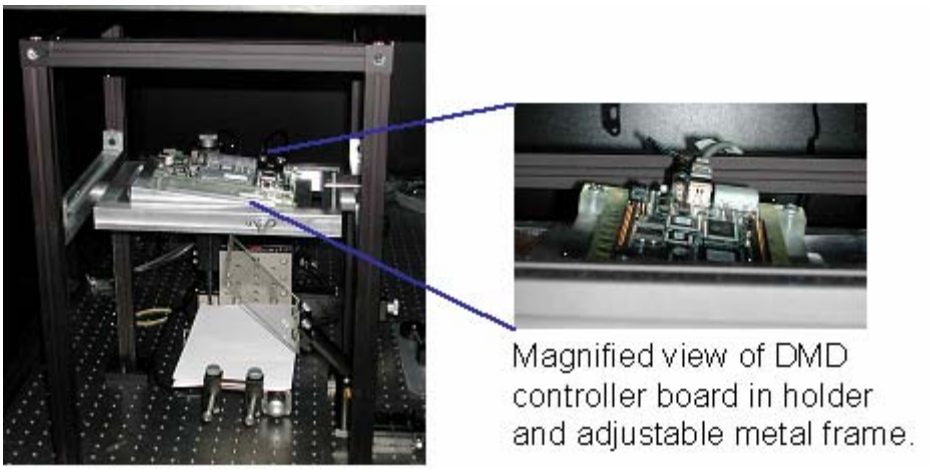

Figure 5.16: Photograph of DMD holder, adjustable frame and metal tower with a close-up view of the DMD controller board held in the tilted position.

Design of the Vat and Elevator for the Liquid Resin

The vat and elevator platform were designed and built on the SLA Viper. The design was not highly optimized, but rather quickly fabricated to allow for testing of the exposure system and the test resins. First, a small platform was built below the stages (Figure 5.17). It has a small cut-out in the back to allow for the passage of wires, and holes are tapped which align to mounting taps on the bracket holding the stages.

Figure 5.17: Photograph showing small, stationary platform mounted below the stages

Next, a vat was designed to sit on top of this platform, resting in the rectangular, recessed area. This vat is basically a small box, with a specialized lid (Figure 5.18). The free-radical polymerization of the experimental resins is highly sensitive to oxygen quenching. Thus, the box is designed to be capable of being flushed with an inert atmosphere, and/or sealed. The large square opening on the lid is designed to fit a small quartz window, allowing the passage of UV light. The two white taps on the lid and sidearm of the vat provide means to plumb a flow of inert gas.

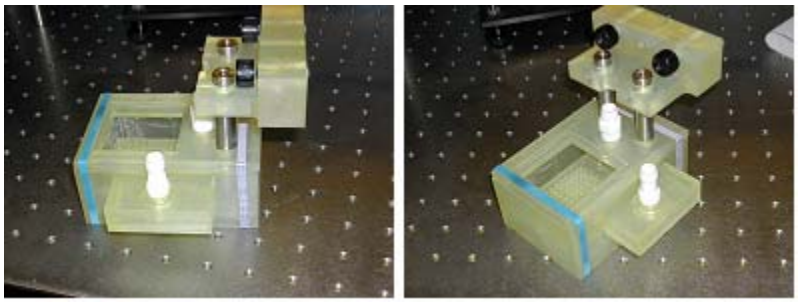

Figure 5.18: Photographs of the vat and stage, assembled with the lid on.

The vat is also designed with two holes to allow for the movement of the elevator platform within the vat. In the photograph on the right side of Figure 5.18, one can see a small perforated platform resting within the vat. This is the elevator platform. The two metal posts coming through the lid connect to the elevator platform, and through the resin piece suspended above in these photographs, connect to the motorized stages.

The fully assembled vat and elevator platform is shown in the next photograph (Figure 5.19). The vat is resting on the stationary platform and the metal posts connected

to the elevator platform are connected to the motorized stage (square block of grey metal with numerous tapped holes for mounting). In this photograph, one may also notice flexible black duct tubing. This provides ventilation directly to the fume hoods, as the acrylate resins can be quite volatile. Also, thin, flexible clear tubing is seen next to the vat, resting on the black metal post. This tubing plumbs nitrogen or argon, to provide an inert atmosphere in the vat.

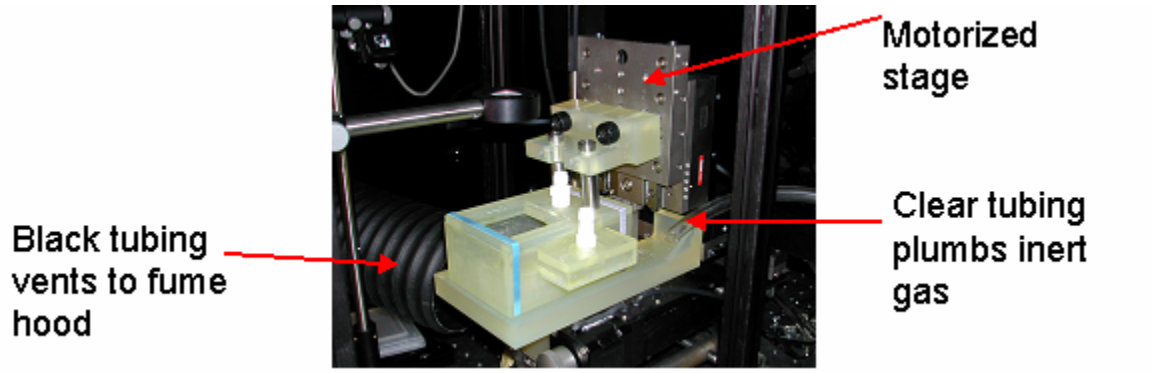

Figure 5.19: Vat and elevator platform, fully assembled.

Selection of Components

The overall system design was highlighted in the previous sections, with an emphasis on the components needed for holding and positioning the mirror array. This section provides a summary of the other main components used in the system.

Light Source

A 1000 Watt mercury-xenon arc lamp is the light source for this system. This component was chosen because it can provide a wide range of light, from infrared through ultraviolet. This range of light wavelength is important as it lends greater flexibility to the design and selection of resin components.

Light conditioning components: Water filter, collimating beam probe

It is necessary to use a water filter directly after the arc lamp to remove the infrared component of the light. This reduces part of the spectra that is responsible for a lot of the heating properties of light, and makes is safer to work with.

The collimating beam probe is used to collimate the light. This particular beam probe is designed for use with a fiber bundle. Initially, a fiber bundle was used to transport the light from the end of the water filter to the optical components further down in the train. However, the losses through the fiber bundle were too high, and the bundle was removed from this system. Instead, the light from the water filter directly enters the collimating beam probe, by using a small tube to connect the two pieces. The downside to this arrangement is that there is still a significant loss at this junction because of the decrease in aperture without focusing.

Shutter

The shutter choice was based on two main characteristics: shuttering speed and shutter aperture. Of course, the shutter also had to be able to handle the amount of light output from the lamp. After investigating several manufacturers, the 76994 shutter from Newport was chosen. This shutter has a large 25 mm aperture, and is capable of up to 40 Hz exposure frequency, making the minimum exposure time 25 ms. The manufacturer

gave assurances that the shutter would operate properly in front of the powerful arc lamp. However, this information proved to be false. The shutter was returned for repair, and the manufacturer claimed there were no issues with the shutter at all. After this repair, the shutter continued to malfunction, and a technical representative finally acknowledged that there could be problems associated with using the shutter in front of the arc lamp due to heating. Using several adapter plates, the shutter position was shifted further down in the optical train, increasing the distance between it and the lamp, and it has since functioned properly.

Filters

The filters in this assembly provide a way of delivering different wavelengths of light to the surface. Filters at 647 nm, 435 nm and 365 nm are available. Currently the filters are changed manually between exposures to produce different wavelength exposures. In the future a mechanical filter wheel could be used to fully automate the system.

TI DMD

Mirror arrays are widely used in many commercial devices, such as projectors and televisions, and the Digital Micromirror Device (DMD) from Texas Instruments (TI) was chosen by A. Limaye for his system. Likewise, we also chose to use a TI DMD, and selected one equipped for use with ultraviolet wavelengths. The UV DMD consists of 786,432 mirrors, in a 1024 x 768 array, as described earlier in this chapter. The recommended illumination by wavelength is shown in Table 5.1 below.

Table 5.1: TI DMD illumination specifications

Wavelength	Maximum recommended intensity
< 400 nm	0.68 mW/cm^2
> 800 nm	10 mW/cm^2

The TI DMD was selected as it is the most well-documented mirror array device, and the most economical. Of the DMD's available, we chose the one designed for use with UV wavelengths. This is important as it offers us greater flexibility in the photopolymerizable resin design. Using the UV DMD allows at least one of the two reactions to be catalyzed with UV light which is significant as many photo-active compounds are sensitive in the UV region of the electromagnetic spectra.

Stages

Stages are needed in this set up to move the elevator platform in the vertical plane (z) for building up each layer. Stages for movement in the horizontal plane (x/y) are also needed in order to stitch together several fields of view to make a larger part. That is, to make larger parts, the vat may be stepped in the horizontal plane, allowing for several projections to make a layer, similar to a mosaic art assembly (Figure 5.20). Without this, the maximum part size would be limited to the size of the projected image from the DMD. While one could use lenses to enlarge this projected image, the minimum feature size would be sacrificed. It should be noted that this image stitching/stepping routine would not necessarily be a difficult transition for use in tissue and cell studies. Current medical imaging often uses this same technique to create larger images from smaller scanned areas.

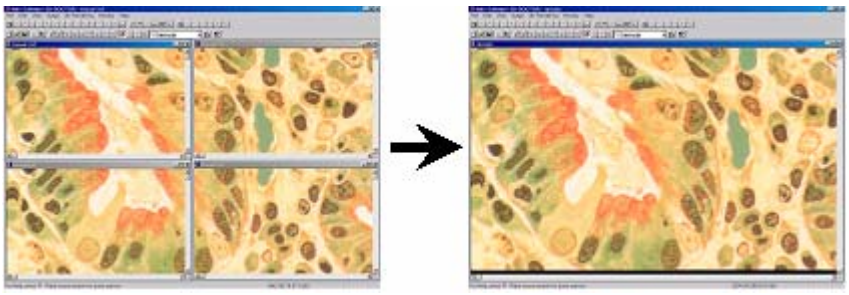

Figure 5.20: Example of image stitch used in medical imaging [10]

The stages for this set up were chosen on precision, accuracy and cost. The build height per layer was the critical minimum dimension. Ultimately, three linear encoded stages with 50 mm of travel were purchased from Thorlabs (LNR50SEK), along with the appropriate motor controllers. The glass scale encoder system provides 20 nm resolution, giving positional accuracy better than 3μm over the full 50 mm of travel, and the bi-directional repeatability is of the order of 100 nm.

Mirror and Focusing lenses

Only one of the two focusing lenses was purchased specifically for this application. The other lens was scavenged from optical components in the lab that were not currently being used. The small mirror directing light to the DMD was also an optical component already present in the lab.

The first lens (closer to the DMD) is a plano convex lens, with a 55 mm diameter and a focal length of 100 mm. This lens was chosen so that it would have large enough diameter to capture all of the light coming off of the DMD, and have a reasonable focal length for the small space. The second lens (closer to the stage and vat surface) is a 25 mm diameter plano convex lens, with a focal length of 85 mm that was found in the lab.

The first lens captures the light coming directly off of the DMD. Because of the physical dimensions of the mirror array, there is a significant amount of diffraction (Figure 5.21), and the second lens captures the diffraction pattern and re-focuses it into the image.

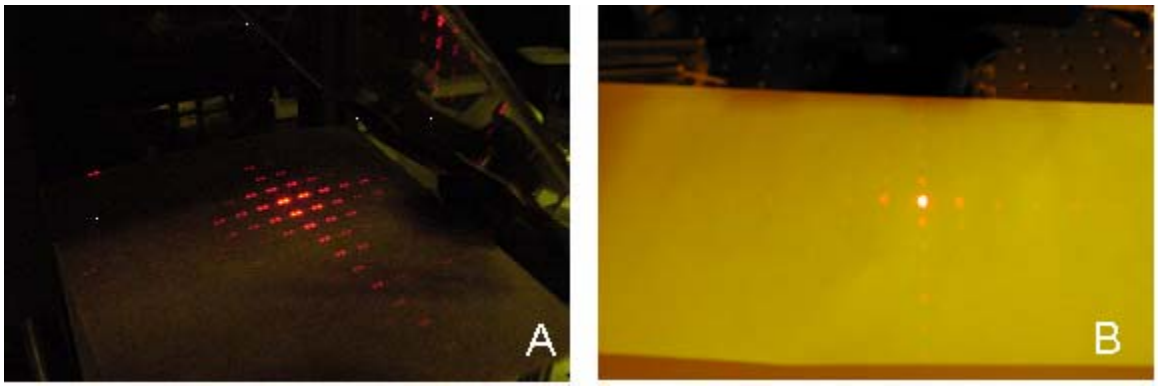

Figure 5.21: Diffraction pattern from mirror array on white paper without any focusing lenses. The array is illuminated by a red laser light and all of the mirrors are "on". This should result in a simple rectangle if focused; however, with no lenses the diffraction pattern is observed. A) Configuration 1: Notice 2 small spots in the diffraction pattern. This comes from the front and back side of the 45^{o} quartz. B) Configuration 2: Notice only 1 dot in the pattern.

SLA Performance

At first, it was difficult to obtain well focused images from the DMD, and there were issues creating images without a rectangular border. The rectangular border was quickly eliminated when we recognized that they were an artifact from the DMD design. That is, TI designed in a "pond of mirrors" (POM) that surrounds the active mirror array. The POM is six mirrors deep on all four sides of the array. These mirrors may be turned off, but are not capable of being turned on. Thus we realized that we were accidentally

capturing the “off” image as our projection. This was easily remedied by displaying the inverse of the images we had been using, and then capturing light from the other direction. With our custom DMD mount, this adjustment was not difficult.

The focusing of the DMD images was more tedious. The lenses were carefully placed by aligning test patterns. Then the exact DMD tilt angle was adjusted, and the lens position re-evaluated. In this manner, the test images slowly came into a very clear focus. Commercial photoresists were used in the focusing study to help visualize the exact light pattern on the imaging plane. Silicon chips were spin cast with AZ 4620 photoresist and exposed to light through the 365 nm filter. The chips were baked on a hot plate and the latent images were examined. The chips were then developed in AZ 421K developer and the resulting patterns were imaged under a light microscope. Figure 5.22 shows some of the results from these imaging studies.

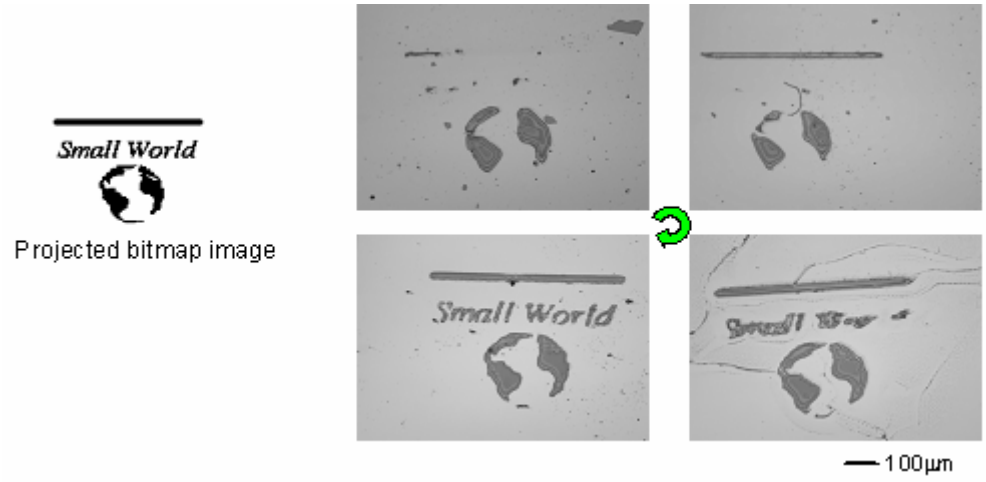

Figure 5.22: Focusing image through successive lens and mirror tilt adjustments. Photographs are of microscope pictures of AZ 4620 after exposure and development.

It was also necessary to measure the intensity of light at various wavelengths, at the plane of the mirror array, and at the focal plane. The intensity probe was set into a post, which was moved so that the probe head was at the mirror plane or the focal plane. The intensities were measured using a 365, 435, and 647 nm filters, as well as using the full beam without a filter (Table 5.2). These intensities are all within the limits set in Table 5.1, except for the full spectrum exposure that is slightly higher than the specification.

Table 5.2: Intensities of light at various wavelengths measured at the point of the mirror array and at the focal plane for part building.

Wavelength	Intensity at mirror array (mW/cm^2)	Intensity at focal plane (mW/cm^2)
365 nm	0.38	0.29
435 nm	1.59	1.55
647 nm	0.2	0.1
Full spectrum, no filter	11.74	7.64

It is possible with our system to resolve down to the single pixels, with about 5 um lines. The resolution images are shown in Figure 5.23. If one recalls the mirror size, this shows our system of lenses gives about a 50% image reduction. By choosing different lenses, one may reduce or enlarge the image as desired for different applications.

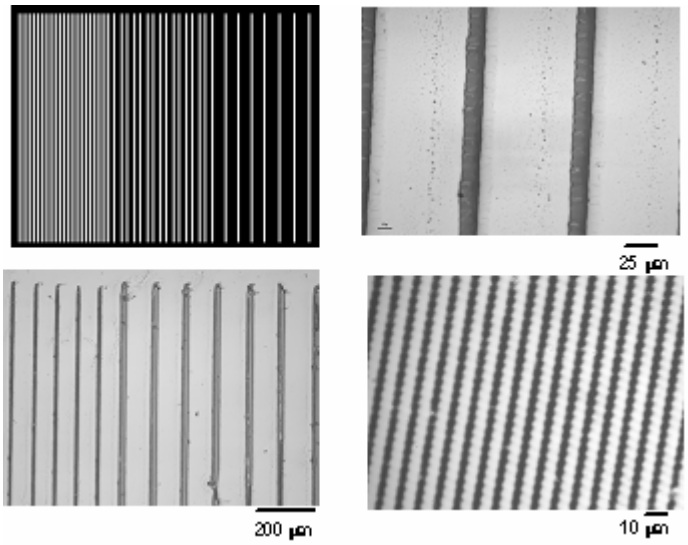

Figure 5.23: Top left is the test bitmap projected by the mirror array. The other three are microscope images showing the line width achieved.

To test the build capability in 3 dimensions, a very simple checkerboard pattern was used. A silicon wafer chip was placed on our elevator platform. The resin used was a test resin composed of tert-butyl acrylate, low viscosity trimethylolpropane triacrylate, Irgacure 2959 photoinitiator and Ciba 784 photoacid generator. The part was built with 10 layers, for a height of approximately 0.05 mm (Figure 5.24).

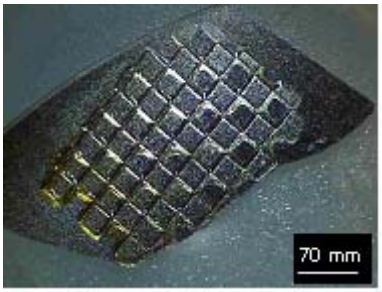

Figure 5.24: Simple part built using the vat system

System Automation

Ideally, this SLA system should run with minimum user intervention. This would allow a user to set up the images for the exposure, assemble the vat and elevator platform, close the optical box, and run the system just using the computer. The motorized stages, shutter and DMD mirror array have been programmed using LabView so that the images, exposure times, and z-height movements are completely automated. However, currently there is no motorized filter wheel, so that changing the wavelength of light must be done manually. Also, eventually the stages and mirror array could be programmed for a stitch function, so that larger parts may be built. The documentation for using the system and automating of the system are given in Appendix A.

Major Component List for SLA System

The Table 5.3 below presents the list of major components used to build the SLA system presented in this chapter, along with actual or estimated costs. Smaller items, such as screws, posts and holders are not included in this list. Some of the components were already in our lab, so not all prices and part numbers were available.

Table 5.3: Major components used to construct the SLA system presented

Quantity	Vendor	Part Name	Part Number	Cost
1	Tyrex Sales	TI UV-DMD		
1	Spectra Physics	Mercury Arc Lamp	1000W Hg(Xe)	Not available
1	Spectra Physics	Liquid water filter	6214	Not available
1	Edmund Optics	PCX Lens Dia: 50.8mm EF:100mm	G08-009	$177.00
1	Edmund Optics	50.8mm Lens Holder	U54-988	$51.10
1	Edmund Optics	Fused Silica Window 50.0 mm sq	G47-231	$110.00
1	Edmund Optics	Fixed Filter Mount 70-40 mm	G54-997	$65.00
1	Newport Corporation	25 mm aperture electronic fast shutter	76994	$693.00
1	Newport Corporation	Shutter driver	76995	$666.00
1	Newport Corporation	Male coupling ring	77829	fix
1	Newport Corporation	Flange: 1.5” male/2” female	66289	fix
1	Newport Corporation	2” Collimating beam probe	76597	$517.00
1	Newport Corporation	Fused silica focusing assembly	77800	$425.00
1	Newport Corporation	3-1 ½ inch step down adapter	66290	$135
3	Thor Labs	50 mm linear encoded TravelMax stage w/stepper actuator & controller	LNR50SEK	$5154/ea
8	Thor Labs	XE 25mm construction rails, 300 mm long	XE25L300/M	$13/ea
Pack of 10	Thor Labs	XE 25 low profile 2 nut	XE25T3/M	$8.50

Summary and Conclusions

Overall, this chapter presents the design, assembly and preliminary results for a mirror-array based stereolithographic apparatus that has the capability to do exposures at multiple wavelengths. Although the design is based on one built by A. Limaye [7], there is a significant difference in the alignment of the mirror array device. While this may seem an esthetic difference, it was designed to eliminate the need for keystone type corrections necessary in a system where the projected image is not perpendicular to the plane of focus. The resulting system is capable of exposing 5 μm lines, which is smaller than the size of an individual mirror due to reduction from the focusing lenses and the individual mirrors can be seen in the projected image as the jagged edges of the lines.

While this system shows a great deal of promise, there are still many aspects that can be optimized. To complete the automation of the system, an automatic filter wheel could be incorporated. This would allow the entire system to run in the closed optical box, without the need for an operator to occasionally change the filters. This is not only a more efficient method, but also a safer laboratory practice, as there is less risk of stray UV light which can cause injury. Also, further optimization of the three-dimensional build process should be done when a new resin is introduced. This includes finding the critical exposure dose and depth of penetration, and a simple procedure for this task is outlined in Appendix D. The optical train may be improved by small reconfigurations. For instance, step down adapters were used to connect some of the optical elements, without a focusing assembly in between. This means there is wasted energy, as the full beam is not being utilized. By focusing the beam before any of the step down plates, a more efficient use of energy can be achieved. Finally, the building of larger pieces may

be pursued once the stitching functions have been programmed into the mirror array and stages.

References

[1] P. F. Jacobs, *Rapid Prototyping & Manufacturing, Fundamentals of StereoLithography*, First ed. Dearborn, MI: Society of Manufacturing Engineers, 1992.

[2] M. Brain, "How Stereolithography (3-D Layering) Works," http://computer.howstuffworks.com/stereolith.htm, accessed May 2007.

[3] "M2 Systems Stereolithography," in *M2 Systems the forefront of product development*, http://www.m2-systems.com/prototyping/stereolithography.php, accessed May, 2007.

[4] "Rapid Prototyping and Manufacturing Institute Homepage," http://rpmi.marc.gatech.edu, accessed May 2007, Atlanta, GA, 2003.

[5] A. Bertsch, S. Zissi, J. Jezequel, S. Corbel, and J. Andre, "Microstereolithography using liquid crystal display as a dynamic mask-generator," *Microsystems Technologies*, pp. 42-47, 1997.

[6] C. Chatwin, M. Farsari, S. Huang, M. Heywood, P. Birch, R. Young, and J. Richardson, "UV microstereolithography system that uses spatial light modulator technology," *Applied Optics*, vol. 37, pp. 7514-22, 1998.

[7] A. Limaye, "Design and Analysis of a Mask Projection Micro-Stereolithography System," in *Mechanical Engineering*, vol. Masters. Atlanta: Georgia Institute of Technology, 2004.

[8] A. Limaye and D. Rosen, "Quantifying dimensional accuracy of a Mask Projection Micro Stereolithography System," presented at Proceedings of the Fifteenth Solid Freeform Fabrication Symposium 2004, Austin, TX, 2004.

[9] "Keystone correction," http://en.wikipedia.org/wiki/Keystoning, accessed May, 2007.

[10] "3D DOCTOR: Vector-Based 3D Medical Modeling and Imaging Software," http://www.ablesw.com/3d-doctor, accessed May, 2007: Able Software Corp., 2007.

CHAPTER 6

DEVELOPMENT OF A RESIN SYSTEM

Introduction

A critical component of any stereolithography (SL) system is the liquid photo-curable resin. These resins are composed of monomers or oligomers along with a photoinitiator. A variety of polymer properties, such as strength and flexibility, may be achieved by careful selection and formulation of these resin components. For the build system proposed in this thesis, there were three main considerations for the resin system. First, the resin must polymerize rapidly so that the part being built solidifies quickly. Second, the final polymer must be capable of undergoing a de-protection reaction when exposed to a specific wavelength of light, distinct from the wavelength used for the polymerization reaction. This requires that the resin system include a cyto-compatible photocatalyst, and a monomer or oligomer with a labile protecting group. Finally, the resin should be biodegradable, so that eventually one is left with only a functional tissue as the scaffold degrades. This chapter details these requirements and the formulation strategies that were employed.

Photopolymerizable Resin

Theoretical Considerations for Photopolymerizable Resin

The first requirement for the resin system is the essential property of all stereolithography (SL) resins; that is, the resin must be capable of undergoing rapid photo-polymerization. The rate of photopolymerization is important for SL, as the

reaction must occur rapidly to provide enough mechanical robustness to the 3D part as it is built so that it can survive the layer-by-layer writing and enable its handling when the writing process is complete. Also, for the second wavelength modification process, it may be difficult to incorporate conventional SL post-processing steps as they could disrupt the chemically patterned surface. Thus, it is especially important for this modified SL process that the initial polymerization events are rapid and complete.

Polymerization is "the process of joining together small molecules by covalent bonds", and there are many variations of this basic process [1]. This process is usually broken down into three essential stages: initiation, propagation and termination (Figure 6.1). These steps are illustrated below, using the polymerization of styrene to polystyrene as an example. When formulating a resin to be photo-curable, one needs to consider all three of these main steps.

The important initiation step sets the main requirements for the resin: a source of radicals and an unsaturated bond for the linkage to occur. For the experimental resin, radicals should only be present in certain areas where the part is to be built. In this case the part is to be built via light, so the initiators of choice are photo-radical initiators (PIs). There are two main requirements that separate this resin formulation from a commercial stereolithographic resin. First, the PIs must be as innocuous to cells as possible; and secondly, the PIs need to be sensitive to a wavelength of light that is distinct from the wavelength of light used for the photoacid generator. Previously, several groups have investigated PI with regard to cell toxicity [2, 3]. The first examines a series of photoradical initiators for use in whole cell encapsulation. The conclusion was that the

Irgacure 2959 initiator was the most cytocompatible and the Irgacure 651 was the least [2]. A second study reinforces these conclusion for a variety of cell lines [3].

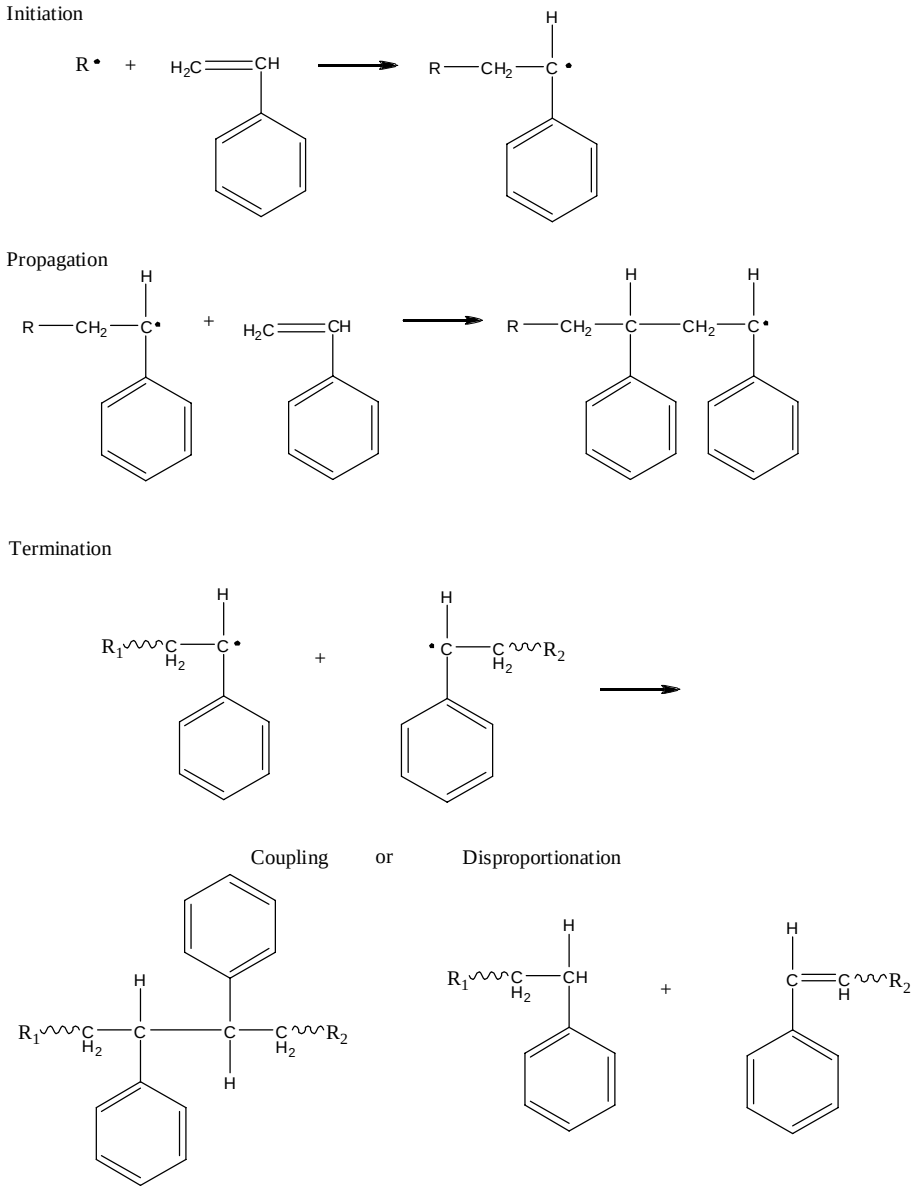

Figure 6.1: Free Radical Polymerization of Polystyrene

The simplest type of unsaturated bond is a carbon-carbon double bond, or vinyl group. Acrylate monomers contain a carbon-carbon double bond which is directly connected to a carbonyl carbon, and thus are a type of vinyl monomer. Figure 6.2 below illustrates the vinyl and acrylate groups.

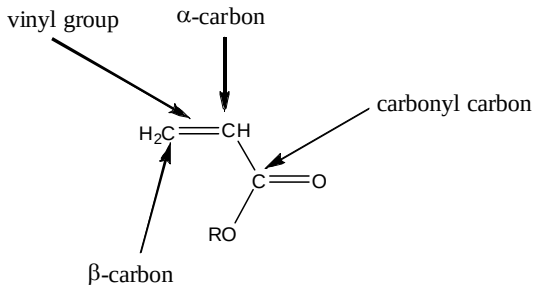

General acrylate structure

Figure 6.2: Chemical structure of acrylates

Acrylic monomers are commonly used in stereolithographic applications. Although the vinyl and acrylate groups only differ by the carbonyl carbon group, the acrylate functional groups generally polymerize much more rapidly [4] which is a great advantage for a SL resin system. For this reason, the main components of the test resin will contain the acrylate functional group for the polymerizable linkage.

Finally, the polymerization reaction should not terminate prematurally. In free-radical polymerization, assuming there is an adequate source of radicals, the main concerns are mechanisms that may inhibit the growing chain from reacting with another monomer unit. An important attribute of stereolithographic resins which avoid this problem is that there is no solvent present to dilute the system. In dilute systems,

growing chains will have lower probabilities of encountering reactive units, and this can limit the extent of reaction. The formulation under development, as with commercial SL resins, will be composed of only reactive units and inititators.

Formulation Strategy for Photopolymerizable Resin

The acrylate linkage was chosen for the main photo-polymerizable linkage as it rapidly undergoes free-radical polymerization [4] and is commonly used in stereolithographic applications [5]. In addition, acrylate polymers are already in use in several medical applications such as contact lenses and bone cements [6]. This linkage will be present in the primary protected monomer unit which will make the protected polymer, as well as a multifunctional cross-linking monomer which will confer structural integrity to the final polymer product.

For the PI, there were two major concerns; the possible toxicity to the cells and the overlap in absorption with the PAG. While the Irgacure 2959 initiator has been shown to be the least toxic 365 nm PI [2, 3], this wavelength has a greater possibility of overlapping with the sensitivity wavelength range for the PAG. The plots below show the absorption spectra for the most cell-compatible PIs and for commercially available initiators and PAGs.

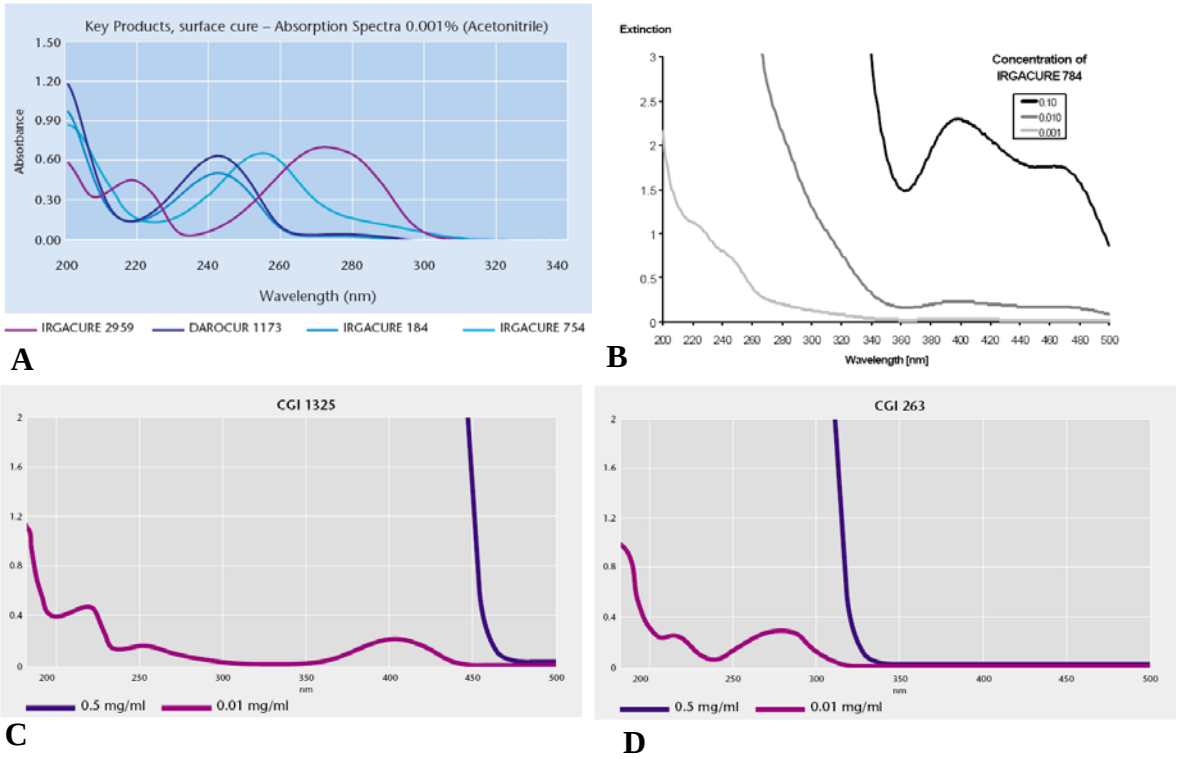

Figure 6.3: Absorption spectra of selected initiators and photoacid generators from Ciba Chemicals all taken in acetonitrile. (A) Initiators 2959, 1173, 184 and 754 (B) Initiator 784 (C) Photoacid generator 1325 (D) Photoacid generator 263

One may notice in the Figure 6.3 plots that the main absorption range for the Irgacure 2959 (Plot A, purple line) is in the 250-300 nm range, which overlaps directly with both the CGI 1325 and CGI 263 PAGs at higher concentrations. The overlap between CGI 1325 and Irgacure 2959 may be minimized at very low concentrations of 1325, however it is not desirable to have this constraint in the formulation. By comparison, the Irgacure 784 inititator has a large absorption range from 380 to 480 nm, which overlaps with the CGI 1325 but is completely distinct from the CGI 263 at any concentration. While it is true that the low wavelength absorption of the CGI 263 does overlap with the 784 absorption, this should not be an issue as long as the photoinitiation event precedes the photoacid generation event. For this reason, the combination of the

Irgacure 784 initiator with the CGI 263 PAG was chosen. It should be noted that the CGI 263 was also shown to be the least toxic PAG in Chapter 2.

Protection Chemistries

Theoretical Considerations for Chemical Protection

The next major characteristic for this resin formulation is that the final polymer must contain a protection group that may be cleaved, changing the surface energy of the material. There are many ways one may approach this design aspect. First, one may consider the group that is to be exposed once the protection molecule is removed. Then, of course, there are a variety of molecules that may be used as the protecting entity.

From the two dimensional cell studies, two simple hydrophilic groups were studied: the hydroxyl (-OH) group and the carboxyl (-COOH) group. The hydroxyl and carboxyl groups were chosen for their relative simplicity and because of the analogy between polyhydroxystyrene and tissue culture treated polystyrene. Analysis of tissue culture treated surfaces demonstrates that both carboxyl and hydroxyl groups are present, and the blocking of the hydroxyl groups reduces cell adhesion [7]. It should be noted that while the carboxyl group is somewhat similar to the hydroxyl group, it also confers a charge to the material. Other studies in literature have shown that the charge of a material is just as relevant to directing cell adhesion as surface energy [8]. Thus, the protection of these two groups was considered in the design of this resin material.

For this design, the protecting group must be capable of being removed in acidic conditions, near room temperature. As one may recall, the mechanism of the chemically amplified resist relies on a photoacid generator (PAG) which upon exposure to UV light

creates a highly acidic local environment, and typically a post-exposure bake step is required to catalyze the de-protection reaction. For this resin, that is to be polymerized and de-protected in the stereolithographic apparatus vat, it is difficult to apply the post-exposure bake step. Thus, it is preferred that the protecting group be labile, under acidic conditions, at temperatures close to ambient conditions.

Fortunately, there are a large number of protecting chemistries that have been studied for both the hydroxyl and carboxyl groups [9]. Two general protection reactions were selected based on the ease of the synthetic routes, and the low energy requirement for de-protection.

Formulation Strategies for Chemical Protection

As stated earlier, there are several protection chemistries that meet the criteria of being acid labile, at relatively low temperatures. Those tested here include protection of the hydroxyl group with 1-ethyoxyethyl ether (EE), tetrahydropyranyl (THP), and the protection of the carboxyl group with THP and methoxymethyl ester (MOM).

The first monomer considered for the main portion of the resin was 2-hydroxyethyl acrylate. This is one of the simplest monomers containing both the acrylate functional group for rapid polymerization, and a hydrophilic hydroxyl group that should be amenable to cell adhesion (Figure 6.4).

Figure 6.4: Structures of general acrylate and 2-hydroxyethyl acrylate

In order for this monomer to be useful in our resin formulation, the hydroxyl group must be capped with a low-activation energy, acid-labile protecting group.

One of the well characterized protecting groups that meets these criteria is the EE. Using the preparation suggested in Greene's Protective Groups [9], the following reaction was attempted (Figure 6.5).

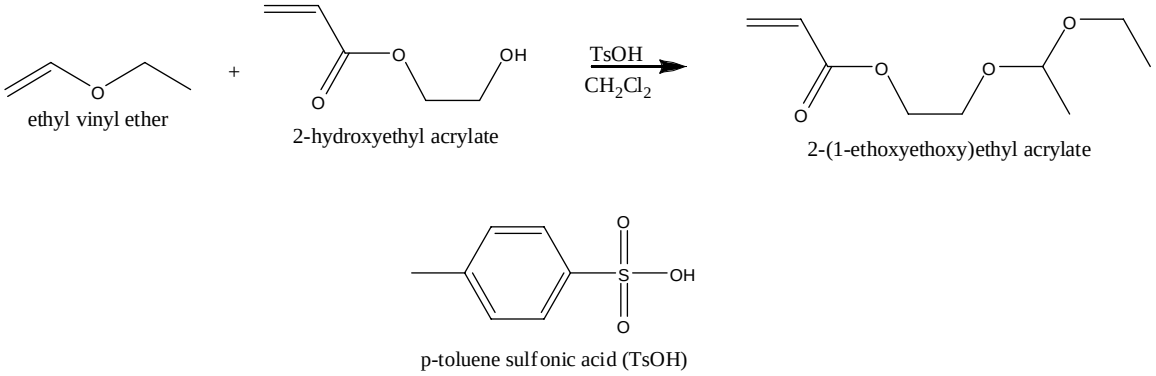

Figure 6.5: Reaction scheme for protection of 2-hydroxyethyl acrylate with ethyl ether

Unfortunately, the resulting product was a very dark red colored liquid, which suggests that a conjugated product was formed. Additionally, the H-NMR of the product was run

by M. Romeo, and shows a very noisy spectrum that was very difficult to evaluate and does not show the expected spectrum for the product (Figure 6.6).

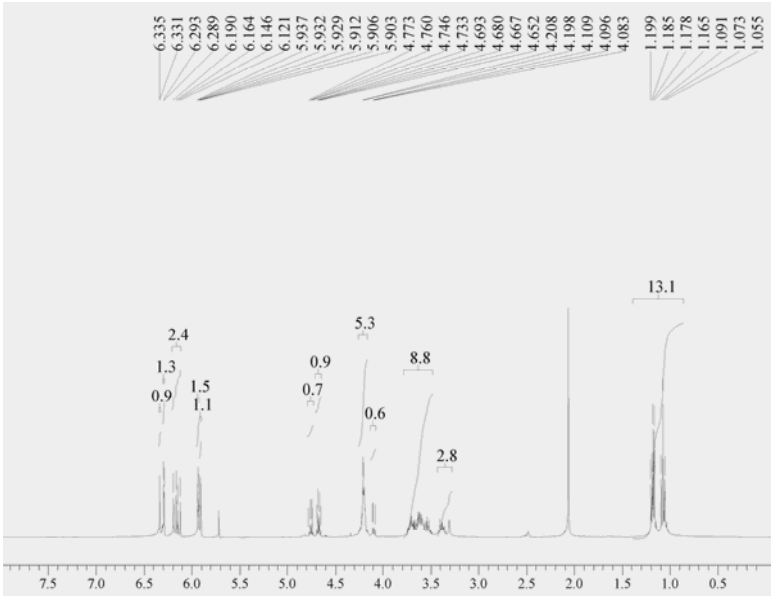

Figure 6.6: NMR Spectra for reaction product from protection of 2-hydroxyethyl acrylate with ethyl ether

Thus, this synthesis route was not pursued further. The details of this reaction preparation are given in Appendix C.

The second reaction that was attempted was protection of 2-hydroxy ethyl acrylate with tetrahydropyranyl (THP), shown in Figure 6.7. This reaction is shown below and the preparation is by Miyashita, Yoshikoshi, and Grieco [10] which is referenced Greene's Protection Groups [9].

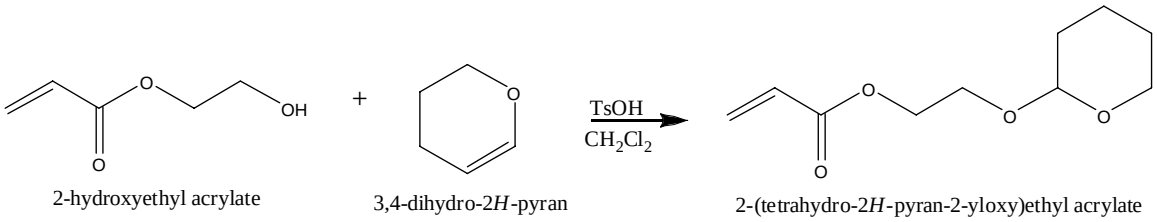

2-hydroxyethyl acrylate 3,4-dihydro-2*H*-pyran 2-(tetrahydro-2*H*-pyran-2-yloxy)ethyl acrylate

Figure 6.7: Reaction scheme for protection of 2-hydroxyethyl acrylate with tetrahydropyranyl (THP) group

This reaction yielded a pale yellow liquid, and the H-NMR of the product verifies that the reaction was successful (Figure 6.8 and Table 6.1).

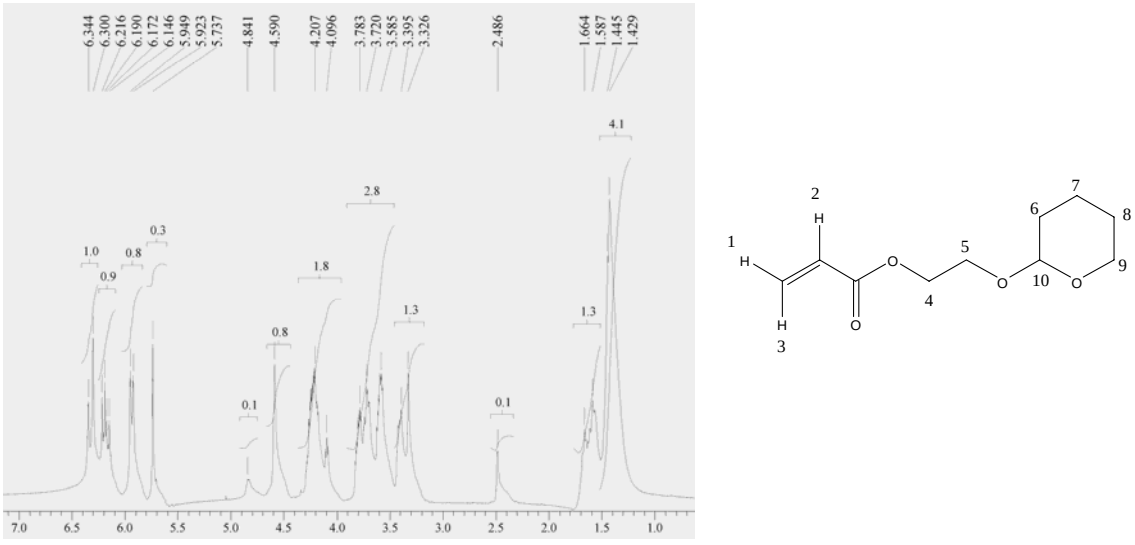

Figure 6.8: H-NMR Spectra of reaction product from 2-hydroxyethyl acrylate protection with THP and desired product with hydrogens labeled

Table 6.1: Hydrogen peak assignments for H-NMR spectra in Figure 6.8.

Hydrogens	Peak shift positions
1, 2, 3	Peaks from 6.3-5.9 that integrate to 1.0, 0.9, 0.8
4	Peaks around 4.2-4.0 that integrate to 1.8
5, 9	Peaks around 3.7-3.3 that integrate to 2.8 and 1.3, for a total of 4.1
10	Peak at 4.59 that integrates to 0.8
6, 7, 8	Peaks around 1.7-1.4 that integrate to 5.4
Small peaks at 2.486, 4.841, and 5.737 are likely from unreacted hydroxyethyl acrylate.	

The reaction product from this THP protection was further analyzed for its protection characteristics. Two resin solutions were compared. The first solution was composed of hydroxyl ethyl acrylate with 1% by weight photoinitiator Ciba 784, and the second was composed of the reaction product with the same amount of the same photoinitiator. Each sample was carefully coated onto a silicon chip and placed in a special exposure box which allows the sample to be kept in a sealed environment during the exposure. The box was connected to a nitrogen cylinder, and a quartz lid was placed on top. The samples were then exposed to UV light at 435 nm for 60 seconds, for a dose of about 1000 mJ. Fourier transform infrared spectroscopy (FTIR) scans were run on each material using the attenuated total reflection (ATR) cell as the films were quite thick. The resulting spectra are shown below in Figure 6.9.

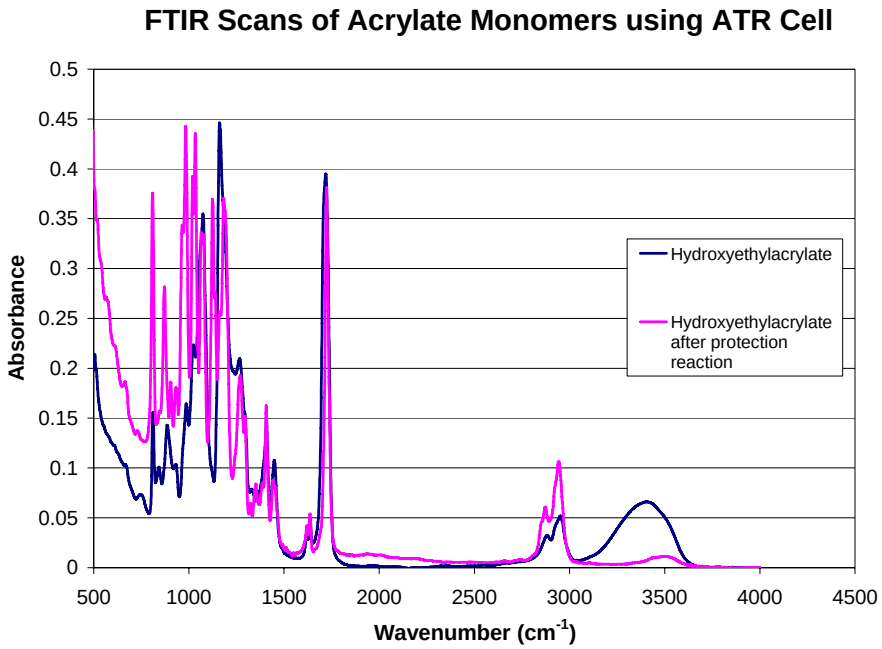

Figure 6.9: FTIR Spectra of Hydroxyethyl acrylate, before and after protection reaction

As one may notice, the scan taken after the protection reaction shows a much smaller peak at 3500 cm^{-1}. The hydroxyl group is known to give a strong peak at 3500 cm^{-1} so this is a clear indication that the protection reaction was nearly complete.

However, the homopolymerization of both the protected and un-protected hydroxyl ethyl acrylate yielded a soft gel, not a hard polymer. Thus, mixed resin formulations were attempted. The idea was that by including a tri-functional acrylate that can act as a crosslinker, a hard polymer could be obtained from the photopolymerization reaction.

Also, the de-protection reaction of the protected polymer was to be tested. Thus, a photoacid generator (PAG) was also included in this resin formulation. The resulting mixture was composed of 325 mg SR 351 LV (trimethylolpropane triacrylate, a

trifunctional acrylate monomer), 560 mg THP-protected hydroxyl ethyl acrylate product, 56 mg of 784 photoinitiator, and 56 mg of 263 PAG. This resin was again tested by photopolymerization on a silicon chip, in the exposure box with an inert nitrogen environment. The chip was first completely exposed to about 1000 mJ of light at 435 nm. Then a black piece of metal with a square cut out of the center was laid on top of the quartz, acting as a mask. The chip was exposed to about 1000 mJ of the full spectrum of UV light from the mercury arc lamp. A post-exposure bake was performed at 100^{o}C for 20 seconds, to fully catalyze the de-protection reaction and to evaporate any un-reacted monomer on the wafer surface. The FTIR scans of the region outside of the square (only exposed to 435 nm) and the region inside of the square (exposed to the full spectrum) are shown below in Figure 6.10.

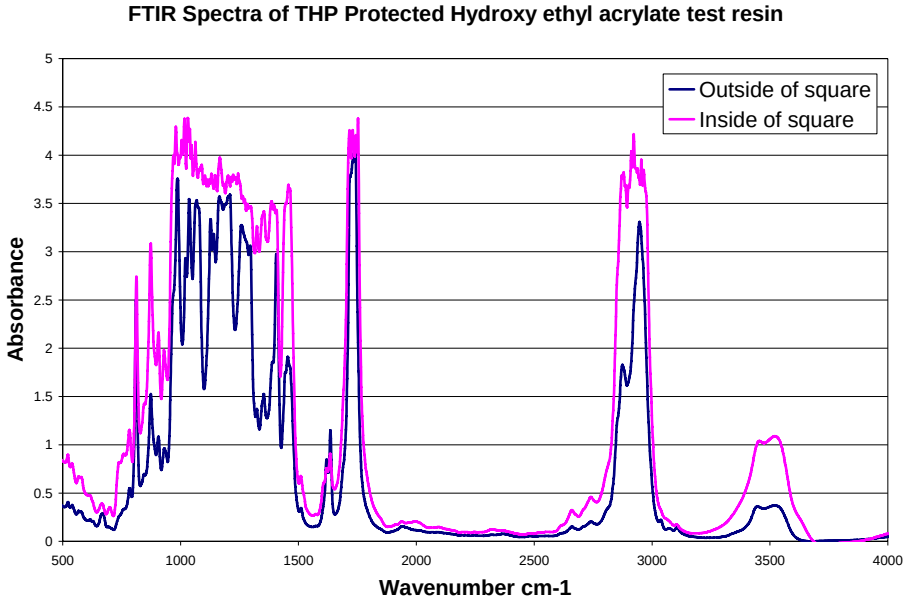

Figure 6.10: FTIR Spectra comparison of test resin in single and double exposed areas

Although the FTIR spectra are noisy, this test was very promising. Again, the hydroxyl group is expected to exhibit a strong peak at 3500 cm^{-1}, and this peak is much stronger in the scan taken in the region inside of the square, which was exposed twice.

With the promising FTIR data, cells were seeded on this sample, however no cell patterning was observed. Briefly, the sample was placed in a Corning Ultra-Low attachment dish with regular serum-containing DMEM media, and the cell suspension was added. After 1 hour of incubation, the media was removed, the chip was washed with DPBS with calcium and magnesium, and fresh serum-containing DMEM was added. This plating was done concurrently with a 2-dimensional polymer study where it was found that carboxyl groups were much more effective at defining cell patterns than hydroxyl groups. Thus, although this resin formulation seems promising chemically, the cell studies suggest that using a resin with a protected carboxyl group would be much more effective.

As the THP protection results showed promise, the next protection reaction that was attempted was a THP protection on methacrylic acid. Structurally, methacrylic acid resembles the hydroxyl ethyl acrylate, in that they are both simple monomers capable of free radical polymerization through the acrylate group. However, in this case, instead of an alcohol group, a carboxylic acid group is present. The desired reaction is presented below in Figure 6.11.

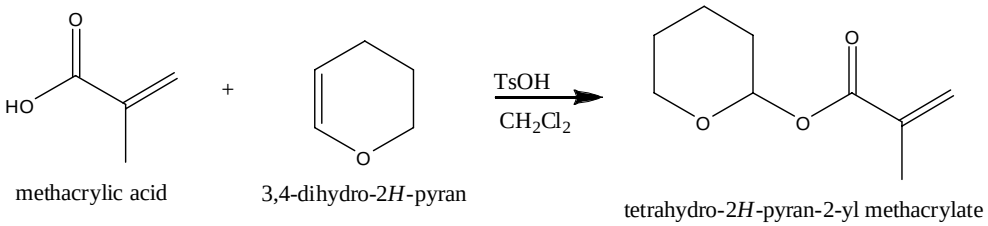

methacrylic acid 3,4-dihydro-2*H*-pyran tetrahydro-2*H*-pyran-2-yl methacrylate

Figure 6.11: Protection reaction of methacrylic acid with THP ether

This reaction was run twice, using two slightly different procedures. Both reactions yielded a highly viscous gel, suggesting that polymerization occurred, instead of only the protection reaction. The H-NMR data obtained, while inconclusive, also suggest that perhaps a polymer was made. Thus, although the THP protection was quite favorable for the hydroxyl acrylate, this route was not pursued further for the methacrylic acid. The details of the reaction procedure are in Appendix C.

The next reaction attempted was the protection of the methacrylic acid with the methoxymethyl ester group (MOM). The MOM group is also well characterized for use in protecting –OH groups on carboxylic acids. This group is also acid-labile and has comparable activation energy requirements to the THP group [9]. Of most importance synthetically, the reaction used to introduce the MOM group to the methacrylic acid is not an equilibrium based reaction. Thus, it should run until all of the reactive groups are depleted, meaning a fully protected monomer sample should be attainable. The desired reaction is shown below in Figure 6.12.

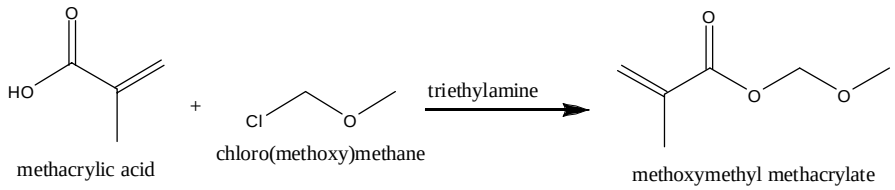

methacrylic acid chloro(methoxy)methane methoxymethyl methacrylate

Figure 6.12: Protection reaction of methacrylic acid with methoxymethy ether

The first time the reaction was run, two phases were obtained: a heavier dark red liquid and a lighter pale product. H-NMR verifies that the pale phase contained the desired product, along with ethyl acetate which is residual solvent (Figure 6.13).

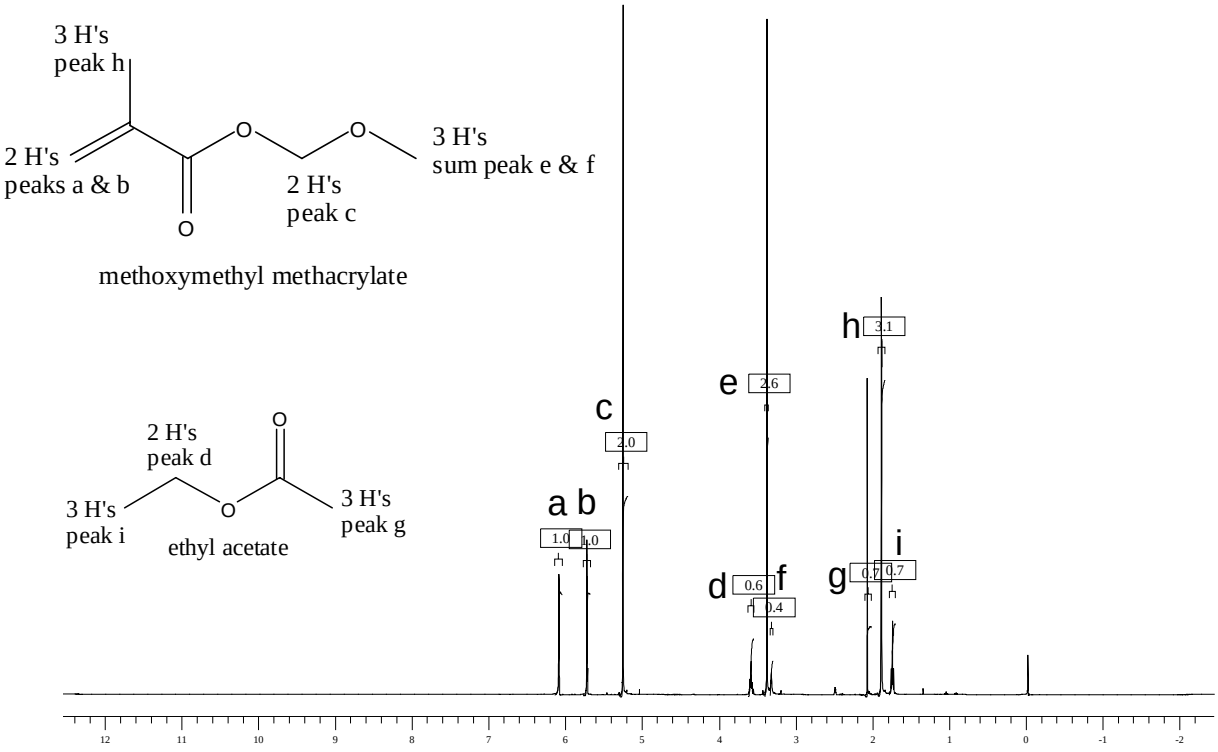

Figure 6.13: H-NMR Spectra of reaction product and residual solvent from methacrylic acid protected with methoxymethyl ether group with structures identifying the hydrogen atoms

Additional purification by simple distillation yielded a relatively pure product. When comparing Figure 6.14 to Figure 6.13, the peaks associated with the solvent, I, D, and G are no longer present. The H-NMR on the dark phase, Figure 6.15, seems to indicate that

polymerization occurred due to the large peak integrating to 10, suggesting a long chain of identical hydrogens. Obviously, this product is undesirable for this study.

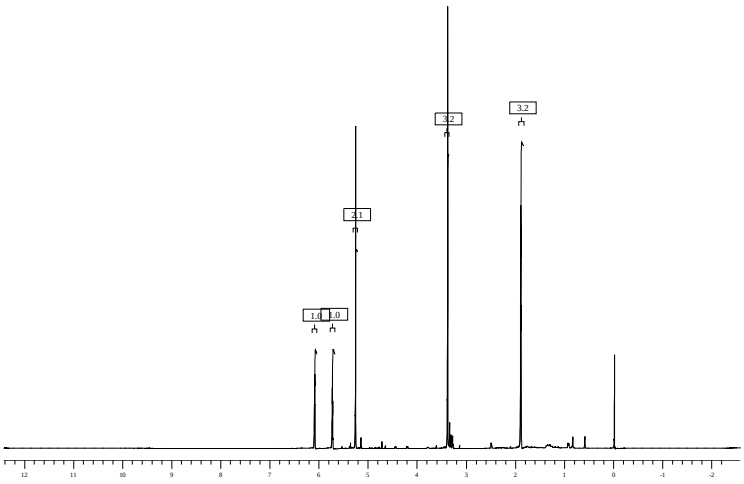

Figure 6.14: H-NMR Spectra for purified product from reaction of methacrylic acid protected with methoxymethyl ether

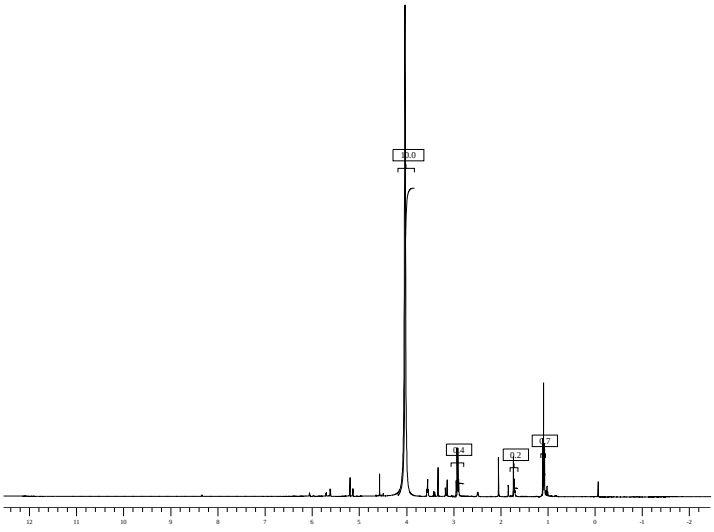

Figure 6.15: H-NMR spectra of dark phase reaction product of methacrylic acid protected with methoxymethyl ether

This reaction procedure comes from a paper by Ueda [11] referenced in Greene's Protection Groups [9], and is detailed in Appendix C.

This reaction product was then tested for polymerization and de-protection. For comparison, the unmodified methacrylic acid was made via free radical solution polymerization. A test resin was made with 200 mg of MOM-protected methacrylic acid (130 g/mol), 200 mg of SR 351 LV tri-functional acrylate (296.32 g/mol), 10 mg of 263 PAG and 10 mg of 784 initiator. The sample was coated onto a glass cover slip and exposed to 1000 mJ of 435 nm light in the exposure box while blanketed with nitrogen. The sample was then exposed to about 1000 mJ of the full spectrum of UV light. The contact angle was measured on the samples, and then they were plated with cells. A comparison of the contact angles of the protected polymer and the methacrylic acid polymer indicate that the de-protection reaction was not successful at the surface of the polymer (Figure 6.2).

Table 6.2: Water contact angles for polymethacrylic acid and protected methacrylic acid resins that have been polymerized and fully exposed to generate acid

Sample	Average Water Contact Angle
Poly(methacrylic acid)	40.5^{o}
MOM-protected MA resin	99.75^{o}
MOM-protected MA resin fully exposed	90.1^{o}

A cell seeding test was run on these samples as well. As with the THP-protected hydroxyacrylate, the samples were placed in a Corning Ultra-Low attachment plate with regular serum-containing DMEM media, and the cell suspension of 15×10^4 cells/ml was added. After 1 hour of incubation, the media was removed, the chip was washed with

DPBS with calcium and magnesium, and fresh serum-containing DMEM was added. The samples were imaged under white light and did not show any clear cell patterning. By comparison, cells grew and spread well on the control surface and on the unmodified poly(methacrylic acid). Representative images are presented in Figure 6.16.

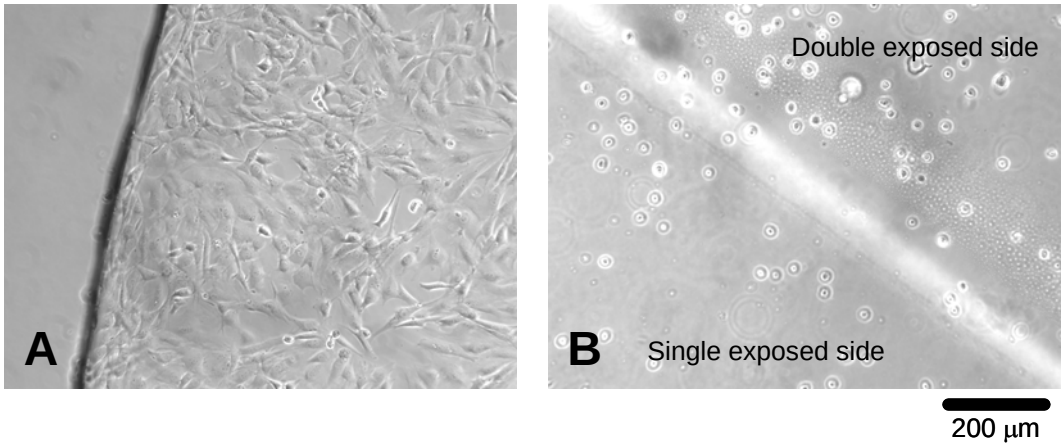

Figure 6.16: Images from light microscope of fibroblasts on (A) poly(methacrylic acid) polymer and (B) Photopolymerized test resin with MOM-protected methacrylic acid monomer, trifuctional acrylate monomer, 784 initiator and 263 PAG. Single exposed surface should be fully protected methacrylic acid and double exposed should be a de-protected surface due to acid generation.

This suggests that the base polymer is a good starting substrate, but difficulties with the deprotection of the carboxylic acid at the polymer surface resulted in poor cell patterning. In addition, there may have been toxicity issues with the photopolymerized samples. Preliminary studies indicate that residual monomer may become trapped in the photopolymer and leached out when bathed in media. These samples were added directly

to the cell media, without a post-cure or wash step, and may have certainly contaminated the cell environment.

Several sets of experiments may be run to determine the exact cause of the patterning failure. First, one should address the chemical de-protection reaction. The water contact angle data indicates that this de-protection was not successful. Broadly, there are three main situations which may have caused the failure of MOM-MA test resin to de-protect. First, the generation of the acid from the PAG molecule may have been inhibited in some manner, thus limiting the extent that the de-protection reaction may occur. Secondly, the de-protection reaction may have been inhibited in some manner, even though there is sufficient acid present. Last, both of these required reactions may have worked well; however, the resin formula may need to be optimized. For example, if too much crosslinker is present, the change in hydrophilicity due to the de-protection reaction may be masked by the hydrophobicity of the crosslinker. However, this scenario is unlikely, as the two monomers were used in equivalent mass loadings, which gives a molar ratio of about 2.3 moles of MOM-MA per mole of SR 351 LV in the final polymer due to the differences in molecular weight. Literature on the hydrophilic nature of methacrylic acid suggests that incorporation of methacrylic acid does significantly lower water contact angles. One paper sites that incorporation of 5-20% methacrylic acid into a control polymer gradually lowered the contact angle from 25^{o} to 18^{o} [25]. This change of 7^{o} in an already hydrophilic system suggests that in this test resin (with a 2:1 ratio of methacrylic acid to SR 351 LV) should demonstrate a much larger contact angle change if indeed the MOM protecting group is fully removed from the surface. Thus, this hypothesis for the failure of MOM-MA to de-protect is the least likely.

To address these hypotheses, the following experiments may be run.

- Acid generation from the PAG fails
    - add pH indicator to resin and run test exposures
- De-protection reaction is inhibited
    - Need for post-exposure bake
        - Run test exposures and after de-protection reaction bake samples on hotplate
    - Exposure box is too dry—de-protection reaction requires small amount of atmospheric water
        - Run polymerization reaction in the N_2 blanketed box environment and remove sample from box for de-protection reaction
    - Crosslinked polymer inhibits the re-generated acid molecules from finding another reaction to catalyze—only small amounts of local de-protection
        - Run de-protection reaction before polymerization reaction. Note that a new PI/PAG combination may be needed because of wavelength overlap (see Figure 6.3).
    - De-protection reaction at the surface is inhibited, perhaps by presence of base in the atmosphere. Base should not be present in the cleanroom atmosphere because base scrubbers are in use. However, the N_2 blanket box has a purge stream of N_2 from a liquid N_2 tank, which can have trace contaminants of base.
        - Compare samples that are de-protected in the N_2 purged box to samples where the de-protection is run outside of the box

        - Compare the IR spectra of samples using a bulk method (transmission mode in the main chamber) to using a surface method (ATR cell or grazing angle)
- All reactions work well, but formula is not well balanced between the amount of multifunctional crosslinker and protected monomer
    - Make several test resins, varying the ratio of protected monomer to crosslinked monomer

Once the chemical reaction is verified, the cell seeding experiments can be run again. It is possible that this step may still fail, even with a good contact angle change and full de-protection. In this instance, the polymer post-processing steps should be examined and optimized. For example, un-reacted monomers may be trapped in the crosslinked polymer, and leach into the cell media environment. The suggested post-processing steps to examine would be a post-cure, to insure there are no un-reacted molecules left in the system, and a wash step to remove any foreign materials.

Degradable Linkage

The last characteristic to be incorporated into this test resin is that the final polymer should be degradable. In the general tissue engineering scheme outlined earlier, one may recall that the final step in the sequence is the degradation of the tissue engineering scaffold, leaving behind only a functioning tissue (Figure 1.1). A straightforward way for this to be incorporated into the design is to include a degradable crosslinking molecule into the resin.

Degradable polymers have received much attention and study due to their great functionality in a wide range of applications such as drug delivery, suture materials, and packaging for consumer goods [6, 12, 13]. It should be noted that there are many terms used to indicate that a material will degrade in a living system. Here, the use of these terms will follow the definition by the Consensus Conference of the European Society for Biomaterials [14]. In this case, biodegradation refers to a degradation event where a biological agent, such as an enzyme or microbe, is the primary component of the degradation process. By contrast, a bioerodible polymer is "a water-insoluble polymer that is converted under physiological conditions into water-soluble material(s) without regard to the specific mechanism involved in the erosion process" [6]. For this resin formulation, one may use biodegradable or bioerodible linkages, as long as they are capable of being incorporated into the final polymer.

Theoretical Considerations for Degradable Linkages

Many degradable polymers have been studied for use in biomedical applications. Some of the major degradable polymer types include polyesters, polylactones, and polyanhydrides. By far, the most widely studied and used are the polyesters. These include poly(lactic acid), poly(glycolic acid), and their co-polymers which have a long history of use as a biodegradable material [12] in applications such as sutures, fracture fixation devices and cell scaffolds [15]. Polycaprolactone is a commonly studied polylactone with a long degradation time of two to three years; however, blends and co-polymers of this material have been developed to increase the degradation rate [16]. Polyanhydrides have been studied often as a degradable polymer for the application of drug delivery [17]; and although their mechanical properties typically limit their use in

load-bearing applications, researchers have developed blends and crosslinkable systems to broaden their use [18, 19]. In addition, polycarbonates and polyorthoesters have been investigated for use orthopaedic applications, and even polymers not typically biodegradable such as polyurethanes and polyphosphazenes have been modified to render them biodegradable. Overall, there are a large number of degradable polymers and linkages that could be incorporated into an SL resin. Table 6.3 shows these common synthetic degradable polymers used in biomedical applications.

Table 6.3: Common synthetic degradable polymers

Polymer	Structure	Degradation products	Biocompatibility
Poly(lactic-co-glycolic acid)	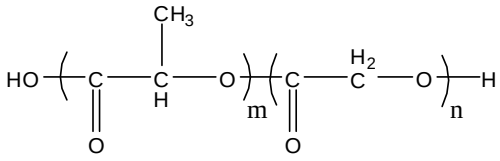 Chemical structure of PLGA polymer. The "m" portion represents lactic acid and the "n" portion represents glycolic acid.	Glycolic acid, lactic acid	Acceptable biocompatibility, some concern for acidic degradation products. Biodegradation by hydrolysis.
Poly(caprolactone)	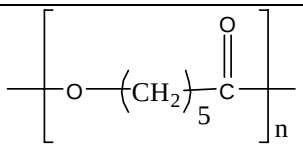 Poly(caprolactone)	Caproic acid	Generally considered non-toxic and tissue compatible
Polyanhydrides	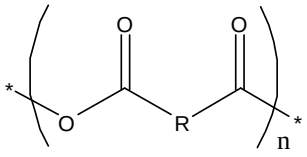 General polyanhydride structure	Dicarboxylic acids	Biocompatible with well defined degradation rates. Degrades by hydrolyixx of anhydride bond.

To incorporate the degradable linkage, the molecule must contain unsaturated bonds where linkages may form so the group is imbedded in the polymer chains. As discussed earlier, the simplest unsaturated bonds include the vinyl and acrylate functional groups. This method of incorporating degradable properties into a polymer has been investigated previously by others. For example, many acrylate end-capped molecules have been studied for the purpose of synthesizing degradable polymers. The Anseth group has studied dimethacrylated anhydride monomers that can react to form cross-linked degradable networks [20], the Mikos groups has investigated poly(propylene fumarate)-diacrylate macromers [21], and Matsuda and Mizutani have used acrylate capped poly(caprolactone-co-carbonate) molecules [22].

While using a di-acrylated degradable monomer would be ideal for this resin system, it would require the synthesis of these specialized monomers. Thus, for the initial proof of concept, a commercially available, di-vinyl degradable monomer was chosen.

Formulation Strategy for Degradable Linkages

The degradable linkage chosen was the simple diallyl fumarate molecule, as shown in Figure 6.17. The two vinyl bonds provide the capability for crosslinking, and the fumarate ester is hydrolysable. Recent literature has shown interest in a related polymer, poly(propylene fumarate). The use and degradation of this polymer has been studied for photo-crosslinking injectable polymer systems [23], akin to an SL resin but using longer oligomeric components instead of monomers. Also, while a mild inflammatory response was noted initially, this polymer does not demonstrate an undesirable long-term inflammatory response when implanted in rats, subcutaneously

[24]. The degradation leads to fumaric acid, which naturally occurs in the body and is found in the Krebs Cycle.

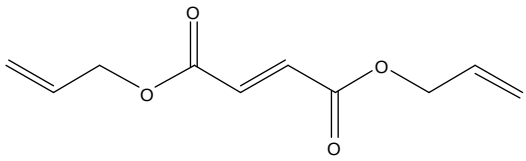

diallyl fumarate

Figure 6.17: Strucutre of diallyl fumarate

A test resin was made with 5 mole% diallyl fumarate, 95 mole % tert-butyl acrylate, and 1% by weight Ciba 2959 photoinitiator, and compared to a test resin made with 100% tert-butyl acrylate and 1 weight % 2959.

Many small disk samples were made by molding the polymers in a specially made Teflon mold (Figure 6.18). Each well for the disk is 7.5 mm in diameter, and 0.5 mm in height (Figure 6.18). The monomer resins were added to each small, disk shaped well, and exposed in a nitrogen atmosphere to about 3.5 J of 365 nm light. This large exposure dose includes what would normally be a post-build curing, so that as much of the resin may polymerize as possible.

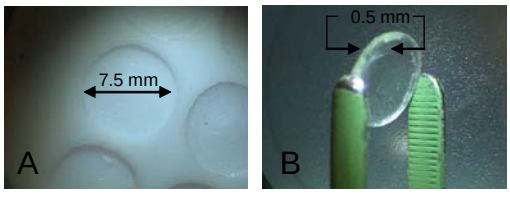

Figure 6.18: Photographs of (A) Teflon disk molds and (B) Polymerized disk sample held by forceps

The parts were carefully removed by flexing the thin Teflon mold to "pop out" the polymer disks. All of the disks were vacuum dried overnight, and then weighed. Each disk was then placed in a small vial with 4 ml of phosphate buffered saline solution without calcium and magnesium. The vials were sealed and kept in an incubator at 37°C. At appropriate time points, a series of 10 vials were removed. The polymer disks were removed from the vials and dried in a vacuum oven overnight before being weighed. The results are shown in the graph below (Figure 6.19).

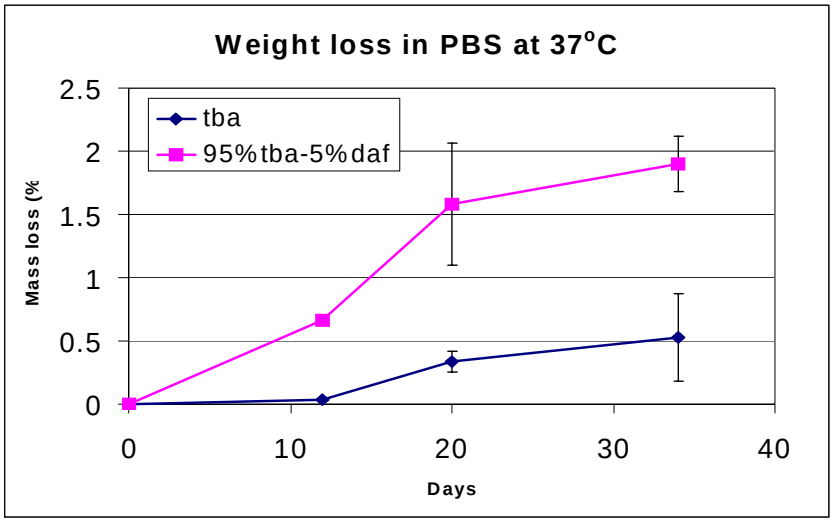

Figure 6.19: Graph of weight loss over time in buffered saline solution for degradation and control samples. Tba represents the samples with only tert-butyl acrylate and no degradable linkages. 95% tba-5% daf indicates the samples composed with 5% of the diallyl fumarate degradable linkage.

While there was a significant increase in the mass lost in the samples that included the diallyl fumarate linkage, the mass loss on all of the samples was very low. This may be expected as simple hydrolysis of an ester, in a buffered solution, is not expected to be

very rapid. However, the results here are promising as they indicate that the degradation of the photopolymer may be controlled by the selection of the type and amount of crosslinking molecule in the resin formulation.

Summary and Conclusions

In summary, several test resins were made with three basic formulation requirements: the ability to undergo light initiated free radical polymerization, ability to undergo acid-catalyzed de-protection reactions, and the ability to be degraded under physiological conditions. The acrylate group was selected as the primary reactive group for polymerization. This was used in the base monomer formulations, as well as in the tri-functional crosslinking molecule. Photoinitiators and photoacid generators were selected that absorb light in distinct regions of the electromagnetic spectrum. The synthesis of several protected monomers was investigated. The successful reaction products were made into test resins. The THP-protected hydroxyacrylate resin demonstrated that photopolymerization with a subsequent photoacid catalyzed de-protection reaction in distinct regions is possible. The MOM-protected methacrylic acid demonstrated that there may be difficulties de-protecting the surface of the polymers, thus resulting in no cell patterning. However, as the methacrylic acid polymer is amenable to cell adhesion and growth, this monomer is still a promising base material. The diallyl fumarate was incorporated successfully in a test resin to demonstrate that tuning the degradation of the final polymer is possible through selection of degradable monomers for the resin.

Although no successful cell patterns resulted from these SL resin materials, there are still possibilities for the use of these materials through optimization. If the acid from the PAG molecule reaction is not being generated, this would have caused the failure of the MOM-MA test resin de-protection. As this is a photo-crosslinked system (due to the multifunctional acrylate included for structural stability), it is possible for small molecules to become trapped in the crosslinked spaces. If this were to occur with the PAG and acid molecules once the PAG is exposed, it may mean that only very few de-protection reactions are catalyzed because while the acid molecule is regenerated after a reaction event, it is unable to be in a position to catalyze a subsequent reaction. This scenario could be probed by including a pH indicator in the resin formula. Then, when the polymer is exposed for de-protection, the color change of the pH indicator would show whether the generation of the acid molecules is problematic. Running the de-protection reaction before the polymerization will also show whether the acid molecules are becoming trapped in the crosslinked matrix and are not effectively catalyzing the de-protection reaction.

The difficulty with de-protecting this test resin based on the MOM-MA may be due the fact that the MOM-MA de-protection reaction has a greater activation energy than expected, and needs to be heated above room temperature for the reaction to happen at an acceptable rate. This could be determined by running a series of MOM-MA samples with a double exposure (one exposure to polymerize the sample and a second exposure to de-protect) and then heating the samples. The contact angles could then be measured and a correlation showing decreasing contact angles with increasing bake temperatures would verify this hypothesis. Another interesting test of this hypothesis

would be to reverse the order of polymerization and de-protection. If the de-protection reaction is catalyzed first, followed by the polymerization, the heat of reaction from the free-radical polymerization may be enough to help catalyze the de-protection reaction. This avenue should also be pursued for comparison and optimization of the overall procedure.

The MOM-MA may also have failed to de-protect if the exposure box was too dry. A small amount of water is needed for the de-protection reaction, and normally the room atmosphere provides this. However, in the N_2 purged environment, there may not be enough water present. To test this idea, one may polymerize the resin, remove the sample from the exposure box, and then expose it for the de-protection reaction. This test may also help determine if contaminants in the N_2 purge are inhibiting the de-protection reaction at the surface of the resin.

Finally, the processing of the polymer prior to cell seeding should be examined. A full post-cure step may be included as well as wash steps. This would ensure that the polymer parts are clean and amenable to cell growth.

References

[1] F. Rodriguez, *Principles of Polymer Systems, Fourth Edition*, Fourth ed. Washington D.C.: Taylor & Francis, 1996.

[2] S. J. Bryant, C. R. Nuttelman, and K. S. Anseth, "Cytocompatibility of UV and visible light photoinitiating systems on cultured NIH/3T3 fibroblasts in vitro," *Journal of Biomaterials Science, Polymer Edition*, vol. 11, pp. 439-457, 2000.

[3] C. G. Williams, A. N. Malik, T. K. Kim, P. N. Manson, and J. H. Elisseeff, "Variable cytocompatibility of six cell lines with photoinitiators used for polymerizing hydrogels and cell encapsulation," *Biomaterials*, pp. 1211-1218, 2005.

[4] T. Y. Leea, T. M. Ropera, E. S. Jonssonb, I. Kudyakovc, K. Viswanathand, C. Nasona, C. A. Guymone, and C. E. Hoyle, "The kinetics of vinyl acrylate photopolymerization," *Polymer*, vol. 44, pp. 2859-2865, 2003.

[5] P. F. Jacobs, *Rapid Prototyping & Manufacturing, Fundamentals of StereoLithography*, First ed. Dearborn, MI: Society of Manufacturing Engineers, 1992.

[6] *Biomaterials Science: An Introduction to Materials in Medicine*. San Diego: Academic Press, 1996.

[7] A. S. G. Curtis, J. V. Forrester, C. McInnes, and F. Lawrie, "Adhesion of Cells to Polystyrene Surfaces," *The Journal of Cell Biology*, vol. 97, pp. 1500-1506, 1983.

[8] K. E. Michael, V. N. Vernekar, B. G. Keselowsky, J. C. Meredith, R. A. Latour, and A. J. Garcia, "Adsorption-Induced Conformational Changes in Fibronectin Due to Interactions with Well-Defined Surface Chemistries," *Langmuir*, vol. 19, pp. 8033-8040, 2003.

[9] P. G. M. Wuts and T. W. Greene, *Greene' s Protective Groups in Organic Synthesis Fourth Edition*, Fourth ed. Hoboken, New Jersey: John Wiley & Sons, 2007.

[10] N. Miyashita, A. Yoshikioshi, and P. A. Grieco, "Pyridinium p-Toluenesulfonate. A Mild and Efficient Catalyst for the Tetrahydropyranylation of Alcohols," *J. Org. Chem.*, vol. 42, pp. 3772-3774, 1977.

[11] M. Ueda, S. Ishibashi, T. Suzuki, and T. Masuko, "Radical-Initiated Homo- and Copolymerization of Methoxymethyl Methacylate," *Journal of Polymer Science: Polymer Chemistry Edition*, vol. 22, pp. 2305-2316, 1984.

[12] S. W. Shalaby and K. J. L. Burg, *Absorbable biodegradable polymers*. Boca Raton, FL: CRC Press LLC, 2004.

[13] R. Langer and N. A. Peppas, "Advances in biomaterials, drug delivery, and bionanotechnology," *AIChE Journal*, vol. 49, pp. 2990-3006, 2003.

[14] D. F. Williams, "Definitions in Biomaterials. Proceedings of a Consensus Conference of the European Society for Biomaterials," presented at Consensus Conference of the European Society for Biomaterials, Chester, England, 1987.

[15] A. P. Gunatillake and R. Adhikari, "Biodegradable Synthetic Polymers for Tissue Engineering," *European Cells and Materials*, vol. 5, pp. 1-16, 2003.

[16] J. C. Middleton and A. J. Tipton, "Synthetic biodegradable polymers as orthopaedic devices," *Biomaterials*, vol. 21, pp. 2335-2346, 2000.

[17] A. K. Burkoth and K. S. Anseth, "A review of photocrosslinked polyanhydrides: in situ forming degradable networks," *Biomaterials*, vol. 21, pp. 2395-2404, 2000.

[18] D. S. Muggli, A. K. Burkoth, S. A. Keyser, H. R. Lee, and K. S. Anseth, "Reaction Behavior of Biodegradable, Photo-Cross-Linkable Polyanhydrides," *Macromolecules*, pp. 4120-4125, 1998.

[19] A. K. Burkoth, J. Burdick, and K. S. Anseth, "Surface and bulk modifications to photocrosslinked polyanhydrides to control degradation behavior," *J Biomed Mater Res*, vol. 51, pp. 352-359, 2000.

[20] D. S. Muggli, A. K. Burkoth, S. A. Keyser, H. R. Lee, and K. S. Anseth, "Reaction Behavior of Biodegradable, Photo-Cross-Linkable Polyanhydrides," *Macromolecules*, vol. 31, pp. 4120-4125, 1998.

[21] S. He, M. D. Timmer, M. J. Yaszemski, A. W. Yasko, P. S. Engel, and A. G. Mikos, "Synthesis of biodegradable poly(propylene fumarate) networks with poly(propylene fumarate)-diacrylate macromers as crosslinking agents and characterization of their degradation products," *Polymer*, pp. 1251-1260, 2001.

[22] M. Mizutani and T. Matsuda, "Liquid photocurable biodegradable copolymers: In vivo degradation of photocured poly(e-caprolactone-co-trimethylene carbonate)," *Journal Biomedical Material Research*, vol. 61, pp. 53-60, 2002.

[23] J. S. Temenoff and A. G. Mikos, "Injectable biodegradable materials for orthopaedic tissue engineering," *Biomaterials*, vol. 21, pp. 2405-2412, 2000.

[24] S. J. Peter, S. T. Miller, G. Zhu, A. W. Yasko, and A. G. Mikos, "*In vivo* degradation of a poly(propylene fumarate)/β-tricalcium phosphate composition orthopaedic scaffold," *Journal of Biomedical Materials Research*, vol. 41, pp. 1-7, 1998.

[25] S. Park, A. Periathamby, and J. Loza, "Effect of surface-charged poly(methy methacrylate) on the adhesion of Candida albicans," *Journal of Prosthodontics*, vol. 12, pp. 249-54, 2003.

CHAPTER 7

SUMMARY AND FUTURE WORK

Summary

Tissue engineering continues to be an area of emerging technologies and promising therapies. With the large healthcare market and the possibilities of tissue engineering therapies to treat a significant number of ailments, it is clear that tissue engineering will continue to grow and develop. There are three main approaches to tissue engineering: the use of isolated cells or cell substitutes to replace those cells that supply the needed function; the delivery of tissue-inducing substances, such as growth and differentiation factors, to targeted locations; and growing cells in three-dimensional scaffolds [1]. There are currently commercial products being developed using all three of these techniques, and there is no universal solution for all tissue engineering problems. Future tissue engineering solutions will utilize an approach that is most appropriate for that particular disease or disorder.

One of the tissue engineering approaches is to create a 3D scaffold, seed it with the appropriate cells and signaling cues, allow the cells to grow and differentiate, and finally implant this engineered tissue into a patient. A critical component to the success of this approach is the design and fabrication of the 3D scaffold. The scaffold must support many functions such as providing mechanical support and structure, facilitating nutrient and waste transport, and supplying physical and chemical cues to the growing cells. Many routes for creating a 3D scaffold have been studied, including 2D layer by layer methods [2], [3], direct fabrication of 3D forms through injectable hydrogels [4],

polymer-porogen methods such as salt leaching [1], and rapid prototyping methods [5], [6], [7]. For the first three methods, it is difficult to create a complex hierarchical structure, either chemically or structurally. However, by adapting stereolithography (SL), a rapid prototyping method, it is possible to develop a method that allows for the direct fabrication of physically complex and chemically structured scaffolds using a single process.

SL is a fabrication method which uses a laser to "write" patterns into a vat containing a photo-polymerizable monomer mixture. The first step in performing SL is generating a computer aided design (CAD) file of the structure of the desired 3D object and slicing it into a series of 2D layers. The next step is to sequentially build up the desired part in a SL tool layer-by-layer from the 2D slice data. In a typical SL apparatus, a movable stage is located within the monomer vat to support the part as it is being formed. To build the part, the stage is first brought within close proximity of the vat surface such that a thin layer of the resin covers the stage. The SL laser is then scanned over the layer according to the 2D data for the bottom slice of the object, resulting in polymerization and solidification of the desired regions of that layer. Next, the stage is lowered into the monomer vat by the thickness of one layer, and the process is repeated with the next 2D data slice. Once the part is finished, it is removed from the vat and excess monomer is washed from the object. Following the washing step, post-processing may be done to improve the properties of finished object.

In order to realize this fabrication method, mixtures of biocompatible monomers and photoinitiators that can be used in conjunction with SL tools to create 3D scaffolds for tissue engineering applications must be developed. Furthermore, beyond the use of

SL to control the physical structure of a polymer object or scaffold, this work develops strategies for using SL methods to also control the local chemical composition of the polymer scaffold surface. To that end, monomers containing hydroxyl and carboxylic acid groups are reactively capped with a "protecting" group (e.g. t-butoxycarbonyl group). The protecting group can be selectively removed in certain areas using exposure to light in the SL tool, via a photo-acid catalyzed reaction. This de-protection chemistry is analogous to the strategy employed for making the "chemically amplified photoresists" (CARs) that are used in microlithography processes for semiconductor fabrication [8]. The de-protection reactions are generally catalyzed by acid, and thus the addition of a photoacid generator (PAG) to a protected monomer material permits local control of the polymer surface chemistry.

It has been previously shown that it is possible to produce the biological equivalent of a photoresist, referred to as a "bioresist", that can be used to direct cell growth on 2-D surfaces [9]. However, using these same polymer materials to directly fabricate 3-D scaffolds is difficult, requiring complex layer-by-layer assembly. The use of similar monomeric materials for SL could present a more facile route for production of 3D, hierarchically structured scaffolds. Also, it is desirable to use more conventional resist materials for cell patterning, to simplify the monomer synthesis.

First, biocompatible materials were identified that can be used in these resist systems. The area of greatest concern was the choice of PAG, as these are small, reactive molecules that could present toxicity problems to the cell culture. Interestingly, the findings from this work show that several PAG are relatively benign to the cell cultures under study, and the recommends a large non-ionic PAG, Ciba 263, as the least cytotoxic.

Once biocompatible PAG molecules were identified, a robust cell seeding method was developed. According to the He paper [9], no special cell seeding procedures are needed to generate cell patterns on bioresist materials. However, when translating the cell patterning to traditional resist materials, it was shown that standard cell seeding methods do not reliably result in cell patterning. Thus, several cell seeding methods were investigated to find a robust way to pattern cells using conventional resist materials. It was shown that seeding the cells in a regular serum-containing media followed by a wash step after one hour of incubation is the best way to produce cells growing in the specified pattern.

This cell seeding method is confirmed by the QCMD findings. First, protein adsorption onto resist materials was examined, and it was found that the least amount of protein adsorbed onto the fully-protected resist materials. These are also the surfaces that resist cell adhesion in the patterning studies. Furthermore, it was shown in whole cell studies that cells do not adhere on the fully-protected surfaces, but rather just settle on the surface. This confirms that the seeding method is appropriate. That is, proteins do not adsorb as readily on the fully-protected surfaces and cells do not adhere well; so rinsing the surface after an hour removes those weakly attached cells, leaving cells only in the patterned areas.

A mirror array based stereolithography apparatus was built in our lab, which allows for exposures at more than one wavelength. Many specialized components were designed and built for this novel system. In particular, a holder and adjustable mount were built to hold the mirror array so that the array is securely held and may be

positioned precisely. Labview code was written to automate the system and small test pieces were made.

With a system capable of two wavelength exposures, appropriate resin materials were synthesized. The protection of several acrylate monomers was investigated. Many of the procedures resulted in a side reaction instead of the desired protection reaction. The most successful monomer synthesis was protecting methacrylic acid monomer with methoxymethyl (MOM) ether. The MOM-methacrylic acid was formulated into a small amount of test resin that was tested for de-protection and cell seeding. This resin was composed of 200 mg of SR 351 LV trifunctional acrylate, 200 mg of MOM-methacrylic acid, 10 mg of 263 PAG and 10 mg of 784 photoinitiator (PI). Samples were coated onto glass cover slips and exposed to only 435 nm light, or the full spectrum. Unfortunately, the water contact angle data showed that the de-protection was incomplete, and the resulting cell patterning study was also unsuccessful. However, when the base monomer, methacrylic acid, was polymerized, it was shown to be a good substrate for cell growth. Thus, it is likely that optimization of the exposure process and post-build cleaning can lead to a positive cell seeding result for this test resin.

It is also desirable for the final polymeric scaffold to be biodegradable. To test this idea, a degradable, di-vinyl group was used as a biodegradable cross-linking molecule. The diallyl fumarate molecule was used in this experiment, and test pieces were photopolymerized in a mold. The pieces were placed in phosphate buffered saline at 37^{o}C and the weight loss of the pieces was recorded. This shows that photopolymerization is capable of incorporating a degradable linkage so the tuning of the degradation of the final polymer is possible through formulation of the starting resin.

Recommendations for Future Work

The combination of photolithographic materials with stereolithography to fabricate tissue engineering scaffolds is still an area with great potential. Many routes for future exist from the work presented, and some of the most interesting and promising ideas are discussed.

The 2D cell patterning methods are very interesting, and have potential to be extended, optimized and used in various cell studies. The process itself, seeding cells in serum containing media with a wash step after one hour of incubation, could be further investigated. In particular, it might be interesting to observe what effect the incubation time has on the pattern fidelity. If shorter incubation times can be used, it would streamline the patterning process. Also, many cell systems are seeded using rocker plates, orbital shakers, or other such devices. It could be very insightful to see how the cells behave when seeded in these conditions with motion and shear forces. Finally, new applications of this 2D cell patterning might be explored. If there is a particular cell function which may be regulated by the spatial orientation of the cell, it would be interesting to examine this by patterning the cells in various shapes and orientations.

Another interesting extension area in the 2D cell patterning would be to examine if more specific cell signaling could be obtained and if there is the possibility for the addition of a second type of cell to the culture. To obtain more specific signaling, one would have to move beyond the simple hydrophilicity switch. Fortunately, the de-protection reaction removes the protecting group to yield an alcohol or carboxylic acid. Both of these are highly reactive groups, and there are chemistries to tether molecules to these them. Thus, it may be possible to follow the de-protection step with a subsequent

reaction to attach a highly specific signaling or adhesion molecule. This may allow for the seeding of special cell types, and a way to direct cell behavior. In order to seed cell co-cultures, it is necessary for the surface which was initially cell non-adhesive to become adhesive. This might be accomplished by a second exposure, after the first cell type has been seeded. Of course, the complication here is that the cells must be robust enough to withstand this process. If alignment of the mask to the substrate surface is possible, the cells would not be directly exposed to UV light. However, the products of the de-protection reaction would be released directly into the cell media.

An interesting extension of the quartz crystal microbalance with dissipation (QCM-D) whole cell experiments would be to use the flow chamber which has an open window. If this could be set up underneath a microscope and video camera, one could observe the cell morphology change along with the frequency or mass change. As the quartz disks and electrodes are not transparent, this set up may only be viewed via top-down microscopy. In addition, this experiment could be run under a continual shear flow of media, and it would be quite interesting to examine the relationship between the flow rate and the cell adhesiveness on the protected and de-protected substrates.

Although the initial resin formulations examined in this work did not immediately yield successful cell patterns, there are other routes that may be explored and the optimization of the systems studied here provides a good starting point. As the MOM-methacrylic acid monomer reaction works quite well, this would be a good material set to begin with for the future work. Also, it is a useful material to start from because the methacrylic acid polymer surface is very amenable to cell adhesion and growth. This material may be used for studies of the extent of polymerization with dose, the amount of

residual monomer or initiator leaching, and the development of a post-build process that would ensure a clean, sterile part suitable for cell seeding. Some of these specific experiments are discussed in Chapter 6.

Along with this, the MOM-methacrylic acid may be used as a basis for optimization of the test resin. Studies of the ratio of MOM-methacrylic acid to the other main components (trifunctional acrylate, PAG, PI, and degradable linkage) will be highly useful in making guidelines for resin formulation. One point of interest would be to understand the amount of protecting group needed to facilitate the cell patterning for this material. It is likely that this will correlate to the contact angle changes monitored in chapters 3 and 4. Also, it will be necessary to balance this requirement with the physical properties needed in a stereolithographic resin; in particular, the resin must polymerize quickly into a solid that can withstand moving up and down on the elevator platform.

Finally, future work may involve optimization of the stereolithographic apparatus. The system is close to being fully automated and by incorporating an automatic filter wheel, the system may be run completely remotely. In addition, once test resins are identified, the important stereolithographic characteristics may be determined for the resin. These include build parameters such as the depth of penetration and the critical exposure dose. The challenge is to determine these characteristics using as small amount of resin possible, due to the difficulty of synthesizing the large quantities typically available in a commercial system. Some of these techniques have been explored through different aspects of work done for this thesis, and an overview is given in Appendix D.

Once complex, 3D parts are built with this system, an entirely new set of experiments may begin. These experiments include the examination of the de-protection

reaction within more complex geometries, the way that cells might be seeded throughout a larger scaffold, and how cell survival varies through a scaffold. At this point, it may be necessary to examine cell growth systems that include some amount of media flow and circulation, such as in a bioreactor environment. Different scaffold geometries may be examined, with different levels of porosity and channel density. There are many complexities that arise when considering a large, 3D system, and ultimately it is these challenges that this system will help investigate and address.

References

[1] P. X. Ma, "Scaffolds for tissue fabrication," *Materials Today (Oxford, United Kingdom)*, vol. 7, pp. 30-40, 2004.

[2] T. H. Ang, F. S. A. Sultana, D. W. Hutmacher, Y. S. Wong, J. Y. H. Fuh, X. M. Mo, H. T. Loh, E. Burdet, and S. H. Teoh, "Fabrication of 3D chitosan-hydroxyapatite scaffolds using a robotic dispensing system," *Materials Science & Engineering, C: Biomimetic and Supramolecular Systems*, vol. C20, pp. 35-42, 2002.

[3] G. Vozzi, C. Flaim, A. Ahluwalia, and S. Bhatia, "Fabrication of PLGA scaffolds using soft lithography and microsyringe deposition," *Biomaterials*, vol. 24, pp. 2533-2540, 2003.

[4] J. A. Burdick and K. S. Anseth, "Photoencapsulation of osteoblasts in injectable RGD-modified PEG hydrogels for bone tissue engineering," *Biomaterials*, vol. 23, pp. 4315-4323, 2002.

[5] K. F. Leong, C. M. Cheah, and C. K. Chua, "Solid freeform fabrication of three-dimensional scaffolds for engineering replacement tissues and organs," *Biomaterials*, vol. 24, pp. 2363-2378, 2003.

[6] G. T. M. Chu, G. A. Brady, W. Miao, J. W. Halloran, S. J. Hollister, and D. Brei, "Ceramic SFF by direct and indirect stereolithography," *Materials Research Society Symposium Proceedings*, vol. 542, pp. 119-123, 1999.

[7] M. N. Cooke, J. P. Fisher, D. Dean, C. Rimnac, and A. G. Mikos, "Use of stereolithography to manufacture critical-sized 3D biodegradable scaffolds for

bone ingrowth," *Journal of Biomedical Materials Research, Part B: Applied Biomaterials*, vol. 64B, pp. 65-69, 2003.

[8] L. F. Thompson, C. G. Willson, and M. J. Bowden, *Introduction to Microlithography*. Washington DC: American Chemical Society, 1994.

[9] W. He, C. R. Halberstadt, and K. E. Gonsalves, "Lithography application of a novel photoresist for patterning of cells," *Biomaterials*, vol. 25, pp. 2055-2063, 2004.

APPENDIX A

DOCUMENTATION FOR MICRO-SLA SYSTEM

This Appendix gives the instructions for operating the Micro-SLA system that was designed and built for this work. It also gives the documentation relating to the automation programming which was done using LabView code. There are three main sets of instructions, so that the equipment may be used without automation, with full automation, or with partial automation. It is important to remember that one should always be wearing UV safety goggles, gloves and a lab coat whenever the UV light is in operation, and that signs stating this hazard and the appropriate protection should be posted on the lab doors. The layout of the system is given in Figures A.1-A.3.

Operating Instructions

System Layout

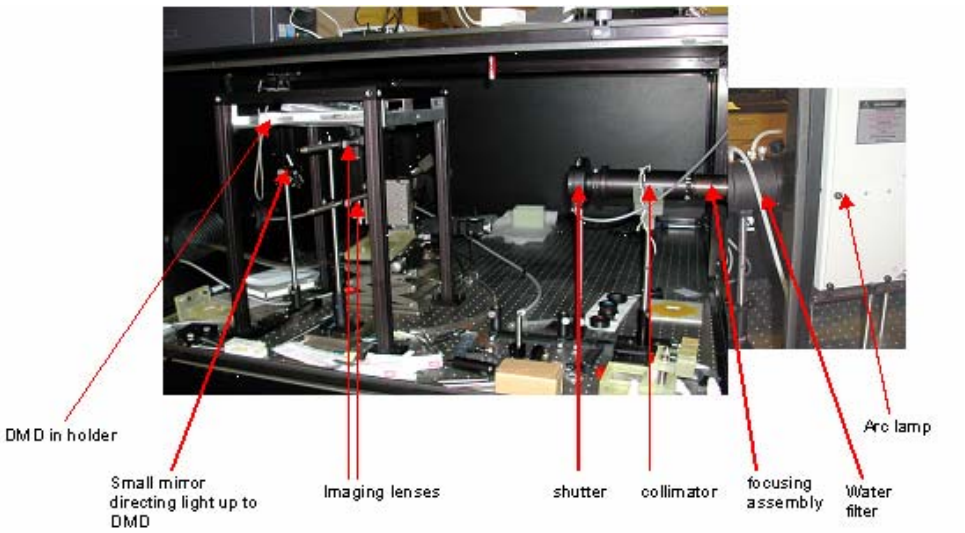

Figure A.1: System Layout, overall configuration

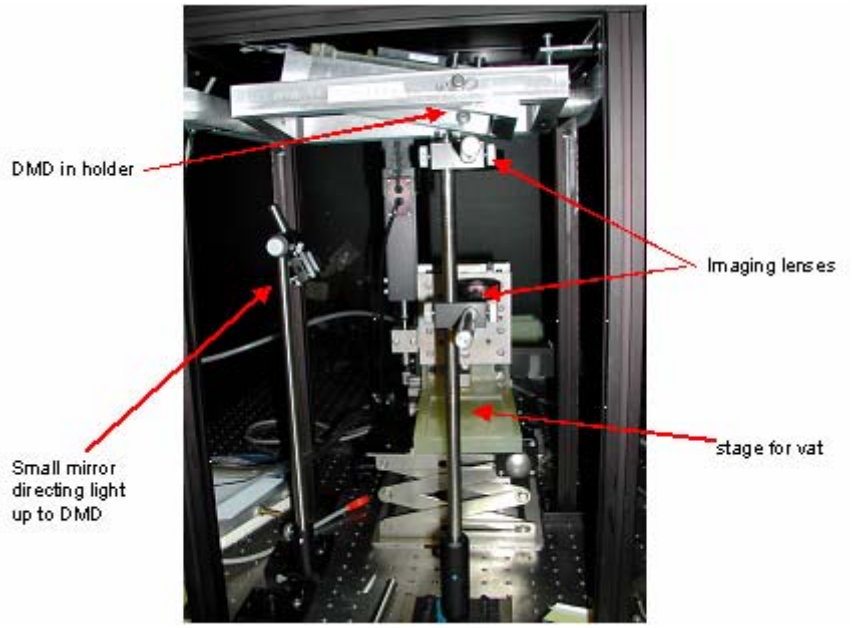

Figure A.2: System layout, detail of the imaging section from the mirror array to the stage for the vat

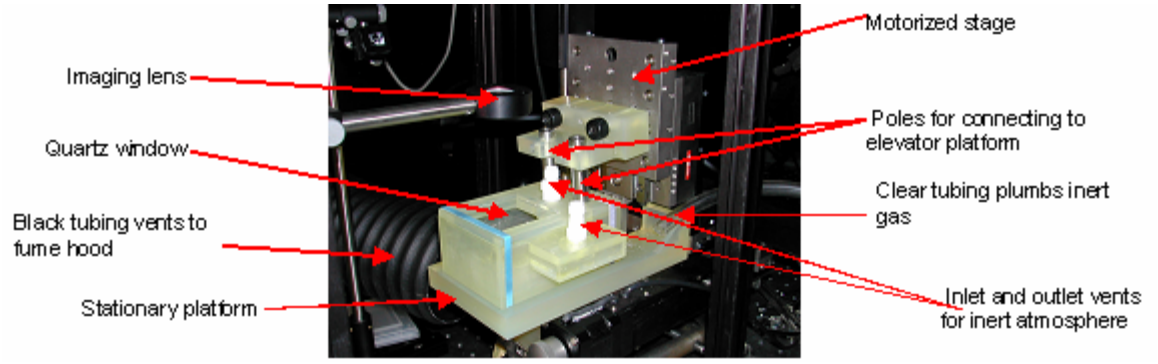

Figure A.3: System layout, detail of the vat assembly and ventilation requirements

Basic Operation of the Micro-SLA System

These instructions are for the basic use of the Micro-SLA system, without the use of any automation programs. Even if one is planning to use an automation program, it is

useful to read these instructions first, as they provide the basics of the operation and can serve as a quick reference guide once one is familiar with using the system. These instructions come from work done by B. Katz in our laboratory to help set-up this system.

Start-up Procedure

1) Make sure all the lamp connections are correct and check the water lines. The lines running to the power supply should be set up according to the HgXe configuration on the back of the lamp housing. Currently, a cold water circulating bath is used to provide cooling water to the water bath. The water lines running to and from the water filter should be connected to this cooling bath, and the bath should be turned on and circulating.

2) Turn on the water to a medium flow rate; make sure all hose connections are secure. Check the water flow rate into the drain to ensure that there are no blockages in the line.

3) Plug in the DMD and connect its USB cord to the computer. Project a checkerboard pattern using the TI software. This pattern is the easiest to use for a quick alignment check.

4) Turn on the stages. Make sure the USB cords are disconnected before turning the stages on.

5) Plug in the stage's USB cords and open ATP config program. Go to the stages tab in the program.

6) If all stages are recognized, exit ATP config and open ATP user.

7) Make sure a suitable platform and vat are connected to the stage. If only running 2D exposures, one may choose to use a platform instead of the vat assembly.

8) Home the X, Y & Z stages.

9) Turn on the lamp.

10) Make sure the wavelength filter is flush against the collimator before opening the shutter. If no filter is needed, use an empty filter holder instead.

11) Check the mirror and make sure the reflected light is hitting the DMD.

12) Check the lenses. First put the UV detector over the top lens and make sure the checker pattern is in the center of the lens. Then place the detector card over the bottom lens and make sure the entire diffraction pattern is being captured. Then check the imaging plane and make sure the image is not distorted. If the image is distorted consult the image troubleshooting section.

13) Adjust the stage so that the image plane is in focus. If the platform connected is the vat system, make sure the focused image is at the top surface of the liquid.

14) Run the desired build or exposure protocol.

Shut down Procedure

1) Close the shutter on the focusing assembly.

2) Turn off the lamp.

3) Close all the programs on the computer including the stage and DMD control programs. Unplug the DMD and disconnect the USB cord.

4) Turn off the stages and disconnect the USB cord.

5) Make sure all photocurable resins are covered and protected.

6) Shut the black box.

7) Turn off the water when the water filter is cool to the touch. It should be cool enough by the end of this procedure.

Quick Troubleshooting Guide

What to do if the stages don't work?

Close the ATP user and ATP config programs, turn off the stages and unplug USB connections. Make sure to do the shut down in that order. Then, restart the computer and disconnect the controller wires on the stage (the part that is supposed to light up green when the stages are working). Reconnect the controller wires. Once the computer is logged back on proceed with step 4 to 6 of the basic start-up procedure.

What to do if the image is distorted?

Plug in the CCD camera. All adjustsments made will be in respect to images seen on the CCD detector. If a horizontal line array has a vertical blur causing the lines to overlap, adjust the x-axis rotation on the gimble mount holding the DMD array. If a vertical line array has a horizontal blur causing the lines to overlap, adjust the y-axis rotation on the gimble mount holding the DMD array. If a checker board pattern has a barreling distortion, adjust the top lens and make sure the projection off the DMD array is centered on the lens. If there is a major blur on either side of the image, make sure the lenses are completely flat along the horizontal.

Detailed Operating Instructions for using the Automated System

These instructions are for using the ventilated exposure box system to build 3D structures. Note, again, that the proper safety precautions should be taken. Wear UV protective glasses, lab coat and gloves at all times when lamp is on, and post signs on the lab doors. Follow all instructions carefully and in the sequence provided (unless otherwise noted). Be extremely careful not to bump the optical display from its original position. These instructions come from work done by J. Stanton in our laboratory to help set-up and automate this system.

Part I: Verify that the UV lamp is set up correctly

1) Place the lamp on the four Edmund Optics metal cylinders with the exiting light path towards the optical set up (inside the black enclosure) and fasten with four screws.

2) Connect the appendage of the exiting light path to the Newport connection to the shutter. Tighten down with small hex key on top of connection piece.

3) Extending from a cold water circulating bath on the table, and to the right of the lamp, is some clear rubber tubing. Attach the tubing to the brass colored connector on the left of the grey lamp body.

Once the lamp is completely assembled, it should look like the figure below (Figure A.4).

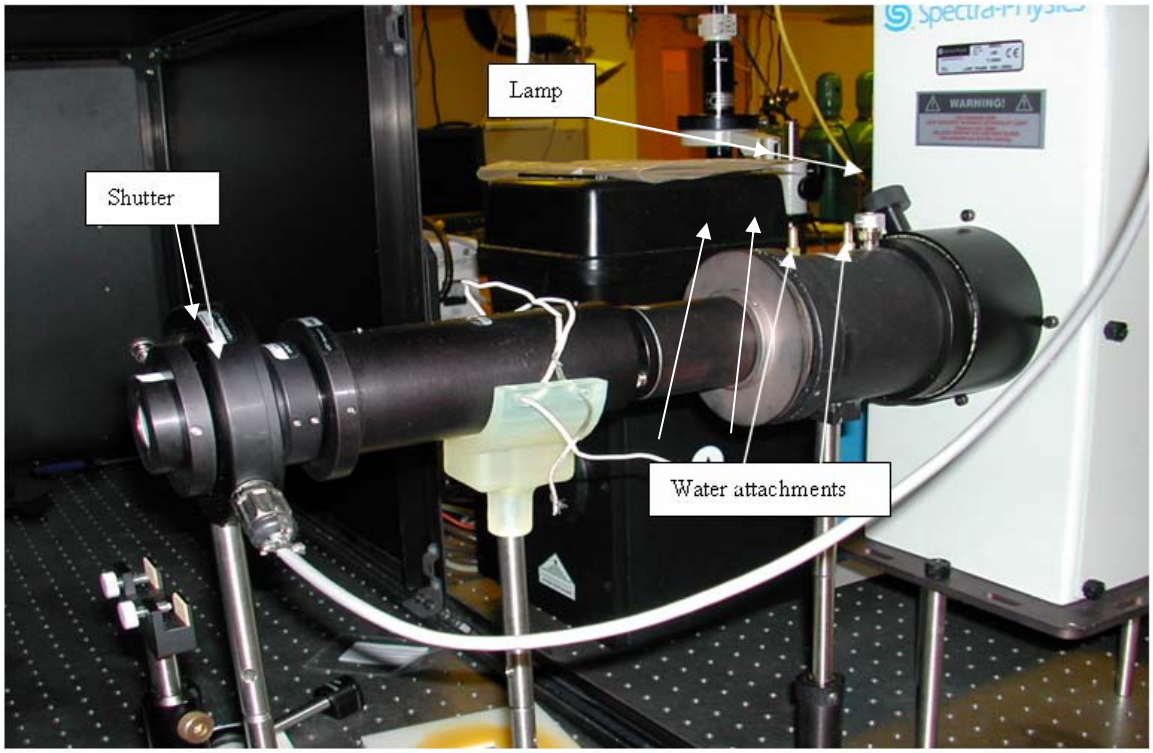

Figure A.4: Photograph showing proper lamp set-up.

4) Locate some clear rubber tubing that is below the table (near your feet) and attach the end to the other brass colored connecter. (This one should be closer to the black enclosure.)

5) Verify the location of the end of the tubing is in the drain under the table so that the exiting water flows directly into the drain.

6) Turn on the circulating cold water bath. Make sure the flow rate is substantial enough to cool the lamp, but not so high as to force the tubing to disconnect.

Note – If any water gets on the table, clean it up promptly.

7) Attach the power cords for the lamp using the directions on the side of the lamp for the Mercury-Xenon set up. (Black and grey cords)

8) Plug in the power supply for the lamp in the wall outlet above the table.

9) Turn on the power source using the black power switch. The display on the front panel should read “0”.

10) Press the “Lamp On” button. (One may choose to delay turning the lamp on until more of the assembly is completed to avoid wearing the required personal protective equipment.) The display on the front panel should read around “1000” when the lamp is ignited. It will fluctuate briefly.

Part II: Power up the hardware.

1) Locate the Newport Electronic Shutter Controller on top of the black enclosure. Verify the silver switches on the front are aligned towards N.C. and REMOTE. Turn on the controller using the power switch located on the back. The power light on the front should light up.

2) Locate the Thorlabs Precision Motor Controller on top of the black enclosure. Turn on the controller using the power switch located on the back. The power light on the front should light up as well as the green signal lights on the metal connection between the cords.

3) Locate the CUI Inc. power supply on top of the black enclosure. Plug in the power supply. This is the power supply for the DMD.

Part III: Completing the set-up

1) On the desktop, double-click the “DMD Discovery 1100 GUI” icon. The following window should open (Figure A.5):

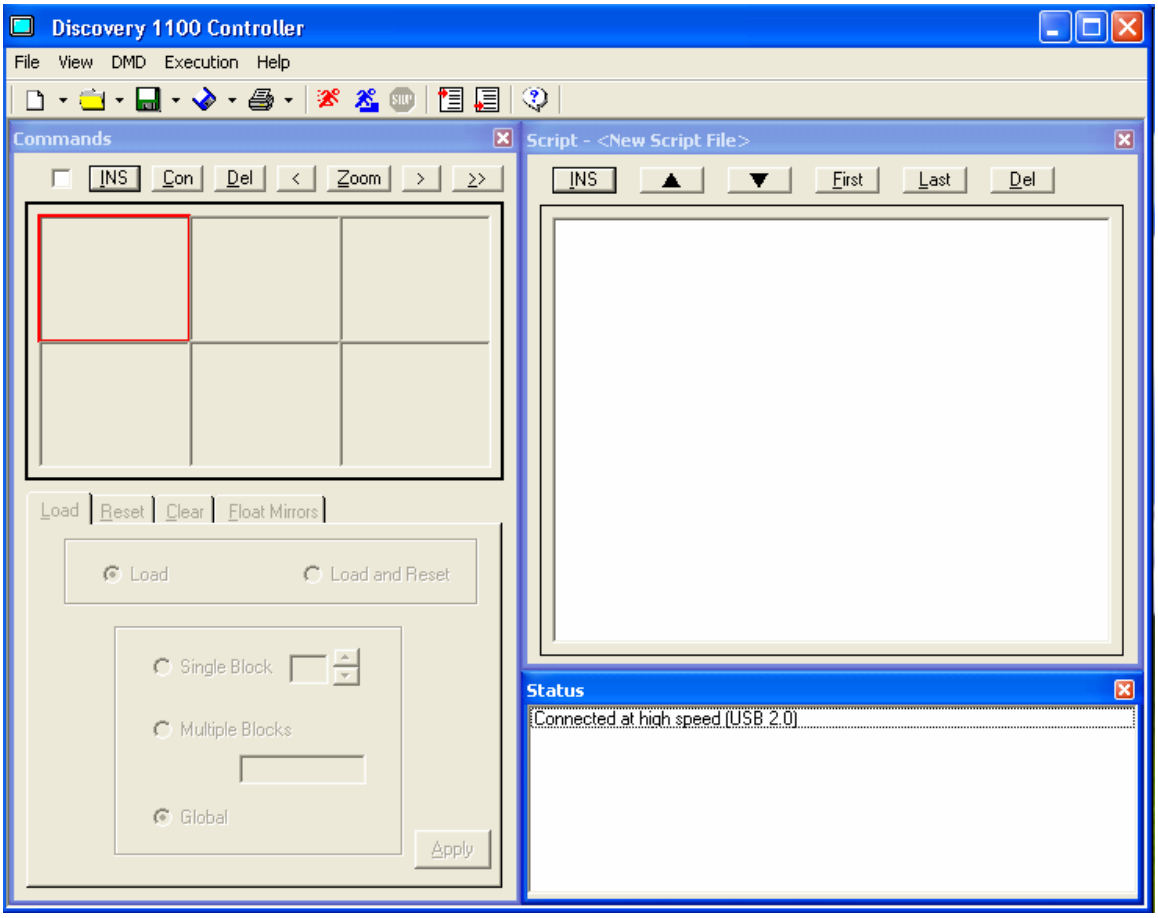

Figure A.5: Discovery 1100 screen layout

If the status does not read some form of “Connected at high speed (USB 2.0)”, close the window, unplug the DMD, and plug it in again. Then open the icon again.

2) Press the “INS” button (on the far left). Click on “white” in the list of images and click open.

3) Still in the commands area, press the “>>” button.

4) Towards the bottom center of the screen, under the “Load” tab, press “Apply”.

5) Then click on the “Reset” tab and also press “Apply”.

6) Up in the main toolbar, press the blue running man seven times. (The highlight should end on “Global” in the Script area and the DMD should be displaying a white picture.)

7) On the desktop, double-click the “APTUser” icon and Figure A.6 should open.

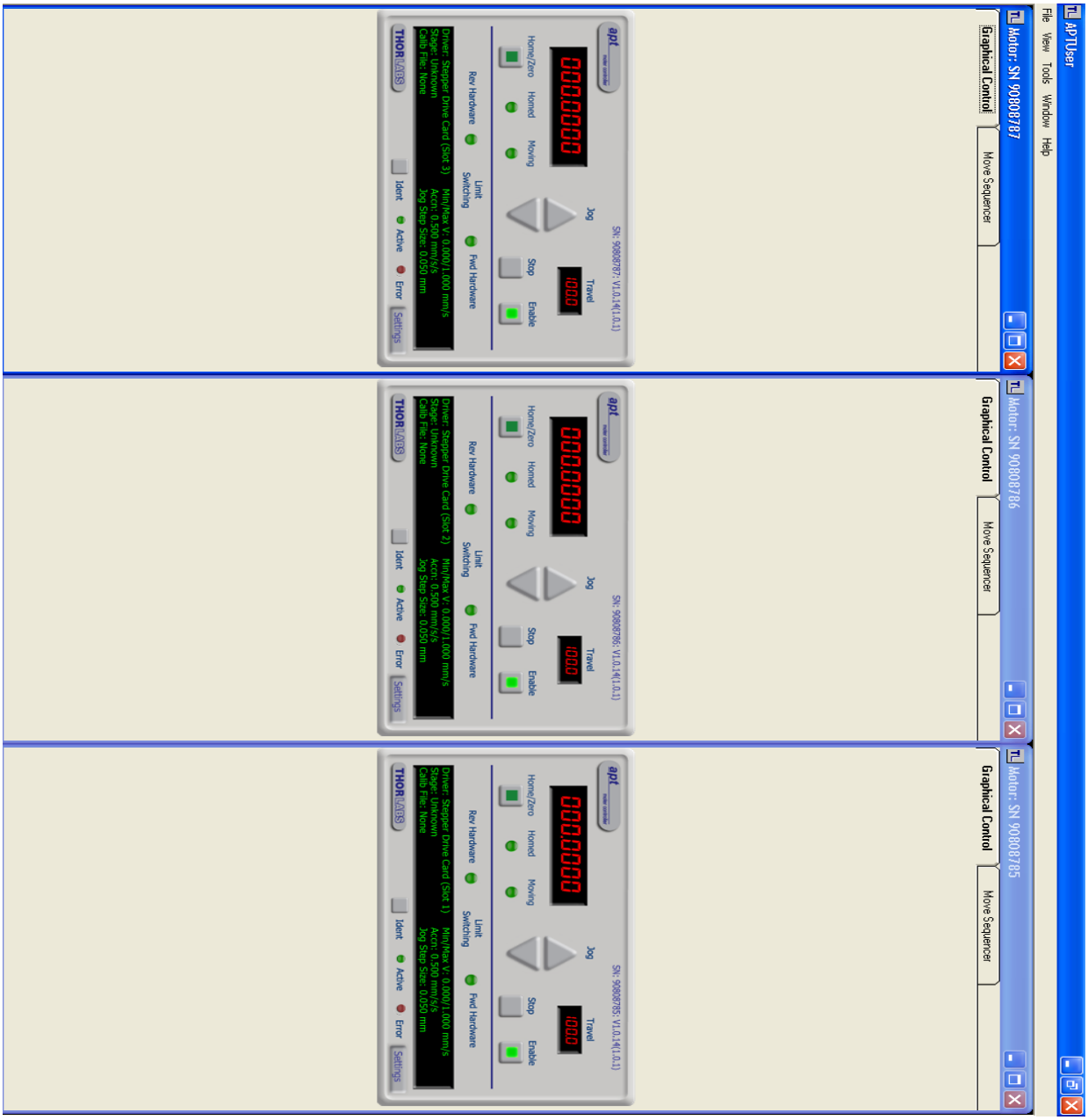

Figure A.6: Screen layout for ThorLabs stage control software

Wait at least 2 minutes for the red positioning values to load. If they do not load, close the window, switch off the Thorlabs Precision Motor Controller, allow the system to rest for 5 minutes, and switch it on again. Then open the icon again.

8) Then, in the same window, press the "Home/Zero" button. This raises the Z axis of the stages to the highest position possible. Then press the Jog up button four times. This lowers the stages down into a region where LabView will recognize them.

9) Verify the vat is set-up for the experiment. If not, assemble in the following manner:

i) Locate the silver small winch device, and place it directly under the two focusing glasses.

ii) Locate the vat and lid (without the venting appendage) and place it on top of the winch (to give extra height).

iii) Locate the foundation piece. This piece is fairly rectangular with an addition on one side to allow attachment to the stationary portion of the stages. It has a rectangular indentation on the top to allow the vat and lid (with the venting appendage) to rest securely on top. Attach it to the stationary portion of the stages (directly below and tucked under the traveling portion) with two screws using the large allen wrench.

Note – The winch and vat and lid (without the venting appendage) should be under the foundation piece, leveling it. Adjust the height of the winch, to provide the appropriate amount of pressure to the foundation to be as level as possible.

iv) Locate the vat and lid (with the venting appendage) and place it in the indentation on the foundation piece. Connect the shelf portion of the vat

to the traveling portion of the stages with the middle holes to allow the downward movement of the shelf during the operation of the LabView program.

Note – This set-up should look like this (Figure A.7):

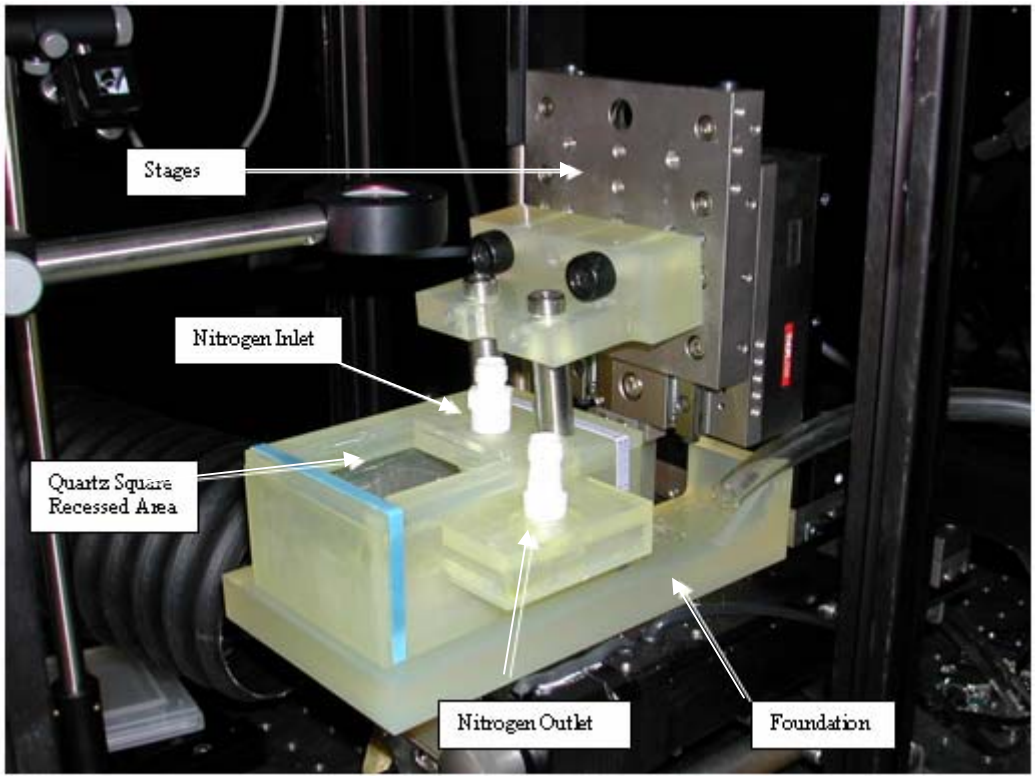

Figure A.7: Proper set up for vat and elevator assembly

v) Place a piece of silicon covered with white paper or a sticker on the shelf. With the lamp on, and wearing all personal protective equipment, switch open the shutter by first switching the REMOTE switch to LOCAL and then switching the N.C. to N.O. Slightly adjust the

arrangement of the setup to achieve the highest level of focus possible. (The absolute height of the stages can be adjusted using the larger winch seated under the stages as a whole.) Replace the piece of covered silicon with the desired building piece. Make sure the building piece of silicon is sized appropriately to allow for the white DMD image display to extend over the edges of the silicon slightly on two (or more) sides.

vi) Switch the shutter control back to the closed setting by switching the N.O. to N.C.

vii) Charge the vat with a monomer/photo initiator solution of choice up to halfway up the height of the shelf. Be sure to drop a few drops of the solution on the surface of the silicon, where the solution covers the picture exposure area.

viii) Attach the inlet nitrogen tubing (the smaller diameter tubing inside the black enclosure) to the connector on the lid of the vat.

ix) Attach the outlet nitrogen tubing (the larger diameter tubing inside the black enclosure) to the connector on the appendage of the vat. (Verify the exit of this tubing is inserted in the black venting tubing).

x) On the opposite side of the table, open the nitrogen valve, near where the tubing is going into the ceiling, until the flow is audible.

xi) Locate the quartz square that can rest in the recessed area around the hole in the lid. Place it there.

xii) On the desktop, double-click the icon “Cool Timer” and set the timer for 5 minutes. Click Start.

xiii) Immediately, flip the switch on the shutter controller from N.C. to N.O. Wait until the timer sounds. Click Stop on the timer and flip the switch back to N.C. Also, flip the other switch from LOCAL to REMOTE.

xiv) Verify the silicon has been fixed to the shelf.

xv) On the desktop, double-click the "Optical LabView Setup" folder. Within this folder, double-click the LabView VI "Indep image display, shuttercontrol, and motor move relative." This front panel looks like Figure A.8.

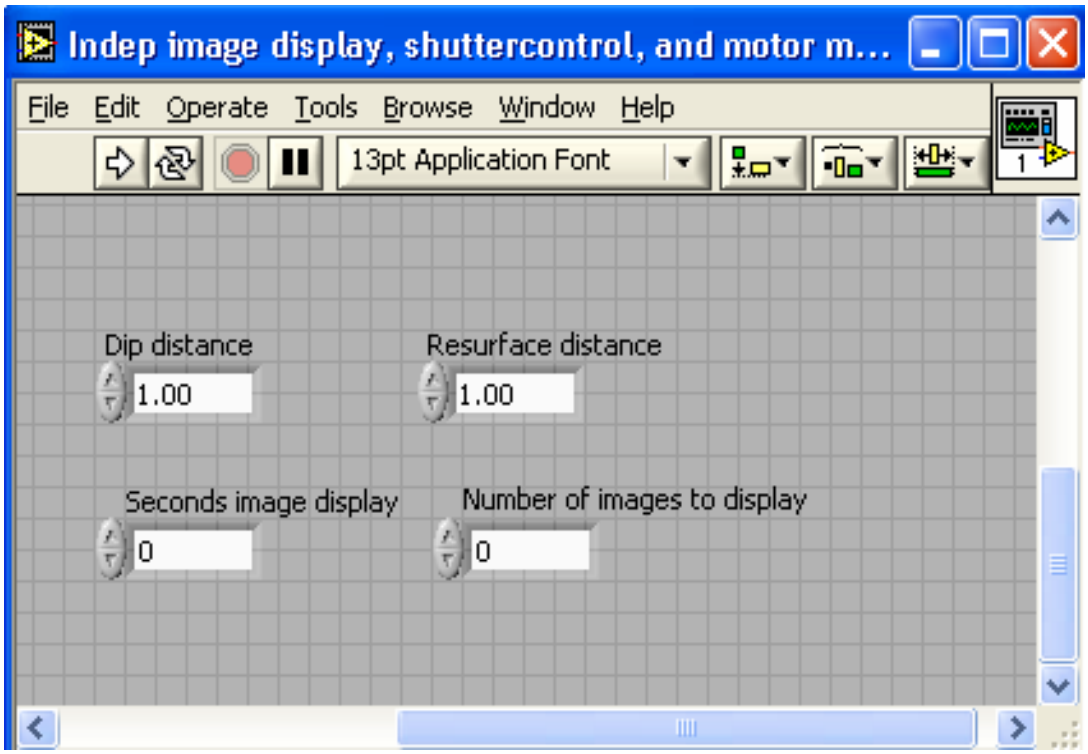

Figure A. 8: Screen layout for Front Panel

xvi) Insert values for the parameters shown on the front panel in conjunction with the build of the structure. “Seconds image display” is the amount of seconds to have the monomer solution exposed with light (the length of time that the shutter is open). The needed exposure time is different for each monomer solution, but is usually about 60 seconds. “Dip distance” is the distance (in mm) of the downward motion of the stage shelf to coat the top layer of the structure in a new layer of monomer to be polymerized (z coordinates). “Resurface distance” is the distance to raise the stage shelf out of the monomer to expose the next layer of the structure (again z coordinates). Also,

Dip distance – resurface distance = height of exposed polymer

So, under normal conditions,

Dip distance = 3.1

Resurface distance = 3.0

These parameters are to be optimized for each experiment.

xvii) Press Control+E. This brings up the block diagram. This diagram should look like:

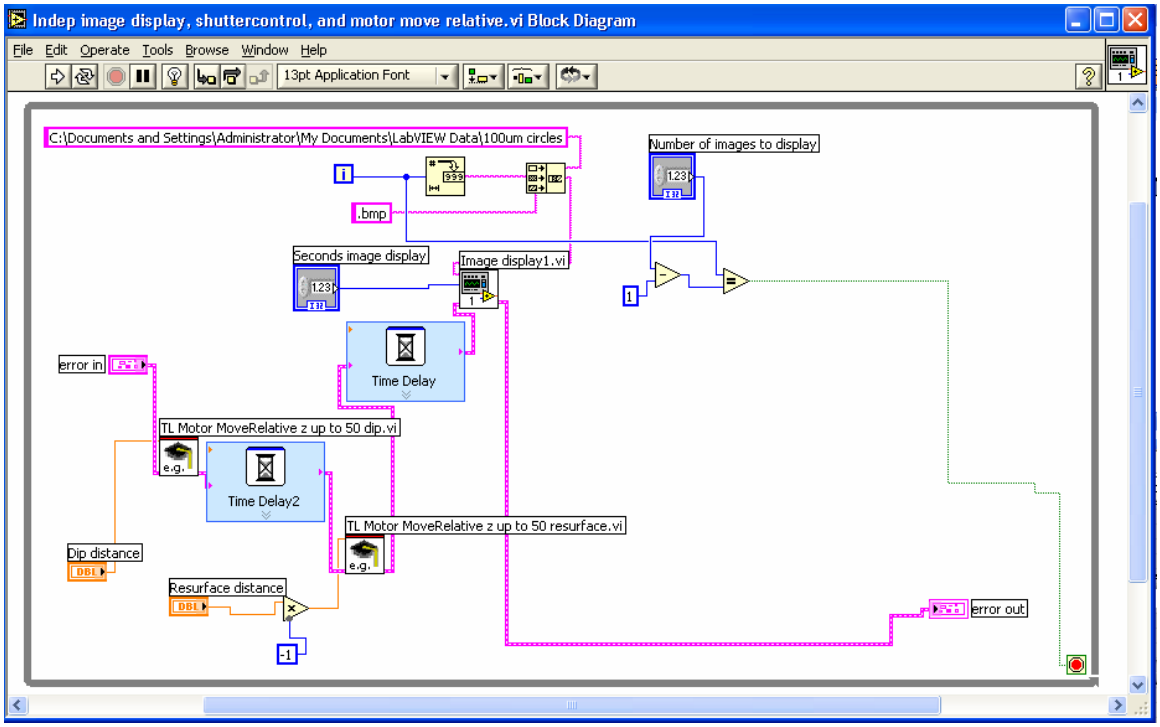

Figure A.9: Screen shot of block diagram

At the top left of the window is a pink box that contains a path. Redefine the path name to retrieve the appropriate images. The images should be labeled in the order they should appear with the exact same path name with the exception of the final number. The numbering should start with zero and continue until all the images have been numbered. They should be in the bitmap format. Type the path in the box, with the exception of the numbering, and the .bmp which will be added by the program.

xviii) Press the button the upper left hand portion of the screen of the block diagram or front panel that looks similar to ⇨. Verify the program is running properly. Allow for the program to run until it stops or shows

an error. If the program shows an error, click ok and then close the shutter if it has been left open.

Note – Troubleshooting: If the program displays an error before finished with the specified number of cycles, close all programs, turn off the computer, unplug the DMD, switch off the shutter control, and then the stages. Turn on the computer but do not log back in until the DMD is plugged in, the shutter control is switched on, and then the stages are switched on. Log back in to the computer and resume at part III (pg. 157).

xix) When the program is done, remove the structure from the vat, built on the silicon.

xx) Turn off all equipment and clean everything touched by the monomer at the end of all experiments. Make sure not to bump the optical setup.

LabView Code

This documentation comes from work done by J. Stanton in our laboratory to help automate this system. This code displays images for a given amount of time, while also moving the stages to the correct position and closing the lamp shutter while the stages were in route. First a vi calls a single image from a text string file path and displays that image on the mirror array for the entered value of milliseconds (ms). Using that template, the program is composed of a series of timed loops, suited for displaying up to 10 images for individually entered ms of display time and then subvi's are placed in strategic locations to control of the stages and shutter. The front panel of this vi looks like this:

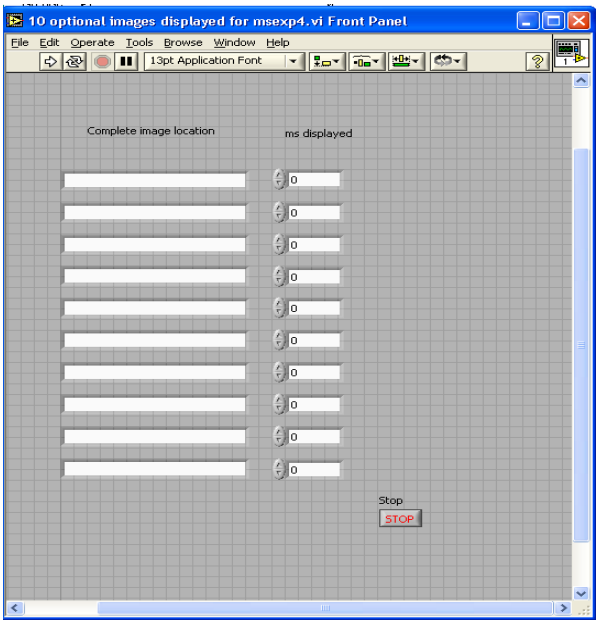

Figure A.10: Screen shot of front panel

The block diagram of this vi looks like Figure A.11 through Figure A.16, shown in the following pages.

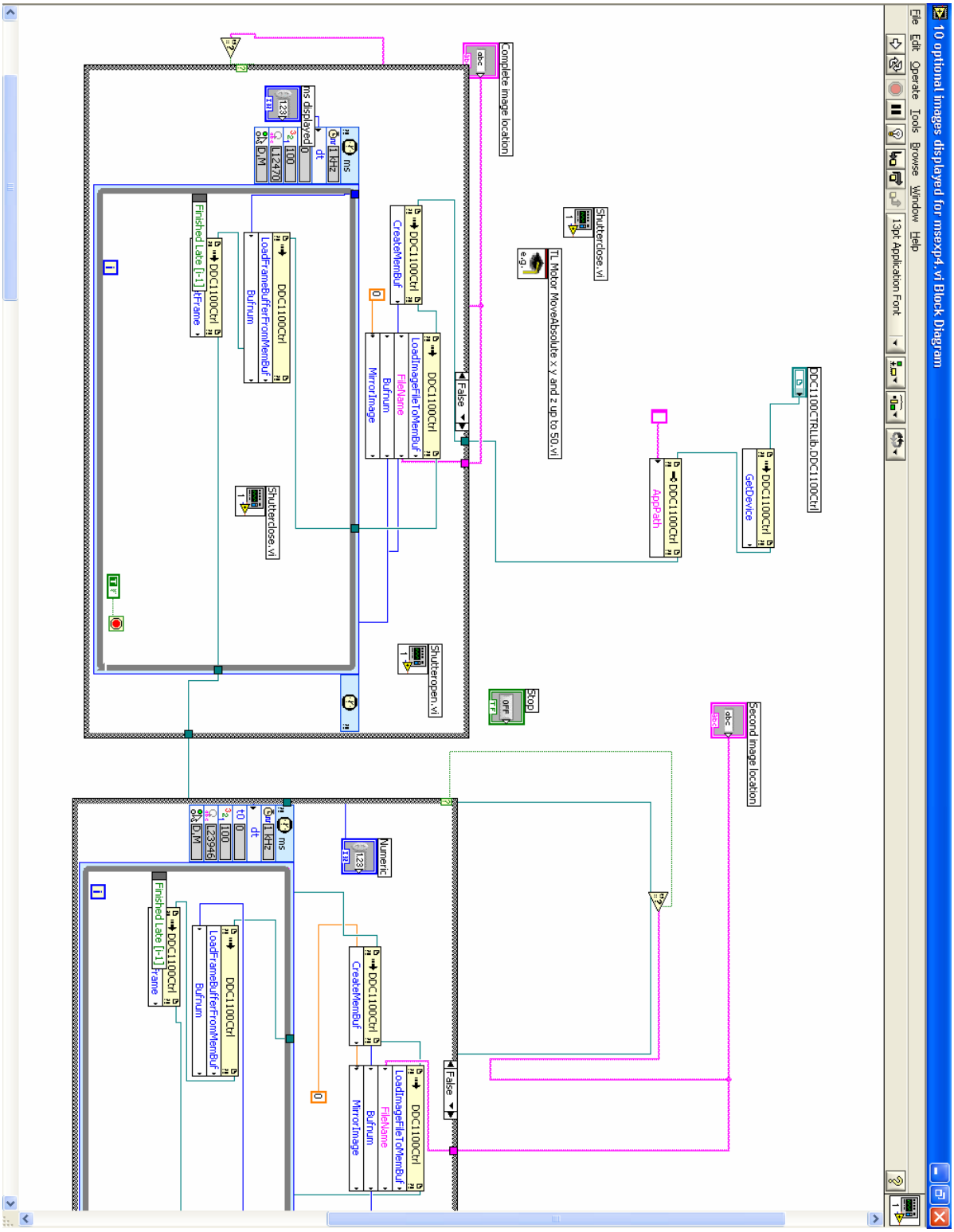

Figure A.11: Overall screen shot of block diagram for control program (pg 1).

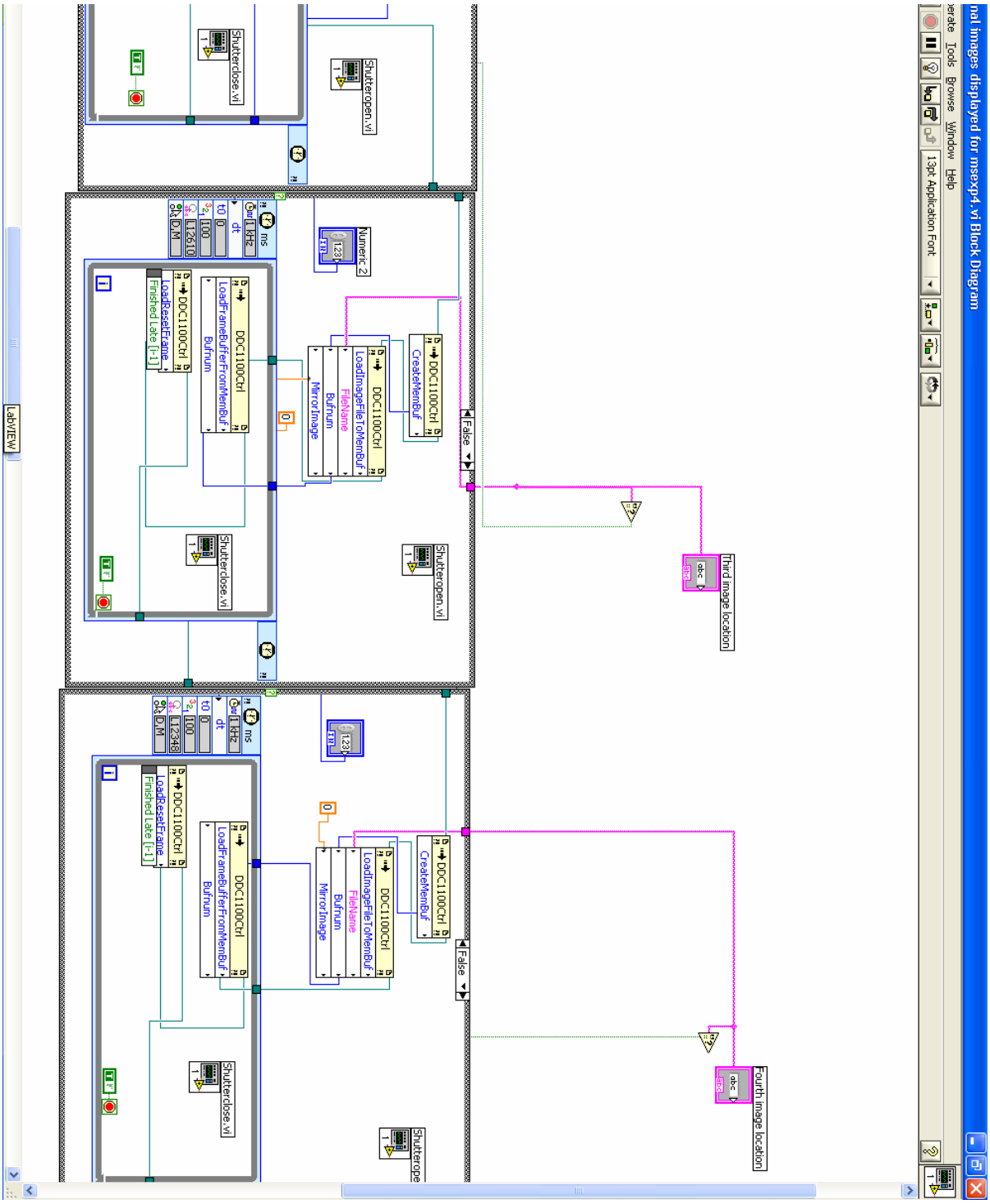

Figure A.12: Overall screen shot of block diagram for control program (pg 2).

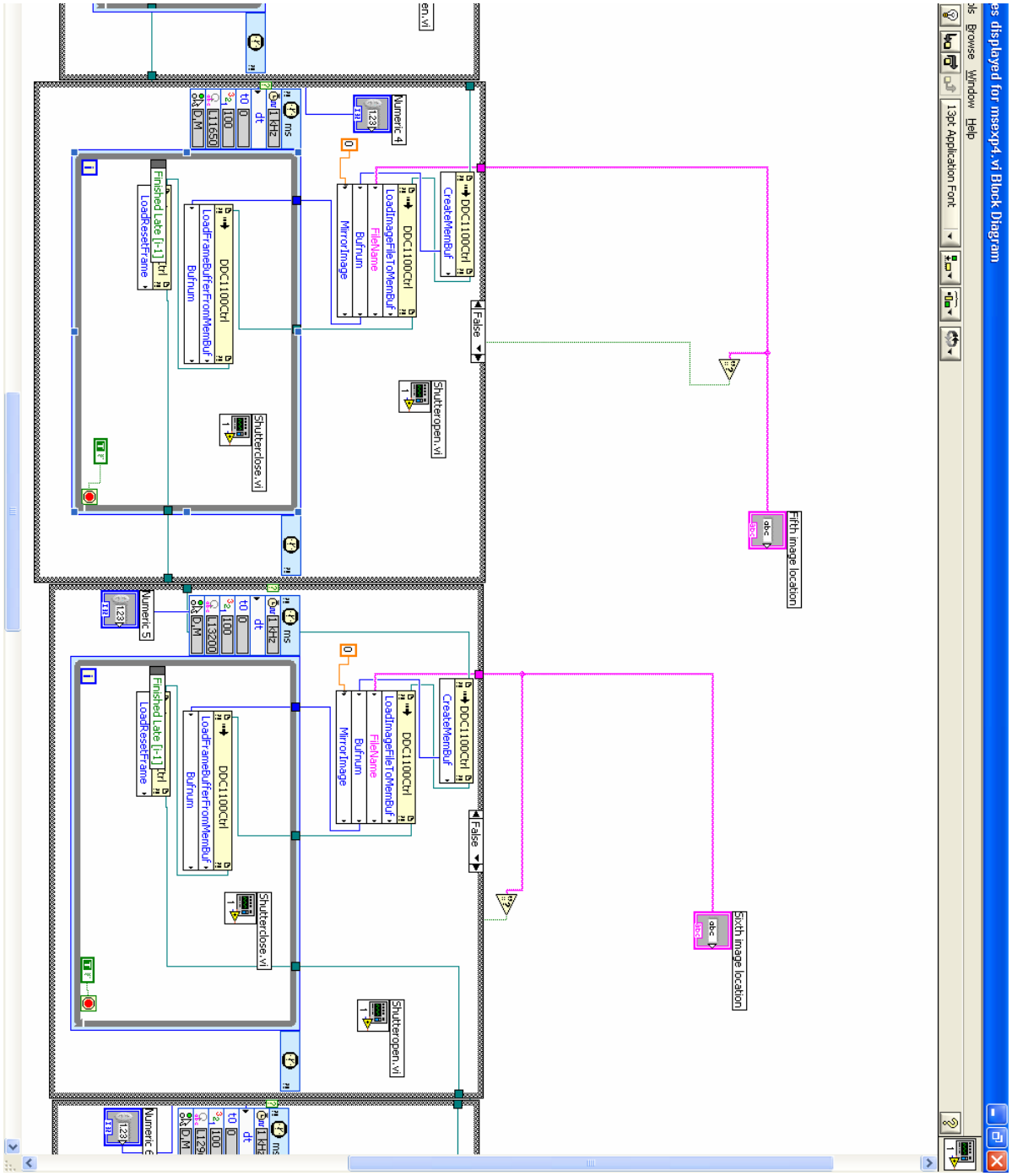

Figure A.13: Overall screen shot of block diagram for control program (pg 3).

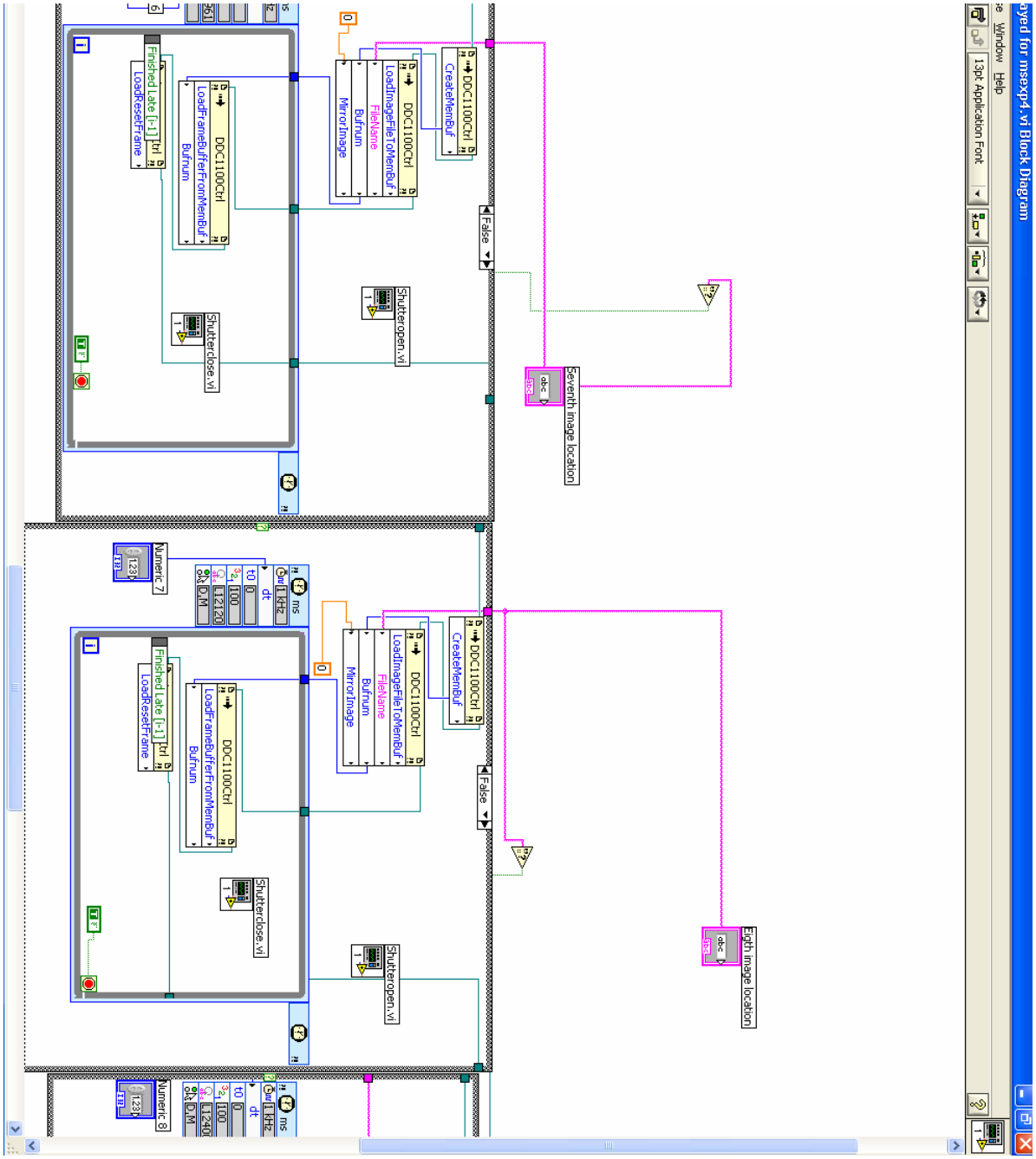

Figure A.14: Overall screen shot of block diagram for control program (pg 4).

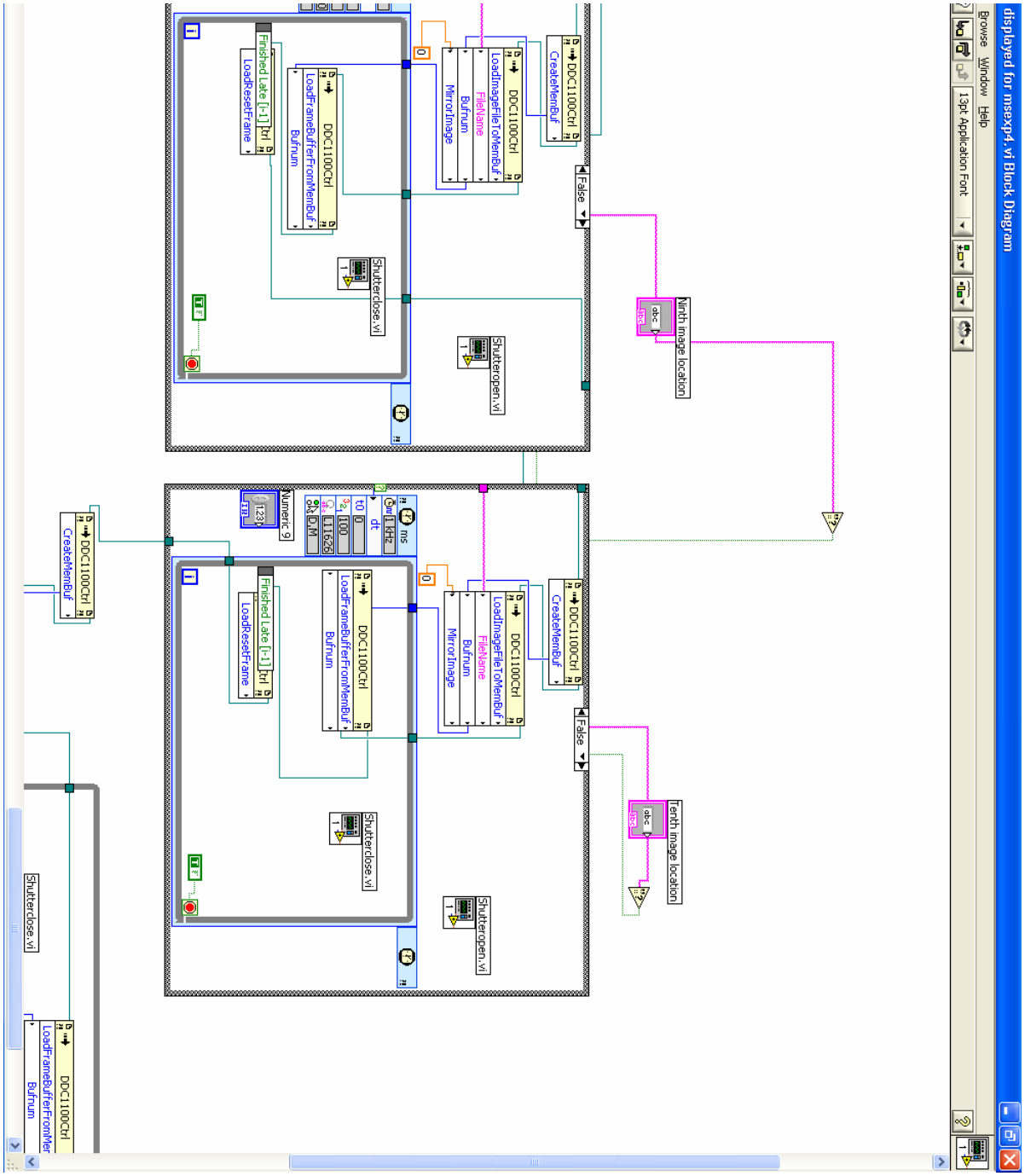

Figure A.15: Overall screen shot of block diagram for control program (pg 5).

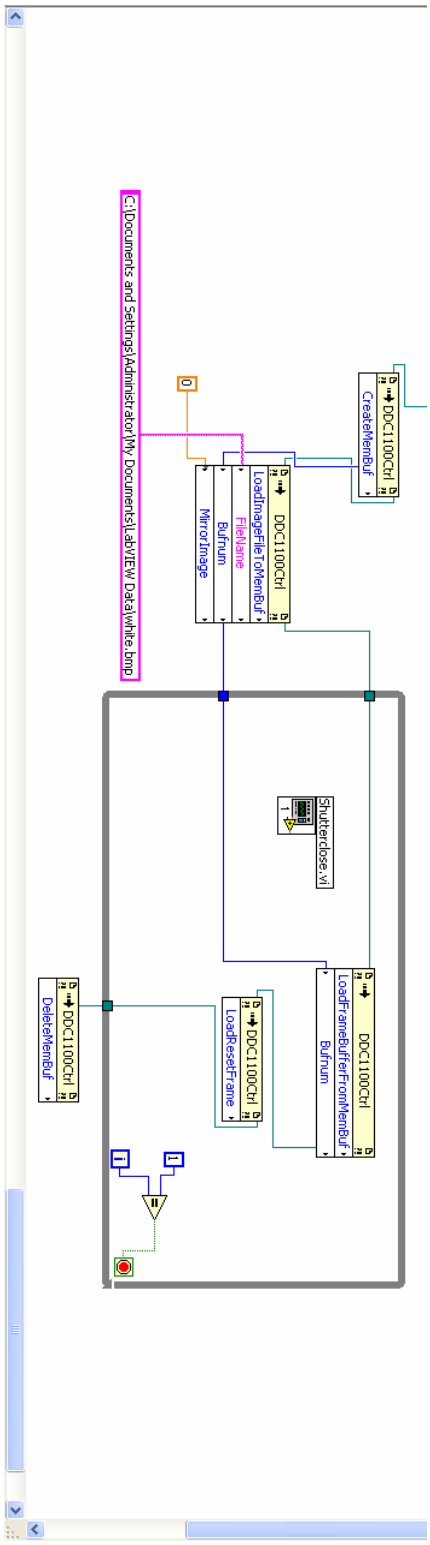

Figure A.16: Overall screen shot of block diagram for control program (pg 6).

As you can see, the vi has several subvi's integrated within it. These vi's are shutteropen, shutterclose, and TL Motor Move Absolute x, y, and z up to 50. Shutteropen and shutterclose are very similar vi's and are modified versions of a vi written by Craig Tabita, shuttercontrol. Their function is to open and close the shutter. The front panels and block diagrams are as follows, respectively (Figures A.17-19):

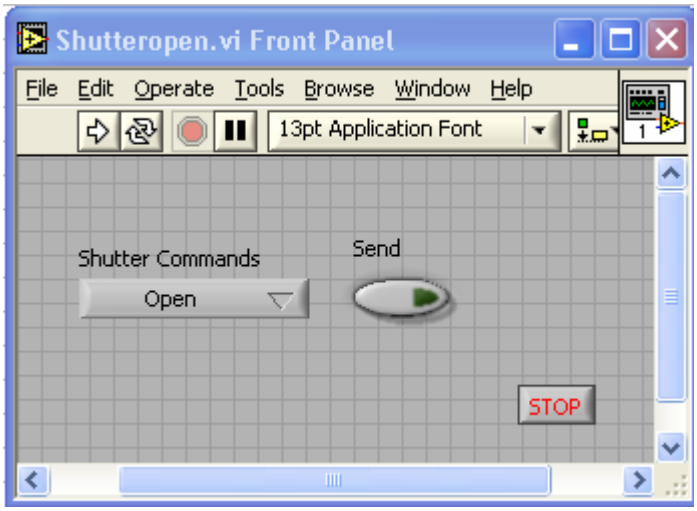

Figure A.17: Shutteropen.vi front panel

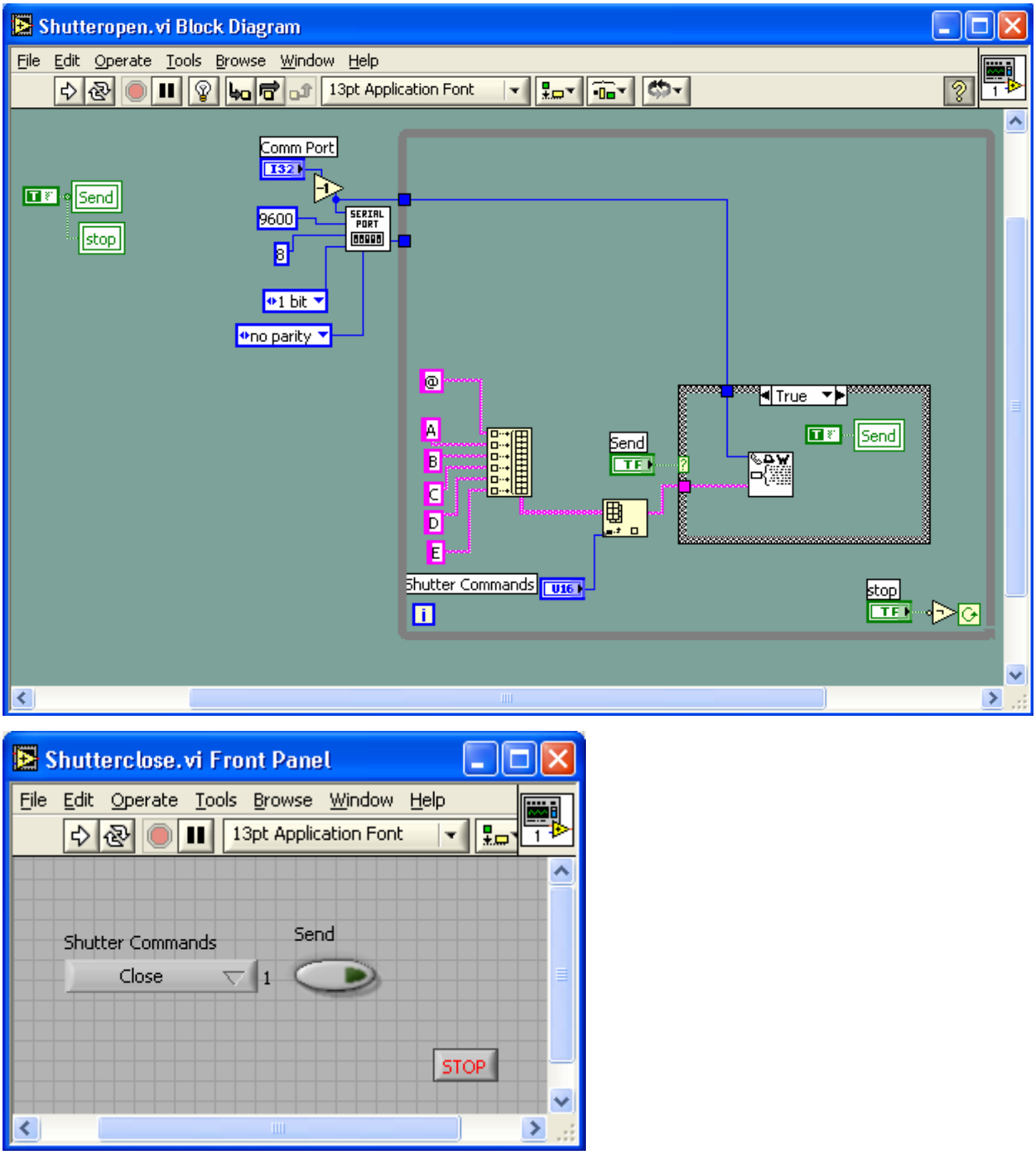

Figure A.18: Shutterclose front panel and block diagram

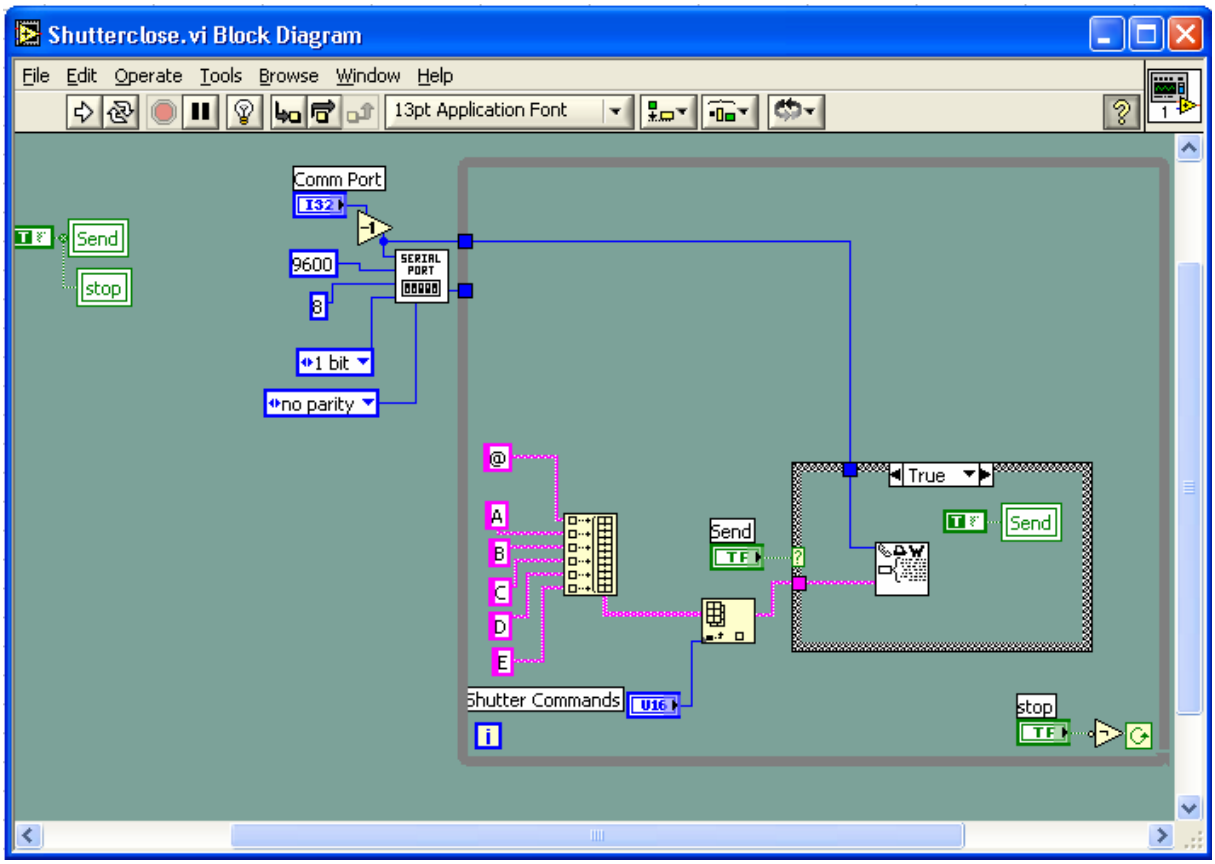

Figure A.19: Shutterclose.vi block diagram

The TL Motor Move Absolute x, y, and z up to 50, and its close relative, TL Motor Move Relative x, y, and z up to 50, are designed to move and control the motorized stages. The front panel and block diagram are as follows in Figures A.20 and A.21.

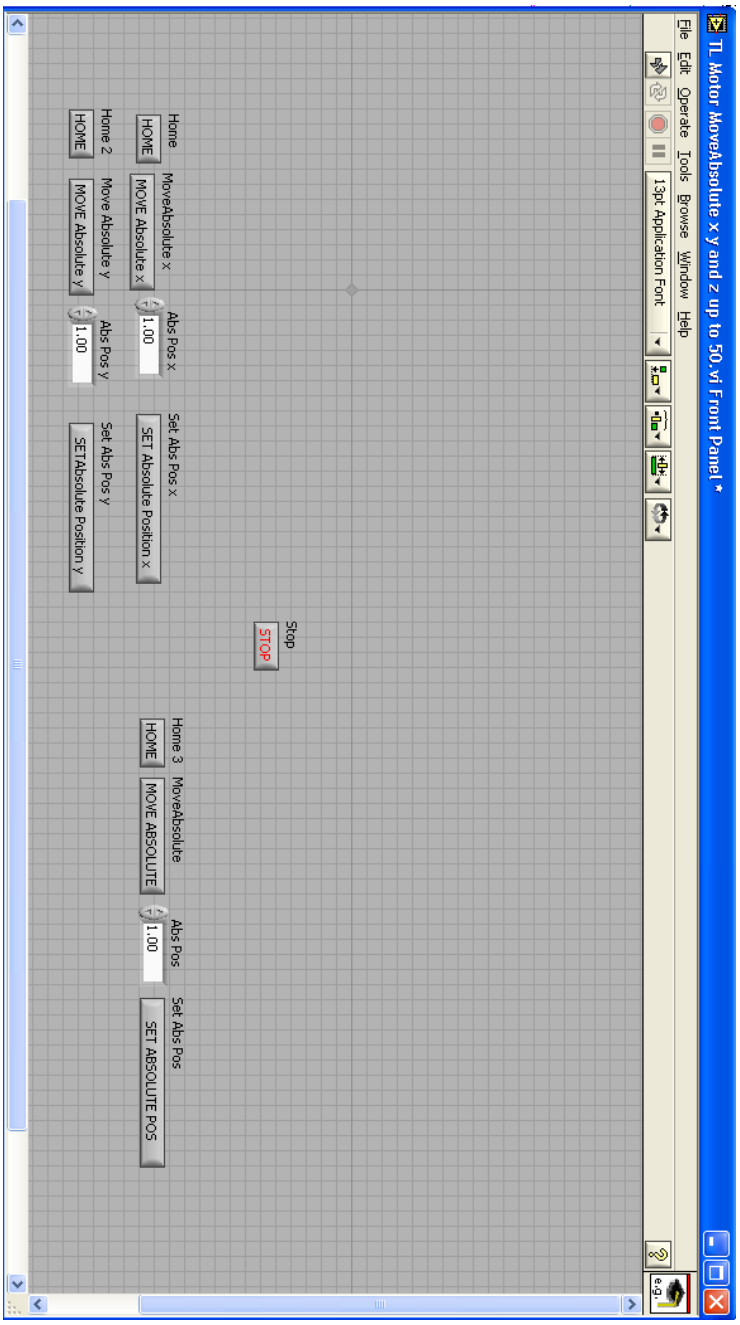

Figure A.20: Motormove front panel

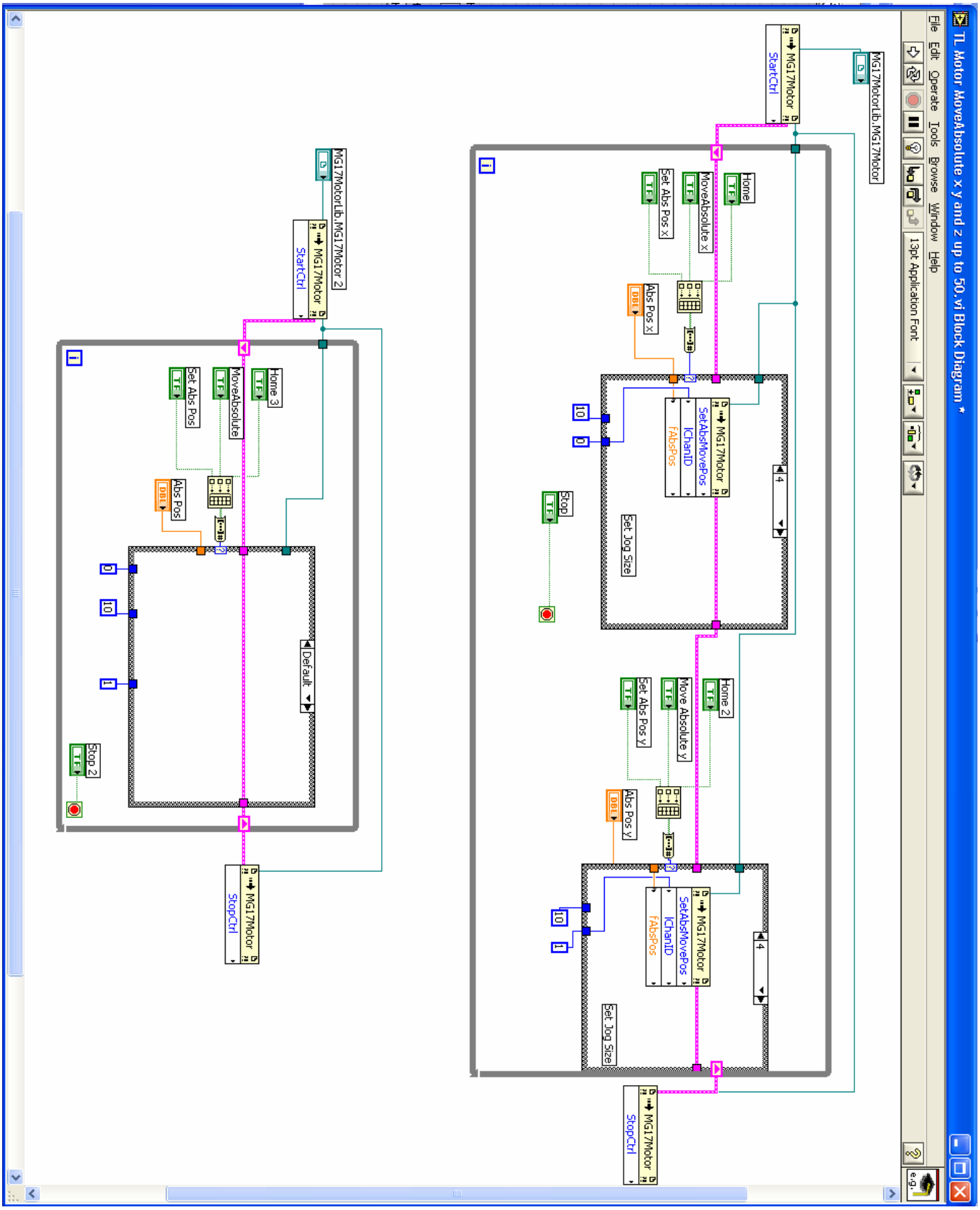

Figure A.21: Motormove block diagram

APPENDIX B

DOCUMENTATION FOR MICRO-SLA SYSTEM:

PART SCHEMATICS

This Appendix gives the documentation used to design and build the custom built pieces for the Micro-SLA system. Many were built on the SLA Viper in the RPMI lab.

Holder for TI-DMD Mirror Array

One of the first pieces that was designed and built was a holder for the mirror array so that it could be securely mounted and handled safely. The mirror array comes only as the device mounted on a printed circuit board. This configuration works well, perhaps, for a design where the mirror array is to be encased and built into a larger electronic breadboard. However, for a device that is to be used in the open, it is difficult to handle and position in such a way that the mirrors are oriented properly in the on and off modes. The following holder was designed using Solid Edge software and built on the SLA Viper.

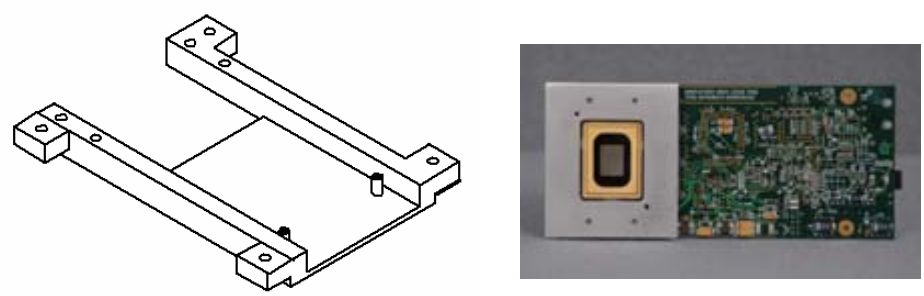

Figure B.1: Isometric view of DMD holder and photograph of TI-DMD, as supplied

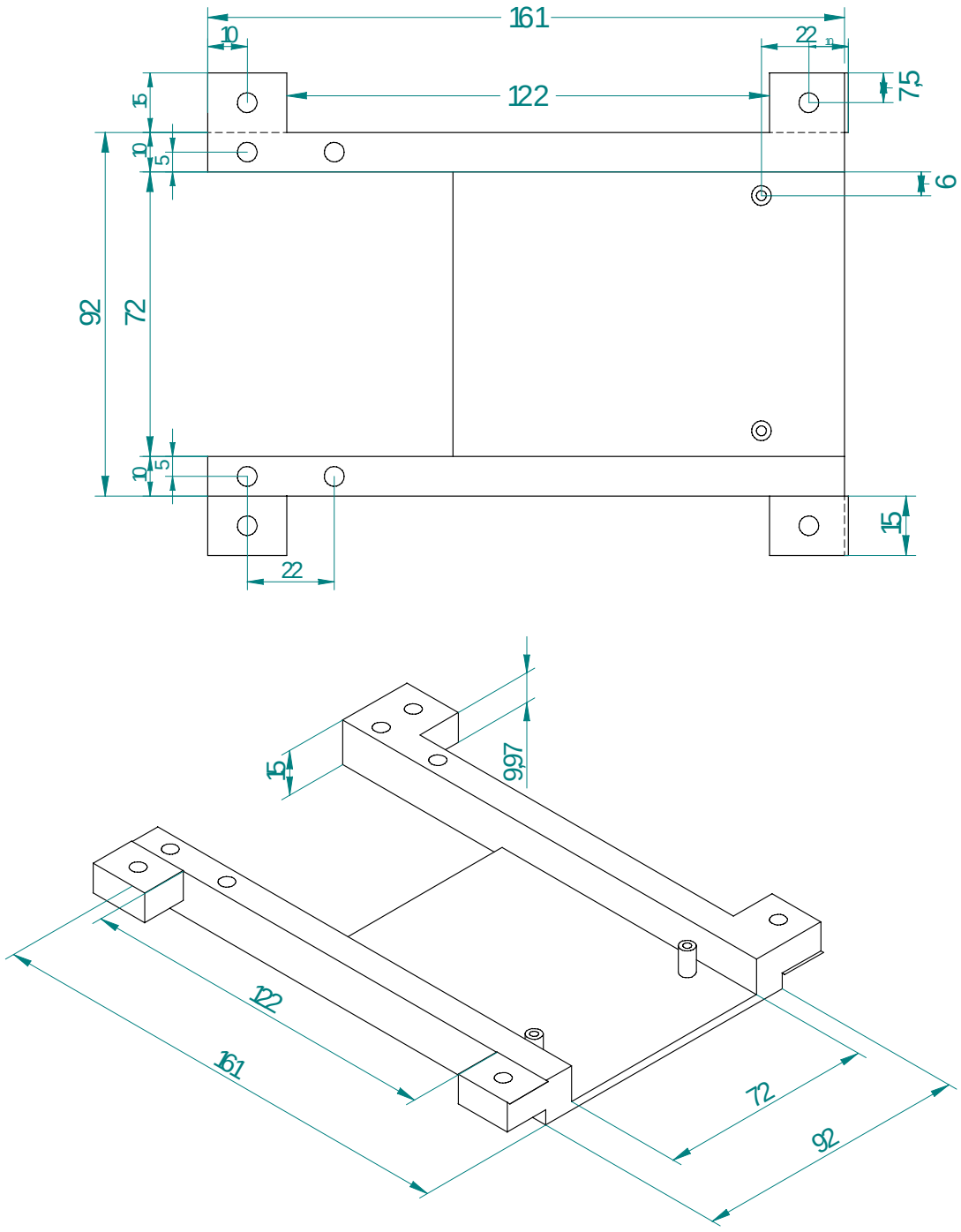

Figure B.2:DMD Holder schematics

DMD Mount Bar

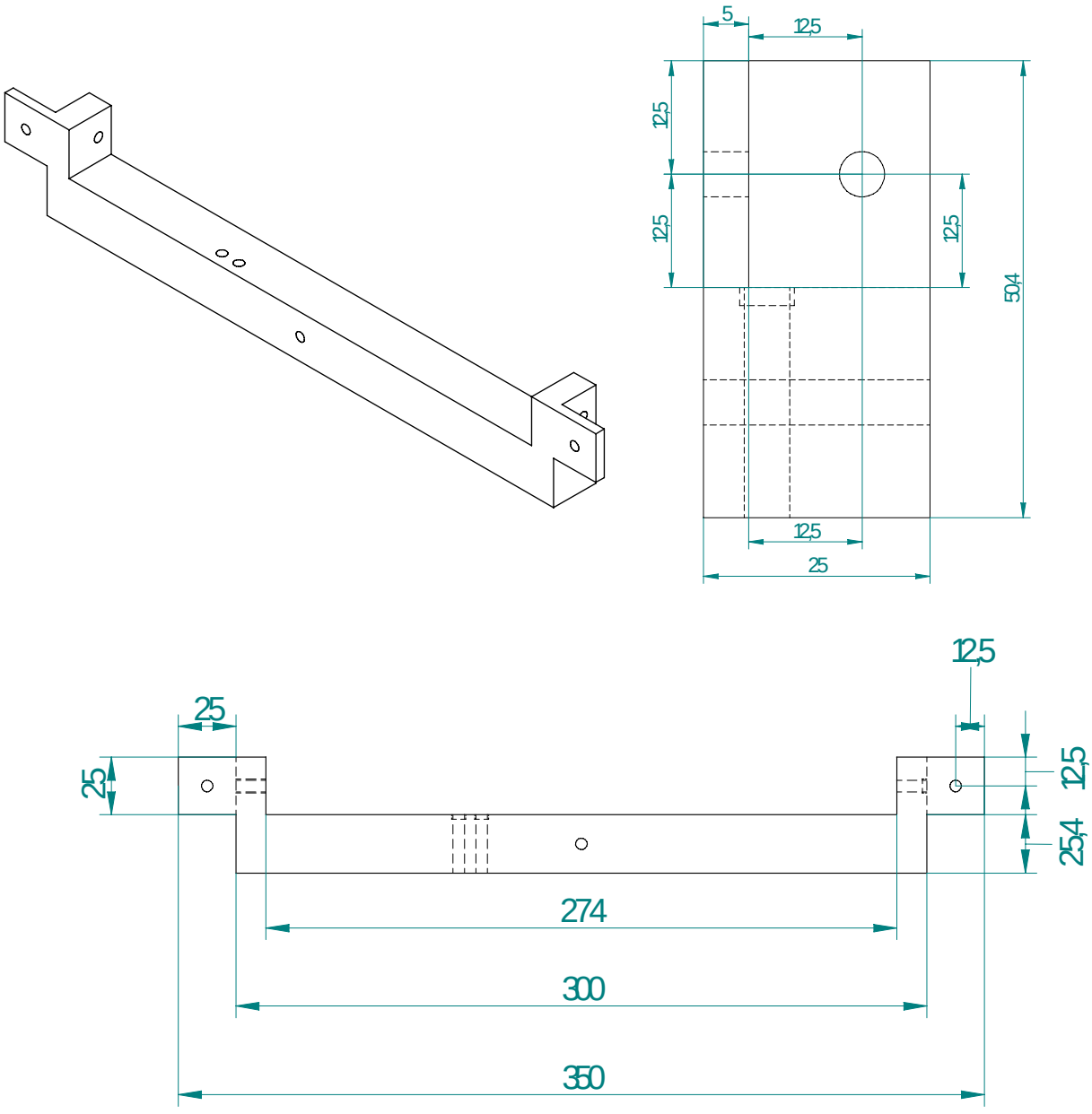

Figure B.3: DMD Mount bar schematics

Gimble Mount

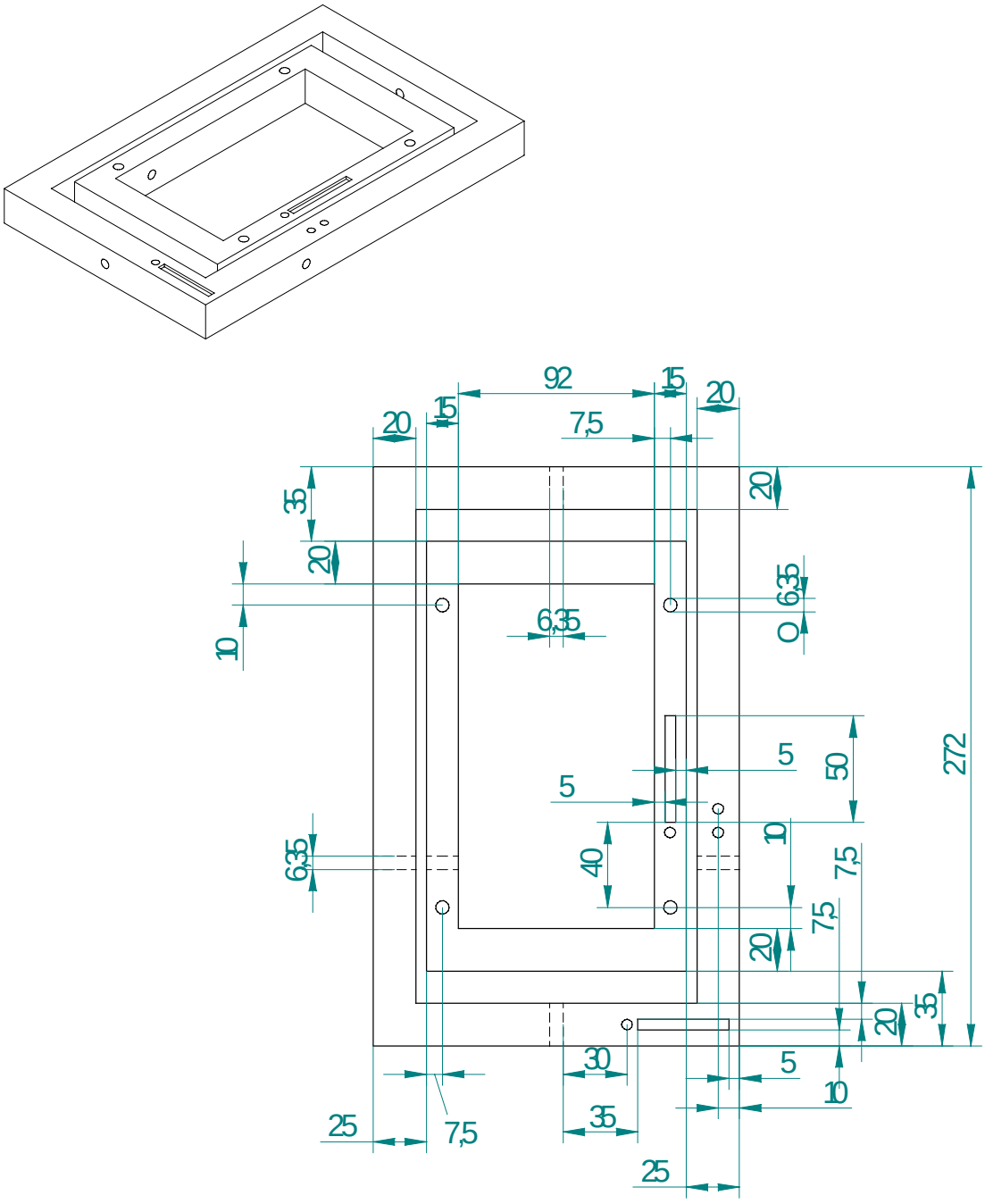

Figure B.4: Gimble mount schematics

Stage

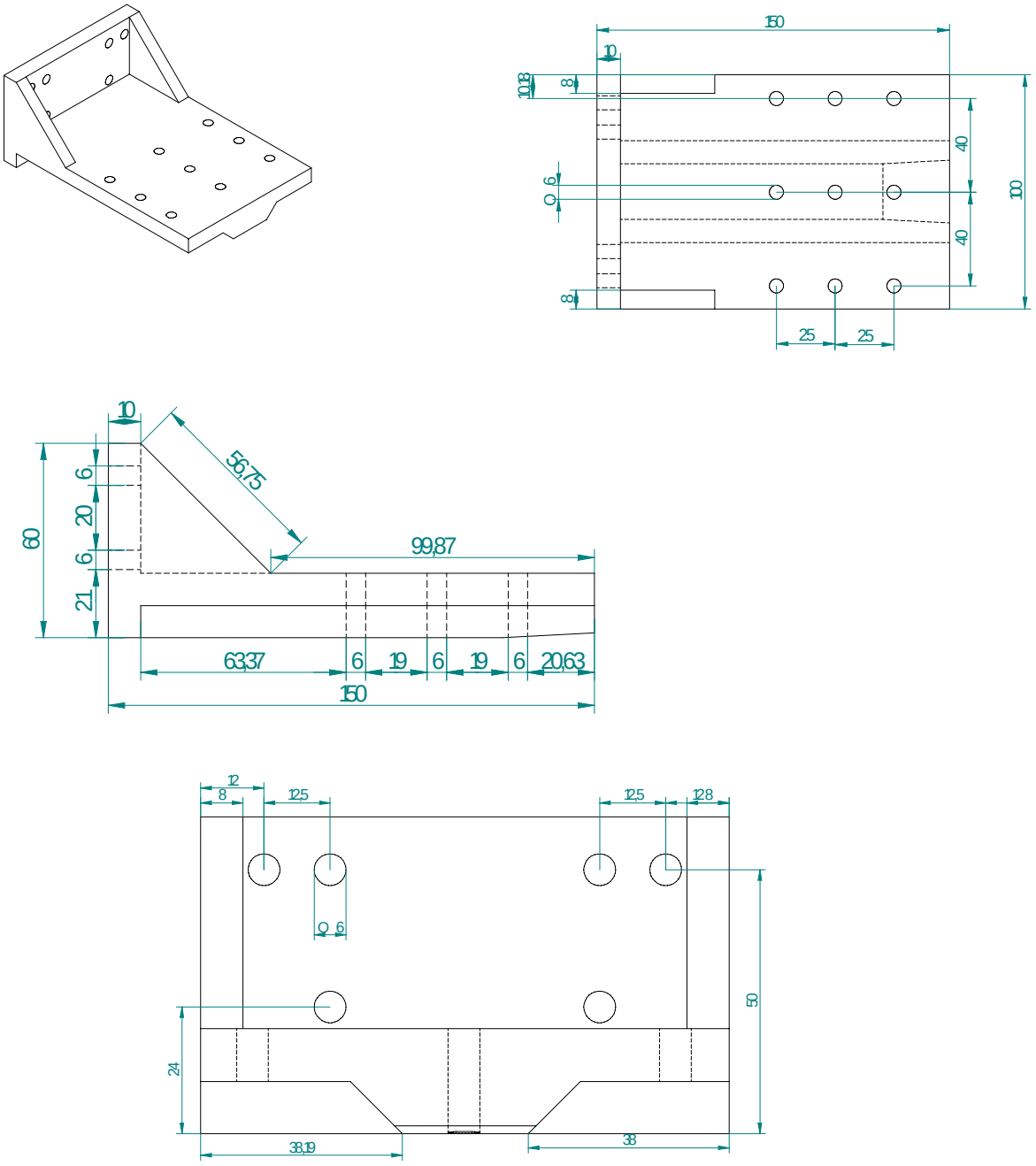

Figure B.5: Stage schematics

Vat

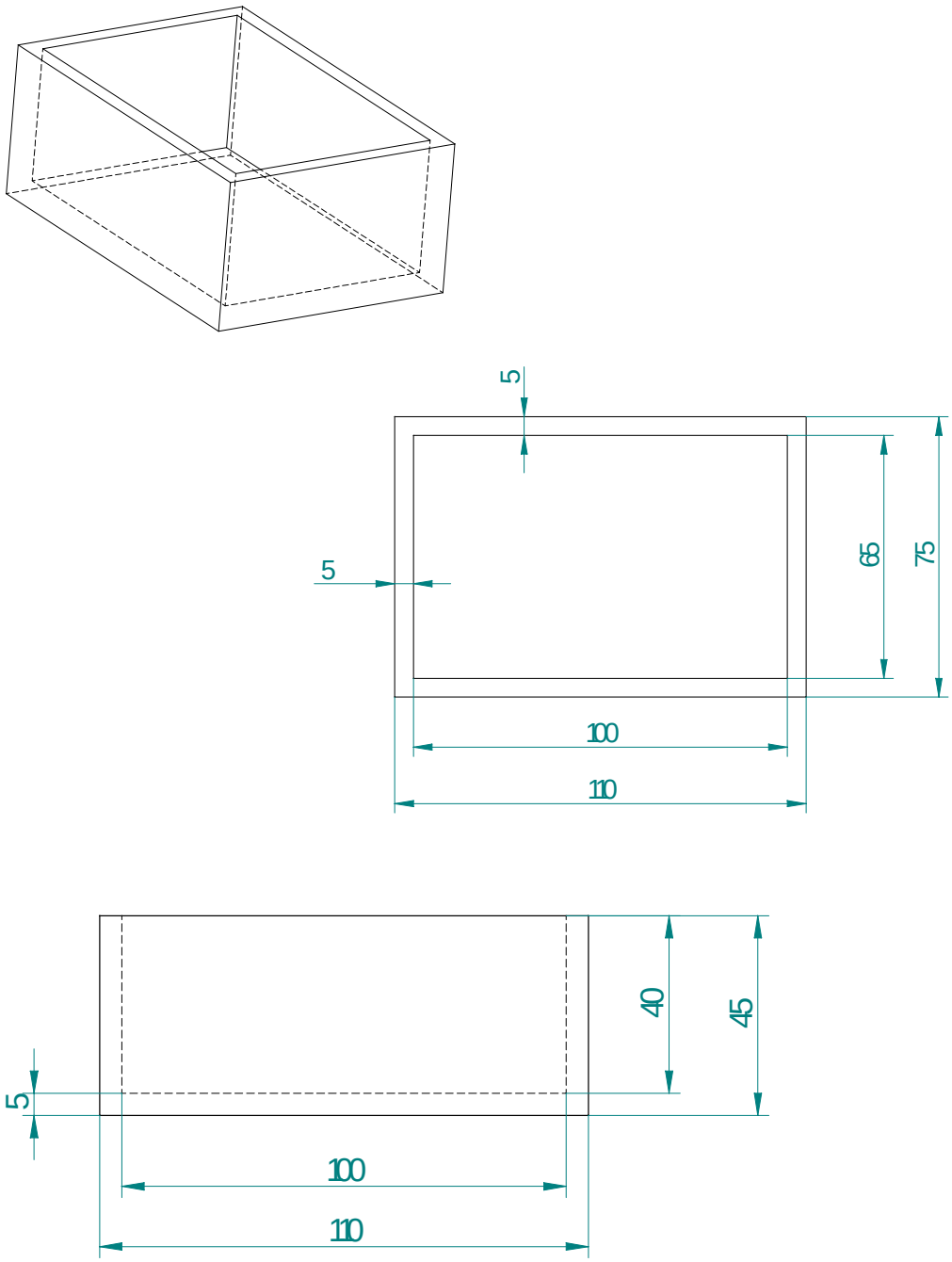

Figure B.6: Vat schematics

Vat Top

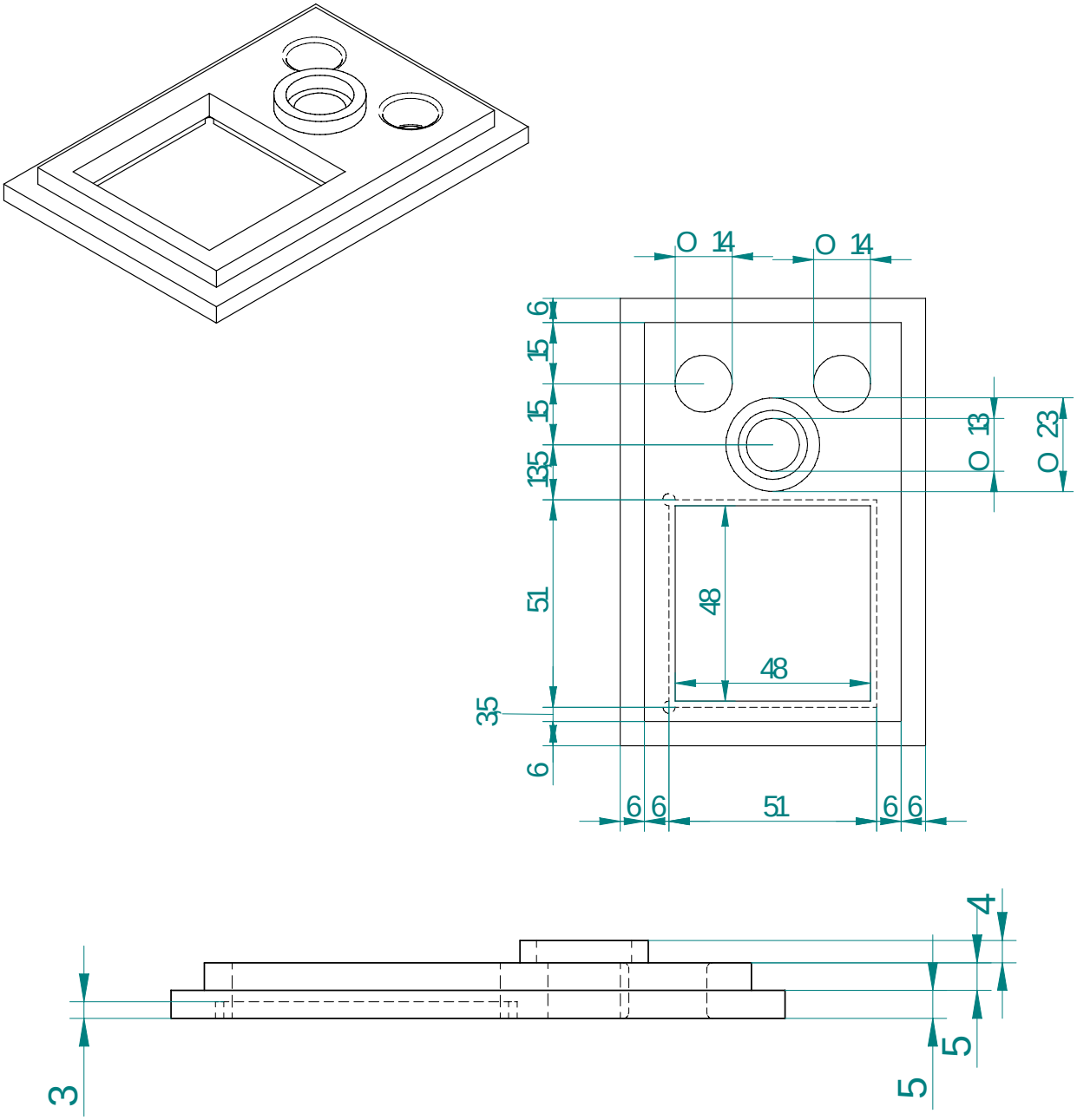

Figure B.7: Vat top schematics

Vat Stage

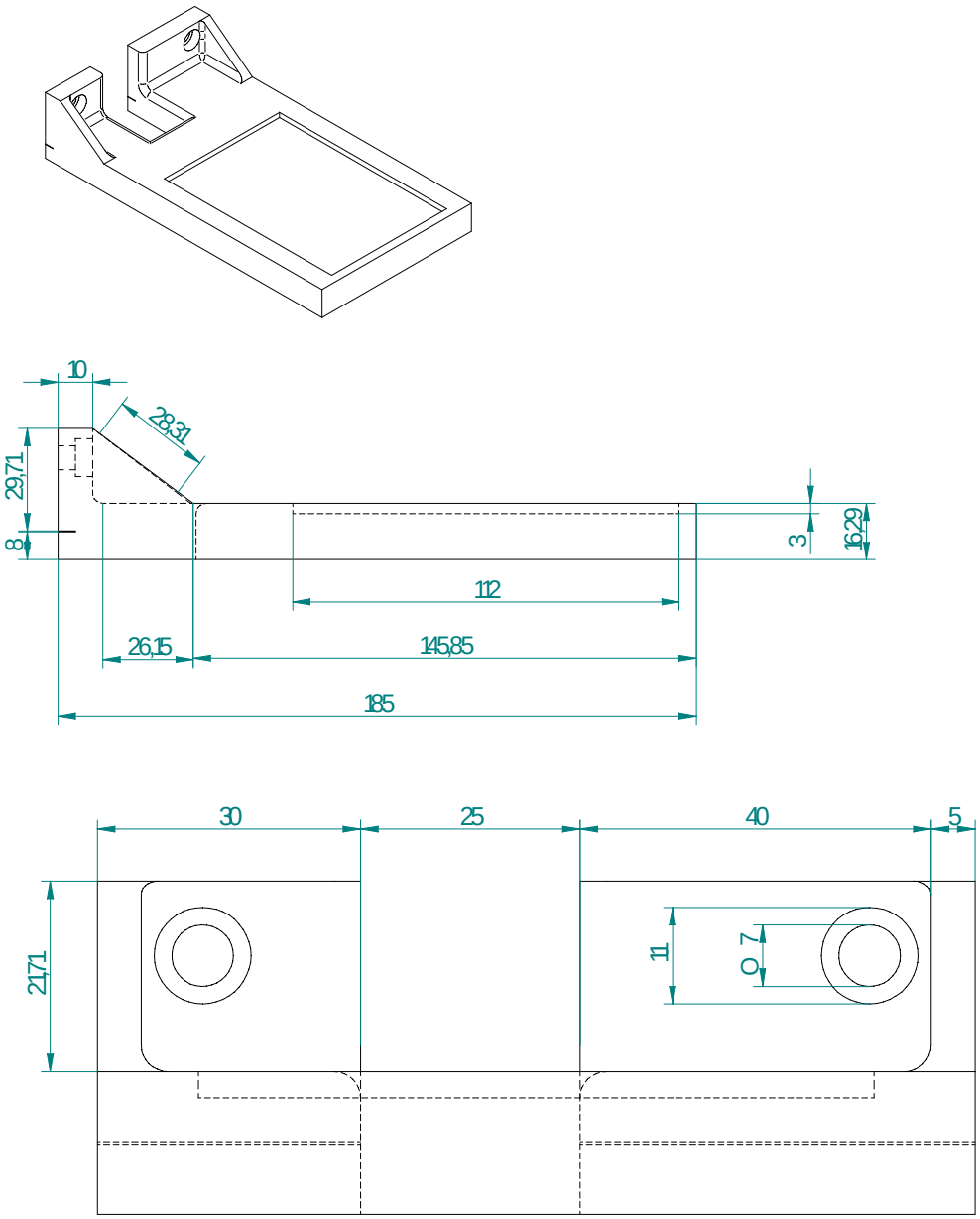

Figure B.8: Vat stage schematics

Elevator Platform

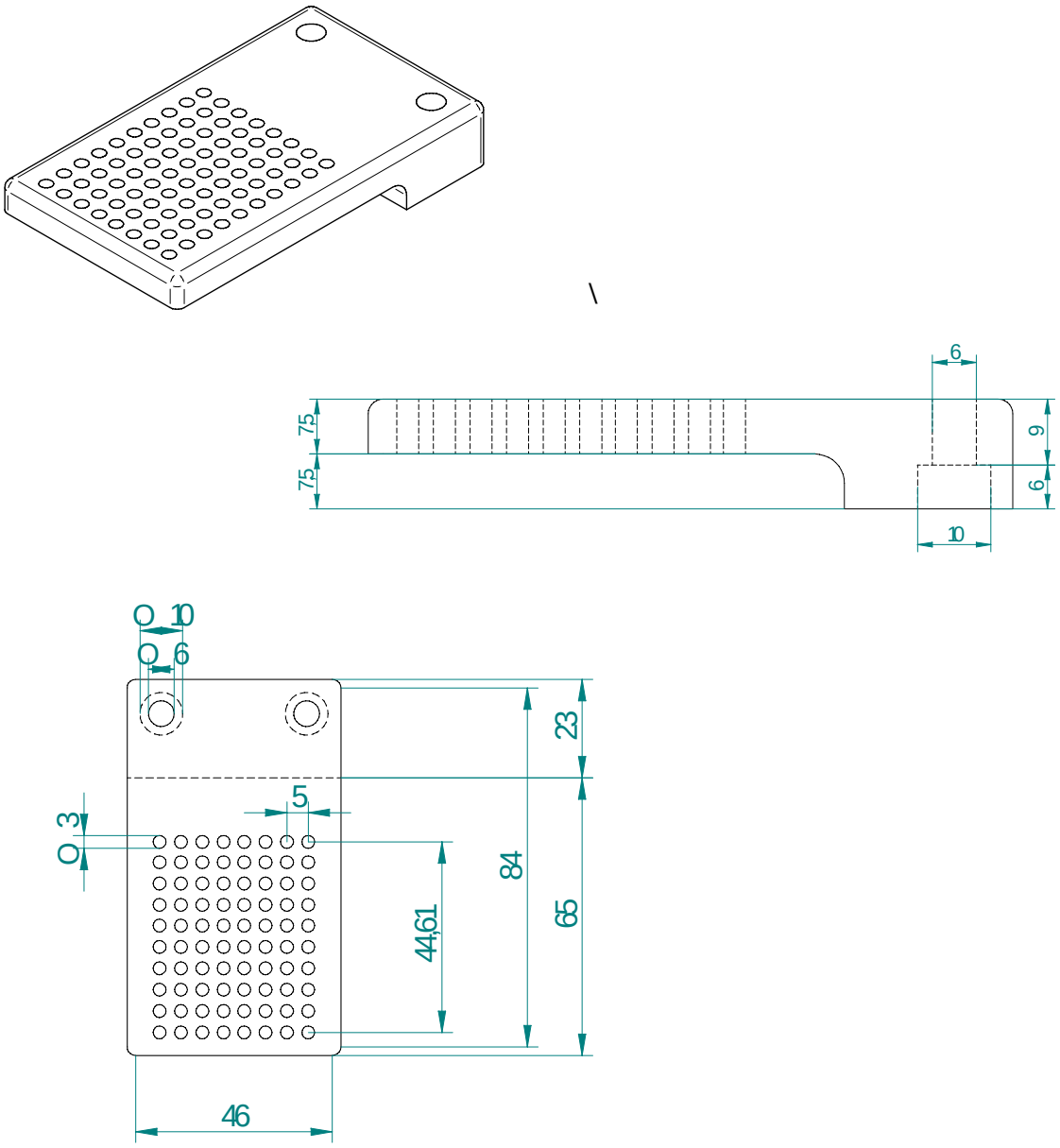

Figure B.9: Elevator platform schematics

Elevator Stage Connection

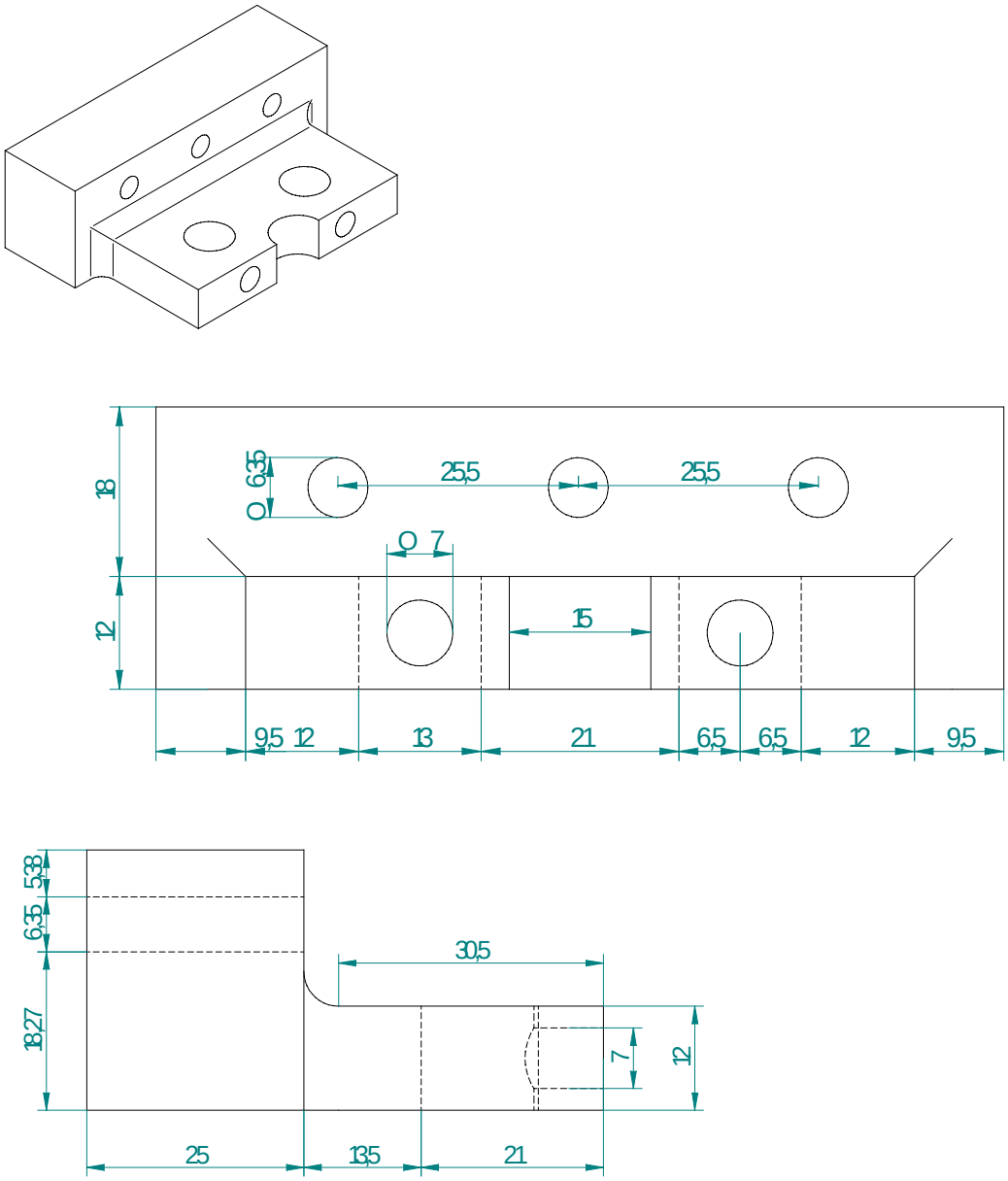

Figure B.10: Elevator stage connection schematics

Lens Holder

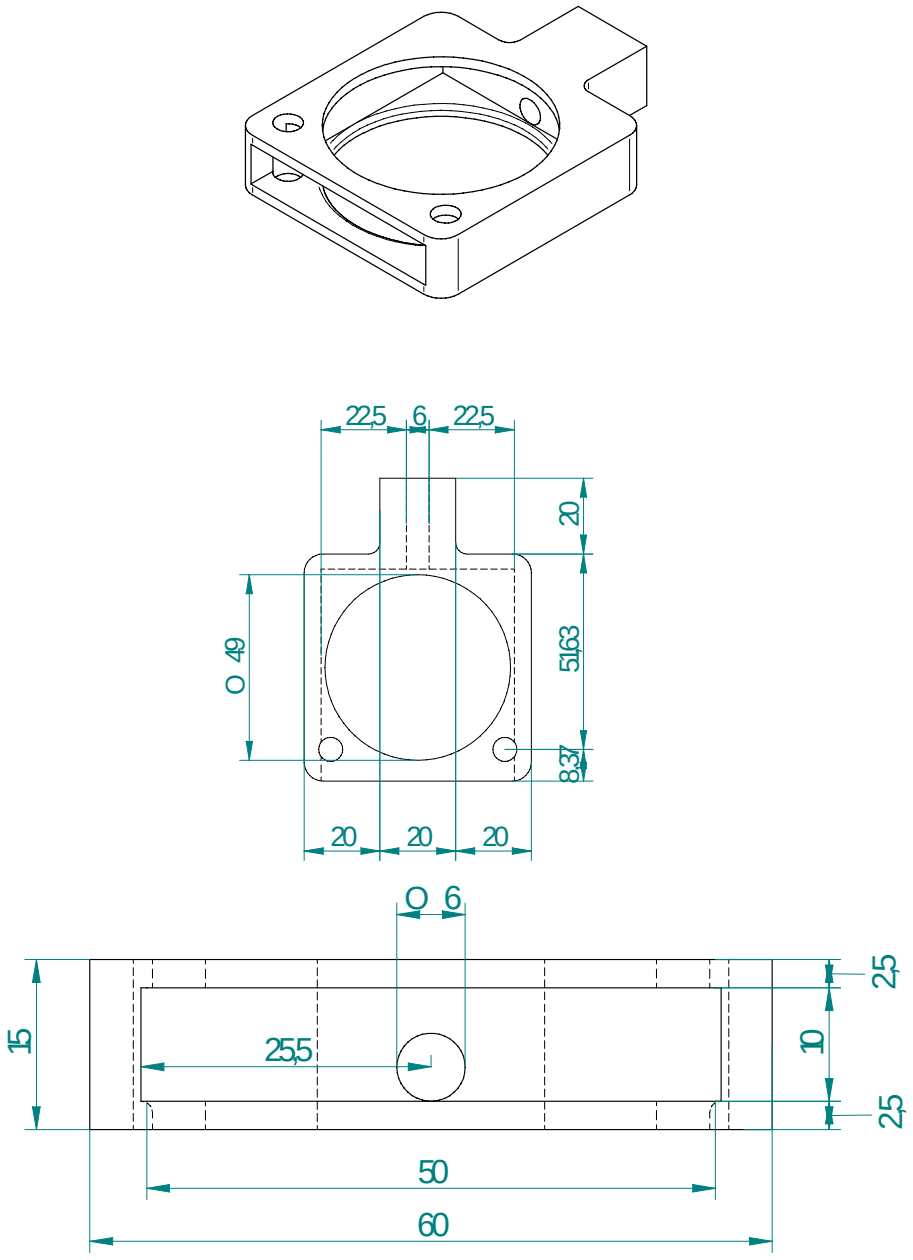

Figure B.11: Lens holder schematics

Tube Holder

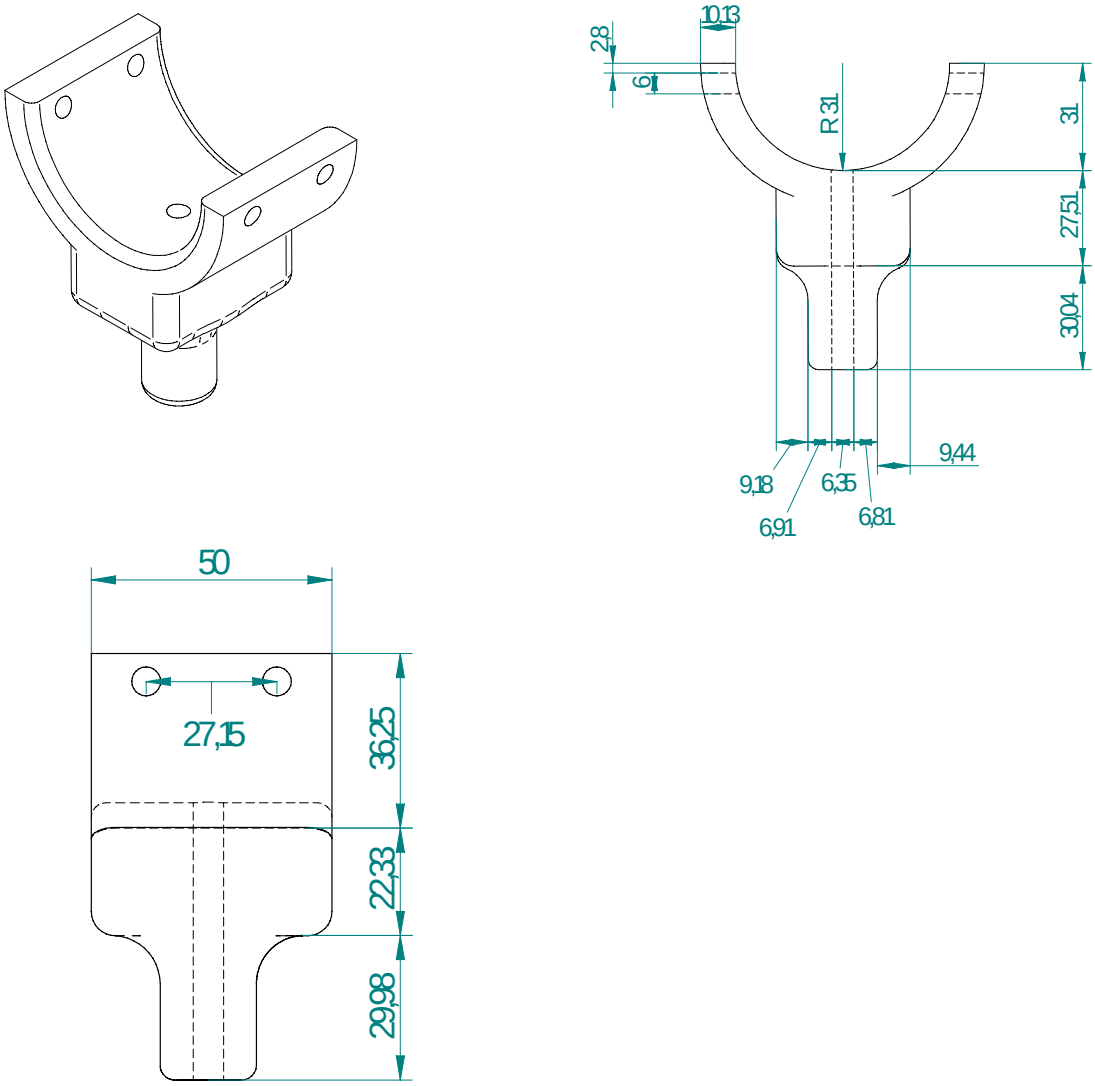

Figure B.12: Tube holder schematics

CCD Camera Stage

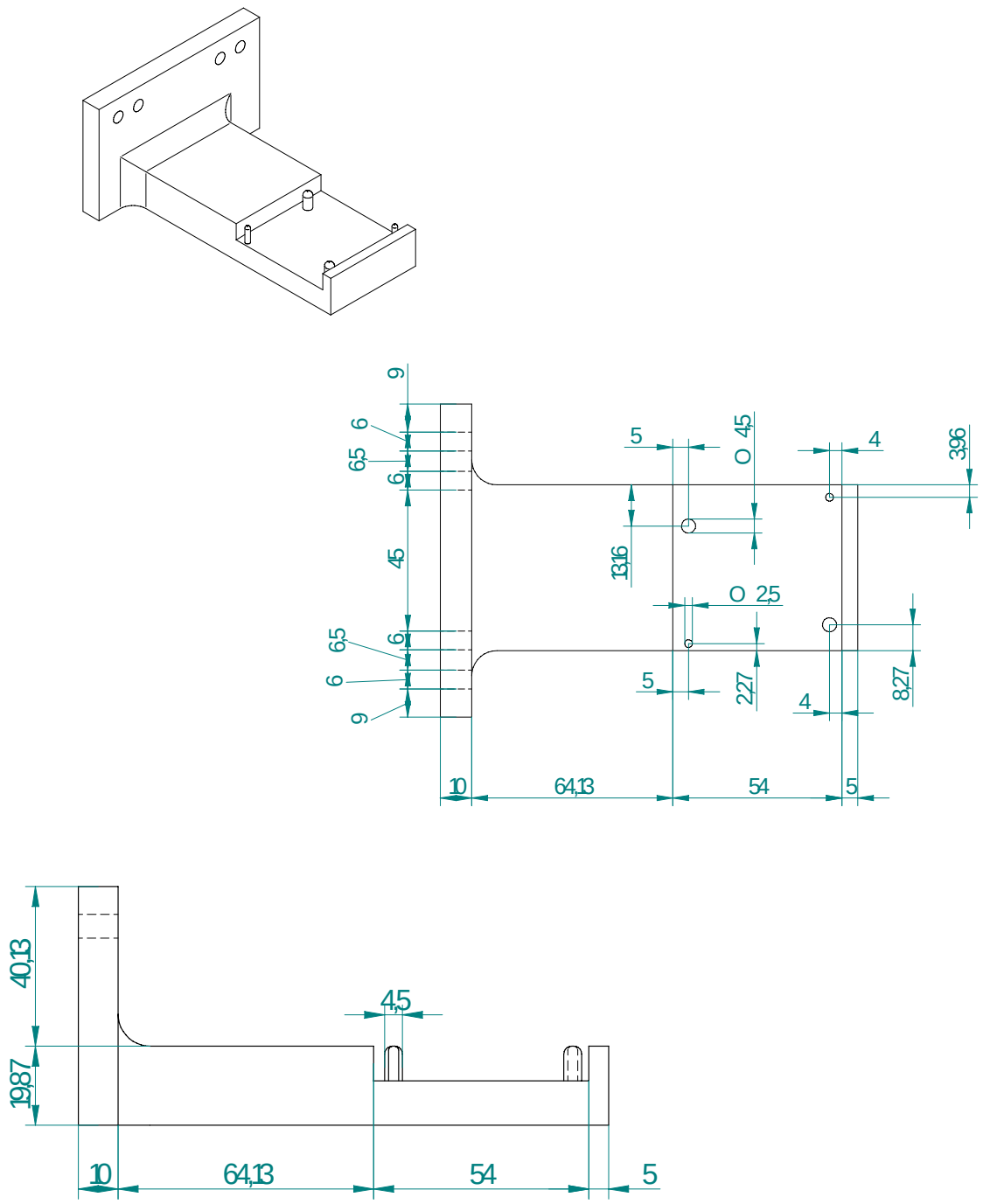

Figure B.13: CCD Camera stage schematics

APPENDIX C

CHEMICAL REACTIONS

Monomer Protection Reactions

In order to realize the fabrication method presented in the thesis, it is necessary to use protected materials so that the acid-catalyzed de-protection reaction may be used to create chemical patterns on the scaffold surface. For stereolithography, the starting materials must be monomers or low molecular weight oligomers. Thus, protected monomers were synthesized and characterized.

Hydroxyethyl Acrylate

Protection of Hydroxyethyl Acrylate with Ethyl Ether

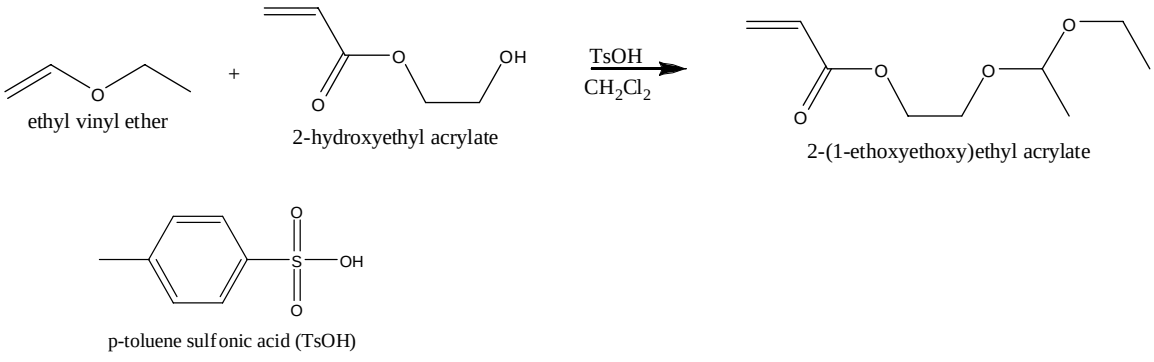

Figure C.1: Reaction scheme for hydroxyethyl acrylate protection with ethyl ether

This reaction was run according to a procedure by Meyers et al [1], cited in Greene's Protective Groups in Organic Synthesis, page 74 [2]. The reaction procedure is as follows.

Molar Equivalent Calculations:

3g of 2-hydroxyethylacrylate * 1mol/116.1g = 0.0258 moles

Ethyl vinyl ether: 1.2 * 0.0258 moles * 72.1 g/mol = 2.23 g

TsOH: 0.1 * 0.0258 moles * 190.22 g/mol = 0.49 g

1) Weigh 2-hydroxyethylacrylate to round bottom flask (3g)
2) Weigh 0.1 molar equivalents of TsOH on weigh paper (0.49 g) and add to flask
3) Mix a little and notice that the TsOH is not completely dissolving in the monomer, as expected.
4) Add about 40 mL of CH_2Cl_2 to flask and mix. Just add enough so that the TsOH dissolves.
5) Weigh out 1.2 molar equivalents of ethyl vinyl ether (2.23 g) in a small bottle and add to flask while stirring
6) Let stir at room temperature for 1 hour. Observe that the solution turned a dark red/brown color.
7) Add saturated $NaHCO_3$ and mix to wash
8) Separate organic layer. Observe that the organic layer is still a dark red/brown color.
9) Remove solvent using roto-vap apparatus.

Protection of Hydroxyethyl Acrylate with Tetrahydropyranyl (THP)

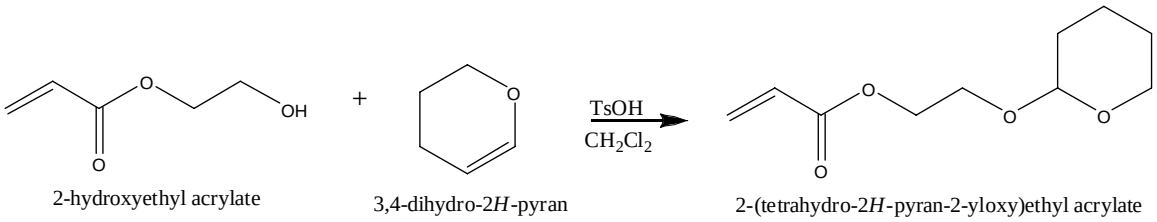

2-hydroxyethyl acrylate 3,4-dihydro-2*H*-pyran 2-(tetrahydro-2*H*-pyran-2-yloxy)ethyl acrylate

Figure C.2: Reaction scheme for hydroxyehtyl acrylate protection with THP

This reaction was run according to a preparation from Miyashita, Yoshikoshi, and Grieco [3] which is referenced in Greene's Protection Groups [2]. The procedure is below.

Molar Equivalent Calculations:

3g of 2-hydroxyethylacrylate * 1mol/116.1g = 0.0258 moles

Dihydropyran: 0.0258 moles * 84.1g/mol = 2.17 g

TsOH: 0.1 * 0.0258 moles * 190.22 g/mol = 0.49 g

1) Weigh out 2-hydroxyethylacrylate into round bottom flask (3 g)
2) Weigh out 0.1 molar equivalent of TsOH (0.49 g) on weigh paper and add to flask. Put a stir bar in and mix.
3) Weigh out 1 molar equivalent of dihydropyran (2.17 g)
4) Add CH_2Cl_2 to flask, about 40 ml, until TsOH dissolves
5) Add dihydropyran to flask slowly while stirring
6) Let stir at room temperature for 3 hours.

7) Make a half-saturated brine solution.
    a. At 60^{o}F a saturated brine solution is 26.4% salt by weight so add 26 g of salt to 200 g of water
8) Add flask contents to brine in separatory funnel
9) Shake the separatory funnel well and let sit.
10) Remove the bottom organic layer into a 100 ml round bottom flask
11) Roto-vap to remove dichloromethane solvent

Methacrylic Acid

Protection of Methacrylic Acid with THP Ether I

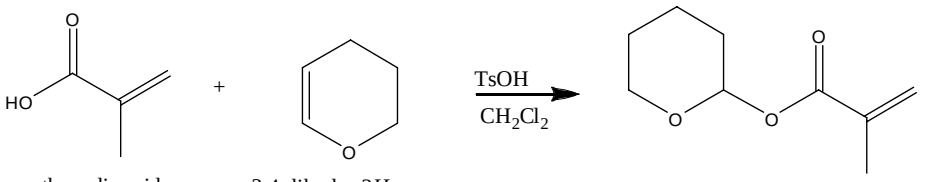

methacrylic acid 3,4-dihydro-2*H*-pyran tetrahydro-2*H*-pyran-2-yl methacrylate

Figure C.3: Reaction scheme for protection of methacrylic acid with THP Ether

This reaction proceeds by the same route as the above protection of 2-hydroxyethylacrylate with THP. Thus, the same preparation was followed.

Molar Equivalent Calculations:

5 g of methacrylic acid * 1mol/86.06g = 0.058 moles

Dihydropyran: 0.058 moles * 84.1g/mol = 5.86 g

TsOH: 0.1 * 0.058 moles * 190.22 g/mol = 1.105 g

1) Add methacrylic acid to round bottom flask
2) Add TsOH to flask. Put magnetic stir bar in and let mix.
3) Add enough CH_2Cl_2 to dissolve TsOH. Added nearly 100 mL and the TsOH still would not dissolve. Had to move to a larger round bottom flask.
4) Slowly add dihydropyran to flask while mixing. The solution immediately started to turn pink, then red, then very dark red/brown. Let stir for 3 hours.
5) Remove about 2/3 of the reaction solution and add to the half-saturated brine solution in separatory funnel. Shake well and then let sit.
6) Remove the organic layer (bottom layer; density of CH_2Cl_2 > density of H_2O)
7) Roto-vap organic layer to remove CH_2Cl_2.

Protection of Methacrylic Acid with THP Ether II

A slightly different procedure for the same protection reaction as above was also attempted. This procedure is from Bernady et el [4].

Molar Equivalent Calculations:

4 g of methacrylic acid * 1mol/86.06g = 0.046 moles

Dihydropyran: 5 * 0.046 moles * 84.1g/mol = 19.34 g

TsOH: 0.01 * 0.046 moles * 190.22 g/mol = 0.0875 g

1) Dissolve TsOH in a minimum amount of CH_2Cl_2.
2) Make solution of methacrylic acid and dihydropyran in CH_2Cl_2 on ice
3) Add TsOH solution to solution from step 2

4) Stir for 10 minutes at 0^{o}C.

5) Remove the ice bath and stir at room temperature for 1.25 hours.

6) Partition solution between ethyl ether and brine/sodium bicarbonate solution

    a. 40 ml saturated brine with 40 ml of sodium bicarbonate

7) Dry with $MgSO_4$

8) Evaporate ether with roto-vap

Protection of Methacrylic Acid with Methoxymethyl (MOM) ether

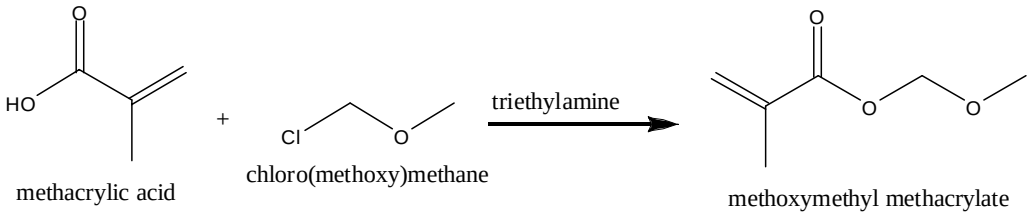

methacrylic acid chloro(methoxy)methane methoxymethyl methacrylate

Figure C.4: Reaction scheme for protection of methacrylic acid with MOM ether

This reaction procedure is from Ueda et al [5].

Molar Equivalent Calculations:

3 g of methacrylic acid * 1mol/86.06g = 0.035 moles

Chloro(methoxy)methane: 1.2 * 0.035 moles * 80.51 g/mol = 3.37 g

Triethylamine: 1.5 * 0.035 moles * 101.19 g/mol = 5.26 g

1) Add triethylamine drop-wise to cold liquid methacrylic acid

a. Note: Freezing point of methacrylic acid is 15^{o}C so add cold water from tap with a few pieces of ice until water is 17^{o}C.

2) Add chloromethyl methyl ether drop wise very carefully. The reaction is somewhat violent with splattering, popping and precipitate splashing everywhere on the flask.
3) Let mix over the weekend.
4) Dilute with 30 ml of ethyl acetate.
5) Filter off precipitate
6) Wash with 10% $NaHCO_3$ aqueous solution
7) Wash with DI H_2O
8) Concentrate by roto-vap

Monomer Polymerization

In order to test the monomers, it was often convenient to first polymerize them and then use the homopolymer. The following procedure was used to polymerize methacrylic acid for testing [6]. A similar procedure can be followed for most polymers that will undergo free-radical polymerization.

Molar Equivalent Calculations:

3.93 g of methacrylic acid * 1mol/86.06g = 45.7 mmoles

2,2'-Azobisisobutyronitrile (AIBN): 0.01 * 45.7moles = 0.457 mmol ➔ 0.075 g

1) Add AIBN to small bottle
2) Add 15 g of ethanol to bottle. Shake to fully dissolve AIBN
3) Add methacrylic acid to 100 ml round bottom flask

4) Add AIBN solution in ethanol to round bottom flask, then add an additional 10 ml of ethanol to flask so the total equals 25 g
5) Blanket the flask contents with N_2 and cap
6) Turn on oil bath to setting 4 on hotplate
7) Heat while mixing to 75 ^{o}C.
8) Let heat and mix overnight
9) Remove from heat and cool to room temperature.
10) Precipitate product in diethyl ether.
11) Collect product by filtering on Buchner funnel
12) Dry product in vacuum oven at 45^{o}C at -24 inHg

Protection Reaction on Polymers

For some studies, it was necessary to synthesize protected polymers. The polymer used in this work was polyhydroxystyrene (PHOST). Two protecting strategies were explored, protection by the THP group and protection by the tert-butoxycarbonyl (tBOC) group.

Tert-butyl carbonyl protected Polyhydroxystyrene

The first protecting group that was considered was the tert-butoxycarbonyl (t-BOC) group (Figure C.5). This group has been widely studied for use in resists [7, 8]; and its benefits include easy and efficient incorporation, its relative stability, and straight-forward cleavage under strong acidic conditions [2]. The general reaction procedure comes from Hansen and Riggs [9].

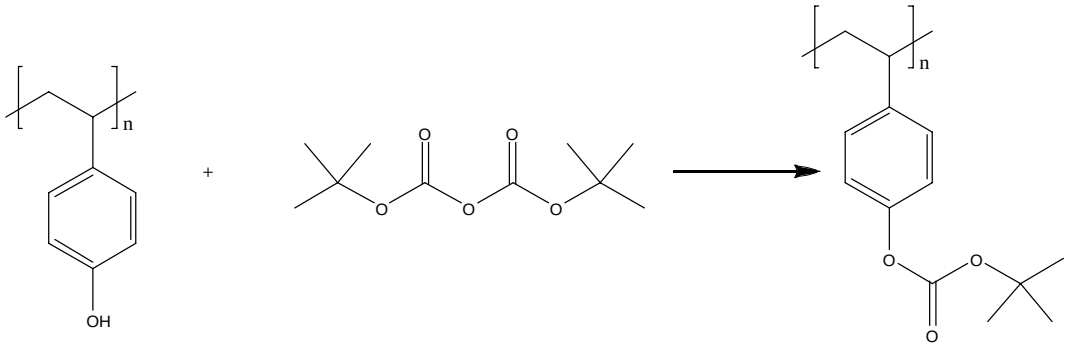

Figure C.5: Reaction scheme for protection of PHOST with tBOC group

Briefly, 2.5 g of PHOST was dissolved in acetonitrile, and 0.3 g of Dimethylaminopyradine (DMAP) was added to this solution. To this solution of PHOST and DMAP was added 5.45 g of ditertbutyl carbonate. The flask was capped with a balloon so that the evolution of CO_2 could be observed as a sign that the reaction was progressing. The reaction was allowed to run for three days, at which time a small amount of the reaction solution was removed from the flask and precipitated in water. The solid was collected, dried in a vacuum oven, and run on H-NMR to determine the degree of protection.

The sample was also run on the thermal gravimetric analysis with mass spectrometer (TGA-MS) machine. The sample was heated with a ramp rate of 5^oC per minute to 230^oC, and then held isothermally for 30 minutes. The mass change is recorded (Figure C.6).

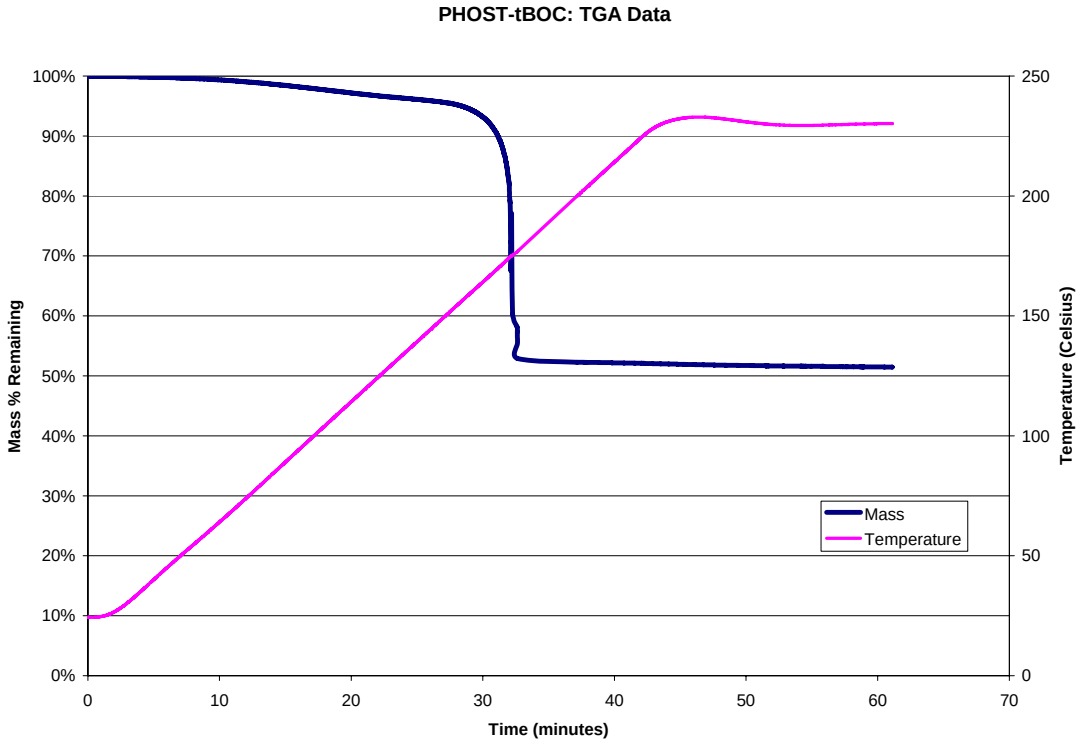

Figure C.6: PHOST-tBOC TGA plot

The major mass loss appears at about 28 minutes into the run, at about 155^{o}C. Using the mass remaining at this point and the final mass remaining, the percent weight remaining is calculated to be 54.4%. The theoretical percent weight remaining is calculated from the molecular weight of polyhydroxystyrene (120 amu) and the molecular weight of the protected polymer (220 amu). For a fully protected polymer, this comes to 54.5%. Thus, the TGA data shows that the polymer is nearly 100% protected, which is in agreement with the FTIR data showing the thermal cleavage of the protecting group (Figure C.7).

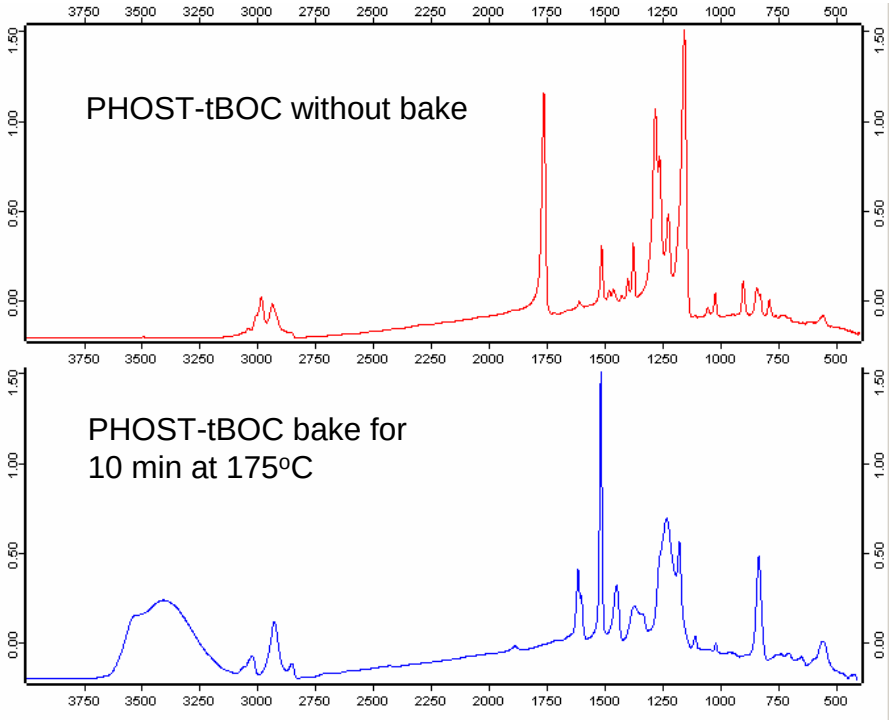

Figure C.7: PHOST-tBOC FTIR plots

Tetrahydropyranyl (THP) Protected Polyhydroxystyrene

The THP protecting group has also been investigated for this work (Figure C.8). The main benefit of this group is that it has lower activation energy for acid-catalyzed cleavage. This means that a high post-exposure bake temperature is not necessary. This is desirable in the case of the final, stereolithographic process. Ideally, the material will polymerize in the vat, be exposed to the wavelength of light that will generate an acid molecule, and the de-protection reaction will occur in those regions as the part is being built. Molecules requiring a high bake temperature to catalyze their de-protection will not work for this fabrication method.

A method for protecting PHOST with the THP group was developed so that protected polymers could be investigated for use as dissolution inhibitors [10], and this procedure has been repeated by C. Berger in the Henderson research group [11].

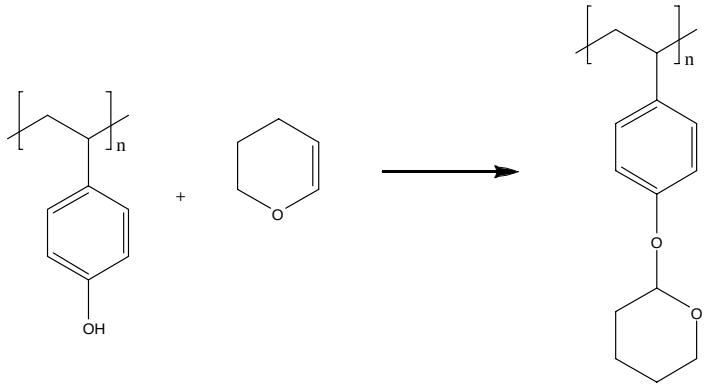

Figure C.8: Reaction scheme for PHOST protection with THP

The protection reaction was preformed under the same conditions as presented in the paper and thesis: "To a solution of 5 g of PHOST and 70-ml ethyl acetate was added 14 g of 3,4-dihydro-2H-pyran and a trace of HCl."[10]. The solution was left at room temperature for 10 days, at which time a small sample was removed and precipitated in petroleum ether. H-NMR was run on the precipitate and the results showed a significant degree of protection. On day thirteen, the reaction mixture was washed with saturated aqueous sodium bicarbonate solution to neutralize any remaining acid, and precipitated in petroleum ether. The recovered polymer was dried in a vacuum oven for 12 hours. The original paper calls for the reaction mixture to be dried over aqueous sodium sulfate for 10 hours; however, this step was omitted due to time constraints.

The sample was also run on the thermal gravimetric analysis with mass spectrometer (TGA-MS) machine. The sample was heated with a ramp rate of 5°C per minute to 230°C, and then held isothermally for 30 minutes. The mass change is recorded (Figure C.9).

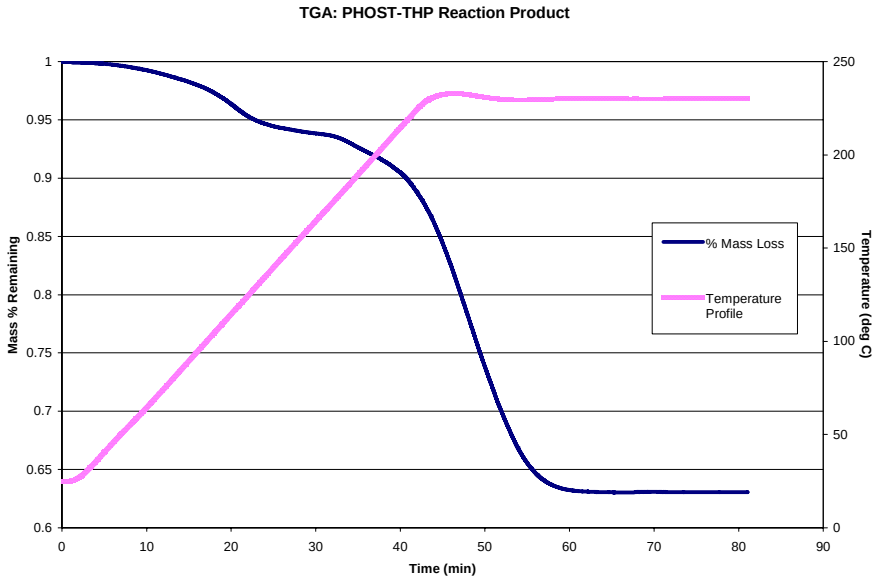

Figure C.9: TGA plot for PHOST-THP

For a 100% protected polymer, one would expect that the fraction of mass remaining would be 0.588 (120/204). From the TGA data, the mass loss calculated from 43-56 minutes is about 0.677, so the polymer is about 87% protected. The mass spectroscopy data matches the hypothesis that the major mass loss from 43 to 56 minutes is from leaving of the THP group. A major fragment with mass 83 shows up at this time point, which correlates to the THP group.

References

[1] A. J. Meyers, D. L. Comins, D. M. Roland, R. Hemming, and K. Shimizu, "Total synthesis of (±)-maysine. ," *Journal of American Chemcial Society*, vol. 101, pp. 7104-5, 1979.

[2] P. G. M. Wuts and T. W. Greene, *Greene' s Protective Groups in Organic Synthesis Fourth Edition*, Fourth ed. Hoboken, New Jersey: John Wiley & Sons, 2007.

[3] N. Miyashita, A. Yoshikioshi, and P. A. Grieco, "Pyridinium p-Toluenesulfonate. A Mild and Efficient Catalyst for the Tetrahydropyranylation of Alcohols," *J. Org. Chem.*, vol. 42, pp. 3772-3774, 1977.

[4] K. F. Bernady, M. B. Floyd, J. F. Poletto, and M. J. Weiss, "Prostaglandins and congeners. 20. Synthesis of prostaglandins via conjugate addition of lithium trans-1-alkenyltrialkylalanate reagents. A novel reagent for conjugate 1,4-additions," *J. Org. Chem.*, vol. 44, pp. 1438-1447, 1979.

[5] M. Ueda, S. Ishibashi, T. Suzuki, and T. Masuko, "Radical-Initiated Homo- and Copolymerization of Methoxymethyl Methacylate," *Journal of Polymer Science: Polymer Chemistry Edition*, vol. 22, pp. 2305-2316, 1984.

[6] S. Graham, A. G. Cormack, and D. C. Sherrington, "One-pot Synthesis of Branched Poly(methacrylic acid)s and Suppression of the Rheological "Polyelectrolyte Effect"," *Macromolecules*, vol. 38, pp. 86-90, 2005.

[7] H. Ito, "Chemical Amplification Resists for Microlithography," *Advanced Polymer Science*, vol. 172, pp. 37-245, 2005.

[8] L. F. Thompson, C. G. Willson, and M. J. Bowden, *Introduction to Microlithography*. Washington DC: American Chemical Society, 1994.

[9] M. Hansen and J. R. Riggs, "A Novel Protecting Group for Hindered Phenols," *Tetrahedron Letters*, vol. 39, pp. 2705-2706, 1998.

[10] H. Shiraishi, N. Hayashi, T. Ueno, T. sSakamizu, and F. Murai, "Nocolak resin-based positive electron-beam resist system utilizing acid-sensitive polymeric dissolution inhibitor with solubilit reversal reactivity," *J. Vac. Sci. Technol. B*, vol. 9, pp. 3343-3347, 1991.

[11] C. M. Berger, "Measuring Acid Generation Kinetics in Photoresist Films via Capacitance Techniques," in *Chemical Engineering*, vol. Doctor of Philosophy. Atlanta, GA: Georgia Institute of Technology, 2004.

APPENDIX D

LOW VOLUME RESIN CHARACTERIZATION STUDY

Introduction

The Windowpane technique is a method developed by 3D Systems engineers to determine the resin characteristics critical exposure (Ec) and depth of penetration (Dp) [1]. Critical exposure is the exposure dose that first changes the liquid monomer to a gel-like state, and the depth of penetration is the depth of that first gel-like state. The procedure is designed for a commercial stereolithographic apparatus (SLA) that uses a Gaussian laser. The procedure specifies the building of five different parts of five "windowpanes" polymerized at increasing exposure levels. The laser fires for tens of microseconds, and the light is reflected by a mirror until the laser turns off. The mirror then moves to reflect light a few bits from the original location, and the laser fires to repeat the cycle. The laser first fires border vectors and then fill vectors, which first "draw" horizontally and then vertically for added strength. The cure depth of the "windowpanes" is then measured with a micrometer and a working curve is plotted that follows Equation D.1.

$$C_d = D_p \cdot \ln \frac{E_c}{E_{av}}$$

Equation D.1: Working curve equation, C_d = cure depth, E_{av}= average exposure, D_p = depth of penetration, E_c = critical exposure.

The Dp is determined to be the slope of the line and the Ec is the x-intercept. The main drawback of the 3D systems method is that it requires approximately 100 mL of resin, which can be expensive and difficult to synthesize.

This project develops a new method to determine the critical exposure and depth of penetration of various resins with a much smaller volume requirement. A low-volume apparatus was designed to determine these characteristics with the volume restriction. The apparatus is capable of blanketing with an inert gas because the oxygen in air can stop the polymerization process by bonding to the free-radicals. The exposure tool that was used emits light at 365nm while the SLA lasers of 3D systems emit light at 355 nm; therefore, a completely consistent result between the two systems is impossible. Three different commercial brand resins, Waterclear 10120, SL-7545, and SL-7560, were tested to determine the calibration curve.

Apparatus and Procedure

The new method developed by this project is referred to as the Square technique because tiny squares are measured instead of windowpanes. Unlike the Gaussian laser used in Windowpanes, collimated light from a UV exposure tool is focused on the apparatus. A plastic mask positioned above the shallow well of monomer allows only light at the very center in a form of a square. The main reason the Square technique uses so much less resin than the Windowpane technique is that supports are not built, and the floating polymerized square part is carefully removed with a metal spatula. The solid square is less than dense than the liquid monomer; therefore, the squares can be taken out

of the well without the top of the square touching the monomer, if appropriate care is shown. Each square is placed *top-side up* on paper towel that has been folded four times. To minimize the amount of monomer around the square part, the part is first gently wiped on the paper towel surface and then set down. After each square is built, the leftover monomer in the well is removed with a pipette, and fresh resin is added to ensure that results are not altered by monomer that has been exposed but not quite polymerized. Three runs are taken at each exposure time, and after four slightly increasing exposure times, the 12 square parts are drained for one hour. To drain the parts, a folded paper towel is placed on all the parts and a weight of approximately 10 grams (a microscope slide works best) is placed over 6 of the parts and another weight is placed over the other six. The square parts are then cured by placing onto a paper towel bottom-side up, and exposed by the UV exposure tool for 45 minutes. The square parts are then measured at the center by a special Windowpane micrometer. The micrometer clicks three times, and at the third click the measurement was taken. The measurement is taken in four places all near the center of the square.

Results and Discussion

The results of the first run of Waterclear 10120, a commercial epoxy/acrylate, is shown in Table D.1, and then plotted in Figure D.1. Only one square was built at each exposure time and the average of the cure depth measurements was used in Equation D.1.

Table D.1: Measurements of one run of Waterclear 10120 at 10.351 mW (values at 355 mW; Ec = 9.7 mW, Dp = 6.3 mils)

Time (s)	Measurement				Average (mils)
10	0.04145	0.04120	0.03945	.04120	40.825
15	0.05435	0.05415	0.05355	.05450	54.1375
20	0.06150	0.06095	0.05880	.05975	60.25
25	0.06675	0.06840	0.06850	.06885	68.125
30	0.07060	0.07270	0.07160	.07290	71.95
	R2= .9945	Ec=23.7	Dp=28.2		

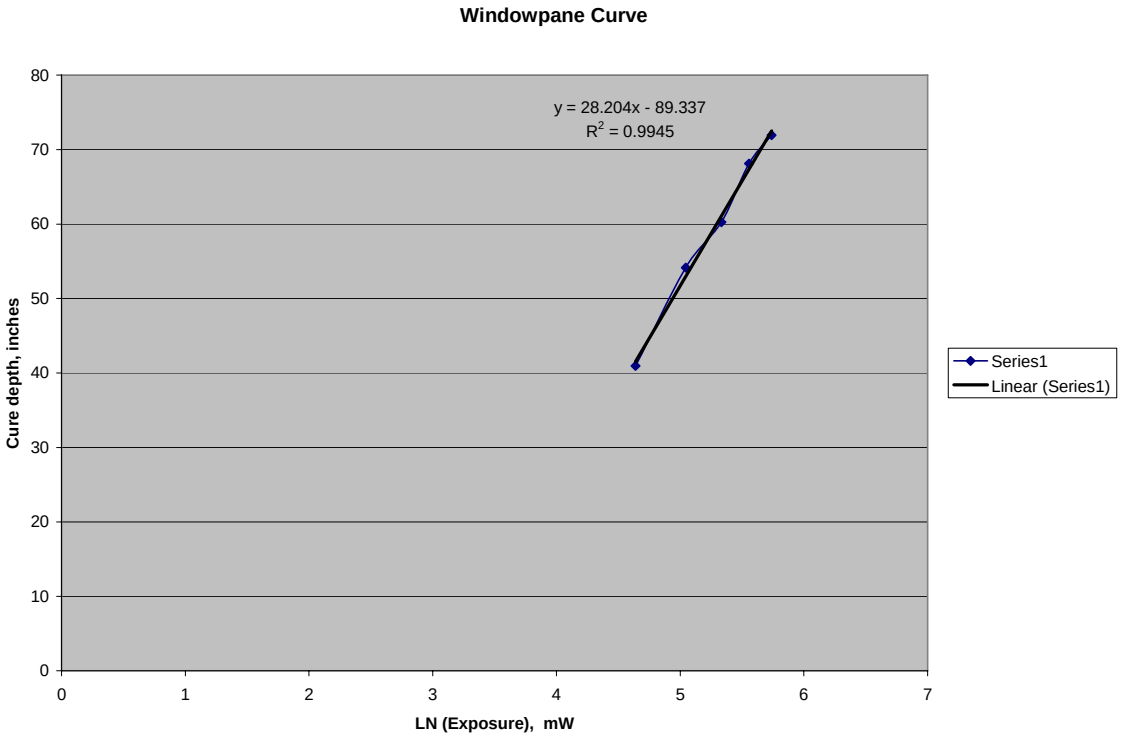

Figure D.1: Working curve of Waterclear 10120 with one run at high exposure times

The R2 value is 0.9945 which suggests a good linear fit. The Ec value of 23.7 mJ/cm2 and the Dp value of 28.2 mils at 365nm are much higher than the literature data of 9.7 and 6.3. Another run was performed to measure consistency, and the experiment was performed at lower exposure times to obtain a more linear curve. The results are illustrated in Table D.2 and Figure D.2.

Table D.2: Measurements of one run of Waterclear 10120 at low exposure times at 9.729 mW.

Time (s)	Measurement				Average (mils)
6	0.02350	0.02360	0.02365	0.02340	23.538
8	0.03575	0.03660	0.03635	0.03625	36.238
10	0.04360	0.04380	0.04425	0.04390	43.888
12	0.04790	0.04895	0.04850	0.04850	48.463
14	0.05360	0.05470	0.05370	0.05115	53.288
	R2= .988	Ec=28.4	Dp=34.6		

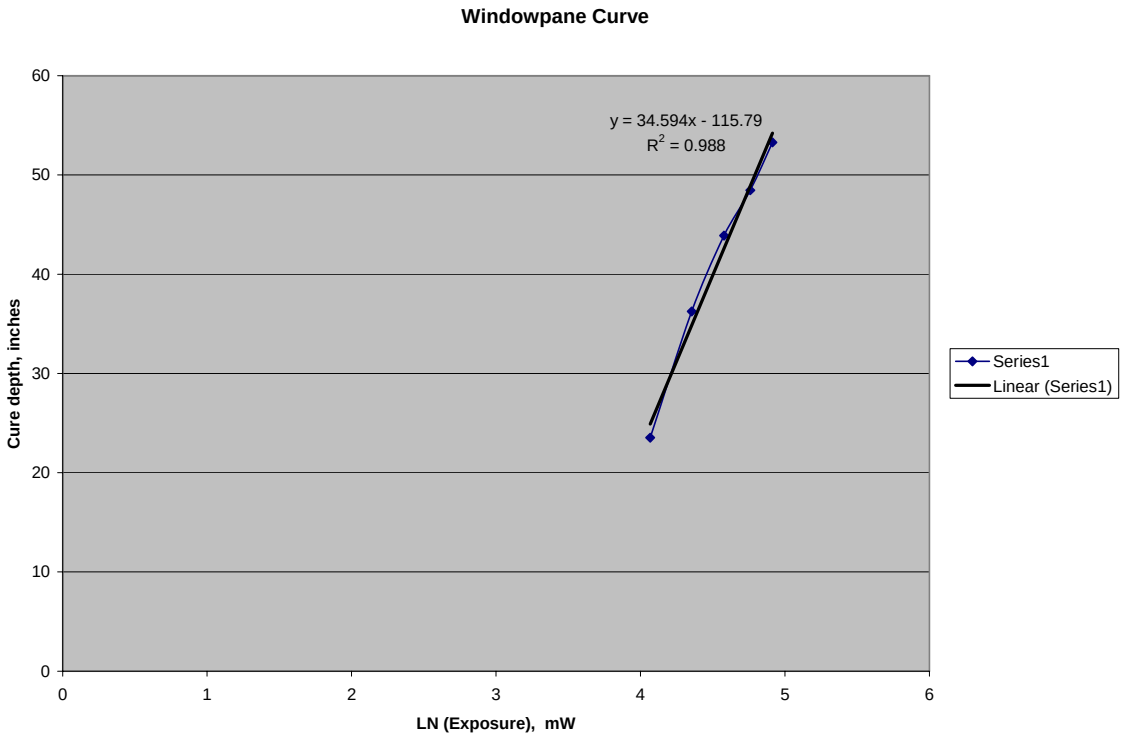

Figure D.2: Working curve of Waterclear 10120 with one run at low exposure times

The first run determined an Ec value of 23.7 and a Dp value of 28.2; the second run determined an Ec value of 28.4 and a Dp value of 34.6. The Ec value is 20% higher and the Dp value is 23% higher in the second run than the first. To obtain a more consistent result, 3 squares at each exposure time will be measured. Also, to determine whether different kinds of resins are off by the same factor, Waterclear 10120, SL-7560, and SL-7545 will be characterized. The results are illustrated in Tables D.3-D.7, and Figures D.3-D.5.

Table D.3: Three runs of SL-7545 at 10.626 mW

Time (sec)	Run 1				Run 2			
10	.03600	.03750	.03720	.03815	.03495	.03530	.03190	.03365
12	.04450	.04340	.04260	.04385	.04175	.04165	.04215	.04180
14	.04850	.04935	.04805	.04925	.04835	.04700	.04790	.04705
16	.05090	.05155	.05170	.05160	.04995	.05020	.05175	.05125
18	.05515	.05470	.0543	.05285	.05400	.05425	.05455	.05300
	R2=.9869		Ec= 28.626	Dp= 28.924	R2=.9846		Ec= 37.78	Dp= 33.807

Time (sec)	Run 3			
10	.03500	.03400	.03655	.03605
12	.03985	.03900	.03945	.04050
14	.04695	.04935	.04655	.04665
16	.05090	.04905	.05265	.05220
18	.05435	.05460	.05255	.05430
	R2=.9831	Ec=37.09	Dp= 33.282	

Table D.4: Average of the three funs of SL-7545 at 20.626 mW

Time (sec)	Run 1 Average	Run 2 Average	Run 3 Average	Total Average (mils)
10	0.037213	0.03395	0.0354	35.521
12	0.043588	0.041838	0.0397	41.70867
14	0.048788	0.047575	0.047375	47.91267
16	0.051438	0.050788	0.0512	51.142
18	0.05425	0.05395	0.05395	54.05
	R2=.9904	Dp=32.004	Ec= 34.527	

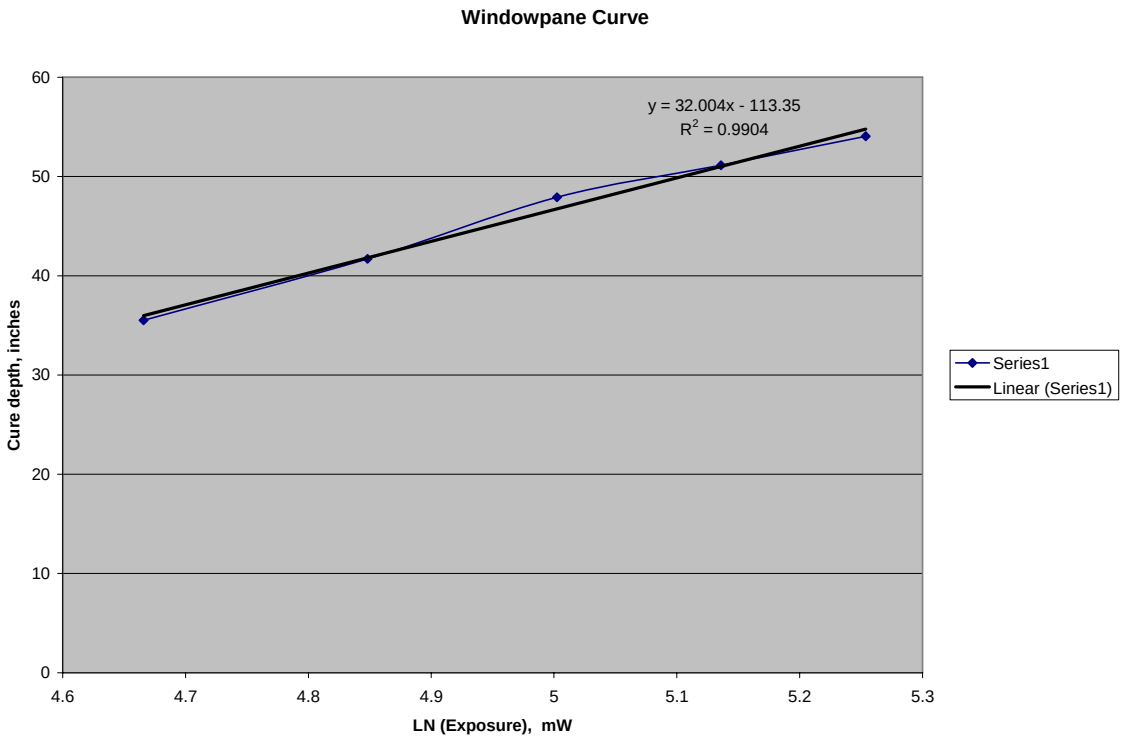

Figure D.3: Working curve of SL-7545 with 3 runs

Table D.5: Each run of SL-7560 at 10.626 mW

Time (sec)	Run 1				Run 2			
10	.03705	.04060	.04150	.03995	.04115	.04040	.04195	.04135
12	.04455	.04395	.04520	.04340	.04390	.04345	.04485	.04520
14	.04875	.04895	.04785	.04820	.04840	.04765	.04795	.04895
16	.05285	.05050	.05185	.05220	.05010	.04875	.04985	.05050
18	.05400	.05545	.05405	.05465	.05290	.05395	.05370	.05290
	R2=.9994		Ec= 21.961	Dp= 25.371	R2=.9881		Ec= 13.925	Dp= 20.258

Time (sec)	Run 3			
10	.04070	.04065	.04120	.04070
12	.0445	.04335	.04350	.04365
14	.04850	.04815	.04715	.04605
16	.05140	.05065	.05100	.04975
18	.05370	.05370	.05295	.05290
	R2=.9939	Ec=16.4286	Dp= 21.719	

Table D.6: Each run of SL-7560 at 10.626 mW

Time (sec)	Run 1 Average	Run 2 Average	Run 3 Average	Total Average (mils)
10	0.039775	0.041213	0.040813	35.521
12	0.044275	0.04435	0.04375	41.70867
14	0.048438	0.048238	0.047463	47.91267
16	0.05185	0.0498	0.0507	51.142
18	0.054538	0.053363	0.053313	54.05
	R2=.9979	Dp=22.452	Ec= 17.592	

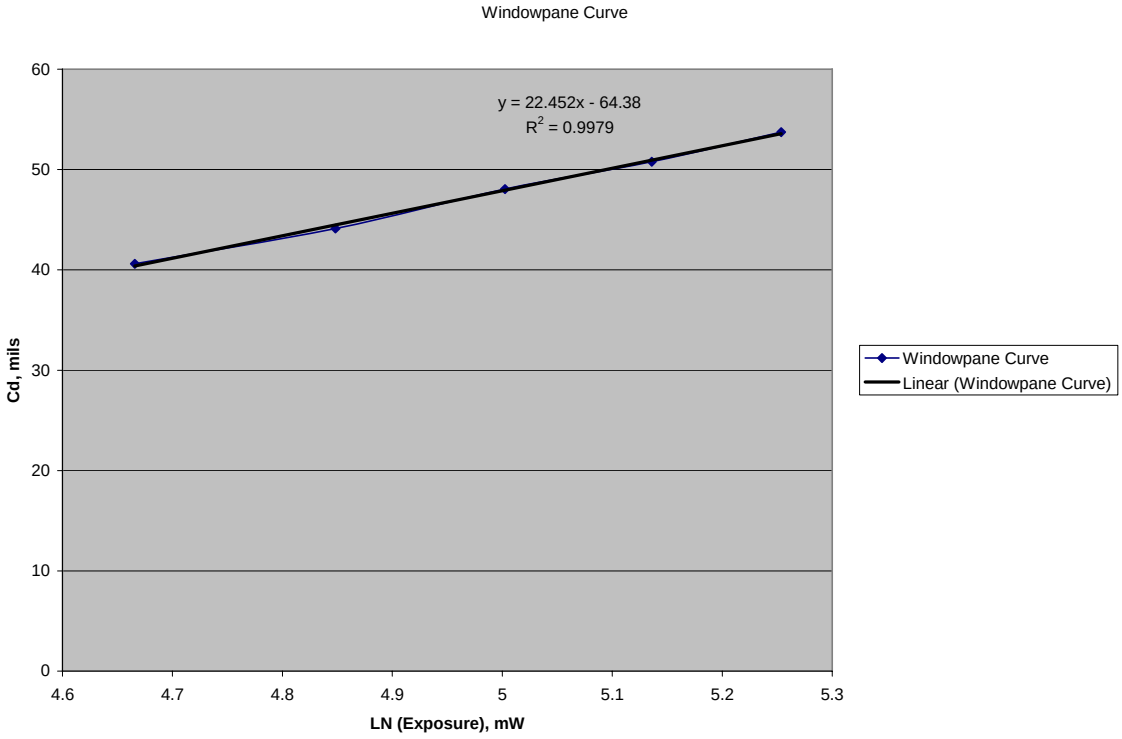

Figure D.4: Working curve of Sl-7560 with 3 runs

Table D.7: Each run of Waterclear at 10.597 mW

Time (sec)	Run 1				Run 2			
12	.05010	.04910	.0485	.0467	.04885	.04800	.04770	.04900
14	.05340	.05345	.05375	.05280	.05415	.05310	.05230	.05355
16	.05585	.05535	.05785	.05850	.05860	.05705	.05665	.05710
18	.06075	.06015	.06035	.06075	.06205	.06125	.06260	.06080
20	.06285	.06365	.06275	.06135	.06375	.06365	.06320	.06315
	R2=.9976		Ec= 14.113	Dp= 24.163	R2=.9938		Ec= 16.927	Dp= 26.402

Time (sec)	Run 3			
12	.05105	.05070	.05020	.04930
14	.05370	.05315	.05315	.05445
16	.05825	.05850	.05855	.05795
18	.06180	.06090	.06130	.06215
20	.06250	.06135	.06135	.06410
	R2=.9767	Ec=10.771	Dp= 21.971	

Table D.8: Average of the three runs of Waterclear at 10.597 mW

Time (sec)	Run 1 Average	Run 2 Average	Run 3 Average	Total Average (mils)
12	.0486	.0483875	.0503125	49.1
14	.05335	.0534125	.0537125	53.49167
16	.0568875	.05735	.0583125	57.51667
18	.0605	.061675	.0615375	61.2375
20	.06265	.0634375	.062325	62.80417
	R2=.9953	Dp=25.005	Ec= 25.3	

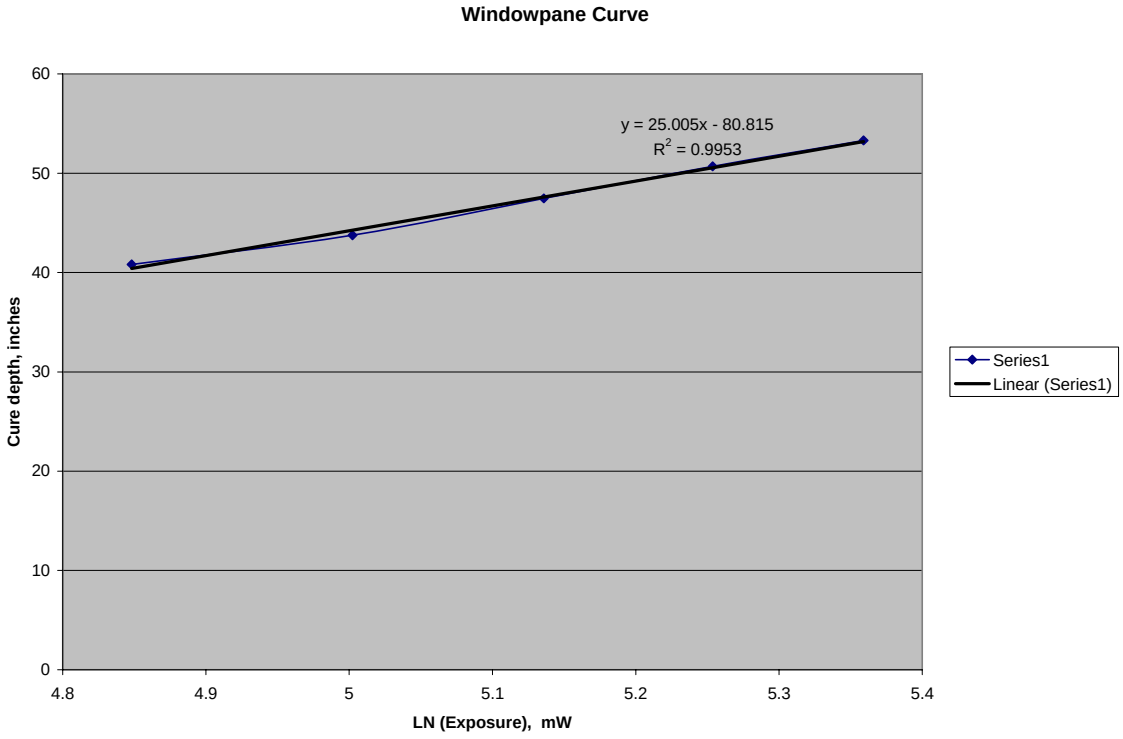

Figure D.5: Working curve of Waterclear with 3 runs

All three plots suggest a good linear fit to the data, but the SL-7545 did not meet the Windowpane standard of an R2 value of 0.995. The factor that each characteristic was off from the literature data is summarized in Table D.9.

Table D.9: First calibration curve

	Waterclear (10120)		SL-7545		SL-7560	
	Ec	Dp	Ec	Dp	Ec	Dp
Experimental	25.3	25.0	34.5	32.0	17.6	22.5
Actual	9.7	6.3	9.6	6.6	5.4	5.3
Factor Off	2.61	3.97	3.59	4.85	3.26	4.25

The depth of penetration of the three resins are off by factors of 3.97, 4.85, and 4.25. The critical exposure of the two polyethylenes are off by 3.59 and 3.26, respectively; while the Waterclear, an epoxy/acrylate mix, is off by 2.61. The causes of this error could be that polyethylenes and epoxy/acrylates do not polymerize the same way under this exposure tool. SL-7545, with the worst linear fit, had the highest factor off in Dp and Ec. Also, some parts did not polymerize evenly throughout the square, and parts were sometimes lopsided as illustrated in Figure D.6.

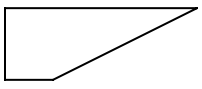

Figure D.6: Lopsided parts due to slightly different apparatus positions

Therefore, the side of the part was measured and not the center.

Thus, several corrections were made, and the three commercial resins were run again. The following corrections were made. The apparatus and radiometer were marked to so they were in the same location for each run. All of the parts were measured at the same location. All of the parts were drained with the same weight (~20 grams for 6 squares). Fresh resins were obtained and were stored carefully, wrapped in aluminum foil.

With these corrections, the three commercial brand resins were run again, but this time only at 4 times instead of 5. The results are illustrated in Tables D.10-18, and Figures D.7, D.8, and D.9.

Table D.10: Run 1 and 2 of SL-7560 at 10.205 mW

Time (sec)	Run 1				Run 2			
14	.04920	.04960	.04905	.04935	.05110	.04870	.04870	.05075
16	.05155	.05105	.05305	.05335	.05340	.05425	.05440	.05335
18	.05460	.05490	.05500	.05480	.05410	.05300	.05615	.05465
20	.05580	.05640	.05580	.05665	.05725	.05520	.05730	.05590
	R2=.9882	Ec= 11.35	Dp= 19.6		R2=.9246	Ec= 7.78	Dp= 17.36	

Table D.11: Run 3 of SL-7560 at 10.205 mW

Time (sec)	Run 3			
14	.05040	.05115	.05125	.05055
16	.05290	.05285	.05200	.05290
18	.05605	.05555	.05440	.05505
20	.05680	.05555	.05635	.05680
	R2=.9849	Ec=6.2	Dp= 16.195	

Table D.12: Average of the three runs of SL-7560 at 10.205 mW

Time (sec)	Run 1 Average	Run 2 Average	Run 3 Average	Total Average (mils)
14	.0493	.0498125	.0508375	49.98333
16	.05225	.05385	.0526625	52.92083
18	.054825	.054475	.0552625	54.85417
20	.0561625	.0564125	.056375	56.31667
	R2=.9889	Dp=17.7	Ec= 8.4	

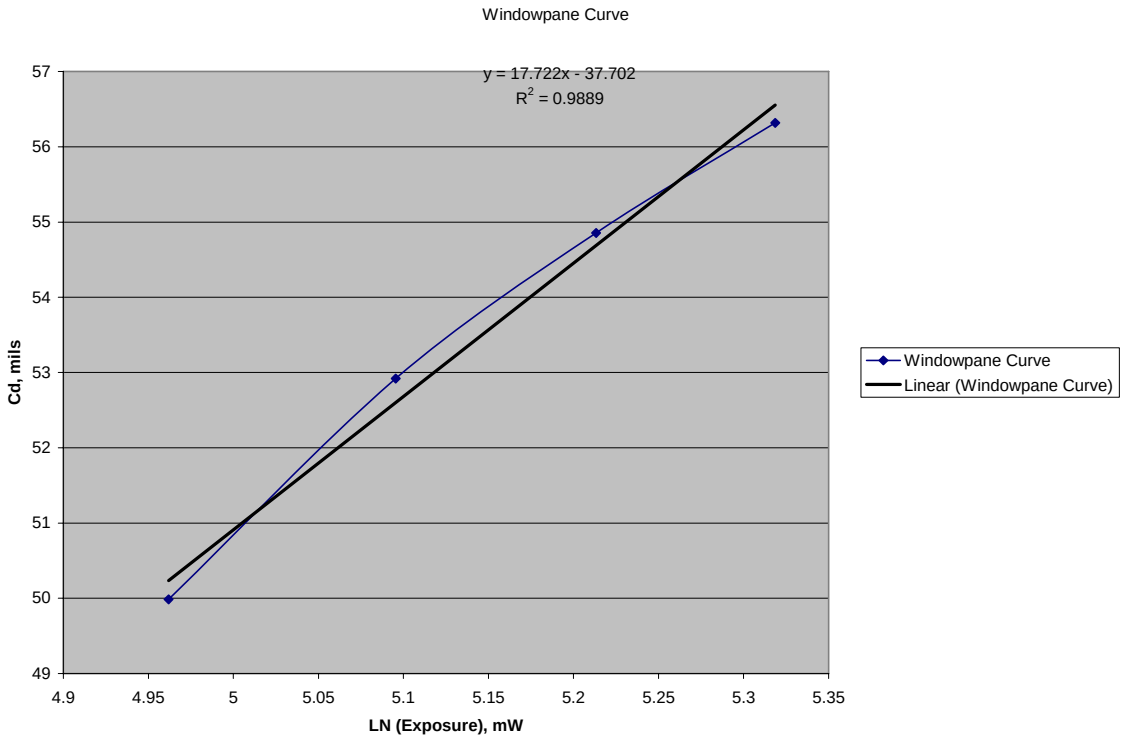

Figure D.7: Working curve of SL-7560 with three runs

Table 13: Run 1 and 2 of SL-7545 at 10.205 mW

Time (sec)	Run 1				Run 2			
14	.04945	.04880	.04875	.04825	.04850	.04885	.04870	.04980
16	.05380	.05390	.05385	.05260	.05490	.05285	.05095	.05250
18	.05535	.05495	.05535	.05575	.05495	.05665	.05575	.05495
20	.05885	.05735	.05885	.05865	.05845	.05815	.05775	.05780
	R2=.9781		Ec= 21.0	Dp= 25.8	R2=.9988		Ec= 20.5	Dp= 25.4

Table D.14: Run 3 of SL-7545 at 10.205 mW

Time (sec)	Run 3			
14	.04985	.04925	.04960	.04990
16	.05235	.05260	.05155	.05315
18	.05525	.05600	.05590	.05595
20	.05840	.05805	.05800	.05825
	R2=.9962	Ec=18.5	Dp= 24.3	

Table D.15: Average of the three runs of SL-7545 at 10.205 mW

Time (sec)	Run 1 Average	Run 2 Average	Run 3 Average	Total Average (mils)
14	.0488125	.0489625	.04965	49.14167
16	.0535375	.052675	.0524125	52.875
18	.05535	.055575	.05575	55.55833
20	.058425	.0580375	.058175	58.2125
	R2=.9983	Dp=25.2	Ec= 20.2	

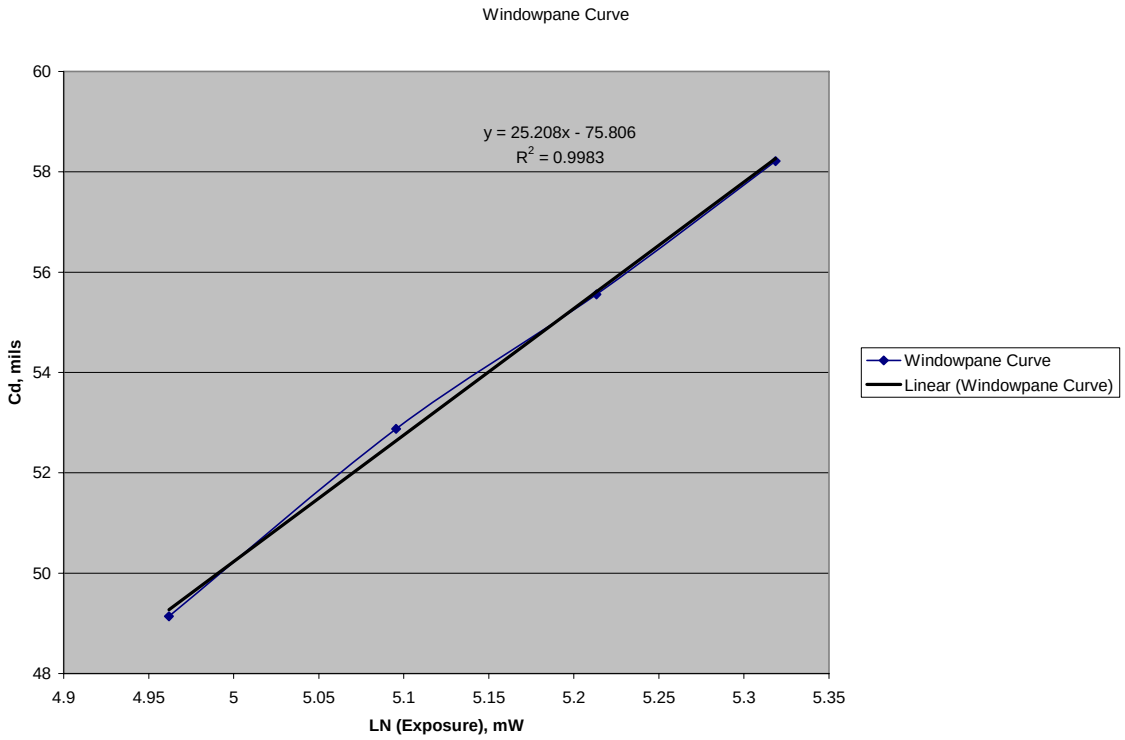

Figure D.8: Working curve of SL-7545 with three runs

Table D.16: Run 1 and 2 of Waterclear 10120 at 10.205 mW

Time (sec)	Run 1				Run 2			
14	.05250	.05465	.05380	.05280	.05325	.05440	.05230	.05310
16	.05540	.05665	.05645	.05640	.05460	.05680	.05690	.05525
18	.05845	.05910	.05900	.05860	.06015	.05910	.05945	.05920
20	.06155	.06200	.06090	.06200	.06125	.06165	.06170	.06125
	R2=.9966		Ec= 13.6	Dp= 22.7	R2=.9937		Ec= 14.9	Dp= 23.6

Table D.17: Run 3 of Waterclear 10120 at 10.205 mW

Time (sec)	Run 3			
14	.05275	.05345	.05240	.05280
16	.05650	.05640	.05705	.05720
18	.05880	.05955	.06025	.05970
20	.06170	.06160	.06125	.06265
	R2=.994	Ec=17.0	Dp= 25.1	

Table D.18: Average of the three runs of Waterclear at 10120 at 10.205 mW

Time (sec)	Run 1 Average	Run 2 Average	Run 3 Average	Total Average (mils)
14	.0534375	.0532625	.05285	53.18333
16	.056225	.055888	.0567875	56.30017
18	.0587875	.059475	.059575	59.27917
20	.0616125	.0614625	.0618	61.625
	R2=.9995	Dp=23.8	Ec= 15.8	

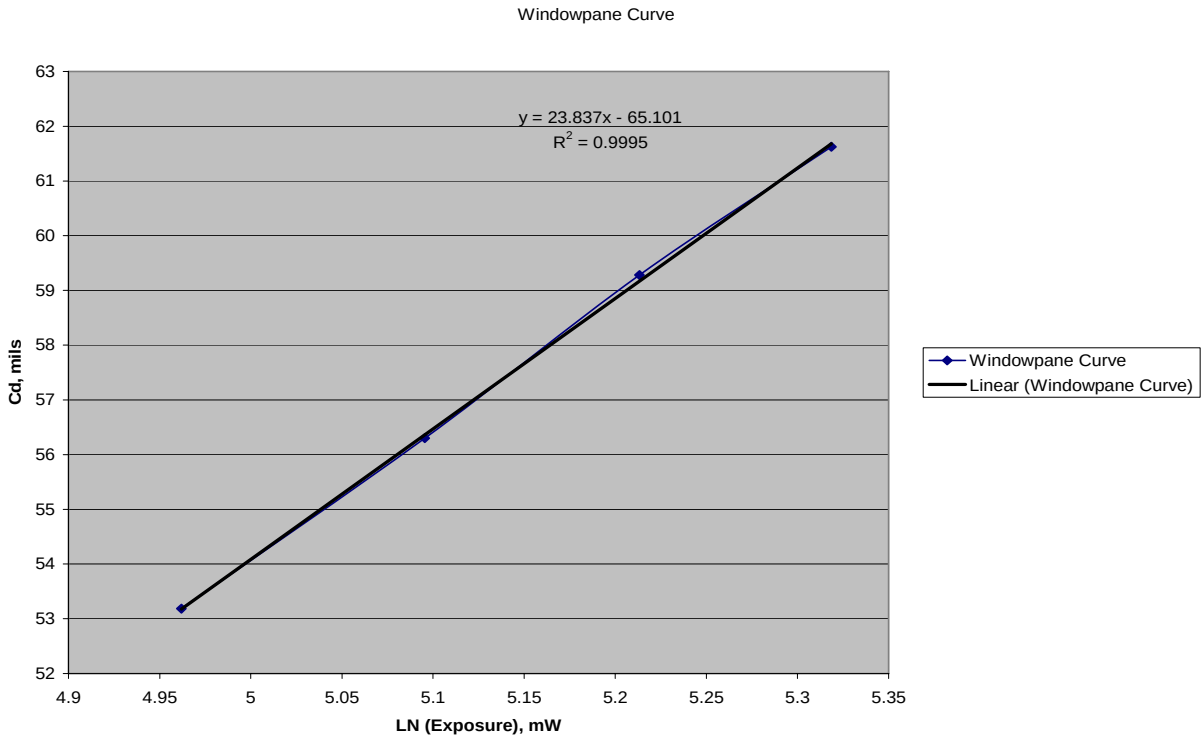

Figure D.9: Working curve of Waterclear 10120 with three runs

All three plots suggest a good linear fit to the data, but the SL-7560 did not meet the Windowpane standard of an R2 value of 0.995. The factor that each characteristic was off from the literature data is summarized in Table D.19.

Table D.19: Second calibration curve

	Waterclear (10120)		SL-7545		SL-7560	
	Ec	Dp	Ec	Dp	Ec	Dp
Experimental	15.8	23.8	20.2	25.2	8.4	17.7
Actual	9.7	6.3	9.6	6.6	5.4	5.3
Factor Off	1.63	3.78	2.10	3.81	1.56	3.34

Summary

This new “Square” method of determining critical resin characteristics provides a means of testing resins using a much lower volume of rein than the traditional Windowpane method. Although the results differ from the commercial resins specifications, the results are self consistent and this method should be sufficient to test new resins for the new system. The main advantage is that this new Square method only requires about 5 mL of resin.

References

[1] P. F. Jacobs, *Rapid Prototyping & Manufacturing, Fundamentals of StereoLithography*, First ed. Dearborn, MI: Society of Manufacturing Engineers, 1992.